The effect of alloying composition and cooling rate on the hot ductility of TWIP steel and mechanical properties of hot rolled HSLA steel

By

Abdullah Qaban

A thesis submitted for the degree of Doctor of Philosophy (PhD) in Mechanical Engineering

School of Mathematics, Computer Science & Engineering

City, University of London

November 2019

Declaration

I hereby certify that this material, which I submit for assessment on the programme of study leading to the award of Doctor of Philosophy is entirely my own work and has not been taken from the work of others and to the extent that such work has been cited and acknowledged within the test of my work.

Publications

1 **Qaban, A**., Mintz, B., Kang, S.E. and Naher, S., 2017. Hot ductility of high Al TWIP steels containing Nb and Nb-V. *Materials Science and Technology*, 33(14), pp.1645-1656.

2 **Qaban, A**., Mintz, B. and Naher, S., 2017. Hot rolled high Al containing steels as a replacement for the control rolled high strength low alloy (HSLA) steels. In *AIP Conference Proceedings* (Vol. 1896, No. 1, p. 130007). AIP Publishing.

3 **Qaban, A**. and Naher, S., 2018. Influence of Al content on the corrosion resistance of micro-alloyed hot rolled steel as a function of grain size. In *AIP Conference Proceedings* (Vol. 1960, No. 1, p. 040017). AIP Publishing.

Conferences

1 **Qaban, A**., Mintz, B. and Naher, S. Oral presentation on the effect of aluminium on the electrochemical corrosion behaviour of HSLA Steel in *AMPT*, 2018, Dublin, Ireland.

2 **Qaban, A**., Mintz, B. and Naher, S. Oral presentation on the influence of Al content on the corrosion resistance of micro-alloyed hot rolled steel as a function of grain size in *ESAFORM*, 2018, Palermo, Italy.

3 **Qaban, A**., Mintz, B. and Naher, S. Oral presentation on the precipitation behavior of AlN and its influence on the microstructure and mechanical performance of a hot rolled C-Mn steel in *the 3rd Euro Congress on Steel and Structural Engineering*, 2017, London, UK.

4 **Qaban, A**., Mintz, B. and Naher, S. Poster presentation on the control of lower yield strength and toughness of hot rolled steel in *the 11th International Conference on Compressors and their System*, 2017, London, UK.

5 **Qaban, A**., Mintz, B. and Naher, S. Oral presentation on hot rolled high Al containing steels as a replacement for the control rolled high strength low alloy in *ESAFORM*, 2017, Dublin, Ireland.

6 **Qaban, A**., Mintz, B. and Naher, S. Poster presentation on control and hot rolling processing of HSLA steel in *the 9th SSC Conference*, 2016, Birmingham, UK.

Acknowledgements

I would like to express my special appreciation and thanks to my primary supervisor Dr Sumsun Naher, she has been a tremendous mentor for me. I would like to thank her for all her generous support and encouragement during my PhD degree. Her guidance and feedback since the beginning of the course have been priceless.

Special thanks to Professor Barrie Mintz for his guidance and help during my PhD course. Despite the technical issues I had with the lab experiments during the project, he was very supportive and encouraging. Many thanks for the time and providing valuable feedback throughout the research project.

Special thanks to Jim Hooker for his aid in the laboratory at City, University of London. I must acknowledge the following universities for their technical support during the project; Warwick University, Open University, Brunel University, Dublin City University and the University of Limerick.

I would like to thank POSCO in South Korea who supported the research project on TWIP steel and special thanks to Dr Shin Eon Kang from POSCO Technical Research Labs for his technical support. I have to thank TATA Steel in the UK for supporting the HSLA steel project and especially Dr David Crowther.

I would like also to thank Professor Ranjan Banerjee for his support and valuable feedback. I'm also glad to be surrounded by extraordinary colleagues, Israt Kabir, Nusrat Tamanna and Bhagya Dasari.

Special thanks go to my family. I would like to express gratefulness to my father who has been always great in encouraging me in the difficult and stressful moments. Words cannot express how grateful I am to my mother who greatly motivated me to work hard toward my goals. I would like to express my thanks to my wife for all the sacrifices that she has made in order to help me to complete my degree. I cannot forget to mention Yousef Qaban and Ahmad Qaban who have been always in my mind and my heart.

Abstract

The current work investigated the influence of alloying composition and thermal treatment on the hot ductility of TWIP (twinning induced plasticity) steel and mechanical properties of HSLA (high-strength low-alloy) steel at room temperature. For TWIP steel, the present work simulated the continuous casting process in the laboratory using hot tensile tests at the temperature range of 700°C-1100°C to assess likelihood of transverse cracking. The tensile specimens were soaked at 1250°C then cooled at 12 or 60°C min^{-1} to the test temperature and then strained to failure at 3 x 10^{-3} s^{-1}. Reduction of area was measured after failure to indicate whether the steel can be cast without transverse cracking occurring. The processing parameters involved the Ti/N content ratio and the cooling rate. Ductility was always good (reduction of area > 40% in the straightening temperature range 800–1000°C, the value required to avoid transverse cracking), independent of Ti/N ratio or cooling rate. A high product of [Ti][N] was found to give improved ductility and a higher N level gave some further benefit. The good ductility is due to B segregation strengthening the grain boundaries and the low S level (0.005%S) limiting the volume fraction of MnS inclusions and restricting AlN precipitation to the matrix. The addition of Nb is beneficial as the precipitation of Nb(CN), on the Ti particles at higher temperatures, will coarsen the precipitates so not only is the fine deformation-induced precipitation avoided but a coarser precipitation enhances ductility. Increasing the cooling rate resulted in a small improvement in ductility due to the refinement of the particle size in the matrix. For HSLA steel, three steels with 0.02%Al, 0.16%Al and 0.16%Al, 0.018%Nb have been examined and their strength and impact behaviour obtained. For the Nb free steels, 0.16%Al steel had a similar strength to the 0.02%Al containing steel~300MPa, but better impact behaviour (40°C lower ITT) with an impact transition temperature (ITT) of -90°C which is attributed to grain size refinement and refinement of the grain boundary carbides. Nb encouraged Widmanstatten ferrite and the formation of lower transformation products like martensite and cannot be recommended as a suitable addition to achieve the benefits of adding higher Al additions. The present work shows that the addition of Nb to this high Al containing steel, although beneficial to strength, giving a lower yield strength (LYS) of 385 MPa, close to that given by some of the control rolled steels, gives very poor impact behaviour with an ITT of only -30°C. The improvement of strength is mainly a result of precipitation hardening by NbCN with some benefit from grain refinement while the deterioration of impact behaviour is due mainly to the formation of lower transformation products, Widmanstatten ferrite and coarse grain boundary carbides. Increasing the cooling rate from 17 or 33°C min^{-1} resulted in a small deterioration in ITT due to the increase of the volume fraction of Widmanstätten ferrite. The finer grain size produced on control rolling prevented the formation of these deleterious phases and adding a high Al addition improved impact performance even when Nb was present.

Contents

LIST OF TABLES

LIST OF FIGURES

LIST OF EQUATIONS

LIST OF TERMS

AHSS	Advanced High Strength Steel
Al	Aluminium
AlN	Aluminium Nitride
Ar	Argon
Au	Gold
B	Boron
bcc	Body Centred Cubic
Be	Beryllium
BN	Boron Nitride
C	Carbon
Cr	Chromium
CR	Control Rolling
Cu	Copper
DIF	Deformation Induced Ferrite
DP	Dual Phase
DRX	Dynamic Recrystallisation
EDS	Energy Dispersive X ray
fcc	Face Centred Cubic
Fe	Iron
Fe-C	Iron Carbon
FEG	Field Emission Gun analyser
FE-SEM	Field Emission Scanning Electron Microscope
FE-TEM	Field Emission Transmission Electron Microscope
FRT	Finish Rolling Temperature
HR	Hot Rolling
HSLA	High Strength Low Alloy
ITT	Impact transition temperature
Kg	Kilogram
LYS	Lower Yield Strength
min	Minute
mm	Millimetre
Mn	Manganese
MnS	Manganese Sulphide
Mo	Molybdenum
MPa	Mega Pascal
N	Nitrogen
Nb	Niobium
Nb(C,N)	Niobium Carbo Nitride
NbC	Niobium Carbide
NbN	Niobium Nitride
Nf	Free Nitrogen
Ni	Nickel

nm	Nanometre
N_t	Total Nitrogen
OM	Optical Microscopy
P	Phosphorus
P_f	Finish Time of Strain-Induced Precipitation
PFZ	Precipitate free zones
P_s	Start Time of Strain-Induced Precipitation
PTT	Precipitation-Time-Temperature
RA	Reduction of Area
Re_h	Ultimate tensile strength
Re_l	Lower yield strength
R_m	Upper yield strength
s	Second
S	Sulphur
Se	Selenium
SEM	Scanning Electron Microscope
SFE	Stacking Fault Energy
Si	Silicon
SiC	Silicon Carbide
ST	Stoichiometric Composition
T	Temperature
TEM	Transmission Electron Microscope
Ti	Titanium
Ti(C, N)	Titanium Carbo Nitride
TiN	Titanium Nitride
Tm	Melting point temperature
TR	Recrystallisation Temperature
TRIP	Transformation Induced Plasticity
TWIP	Twining Induced Plasticity
UTS	Ultimate Tensile Strength
V	Vanadium
V(C,N)	Vanadium Carbo Nitride
VC	Vanadium Carbide
VN	Vanadium Carbide
W	Tungsten
µm	Micrometre
WF	Widmansttatem Ferrite

LIST OF SYMBOLS

%	Percent
~	Approximately
°C	Degree Celsius
A_0	Cross-sectional area before test
Ac_1	Temperature at which austenite begins to form during heating
Ac_3	Temperature at which transformation of ferrite to austenite is completed during heating.
Ae_1	Start temperature of austenite formation under equilibrium conditions
Ae_3	End temperature of austenite formation under equilibrium conditions
Ae_4	Temperature at which delta-ferrite transforms to austenite during cooling at equilibrium
A_f	Cross-sectional area after test
Ar_1	Temperature at which transformation of austenite to ferrite or to ferrite and cementite is completed during cooling
Ar_3	Temperature at which austenite begins to transform to ferrite during cooling
D_f	Final diameter
D_i	Initial diameter
d_α	Grain size
ε	Strain
k_{A3}	Gradient of transformation temperature per unit content from austenite to ferrite
k_{A4}	Gradient of transformation temperature per unit content from liquid to austenite
Tγ	Austenite composition temperature
Wt-%	Weight Percent
α	Ferrite(alpha iron)
γ	Austenite (gamma iron)
δ	Ferrite (delta iron)
ἑ	Strain rate
σ_{UTS}	Ultimate Tensile Strength
σ_y	Yield Strength

1 Introduction

1.1 Background of research

Many types of steel are being developed to provide good mechanical properties to meet the industry requirements which are high strengths and better toughness. Generally, the mechanical behaviour of steel depends on the processing parameters that control the microstructure and precipitation kinetics of carbide, nitride and sulphide forming elements. Thus, the mechanical properties of the finished product are mainly dependant on what happens after casting. However, to achieve these good properties, the hot ductility must be adequate to allow straightening to occur during the continuous casting operation without cracks forming. Many of the new steels that are being developed require having a higher than usual Al content to develop the required room temperature mechanical properties and this sends up danger signals because steels with higher than the recommended Al additions are noted for giving cracking during continuous casting. This arises because AlN precipitation occurs mainly at the austenite grain boundaries rather than in the matrix of the grain often as a thin film covering the grain surface and so is particularly notorious for causing intergranular failure (e.g rock candy failures).

Al has been used for many years as a deoxidiser and grain refiner but only in small quantities, 0.02 to 0.04 wt-% and within this range cracking does not normally occur.

However, very high Al additions, 1-2%, are now being added to TRIP (Transformation induced plasticity) and TWIP (Twinning induced plasticity) steels. In the case of the TRIP steels, the steel is a microalloyed steel that has a high Al and/or high Si or P addition

The elements, Mn, Al, Si and P are all ferrite formers. The conventional TRIP steel is a low C steel, (0.15%C) with 1.5%Si and 1.5% Mn. However, high Si levels make it difficult to galvanize and form unsightly stains on the surface. Al or P can replace Si and do not give this problem. With these steels and a suitable heat treatment it is possible to produce a steel which has a small amount of austenite, which on deforming will transform to martensite and thus strengthen the regions which would otherwise thin down and fracture. Hence, necking is prevented and very high elongations are attained at room temperature. The steel can also because of the microalloying elements that are added achieve very high strengths.

This is very different to the situation in most structural HSLA steels which are "ferrite/pearlite" at room temperature and the properties that are present in the finished product are dependent particularly the yield strength on the ferrite in the structure.

The present research work, however, is aimed at improving the hot ductility of TWIP steels. In contrast to TRIP steels they are fully austenitic at room temperature and their high ductility and strength are due to an entirely different mechanism which depends on twinning. Twinning is a feature of fcc structures like copper, brass and stainless steel. The high C and Mn contents of the steels ensure that they are austenitic at room temperature. Adding high Al additions to the steels makes them more difficult to cast and this has hindered their development. Al reacts strongly with oxygen readily forming Al_2O_3 and the particles often clog up the nozzles on the ladle during melting and AlN precipitation on cooling cause intergranular failure. Thus although the finished product has exceptional properties, the problem with the steel is the difficulty in casting it. Much work has been carried out in the Department already to establish the optimum composition to avoid cracking during casting and the present work is a continuation of this

Another area where high Al additions are being considered is in the hot rolling of steels. Here a smaller addition approx.0.2wt-% but nevertheless much greater than the customary addition is being added, as it has been shown to improve the impact performance for reasons yet to be fully established. Here the influence of Al on the strength and impact behaviour are examined and follows up again on previous work in the Department.

With this interest in adding higher Al additions, two aspects have been examined in the present work. One is on the hot ductility of TWIP steels and the other is the hot rolling of high Al plain C-Mn steels.

There are two part of this thesis. First part of the thesis concentrated on TWIP steel which is a relatively new and an advanced steel which offers very high strength levels with good ductility. The combination of both properties has made TWIP steel an attractive option for the automotive industry for weight reduction and less CO_2 consumption. However, production of TWIP steel through continuous casting is difficult due to the formation of transverse cracks at the slab surface during processing.

The second part of the thesis is concerned with hot rolled HSLA steel. HSLA steel, also known as microalloyed steel, has excellent strength and fracture toughness this being obtained by the addition of micro quantities of elements, $\leq$0.05%, such as aluminium, titanium and niobium.

However, the mechanical properties of hot rolled HSLA steel still cannot meet the increased requirements of the industry and so control rolled steel has become more popular. The control rolling process is an expensive technique that requires advanced equipment, more labour and longer processing time. The extent to which Al and Nb can be used to improve the properties of hot rolled steels has been investigated with the aim of obtaining mechanical properties similar to those given by the more expensive, control rolled or normalised route, eg. API X52 line pipe.

1.2 TWIP steel

1.2.1 Introduction

TWIP steel is a relatively new type of steel. The term 'TWIP' refers to Twinning Induced Plasticity and it describes the twinning phenomenon of the steel during plastic deformation. Extensive amount of twins are generated so splitting up the grains into sub-grains in which the twin boundaries behave similarly to grain boundaries. Hence, they provide higher resistance to dislocation movement and so can accommodate the fast accumulation of the high dislocation density and allow a high degree of work hardening. This gives TWIP steel its exceptional combination of high strength and ductility at room temperature (Figure 1-1).

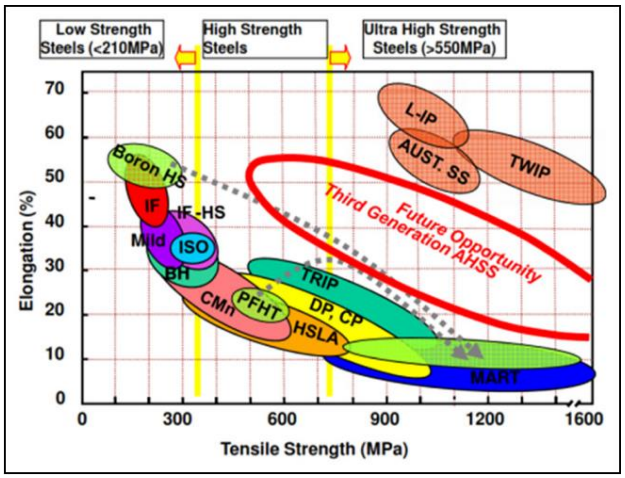

Figure 1-1Map showing ultimate tensile strength and elongation for various classes of the high-strength steel sheet using this as the engineering measure of good properties [1,2].

A twin is a stacking fault caused by the planes of atoms used in building up a fcc crystal forgetting their sequence ABCABCABC and going for example to ABCBCABCBACBA – the line where they meet is the sharp boundary seen under the microscope (Figure 1-2). The line represents the change from fcc to hcp. In order to produce these twins a certain amount of energy is needed called the stacking fault energy (SFE).

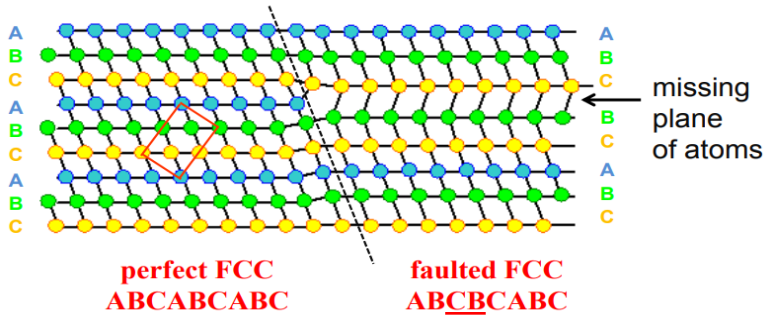

Figure 1-2 Schematic diagram showing a stacking fault sequence in a fcc crystal structure [3].

When only a little amount of energy is needed, the SFE is low and a large number of twins form. This can readily be seen under the microscope when comparing the fcc structures of annealed brass, copper, austenitic stainless steel and aluminium. Brass has the lowest SFE and has a large number of twin boundaries while aluminium, which has a high SFE, does not twin. Careful control of stacking fault energy (SFE) is crucial to establish the appropriate level of twinning through alloying. The stacking fault energy is solely controlled by the composition (Table 1-1).

Table 1-1 Stacking fault energy values of common metals and alloys [4].

Metal or alloy	Stacking fault energy (mJ m^{-2})
Al	180
Ni	75
Cu	75
Brass	25
Stainless Steel	20
(TWIP steel) Fe-22%Mn	15
Fe-25%Mn	21
Fe-28%Mn	41

Low SFE facilitates twinning formation but must not be outside the critical range 20 to 47 mJ m^{-2} [5]. Lower SFEs <20mJ m^{-2} introduce too many boundaries giving an enormous degree of work hardening which changes the structure into martensite while higher SFEs >47mJ m^{-2} favour a dislocation glide mechanism rather than twinning. For Fe–0–29%Mn, binary steels, the stacking fault energy (SFE) drops with increasing Mn concentration up to approximately 13 wt-%, and then rises again according to thermodynamic calculation [6,7].

The high manganese content (15-30%) is needed as although the SFE is raised it is necessary to stabilise the austenitic structure at room temperature [8]. The experimental SFEs for the 22, 25 and 28%Mn alloys are 15±3, 21±3 and 39±5 mJ m^{-2}, respectively. The large increase in SFE

energy above 25 wt-%Mn is consistent with experimental observations that show that there is a sharp reduction in the ε-martensite start temperature for additions of Mn above 25 wt-% in binary Fe-Mn alloys [9]. In addition, although the high level of aluminium content (1-2%) raises the SFE, it has become a favourite addition as it prevents delayed fracture in deep drawn products and of course reduces the weight, this being so important in the car industry [10]. TWIP steels either have Al or Si present to give the TWIP effect.

The SFE is determined by the chemical composition of the material. A typical correlation is shown in *Equation 1* proposed by Rhodes and Thompson [11] and *Equation 2* proposed by Dai et al. [12]:

Equation 1

$$SFE\ (mJ\ m^{-2}) = 1.2 + 1.4Ni + 0.6Cr + 7.7Mn - 44.7Si$$

Equation 2

$$\gamma^{300}\ (mJ\ m^{-2}) = \gamma^{0} + 1.59Ni - 1.34Mn + 0.06Mn^{2} - 1.75Cr + 0.01Cr^{2} + 15.21Mo - 5.59Si - 60.69(C + 1.2N)^{1/2} + 26.27(C + 1.2N)(Cr + Mn + Mo)^{1/2} + 0.61[Ni(Cr + Mn)]^{1/2}$$

where the symbol for the alloying elements represents their weight percentage. γ^{300} represents the value of SFE at room temperature and γ^{0} denotes the value of SFE of pure austenitic iron at room temperature.

In addition to Al or Si, more alloying elements are added for further improvement of properties depending on the desired application i.e. a typical TWIP steel has a strength level of 800 MPa and this can be raised to 1000 MPa by the addition of Nb, ~0.03% [13]. This high level of strength combined with excellent ductility make TWIP steel an attractive option for use in the automotive industry for weight reduction, lower petrol consumption and reduced emissions [13]. Due to its high toughness and strength, TWIP steel is mainly used in impact protection structures of automobiles, such as B-pillar members, crumble zones and side impact bars [14].

1.2.2 Motivation

The present work is designed to examine the influence of high N contents on the hot ductility of TWIP steels in detail. Much of the previous work has been on low N steels, approximately 0.005%, but these days more and more steel is being recycled in electric arc furnaces leading to higher N levels of 0.01%N. Precipitation of nitrides can reduce the hot ductility so Ti is often added so that only TiN forms and provided the precipitation is coarse, ductility is not affected.. Thus, if the [Ti] x [N] product is sufficiently high all the N is taken out as TiN. Although there is more precipitation, it is generally too coarse to influence the hot ductility. It is therefore

important to establish the optimum Ti and N levels to achieve this and give the optimum hot ductility.

In addition to Ti additions being beneficial, B has also been found to be needed to obtain good ductility in these TWIP steels provided B can segregate to the boundaries and not form BN. The B in solution is able to strengthen the grain boundaries.

Previous work [15] has examined a steel with a high Ti/N ratio of 7;1, so that typically to remove all the N, the Ti level is 0.07% in a 0.01%N steel. As long as the stoichiometric composition for TiN is attained (Ti/N ratio 3.5:1) all the N will be taken out of solution as TiN so that B can segregate un-impedingly to the boundaries. A lower Ti level should also have the desired effect but the stoichiometric composition often gives fine precipita-tion leading to poor ductility. Nevertheless, the stoichiometric composition needs to be examined at these high N levels to examine whether a reduced Ti level may be used.

Cooling rate in previous work [16] has generally been 60°C min^{-1} which is higher than the recommended cooling rate of ≤25°C min^{-1} needed to coarsen the TiN particles to obtain the maximum ductility or to give the maximum segregation for B. In this exercise the cooling rates will be 12 and 60°C min^{-1} for comparison. This cooling rate is the average cooling rate that takes place during secondary cooling on continuous casting so is commercially very relevant.

Previous work [17] has concentrated on the simpler high Al, TWIP steel giving a strength level of 800MPa. However, if a higher strength level is required~1000MPa then Nb needs to be added. Nb additions particularly give poor ductility in peritectic C, HSLA steels. The present exercise examines the influence of Nb on the hot ductility of high Al, high N, TWIP steels containing B and Ti.

This examination should establish the most suitable composition for preventing transverse cracking in the continuous casting of the highest strength high Al, TWIP steels containing Nb.

1.3 Hot rolled HSLA steel

1.3.1 Introduction

In hot rolled high-strength low-alloy (HSLA) steel, again both the avoidance of transverse cracking during casting and the room temperature properties are important. HSLA steels, also known as microalloyed steels have excellent strength and fracture toughness this being obtained by the addition of microquantities of elements, ≤0.05%, such as aluminium, titanium, niobium etc. These steels are popular in the industry due to their good combination of strength,

toughness and weldability [18,19]. The selection of alloying elements and their contents are governed by the desired properties. Therefore, HSLA steel is classified into several grades, each of which has a specific combination of properties, based on their application. HSLA steel is used for oil and gas pipelines, offshore structures, ship construction, bridges, power transmission towers, storage and transporting tanks [19,20]. HSLA steel is also popular in the automobile industry because it offers high strength-to-weight ratio and low impact transition temperature besides its cost effectiveness. HSLA steel is estimated to contribute one-third of the body structure mass of vehicles around the world (Figure 1-3), and it is gradually increasing [21]. It is suitable for the manufacturing of vehicles' structural parts including chassis components, cross members, reinforcement's parts, longitudinal beams and suspension systems.

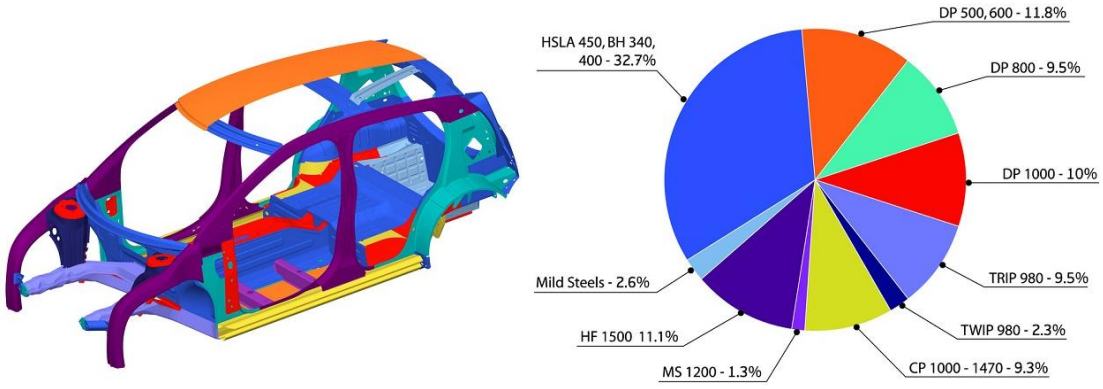

Figure 1-3 Types of steel used in the manufacturing of body structural vehicles [14].

In conventional carbon steel, the ultimate tensile strength can be enhanced by addition of high amounts of carbon but generally carbon is not a favoured element when considering ductility and weldability [22]. The addition of other alloying elements, such as aluminium, niobium, vanadium and titanium, can compensate for the strength loss caused by the low carbon content, without affecting other properties. Therefore, most of HSLA steel used nowadays contain low carbon, as low as 0.06%. HSLA steel offers two or three times the yield strength exhibited by plain carbon-manganese C-Mn steel [21].

1.3.2 Motivation

Previous work [23] has investigated the impact behaviour of hot rolled steel at various Al contents (0.02-2%). Increasing the Al content from 0.02 up to 0.16% was found to reduce the ITT considerably from -60 to -100°C without influencing the strength. In addition, Al slowed down the diffusion rate of carbon and obstructed the growth of grain boundary carbides thus improving the impact behaviour. However, further increase of Al beyond that level caused the

impact behaviour to deteriorate dramatically due to the formation of martensite whose volume fraction increased as a function of Al content.

A further study [24] was carried out to assess the role of nitride formers, i.e. Ti, Al, Zr and B, on the properties of C-Mn hot rolled steels. It was observed that Al was the most effective element for achieving a good combination of strength and toughness. Despite the coarse grained-microstructure ~7-8$mm^{-1/2}$, the addition of 0.16%Al to a plain C-Mn steel realised a strength level of 295MPa and a very low ITT of -100°C. This improvement in impact behaviour was attributed to a refinement of the grain boundary carbides and removal of N in solution.

The solid solution hardening effect of Al has also been separately examined from the impact behaviour in hot rolled ferrite/pearlite steels [25] and it was found that the addition of 1%Al enhanced the yield strength by 70-80MPa. However, at low Al concentrations (0.02-0.08 wt-%), the solid solution hardening of Al is unnoticed due to removal of N as AlN occuring at the same time. At high Al concentrations (1-2 wt-%), the solid solution hardening of Al is also obscured due to the fact that Al favours martensite formation leading to pre-yielding of the ferrite. In order not to obtain martensite it was recommended to reduce the carbon content from 0.1% to 0.06%C.

The effect of Al on strength and impact behaviour of hot rolled plain C-Mn steels was further studied as a function of nitrogen content [26]. In low nitrogen steels (0.001 wt-%), there was no grain refinement because the N level was too low to have an effect on strength or impact behaviour. Al was found to contribute to solid solution hardening and refine the grain boundary carbides giving better impact behaviour. Raising the N content to 0.003-0.005% improved the impact behaviour in the 0.16%Al containing steel due to grain refinement induced by AlN precipitation.

Based on previous studies, it is recommended to keep aluminium content at 0.16% and to increase the nitrogen level in the hope of grain refinement and reduce the carbon content in order to get the maximum potential of the Al addition. Furthermore, it is suggested to add niobium to gain an additional strength to these steels through precipitation hardening and grain refinement. This may result in hot rolled HSLA steels with similar properties to those obtained by control rolling at the lower end of the strength spectrum.

1.4 Aim of the thesis

The first part of the thesis concentrates on TWIP steel, which is generally produced by continuous casting. However, due to the high alloy content of this steel, it becomes difficult to

cast without transverse cracking occurring [15,27]. The problem arises during the straightening stage in continuous casting, in which the surface and the edges of the strand are put into tension, leading to transverse cracking. This requires further processing of the steel strand which may include scarfing of the surface and trimming off the cracked edges, increasing the scrap losses and processing time and therefore the cost. Therefore, it is essential to optimise the alloying composition and processing parameters to avoid such a problem without compromising properties at room temperature. Despite the beneficial influence of Nb in enhancing the room temperature strength of TWIP steel, precipitation of NbC(N) encourages formation of transverse cracks. The addition of titanium can eliminate the negative effect of Nb on casting but the optimum content required and the mechanism by which this improvement takes place is still in question. The characteristics of the Nb and Ti precipitates such as size, volume fraction and location play a critical role in improving casting process and eliminating the formation of cracks. These characteristics are optimised by cooling rate and hence a better understanding of both factors; heat treatment and chemical composition need to be established. In this work, simulation of continuous casting operation is carried out using a hot tensile test to simulate the straightening operation in continuous casting and this has been found to be reliable in evaluating a steel susceptibility to cracking through establishing hot ductility curves [28]. Generally, the first part of the thesis has been carried out to define the optimum composition and cooling rate for reducing the likelihood of transverse cracking in high Al containing TWIP steel. In particular, this work aims to examine the effect of Ti/N ratio and cooling rate (60 and 12°C min^{-1}) on the hot ductility of TWIP steel.

The second part of the thesis concentrates on trying to improve the properties of hot rolled HSLA steels. The most desirable properties required of HSLA steel are a high yield strength and good impact behaviour. Improving both properties is a challenge due to the fact that the improvement of strength normally leads to deterioration in impact behaviour and vice versa. As mentioned previously, these properties are governed by the chemical composition and thermal history. A steel with normal Al content of 0.02-0.04%Al results on hot rolling in a coarse austenite grain size leading to a coarse grained ferrite at room temperature and often low temperature transformation products including martensite, upon transformation. Impact behaviour is therefore poor as well as strength. Properties after casting can be substantially improved by normalising, control rolling and more recently control rolling followed by direct rolling. In all these cases, the grain size is refined, giving higher strength and an improvement in notch toughness. However, all these routes are more expensive and many smaller steel plants

do not have control rolling facilities. There is therefore a need to improve the properties of hot rolled steel. Nb is known to enhance strength but at the expense of impact behaviour depending on its content. Previous work has indicated that high Al additions can improve the impact behaviour without influencing strength or vice versa. Therefore, Al when added should to some degree compensate for the deterioration in impact behaviour on adding Nb and so be very useful in improving the hot rolling properties. It is not known with certainty whether the high Al content improves impact performance because 1) it enables more AlN to be precipitated out so enhancing any possible grain refinement 2) it is by the removal of the interstitial hardening by N or 3) because Al refines the carbides situated at the boundaries. All of these possibilities would give the better impact behaviour. Cooling rate has also been examined so as to avoid lower transformation products which can lead to impact deterioration.

2 Literature review: hot ductility of TWIP Steel

2.1 Continuous casting

One of the most advanced casting technologies used in processing steels is continuous casting. The process allows homogenisation of mechanical and structural properties all along the strip or plate [29]. The technique covers various types of steel and it is becoming more popular in the advanced steel manufacturing factories for the large scale production of steel products [29]. The full continuous casting process is presented in Figure 2-1. The process starts by heating the steel up to the melting temperature in a furnace. The molten steel is then poured into a ladle so that treatments such as degassing, alloying and setting up the liquid to the required temperature can be applied. The liquid steel is then fed into a holding bath known as tundish via a refractory tube. The tundish is a reservoir which allows the steel to flow smoothly into an oscillating water cooled copper mould at a controlled rate so that there is no overflowing. Lubricants are added to enhance thermal insulation of the liquid steel and to avoid sticking occurring when the strand moves down.

The steel strand moves from the vertical to the horizontal axis gradually by the rollers through a curved path. The strand is straightened and then cut into conveniently sized billets. These are then allowed to cool to room temperature before rolling to the required thickness. The cold billets are then inspected for cracks and other flaws. The slabs are, when necessary, repaired or rejected. The sound billets are then reheated to 1200-1250°C and rolled to their final gauge. More recently direct rolling immediately after casting has been included in the finishing procedure for plate and strip steel with further savings in cost [30].

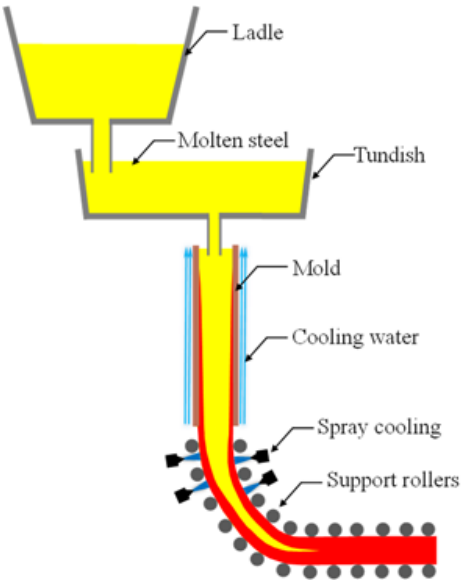

Figure 2-1 Schematic description of the continuous casting process of steel [31].

However, because the surface and the edges of the strand are put into tension during straightening, cracks are prone to form in some of the more sensitive grades of steel. This requires further processing of the steel strand which may include scarfing of the surface and trimming off the cracked edges, increasing the scrap losses and processing time and therefore the cost.

In the last three decades, strong carbide and nitride forming elements such as Ti, Al, Nb and V have been added to different types of steel to enhance strength and toughness through grain refinement and precipitation hardening [32]. However, the carbides and nitrides that form, as well as the presence of high alloying additions, increase the steels susceptibility to transverse cracking occurring on the surfaces and edges of the slabs (Figure 2-2). These precipitates form at the austenite grain boundaries and the tensile forces obtained on unbending in the continuous cast strand cause intergranular cracks to form. Microscopically, cracks have been found to form along austenite grain boundaries associated with chain-like precipitates. This issue has received much attention by metallurgists trying to solve such a complex issue due to the various factors that can contribute to the formation of transverse cracks [33].

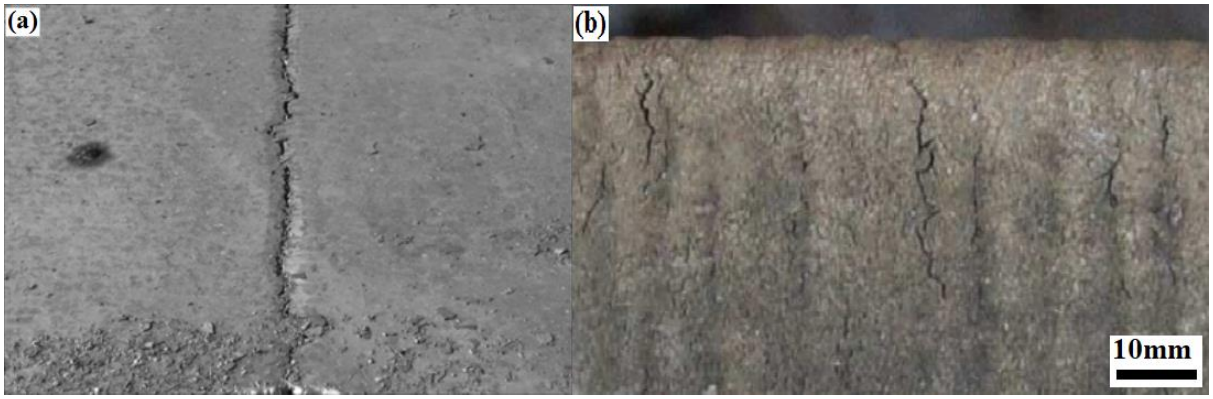

Figure 2-2 Formation of cracks during continuous casting (a) on the surface, (b) in the edge of bloom. Note the ripples in the surface called oscillation marks which are formed by the water cooled Cu mould oscillating up and down [34,35].

Some researchers [36] have attributed the cracking mainly to the alloying composition as shown in Figure 2-3. However, other researchers [37] claimed that cracks are caused by the casting temperature which if not controlled properly can cause bi-films to form over the grain surface so causing embrittlement between austenite grains. Transverse cracking is particularly a problem in certain steels and this affects the production continuity and reduces the production rate of the slabs. This causes a serious economic problem in the steel industry as crack-containing slabs might be directly rejected depending on the crack size [38]. A defect free steel surface is desired, particularly with direct rolling were no pre-inspection of the surfaces can

take place prior to rolling. It can be seen that research work is therefore needed to understand what initiates transverse cracks and then encourages them to propagate during continuous casting so that the steel industry can be guided into how to avoid them.

The transverse cracks have been found to initiate in the mould and propagate when the bending/unbending operation takes place. The straightening operation which puts the surface into tension propagates the cracks which start at the surface and propagate below the surface. Microscopic examination shows that the cracks propagate along the grain boundaries of the columnar grains that form at the surface.

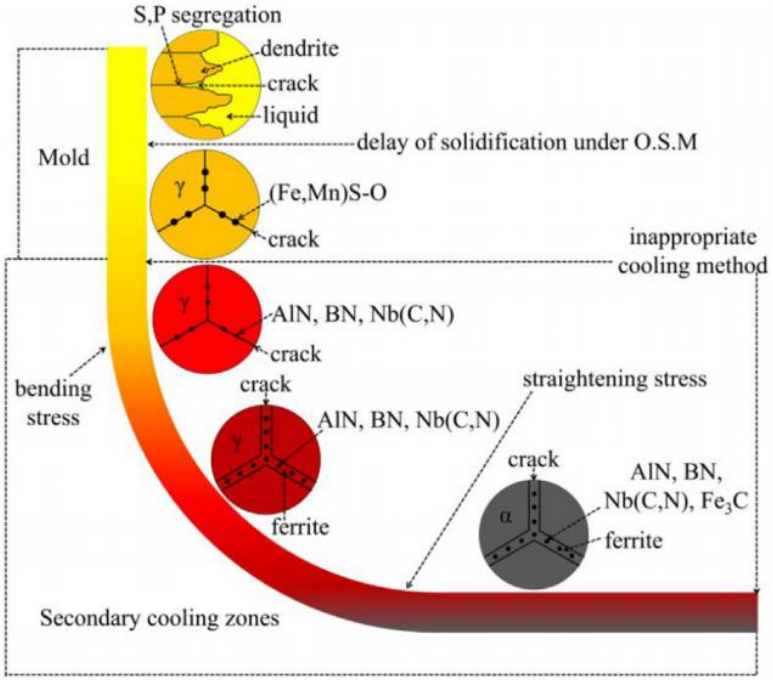

Figure 2-3 Effects of alloying composition on crack initiation and propagation during continuous casting of steel slabs [36].

2.1.1 Simulation of continuous casting in laboratory

A simple hot ductility test has in the main been used to simulate the straightening operation in continuous casting and this has been found to be very beneficial in evaluating a steels susceptibility to cracking [39]. The tensile sample is first heated to 1250°C to take all the carbides and nitrides into solution; the condition they were originally in, on casting. This will generally take the precipitates of AlN, Nb(CN), VC and VN back into solution but not TiN. The solution temperature is sufficiently high to produce a very coarse grain size 200-300um. This is of course finer than the columnar grains in the as cast state (500-1000um). The strain rate used in the tensile test is chosen to be the same as that undergone in the straightening operation. Hot ductility curves are produced by tensile testing at elevated temperatures. The

curves can be obtained by measurement of the percent elongation or more commonly by measuring the percent reduction in area (%RA) at fracture using *Equation 3*:

Equation 3

$$\%\mathrm{RA} = \frac{\text{Decrease in area}}{\text{Original area}} = \frac{\mathrm{D_i^2} - \mathrm{D_f^2}}{\mathrm{D_i^2}}$$

where D_i is the initial diameter and D_f, the final diameter.

The %RA is recorded and then plotted against the test temperature to obtain the hot ductility curves.

The higher the value is, the less likely, the steel will be prone to transverse cracking during continuous casting. Mintz [40] reported that %RA must not be less than 40% in order to avoid transverse cracking. Percent reduction of area (%RA) has been used extensively to evaluate hot ductility in most of the literature surveys [41]. However, recent work by Jansto [41] showed that strain energy, i.e. the integration of the stress/strain curve, could be more accurate in assessing hot ductility behaviour. Moreover, in disagreement with the majority of published hot ductility data, 10% RA was found to be sufficient to ensure crack-free casting rather than the 40% RA which is often quoted. However, these differences are likely to stem from their different heating schedules; shorter holding times before tensile testing being more deleterious as less static precipitation occurs before straining and thus there is more available for precipitating as the finer more detrimental strain induced dynamic precipitation.

Even though there are differences (see next section) in behaviour between the commercial continuous casting operation and the hot ductility tensile test, the test has been found very useful in controlling transverse cracking. In ferrite/pearlite constructional steels, electron microscope examinations show there is little difference in the microstructure of cracked hot tensile sample compared to that in transverse cracks.

2.1.2 Parameters that affect accuracy of hot ductility measurements

As mentioned, the conditions in the test are set to simulate, as closely as possible, the conditions pertaining to the straightening operation during continuous casting [42]. The most important three factors that need to be carefully controlled are the holding temperature, strain rate and cooling rate [42,43]. In the test, the sample is heated up to a temperature level at which all the alloying elements can dissolve in order to obtain the same microstructure evolution such as grain size and precipitation behaviour as in the as-cast state. This temperature is chosen based

on the alloying composition, as elements have different dissolution temperatures but generally for Nb and V containing steels, 1300°C is sufficient to take the carbo-nitrides back into solution The strain rate is set to the same level that is used during the straightening operation, which is estimated to be 3 x 10^{-3} or 1.5 x 10^{-2} s^{-1}, this being the strain rate for thick and thin slab casting respectively [20]. The cooling rate to the test temperature is taken to be the average cooling rate, close to the surface of the strand. Cooling rate depends on the thickness of the slab and it is estimated to be ~60°C min^{-1} for conventional continuous casting, 250mm slab [44] and ~200°C min^{-1} for thin slab casting, 50mm thick slab [45]. Slab casters tend to cast sections that are much wider than thick. Conventional slabs lie in the range 100–1600 mm wide by 180–250 mm thick and up to 12 m long with conventional casting speeds of up to 1.4 m/minute.

It is important to emphasise that dynamic recrystallisation (DRX) does not occur on bending during continuous casting due to the low strain (1-2%), and coarse grain size. Previous reviews [42,46] showed that increasing strain rate from 10^{-3} s^{-1} to 10^{-2} s^{-1} raised the %RA of steel by ~25% due to less time for grain boundary sliding and development of cracks, so improving ductility.

Dynamic recrystallisation by forming a finer grain size and allowing grain boundaries to escape from their growing cracks and thus stunt their growth, will always improve ductility.

Thus, because of the lack of dynamic recrystallisation in the bending operation the use of hot ductility curve in predicting cracking behaviour at temperatures higher than that for dynamic recrystallisation must be treated with caution.

Increasing the strain rate which will again always improve hot ductility in the commercial continuous casting operation has only limited applicability as there is little one can generally do to increase the strain rate in the commercial operation.

Furthermore, cooling conditions in continuous casting are relatively more complex and may not be precisely simulated by the simple cooling conditions in a laboratory tensile test [17]. A typical cooling schedule in continuous casting involves a rapid drop of temperature from the melting point, followed by a rise after which the temperature oscillates (Figure 2-4). The first rapid drop in temperature is called primary cooling and the second part is called the secondary. In the secondary cooling stage, the strand temperature increases as it passes through the rollers then decreases as it is sprayed with water when it exits the rollers. Despite the difficulty of simulating the commercial continuous casting cooling conditions in the laboratory, it has been

shown by Spradbery et al. [47] that adding an under cooling step improves the agreement between the laboratory test and commercial experience.

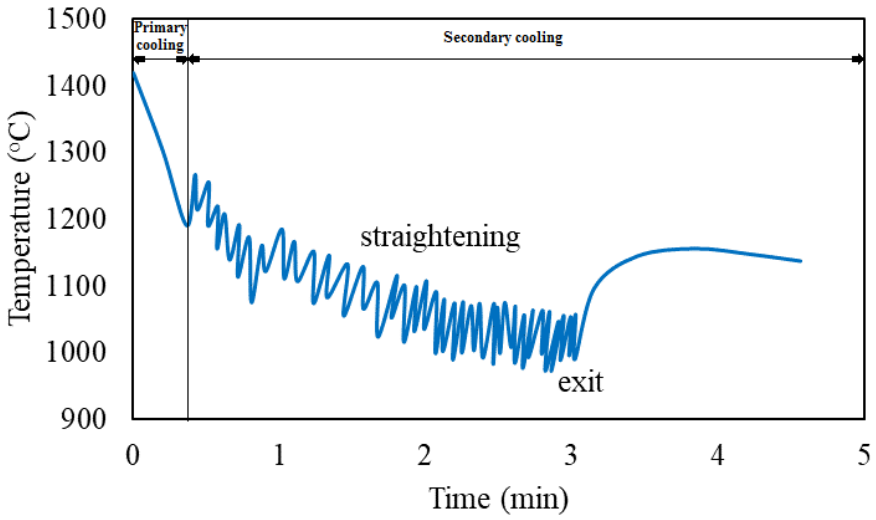

Figure 2-4 A typical cooling curve in continuous casting showing how the strand surface temperature for micro-alloyed steel varies with time after casting [48].

2.2 Hot ductility behaviour of steel as a function of phases, grain size and precipitation

The temperature range in which the straightening stage takes place, is in the range of 1000-700°C. This temperature range is very critical since hot ductility can be very low within this range with a conventional steel (Figure 2-5). In such a "ferrite/pearlite" steel, the hot ductility behaviour passes through three stages. In the high temperature range >1000°C, the hot ductility is high due to dynamic recrystallisation. In the low temperature range <700°C, the hot ductility is high due to the formation of the soft ferritic phase at the expense of the harder austenite [49]. Ferrite has more slip systems than the more closely packed austenite phase and is able to recover more readily than austenite.

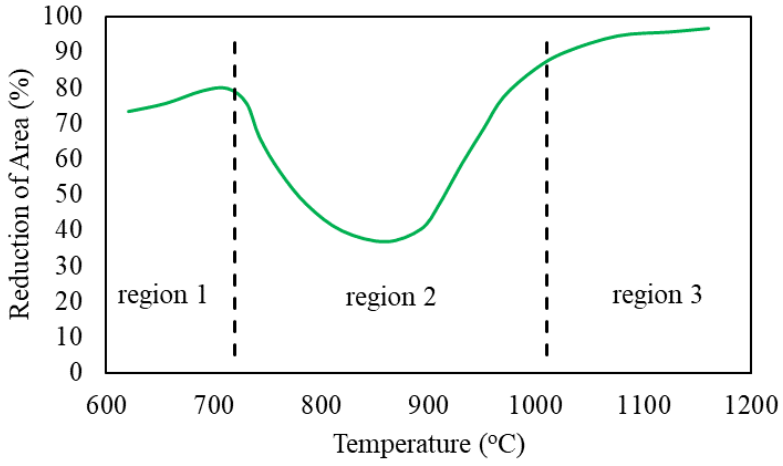

Figure 2-5 Hot ductility behaviour of a typical HSLA steel [49].

The deterioration of hot ductility in the middle stage, the trough, can be attributed to one of three mechanisms. Firstly, during cooling from the austenite, the ferrite nucleates intensively at the austenite grain boundary forming thin films at the start of transformation, the Ar_3 (Figures 2-6 and 2-7). During normal transformation these films rapidly thicken up as the test temperature is lowered. However, deformation, which always concentrates at the boundaries, speeds everything up so equilibrium is achieved. The transformation temperature locally is now raised to the Ae_3. Thin films of ferrite can now form over a wide range of temperature from the Ae_3 to just below the Ar_3; (this difference can be as much 200°C).

Because the thin film of ferrite is so much softer than the austenite that it is surrounding the majority of deformation takes place in the ferrite when the bending operation takes place leading to very low ductility intergranular ductile failure, i.e. although the ferrite is very ductile the strain concentrates mainly in the ferrite instead of uniformly throughout the austenite grains.

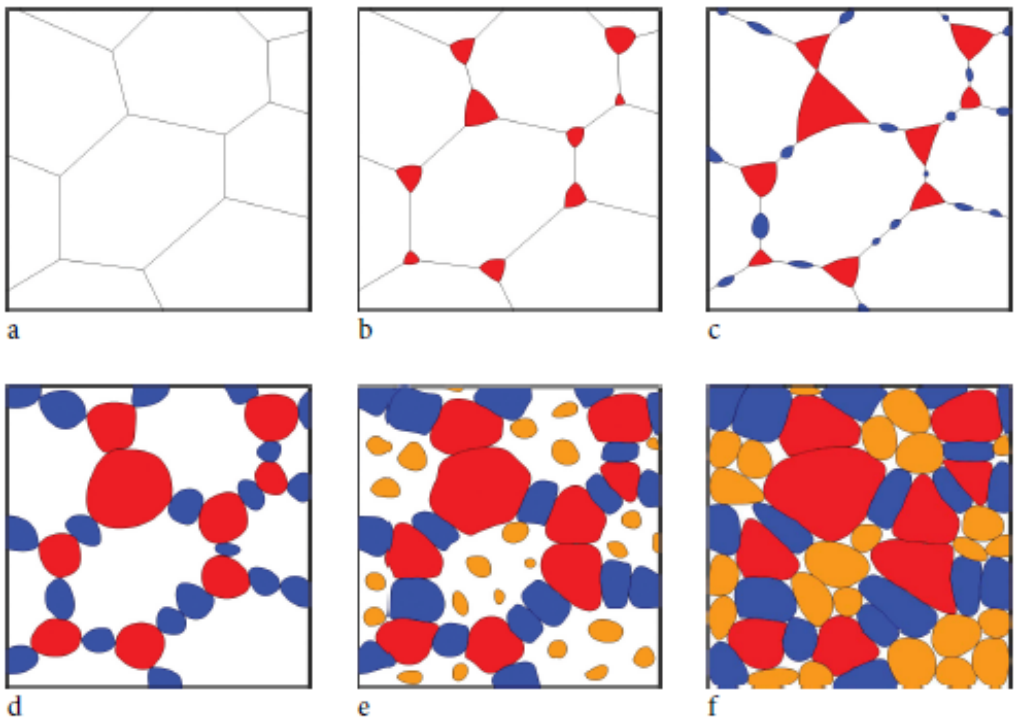

Figure 2-6 Schematic illustration of possible phase transformation development under static conditions: (a) austenite grain structure; (b) ferrite nucleation (red colour) on austenite grain corners; (c) ferrite growth on grain corners and nucleation on grain boundary faces (blue colour); (d) ferrite growth on grain corners and boundaries and impingement on the grain boundaries; (e) ferrite nucleation on defects in former austenite grain interiors (orange colour); (f) grain growth [50].

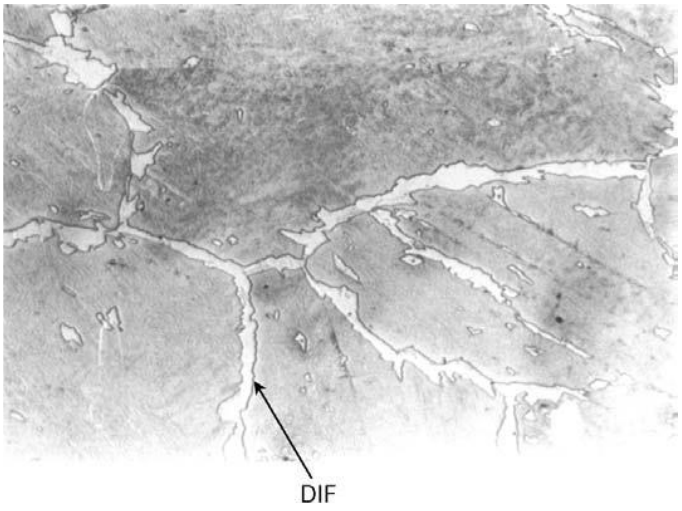

Figure 2-7 Deformation induced ferrite (DIF) formed in a tensile sample tested well above the Ar_3 close to the Ae_3 temperature x400 [51].

Secondly, since precipitates nucleate more readily at grain boundaries than they do in the matrix, precipitate free zones (PFZ) are often formed in the regions adjacent to the austenite grain boundaries. These PFZs are softer compared to the matrix and behave similarly to having a thin film of the soft ferrite surrounding the austenite grains. The stress then concentrates on the PFZ, leading to intergranular failure. A typical steel microstructure with precipitate free zones is shown in Figure 2-8 [52].

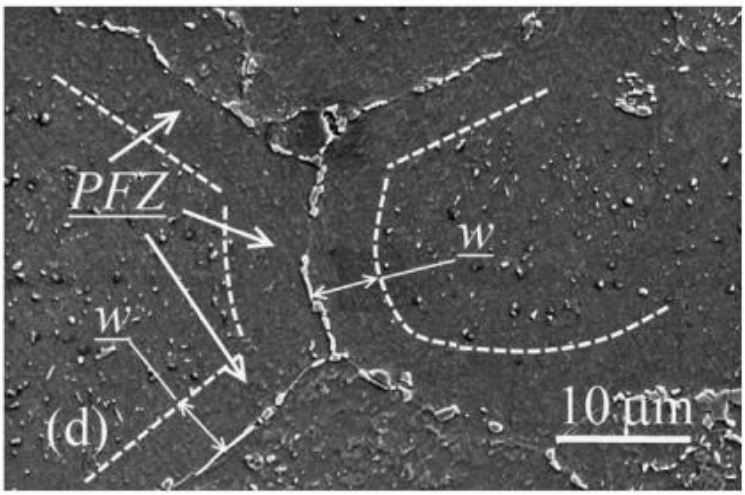

Figure 2-8 SEM microstructure showing the precipitate free zones (PFZ) and their width (W) [52].

The third mechanism contributing to intergranular failure is grain boundary sliding [19]. The movement of the grain boundaries by sliding at triple points, where three grain boundaries meet as shown in Figure 2-9, leads to a large concentration in local stresses which can cause severe damage by rupture of the grain boundaries leading to poor ductility. This rate of sliding increases with time and temperature. These fractures surface have a flat very brittle appearance.

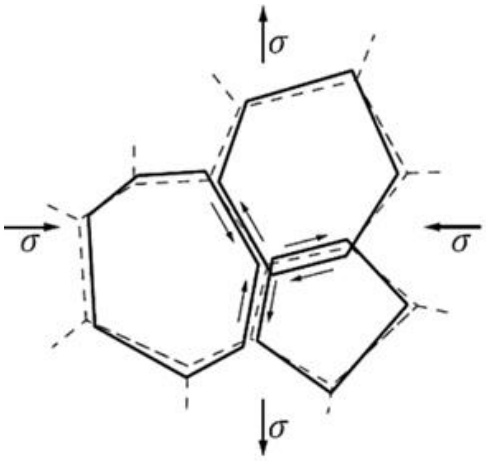

Figure 2-9 Schematic diagram of grain boundary sliding at a triple point [53].

At the high-temperature end of the second stage, above the Ae_3, hot ductility improves significantly due to dynamic recrystallisation (nucleation of new grains at the grain boundaries) taking over any further grain boundary sliding, by allowing the boundaries to move and isolate any cracks that are forming. In addition, due to the high recovery rate of ferrite at high temperature and the fact that the dynamically recrystallised austenite grains are relatively finer, hot ductility can improve. At the low-temperature end of the second stage ~720°C, sufficient ferrite forms on transformation, (generally in excess of 40% ferrite) so strain localisation can no longer occur and as a result hot ductility improves.

In general, grain boundary precipitation is considered detrimental especially with very fine precipitation or as the precipitate size increases, higher volume fractions. In such a case, it becomes easier for cracks to propagate and link up leading to intergranular fracture [42].

Since TWIP steel is alloyed with a high concentration of Mn and C, the phenomenon of phase transformation to give a thin film of ferrite does not occur as the structure is solely austenitic. Therefore, the hot ductility in TWIP steel is mainly influenced by dynamic recrystallisation, grain size, and precipitation behaviour.

Cracks initiate at the grain boundaries and chemical composition has been found to play a critical role in minimising intergranular cracking. Many investigations have been conducted to assess the influence of different alloying elements and the role of precipitation in affecting transverse cracking behaviour. In addition, heating and cooling schedules prior to rolling have been experimentally optimised to reduce the likelihood of transverse crack formation.

2.3 Factors influencing hot ductility

2.3.1 Cooling rate

Cooling rate has been found to influence the microstructure evolution and so the hot ductility of steel. Cooling rate affects hot ductility through controlling the temperature and time available for diffusion and as a consequence controls the nucleation site, size and volume fraction of precipitation [54]. It is well established that coarse size particles are desired to promote hot ductility (Figure 2-10) and slow cooling rates can provide more time for the precipitates to grow [55]. Nevertheless, the rate of improvement can be seen to decrease as the precipitate size increases (Figure 2-10). Frequently, when the precipitate size is ≤ 10-15nm ductility is poor and transverse cracking will occur.

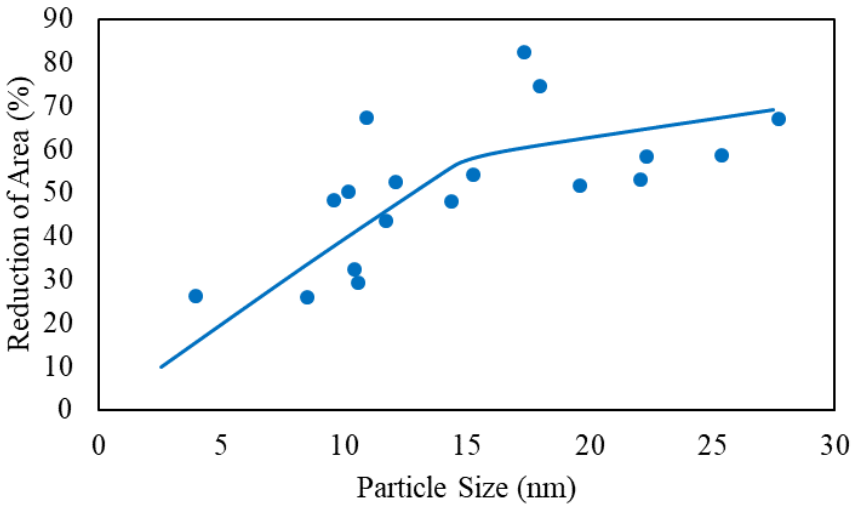

Figure 2-10 Effect of particles size on %RA for Ti-bearing steels [55].

Abushosha et al. [56] have investigated the effect of cooling rate on the hot ductility of plain C-Mn steels and found that reducing the cooling rate from 60 to 10°C min^{-1} caused the hot ductility to improve. The marked decrease in hot ductility at the higher cooling rate was found in this case to be caused by the presence of finer MnS particles at the boundaries as precipitates were not present.

A recent study by Kang et al. [57] on the influence of cooling rate on the hot ductility behaviour of TWIP steel showed that increasing the cooling rate from 60 to 180°C min^{-1} led to a significant deterioration in hot ductility (Figure 2-11). Finer precipitation of MnS and AlN, at the grain boundaries, was observed at the faster cooling rate, which increased the flow stress applied on the boundary. In addition, by reducing the distance between the particles, crack propagation and linking up were found to be easier, so weakening the boundaries and hence

leading to intergranular fracture. It is interesting to note that in austenitic steels because of the absence of the ferrite film there is not a normal ductility trough and generally ductility does not change very much until DRX occurs at the higher temperatures. The hot ductility of TWIP steels can from Figure 2-11 to be poor falling well below the R of A value needed to avoid transverse cracking (40%).

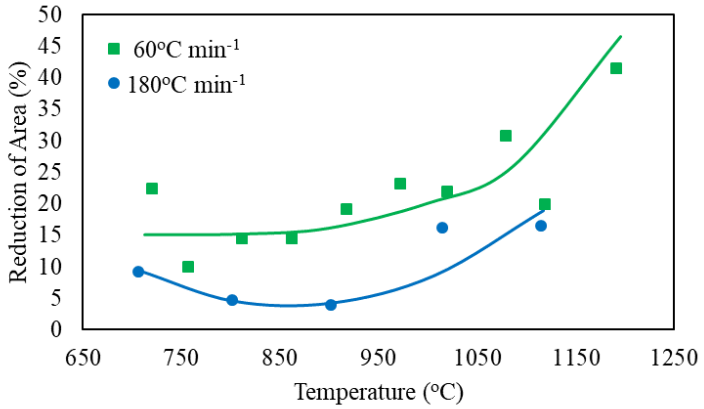

Figure 2-11 Effect of cooling rate on %RA of as cast TWIP steel with the composition: 0.6%C, 0.2%Si, 18%Mn, 0.01%P, 0.006%S, 1.4%Al, 0.03%Nb, 0.1%V and 0.003%N [57].

It was reported also by Kang et al. [15] that reducing the cooling rate from 60 to 12°C min^{-1} for a B-bearing, Nb containing TWIP steel (0.002%B) gave a further improvement of hot ductility, with %RA close to that needed to avoid transverse cracking (Figure 2-12). This was justified by the slower cooling rate allowing more B to segregate to the boundaries and strengthening them. It is well established by many of the earlier researchers that the kinetics of B segregation to the boundaries is dependent on cooling rate but the segregation is none equilibrium so there is a range of cooling rates that will give good ductility [58,59].

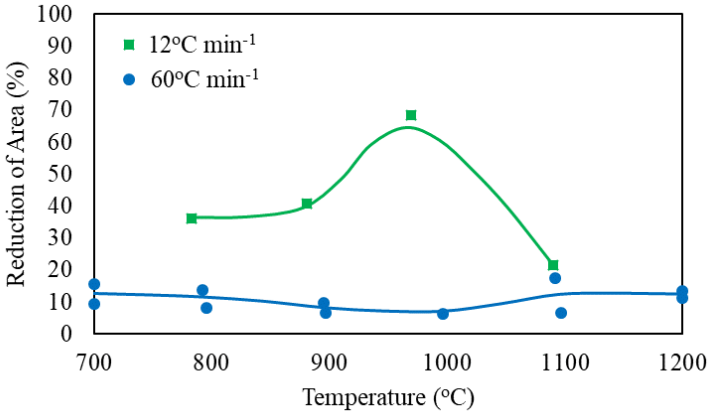

Figure 2-12 Influence of cooling rate on the hot ductility of as cast TWIP steel with the composition: 0.55%C, 0.07%Si, 18%Mn, 0.02%P, 0.002%S, 1.2%Al, 0.016%Nb, 0.049%V, 0.002%B and 0.006%N [15].

For TWIP steels, the boron is used to improve hot ductility and this only takes place if it can segregate unimpededly to the boundaries and not form a nitride. It must always be in solution to do this and not precipitate out at the boundaries. Ti is therefore added to combine with all the N, so that AlN and BN precipitation cannot occur. However, the TiN particles must be coarse to avoid cracking problems so slower cooling rates are required, 12°C min^{-1} [20]. However, the situation becomes more complicated in the presence of Nb which normally precipitates as Nb(CN) particles in a fine form within the matrix and the boundaries leading to a very poor hot ductility [60,61]. It was concluded that the detrimental influence of Nb can be eliminated by reducing the cooling rate from 60 to less than 25°C min^{-1}, so giving rise to coarser Nb(CN) particles. Kang et al. [15] reported that the optimum cooling rate for the Nb containing TWIP steel is 12°C min^{-1} leading to a significant improvement in hot ductility which is sufficient to prevent transverse cracking during the straightening operation (Figure 2-12).

Although a slower cooling rate has been reported to promote hot ductility, there is an optimum minimum cooling rate. B segregation is non-equilibrium and therefore there is a range of cooling rates causing this segregation. Yamamoto et al. [61] reported that the optimum cooling rate for the maximum segregation of B at grain boundaries was 10°C min^{-1}. Another paper by Cho et al. [62] on low alloy steel found a marked improvement in hot ductility by reducing the secondary cooling stage of the slab after solidification. It has also been shown that taking the average cooling rate which includes both the fast primary (600°C min^{-1}) and slower secondary (often 12°C min^{-1}) for the cooling rate used for the tensile specimens does not give the best simulation. Generally it is the secondary cooling rate for thick slab casting, often 12°C min^{-1} which controls the growth of the precipitates and is therefore a better choice than the average of the primary and secondary cooling rates.

It can be concluded from previous work [56,57] that there is general agreement that slower cooling rates give enhanced hot ductility. Practically, cooling rate is dependent on the casting process and the form of steel to be cast, e.g. thicker slabs have slower cooling rates compared to the thinner ones. Some adjustment can be made to the cooling rate by altering the water flow of the cooling sprays but this is generally limited.

2.3.2 Strain rate

Besides deformation temperature, hot ductility behaviour of metals is significantly affected by strain rate [63]. Again, commercially there is little that can be done to alter the strain rate for a given thickness this being dependent mainly on the size of the rolls at the straightener.

The hot ductility of low carbon steel was investigated by Mišičko et al. [64] as a function of strain rate (1 x 10^{-3} and 1 x10^{-2} s^{-1}) between 1000 and 1300°C. The higher strain rate was reported to deteriorate hot ductility and this was ascribed to deformation induced precipitation of Al based particles along the austenite grain boundaries leading to intergranular failure. However, the temperature range examined was too high for the normal straightening operation and to be commercially useful information.

In contrast and more generally, higher strain rates do markedly improve the hot ductility of microalloyed steel and when sufficiently high lead to no ductility trough as reported by Großeiber et al. [65]. Hot ductility gradually improved as strain rate increased, and the fracture mode steadily increased from intergranular to transgranular. Higher strain rates gave less time for precipitates to segregate to grain boundaries, so making it difficult for voids to form and propagate. They also gave less time for grain boundary sliding to occur.

Carpenter et al. [66] suggested that the detrimental influence of lower strain rate is enhanced when the steel is highly alloyed. This is attributed to the higher volume fraction of precipitates obtained which delay the onset of dynamic recrystallisation and recovery. Intergranular cracking is then initiated as a result of grain boundary sliding. It is very important to note that dynamic recrystallisation does not take place during the straightening operation as the grain size is so coarse and the strain is too low.

Wang et al. [67] have assessed the hot ductility behaviour of austenitic steel at various strain rates in the temperature range of 900-1200°C and concluded that strain rate influences hot ductility through the following mechanisms: strain distribution, amount of dynamic recrystallisation, grain size and dynamic recovery. Higher strain rates enhanced the kinetics of dynamic recrystallisation, so giving finer grains and preventing hot cracking. Furthermore, reducing strain rate led to a higher strain gradient from the matrix to the grain boundary, thus enhancing hot cracking. It can be concluded that higher strain rate generally is beneficial in improving hot ductility in the straightening temperature range of 700 to 1000°C (Figure 2-13).

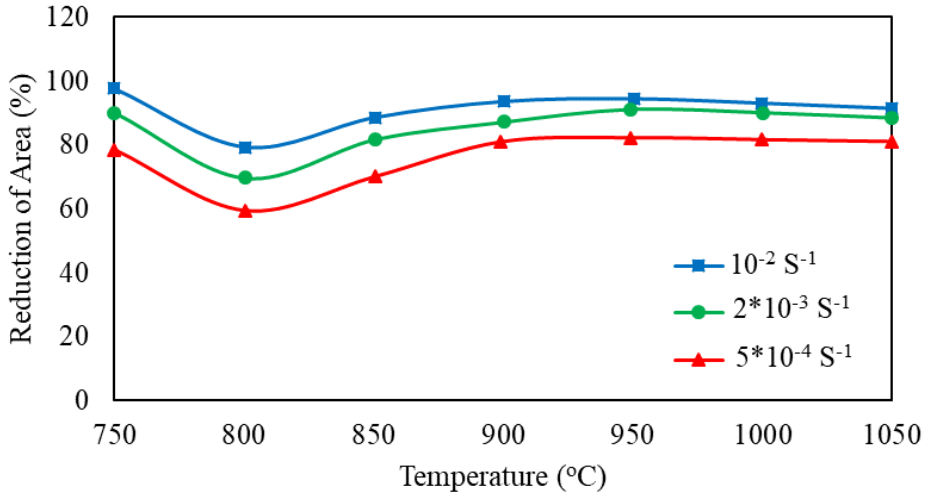

Figure 2-13 Influence of strain rate on hot ductility of steel for the base composition: 0.044%C, 1.45%Mn, 0.22%Si, 0.007%S, 0.012%P, 0.017%Al and 0.01%N [68].

2.3.3 Comparison between the effect of strain rate on hot ductility in continuous casting and in hot tensile testing

In continuous casting at the bending stage, the grain size is too coarse and the strain too small to activate DRX at the normal temperature range for the straightening operation. Increasing temperature enhances the recovery rate, which results in better hot ductility. However at the same time, due to the absence of DRX, grain boundary sliding (GBS) occurs and its rate increases with time and temperature leading to poor ductility. When the steel is fully austenitic on bending, as is the case for TWIP steels, both phenomena occur simultaneously and the improvement in hot ductility caused by the recovery is roughly balanced by the deterioration caused by the grain boundary sliding.

In hot tensile testing, the higher the strain rate, the less time is available for GBS to take place. This gives less time for cracks to form at the boundaries, and it has been observed that doubling the strain rate could reduce the cracks length by a half [42]. Therefore, increasing strain rate $\dot{\varepsilon}$, increases the level of strain to failure ε_f, as shown in Figure 2-14.

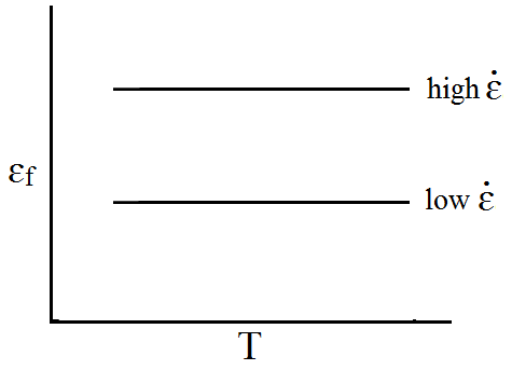

Figure 2-14 The influence of strain rate $\dot{\varepsilon}$ on strain to failure ε_f as a function of temperature T

The occurrence of DRX changes the whole situation as the new recrystallised grains can move away from the cracked boundary easily, making it difficult for cracks to continue propagation, so improving ductility. Typical stress-strain behaviour of steel is shown in Figure 2-15(a) before the onset of DRX and in Figure 2-15(b) when DRX can occur.

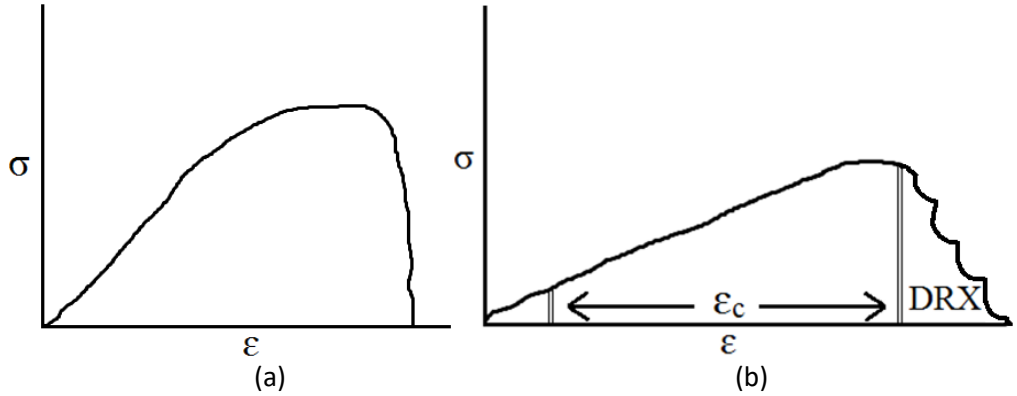

Figure 2-15 Schematic diagram showing stress-strain curves for steel (a) without recrystalisation, (b) with recrystallisation.

The typical changes that occur in the stress/strain curves are shown, as the test temperature increases, in Figure 2-16, when there is no DRX (744 to 825°C) to when DRX becomes established at ~836°C. DRX causes the stress to decrease and then increase with further deformation at the same time as the tensile specimen necks down to failure.

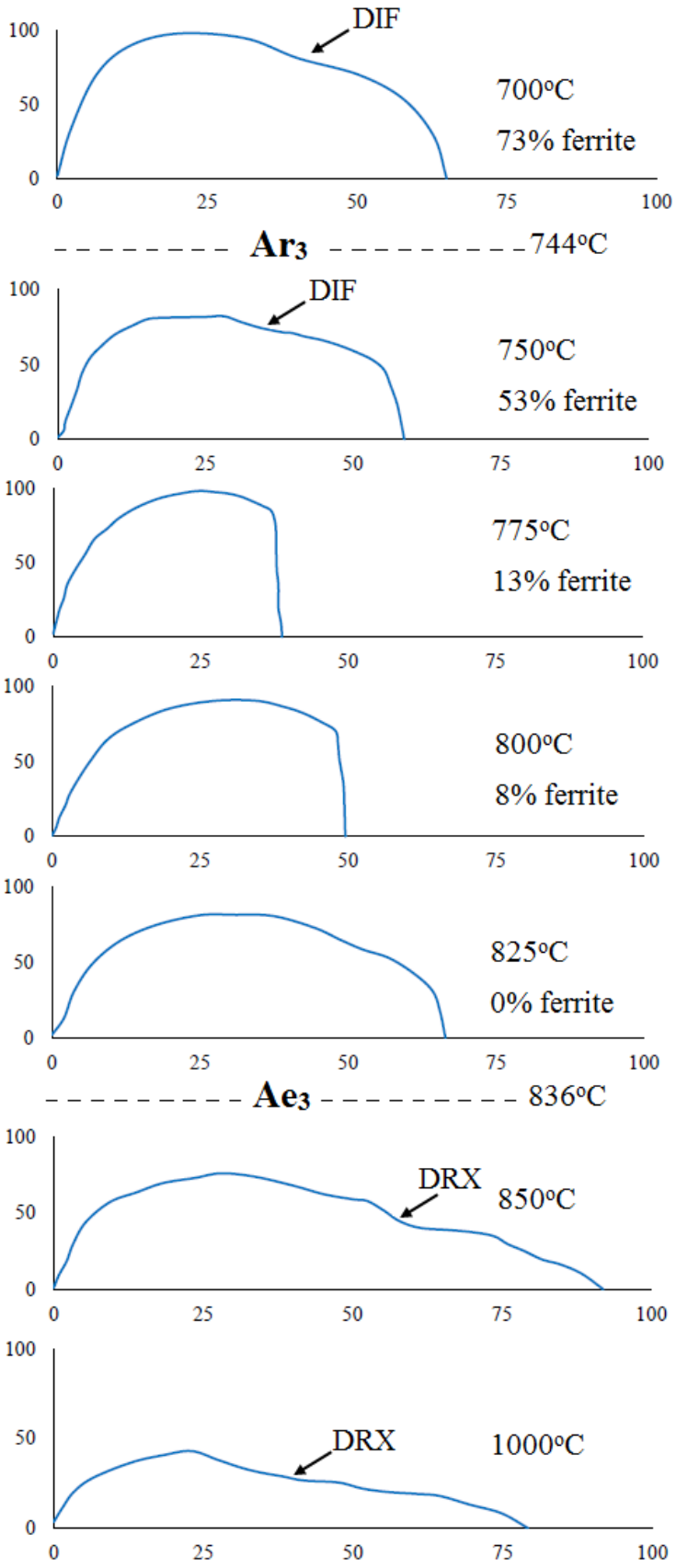

Figure 2-16 Changes that occur in the stress/strain curves in the temperature range (700-1000°C) [42].

The main parameter affecting DRX is the critical strain required for DRX, ε_c, which is the strain required for the onset of DRX, and its value depends on the deformed original unrecrystallised grain size and strain rate. The new recrystallised grains form by a bulging out of the boundary of the original grain (Figure 2-17). The finer the original grain size is, the more nucleation sites are available so less critical strain is required for the onset of DRX. The driving force for formation of new grains is estimated by the strain energy difference between the original grain and the recrystallised grain. In a given time, increasing the strain rate gives higher dislocation density in the recrystallised grains and thus the driving force across the boundary increases making it harder for DRX to occur, so a higher ε_c is needed. However, at low strain relevant to the straightening operation, DRX does not occur and the dislocation density builds up and ductility deteriorates.

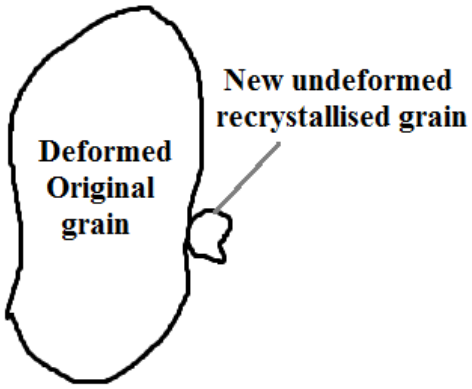

Figure 2-17 Schematic diagram showing nucleation of a new grain on the boundary of the deformed original unrecrystallised grain.

Previous work [20] has shown the critical strain needed for dynamic recrystallisation to occur is a function of the strain rate and grain size (Figure 2-18). The temperature for dynamic recrystallisation is extrapolated from the point at which the curve for ε_c against temperature intersects with the curve for strain to fracture, ε_f, against temperature. It is seen that increasing strain rate leads to better hot ductility, reflected by the narrower and shallower trough (Figure 2-18(b)). Furthermore, refining grain size by decreasing ε_c was found to reduce the depth and width of the trough significantly (Figure 2-18(c)). The reasons for the hot ductility improvement that occurs on increasing the strain rate and refining the grain size are very different with regards to the enhancement of DRX. Refining the grain size encourages DRX [69] whilst increasing the strain rate makes it more difficult for DRX to occur.

Increasing the strain rate has an enormous influence on improving hot ductility even though it increases ε_c because grain boundary sliding is radically reduced, improving the strain to fracture ε_f, (Figure 2-18(b)). The value of ε_c can be calculated using *Equation 4* [70].

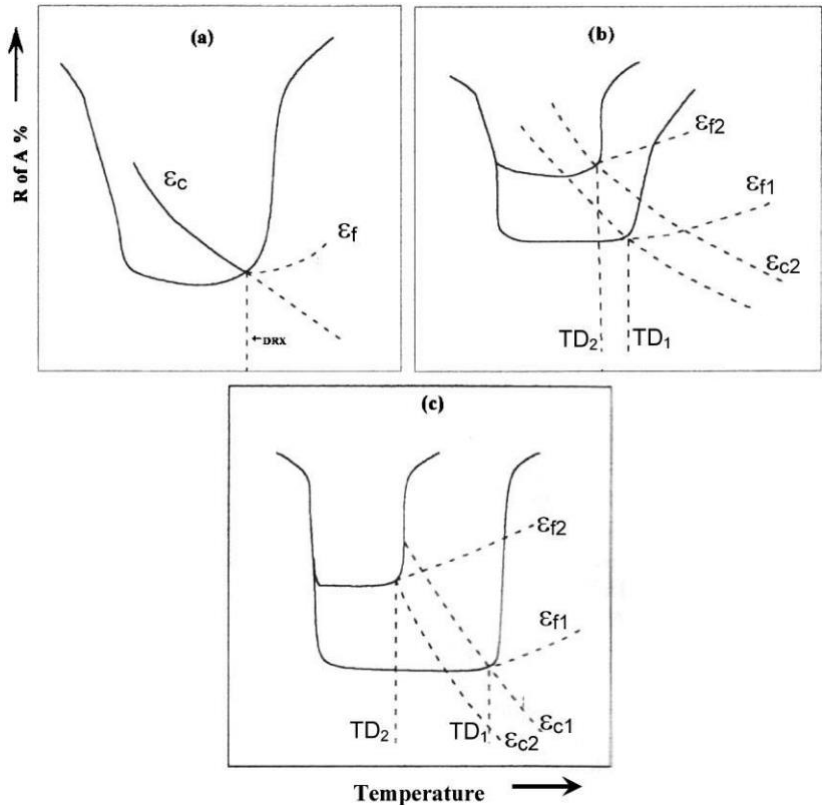

Figure 2-18 Schematic diagram showing (a) how the width of the hot ductility trough is affected by the dynamic recrystallisation (DRX), (b) the influence of strain rate on the depth and width of the trough ε_{c1} and ε_{f1} refer to the lower strain rate. ε_{c2} and ε_{f2} refer to the higher strain rate and (c) the influence of grain size on the depth and width of the trough, ε_{c1} and ε_{f1} refer to the coarse grain size, ε_{c2} and ε_{f2} refer to the finer grain size [20].

Equation 4

$$\varepsilon_c = A d_o^{1/2} Z^n$$

where Z donates the Zener-Hollomon parameter, d_o represent the initial grain size while A and n are constants (n = 0.15). A finer grain size gives a smaller ε_c while increasing the strain rate increases ε_c

The value of Z can be obtained by *Equation 5* [70]:

Equation 5

$$Z = \dot{\varepsilon} e^{Q/RT}$$

where Q in the activation energy for deformation of the austenite phase, T denotes the absolute temperature.

2.3.4 Grain size

It is well established that optimising microstructure, particularly grain size, is essential to control mechanical properties at room temperature and hot-flow characteristics not only for steel but for all metals [71]. Hot ductility could be considerably improved by refining the austenite grain size in plain C-Mn steel in the temperature range 650-1000°C as reported by Mintz and Crowther [72]. They showed that refining the grain size increased the reduction of area and the hot ductility trough was always narrower and less deep (Figure 2-19).

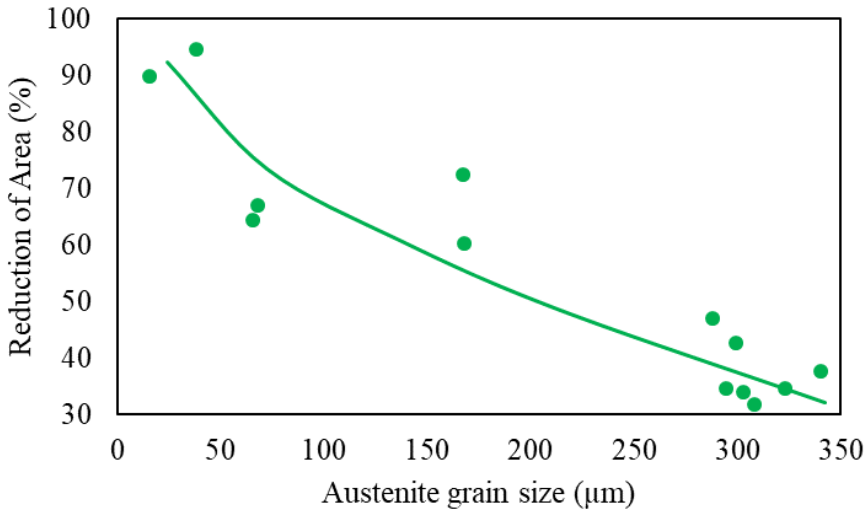

Figure 2-19 Effect of grain size on %RA for C-Mn steels tested at 750°C [72].

Ouchi and Matsumoto [73] also have shown the hot ductility of C-Mn-Al and C-Mn-Al-Nb steels is not significantly influenced on refining the grain size from 1000 to 300µm as the change in R of A will be small. However, Schmidt and Josefsson [74] have also reported that transverse cracking can be considerably reduced in microalloyed steel by refining the austenite grain size through introducing a suitable secondary cooling pattern. They suggested that the amount of cracking gradually decreases as the grains become finer and hence a steel free of defects could be obtained during the straightening operation. Mintz and Crowther [75] have shown that refining grain size in microalloyed steels from 300 to 150µm at 850°C increases the reduction of area by ~20% which is often enough to avoid transverse cracking and low-ductility intergranular failures.

It can be seen from Figure 2-19 that refining the grain size always improves ductility but the influence of refining the grain size as the grain size coarsens becomes less and less and for grain sizes ≥300um the changes are small and this accounts very much for the reported variations.

Many studies [75-78] have suggested that refining the grain size would improve the hot ductility of metals. Evans [79] justified such a behaviour by the considerable reduction of sliding rate when the grain size is refined giving a reduction in grain boundary cavity growth rate. In addition, cracks in the grain boundary must grow through triple points (Figure 2-9) and the fewer they are, as in the coarse grains, the easier the cracks can develop and the steel becomes more susceptible to intergranular failure.

Control of grain size can be achieved by either optimising heat treatment or alloying composition. This is always accompanied by a change in the precipitation behaviour which clearly influences the hot ductility and hence it becomes very difficult to differentiate between the influence of grain size and precipitation on hot ductility which probably accounts again for the uncertainty in literature.

2.4 Influence of alloying composition on hot ductility

2.4.1 Carbon

Crowther and Mintz [80] stated that increasing carbon content from 0.04 to 0.28% in a plain C-Mn steel moved the hot ductility trough to lower temperature as a consequence of increasing the C level lowering the Ae_3 temperature and the temperature at which the thin film of deformation induced ferrite can form. Increasing the C level also lowers the Ar_3 so the whole hot ductility curve is moved to lower temperatures, Figure 2-20.

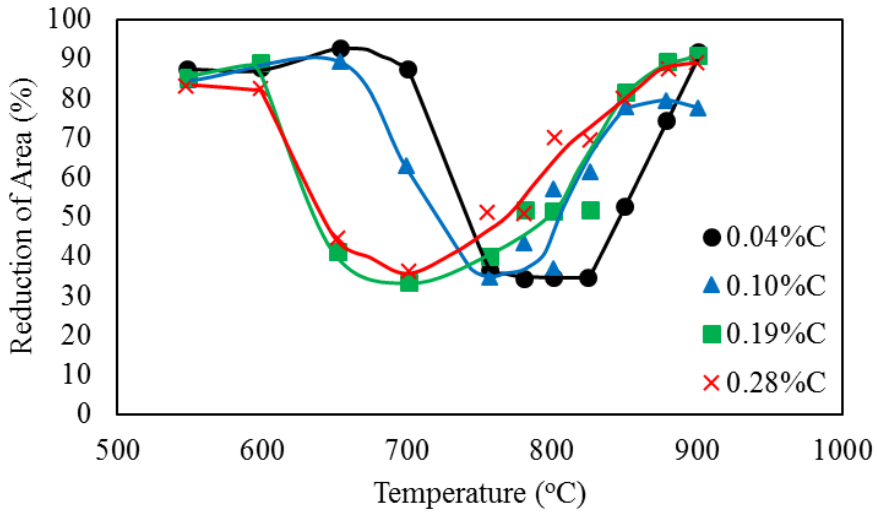

Figure 2-20 Influence of carbon content on the hot ductility curves for ferrite/pearlite steels for the base composition: 1.5%Mn, 0.2-%Si, 0.013%S, 0.002%P and 0.004%N [80].

The minimum hot ductility was found to take place during the formation of thin ferrite films along the austenite grain boundaries by deformation induced transformation. The soft ferrite films allowed strain concentration along the boundaries causing voids at the MnS inclusions, which eventually link up to cause intergranular failure.

Increasing carbon content above 0.28%, which is more relevant to the current work on TWIP steel, besides moving up the Ae_3 temperature, was reported to raise the activation energy for dynamic recrystallisation (Figure 2-21) which would mean that the critical strain needed for dynamic recrystallisation is subsequently increased. As a result, sliding at austenite grain boundaries is increased and becomes sufficient to encourage coalescence of cracks leading to intergranular failure in the austenitic phase giving worse hot ductility and extending the trough.

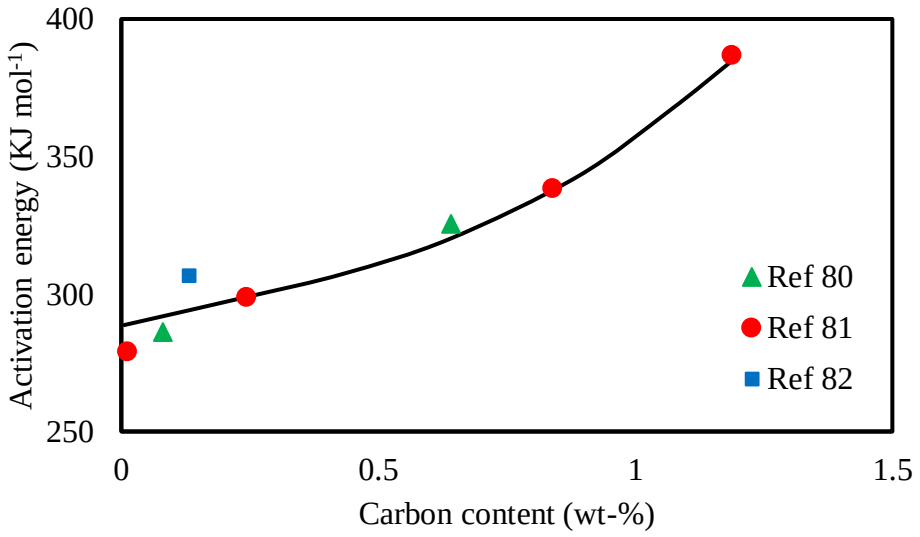

Figure 2-21 Influence of carbon content on activation energy [80-82].

In case of Nb-bearing steel, the deleterious influence of carbon becomes more pronounced as reported by Mintz and Mohamed [83] due to Nb(CN) precipitation. The steel examined was in the re-heated condition and showed the worst hot ductility at higher carbon content due to the higher volume fraction of NbCN precipitates at the austenite grain boundaries.

The same type of steel was examined by Mohamed [84] who observed a deterioration in hot ductility with increasing carbon content to a specific limit in the as-cast state. The work evaluated the hot ductility behaviour of low alloyed Nb-bearing steels based on carbon content (0.014-0.18%C). He observed that increasing carbon content up to 0.14% was detrimental to

hot ductility but suggested this was due to grain coarsening, while a higher carbon content of 0.18% improved hot ductility considerably due to grain refinement (Figure 2-22).

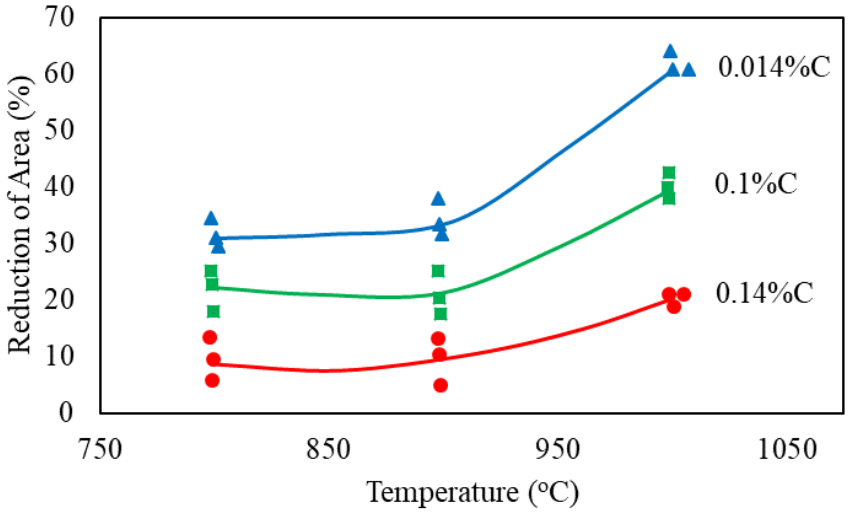

(a)

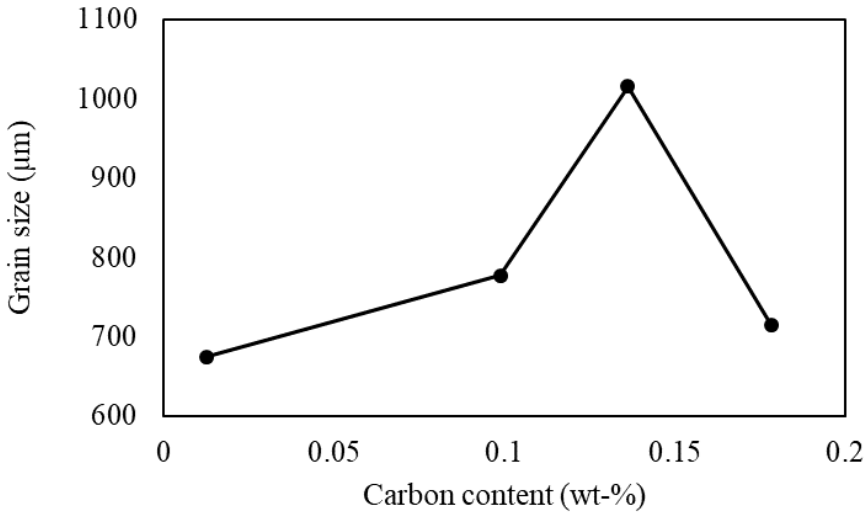

(b)

Figure 2-22 (a) Effect of carbon content on %RA in low alloyed steel, (b) effect of carbon content on austenite grain size at 1100°C in low alloyed steel for the base composition: 1.5%Mn, 0.4%Si, 0.006%S, 0.01%P, 0.03%Al, 0.03%Nb and 0.007%N [84].

He suggested that this is a consequence of the peritectic reaction where below the C peritectic level the two phases δ ferrite and γ are present enabling grain refinement to take place on transformation and at higher C contents the two phases, liquid and austenite are present so that grain refinement is again possible (Figure 2-23).

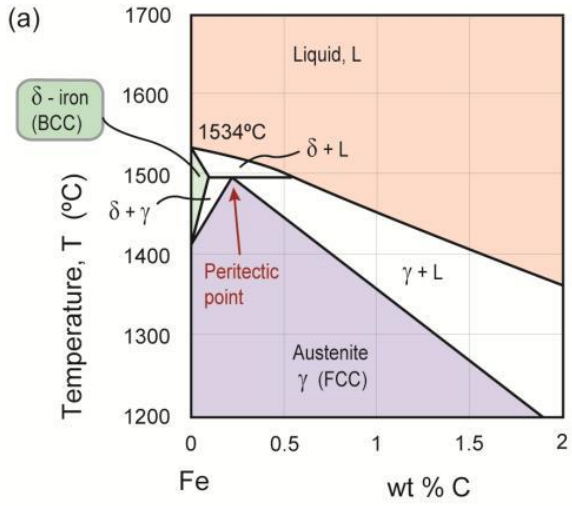

Figure 2-23 Peritectic part of the constitutional Fe-C diagram [85]. Note peritectic occurs at the highest temperature at which the transformation to austenite takes place.

In the as-cast state, transformation changes above the Ae_3 become important in controlling the austenite grain size and the peritectic carbon gives rise to a coarser austenite grain size and this can dominate the hot ductility behaviour. However, it is obvious from the peritectic diagram that the peritectic carbon point corresponds to the highest temperature for austenite to form on solidification so would be expected to have the coarsest grain size. Increasing or decreasing the C content on either side of the peritectic point leads to lower temperatures for the formation of austenite again leading to a finer grain size. This would seem a better explanation as ductility is found to be better at low C levels with less cracking in contradiction to Mohammed's [84].

Therefore, the effect of carbon on hot ductility becomes more pronounced in the as-cast state for plain C-Mn and low alloyed steels. In the case of TWIP steels in which no phase transformation takes place, the effect of carbon on hot ductility can be evaluated by the grain size and the precipitation characteristics of carbide forming elements.

2.4.2 Manganese and Sulphur

Manganese is added to TWIP steel at high concentrations to preserve the austenitic structure and control stacking fault energy [86]. Normally, Mn can act as a deoxidising agent by removing oxygen out of the melt into the slag during casting by forming manganese oxide compounds [87]. When discussing the influence of Mn on the hot ductility, sulphur has also to be taken account of due to the fact that Mn is a strong sulphide forming element so both elements will be discussed in this section. In the absence of Mn or when there is a low ratio of Mn/S, Fe-sulfides can form at high and medium temperatures, where the straightening

operation takes place [88]. The low melting point of this phase triggers formation of cracks whereas their propagation is governed by the morphology, size and volume fraction of these precipitates [89]. Therefore, Mn has always been added to steel alloying composition since it has a greater affinity to S than Fe, and MnS has a much higher melting point than FeS so preventing the negative effects of S precipitation. The precipitation behaviour of MnS and AlN is predicted as a function of temperature for the composition presented in Figure 2-24.

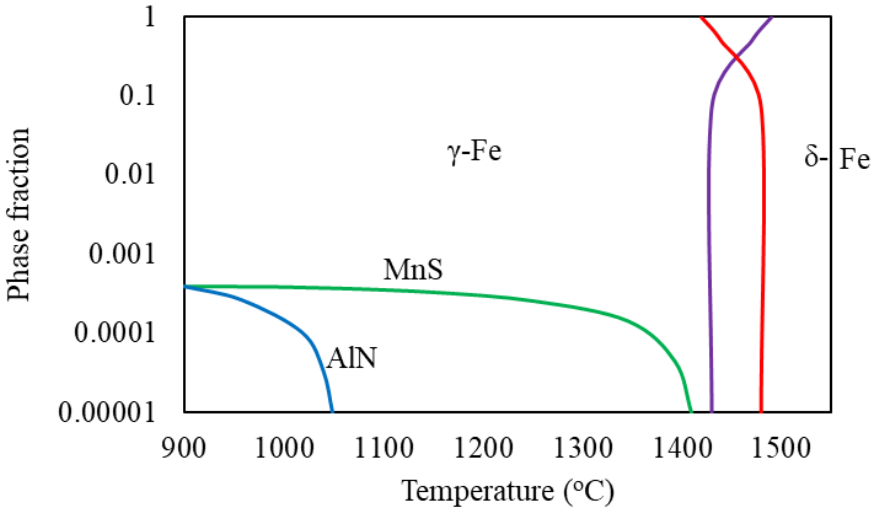

Figure 2-24 Phase temperature diagram for AlN and MnS steel with the composition: 0.040%C, 0.06%Si, 0.46%Mn, 0.017%P, 0.010%S, 0.017%Al and 0.0056%N [90].

Previous work [91,92] has shown that MnS particles are easily deformed during hot working due to the fact that MnS particles are relatively softer than the steel iron matrix they are residing in and so elongate out along the rolling direction. MnS precipitation has been shown to be beneficial in retarding grain growth in the austenite [93-95]. Based on previous experiments, the degree at which MnS particles can influence hot ductility is dependent on their size and distribution and the finer and greater the volume fraction the easier it is for cracks to develop [96,97]. As a matter of fact, MnS particles form at high temperature, typically 1380°C, and act as nucleation sites for AlN precipitation at temperatures below 900°C as reported by Steenken et al. [98]. Since MnS precipitates preferably in the matrix, the detrimental influence of AlN precipitation is minimised since AlN precipitates mainly at grain boundaries, and so provides nucleation sites for void formation that continuously grow to interlink resulting normally in lower hot ductility. This is particularly important in TWIP steel which contains higher amounts of Al [99]. Lückl et al. [100] examined the influence of cooling rate on the behaviour of MnS/AlN precipitation in low carbon steel under a reheating schedule. They found that faster cooling gave finer and denser MnS/AlN particles which could obstruct the rate of dislocation

movement due to dislocation pinning due to the sufficiently dense distribution of these particles, resulting in lower hot ductility in the austenite region (Figure 2-25).

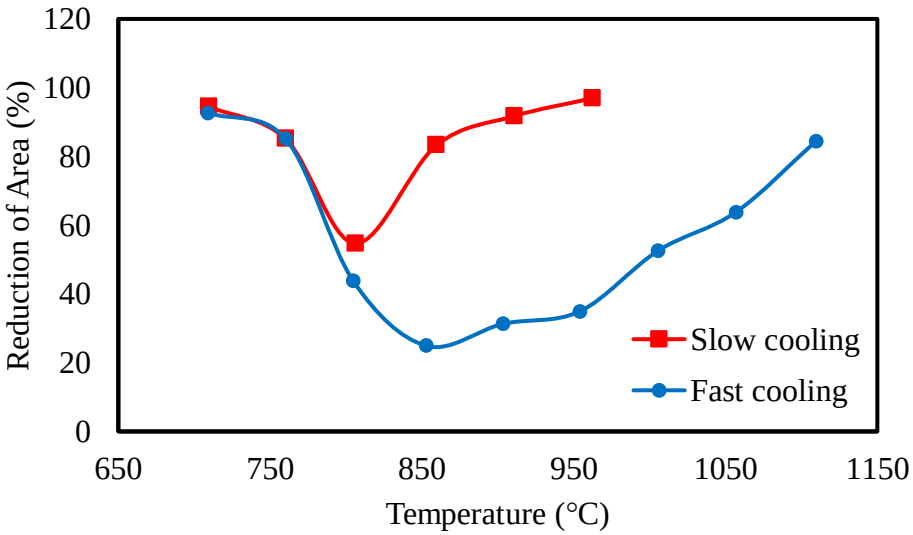

Figure 2-25 Reduction of area for fast and slow cooling of low carbon steel, the fast cooling rate being 250°C min^{-1} and the slow cooling rate 190°C min^{-1}, the composition: 0.104%C, 0.044%Si, 0.43%Mn, 0.009%S,, 0.046%Al, 0.0009%Ti, 0.025% and 0.0056%N [100].

It is therefore recommended, besides utilising slower cooling rates, to reduce the amounts of both S and Al in order to coarsen and reduce the density of these particles [53]. Liu et al. [101] investigated the influence of Mn content on the hot ductility of TWIP steel and observed that as Mn level increases from 15 to 23% the hot ductility first increased and subsequently deteriorated (Figure 2-26). They observed that the MnS particles were located within the matrix but the distribution was inhomogeneous with there being severe Mn segregation in the interdendritic zone. Moreover, the maximum fraction of dynamically recrystallised grains occurred at the lowest Mn content. This fraction dropped significantly on increasing the Mn level and grain boundary sliding was promoted. Furthermore, the effect of C microsegregation was accelerated by Mn addition since a higher amount of C microsegregation occurred as Mn content increased. As expected, mixed ductile-brittle fracture was observed for the low Mn content while the high Mn steel exhibited brittle type fracture. Cabanas et al. [102] showed that in hot rolling, higher Mn additions retarded the dynamic recrystallisation of Fe-Mn binary alloys. Lan et al. [55] also showed that the addition of 22%Mn to TWIP steel led to Mn microsegregation and microporosity in as cast structures, hence reducing the matrix homogeneity and giving poorer hot ductility.

Again, it should be noted that dynamic recrystallisation does not normally occur on straightening because the strain on straightening is too low and grain size is too coarse so this does not address the commercial problem.

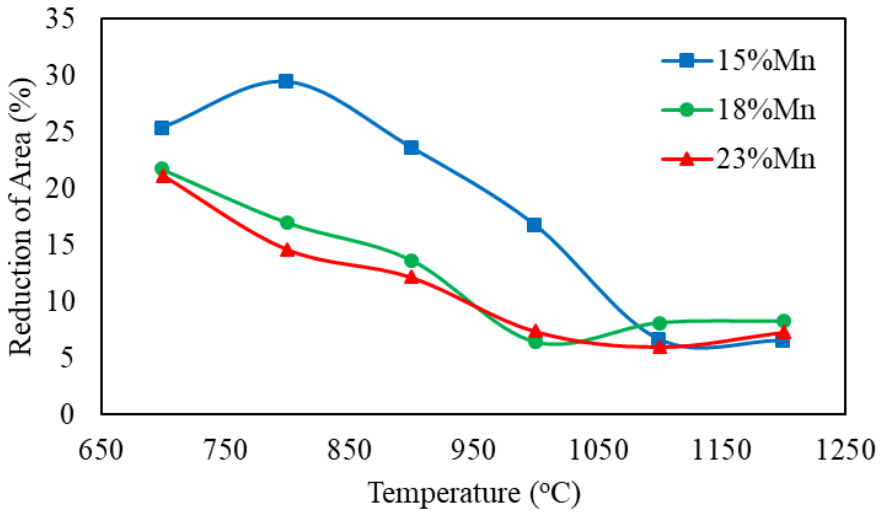

Figure 2-26 The hot ductility of TWIP steel at different Mn contents for the base composition: 0.6%C, 0.008%S, 1.5%Al and 0.01%N [101].

In contrast, Banks et al. [103] observed that the increase of Mn content from 0.25 to 1.6% in the high temperature processing (HTP) of Nb-Ti linepipe steel activated the recrystallisation kinetics leading to finer and a more homogeneous microstructure.

In the presence of copper (Cu), which may be present as a residual or picked up from the Cu mould on casting, it was recommended to minimise sulphur addition to avoid formation of MnS particles as these may also act as preferred sites for Cu concentration causing hot shortness and so deteriorating the hot ductility [104].

2.4.3 Aluminium

Traditionally, the steel industry has used low concentrations of aluminium as a deoxidising agent in steel to form aluminium oxide to scavenge oxygen during casting and minimise porosity. Presently, aluminium has attracted more attention due to its considerable influence on grain refinement by inhibiting grain growth in steels [105].

Higher contents of Al in plain C-Mn steel were found to raise the Ae_3 temperature so ferrite bands form prematurely resulting in a wider hot ductility trough. This phenomenon is enhanced with the presence of high amounts of N, resulting in finer and a higher volume fraction of AlN precipitates, increasing the susceptibility to intergranular fracture [106]. These precipitates form during solidification and later during cooling after rolling [107]. The AlN often

precipitates in a very fine thin film covering the grain surface leading to cracking. However, high amounts of Al (1-2%) are needed in TWIP steel in order to control the stacking fault energy and achieve extensive twinning during deformation at room temperature [108].

Recent work by Liu et al. [101] have examined the effect of Al content on the hot ductility of TWIP steels, the steel having, 18%Mn, 0.009%N and 0.008%S. The study showed that reducing Al additions from 1.5 to 0.75% improved the hot ductility only slightly by 8% (Figure 2-27). At both Al levels, hot ductility was always poor, being below 40% throughout the temperature range 700-1200°C. In contrast, a significant improvement in hot ductility was achieved when Al was at the very low level 0.002%, hot ductility being over 40% in the same temperature range.

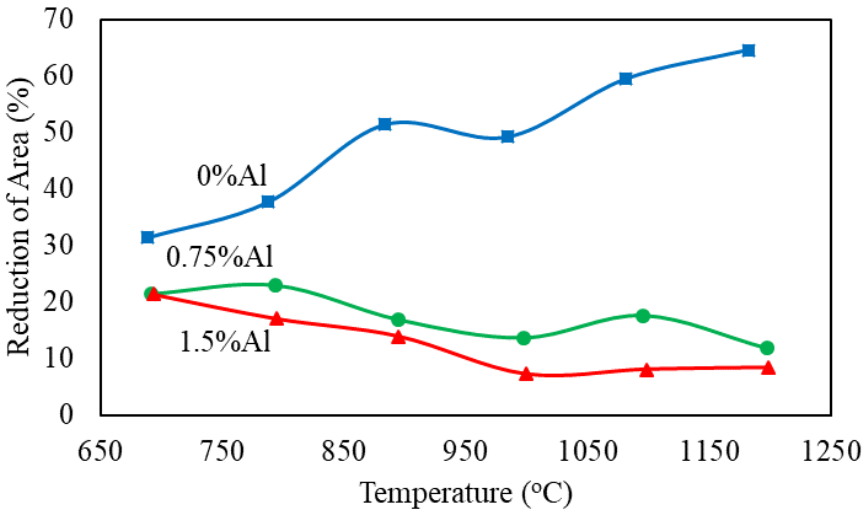

Figure 2-27 The hot ductility of TWIP steel at different Al content for the base composition: 0.6%C, 0.008%S, 18%Mn and 0.01%N [101].

It was concluded that the equilibrium precipitation temperature of AlN increased noticeably with the increase of Al content (Figure 2-28) resulting in a dramatic increase in volume fraction of AlN particles. The excessive volume fraction of "fine" AlN particles in the high Al-bearing steel was found to be very effective in obstructing dynamic recrystallisation and enhancing grain boundary sliding by pinning the grain boundaries leading to poor hot ductility [46]. Previous work [109,110] has also confirmed that a high addition of Al encourages AlN precipitation up to very high temperature in TWIP steels. Indeed, it is well established that higher Al concentrations make it easy for AlN to precipitate out, in comparison with plain low Al-bearing C-Mn steel [111,112].

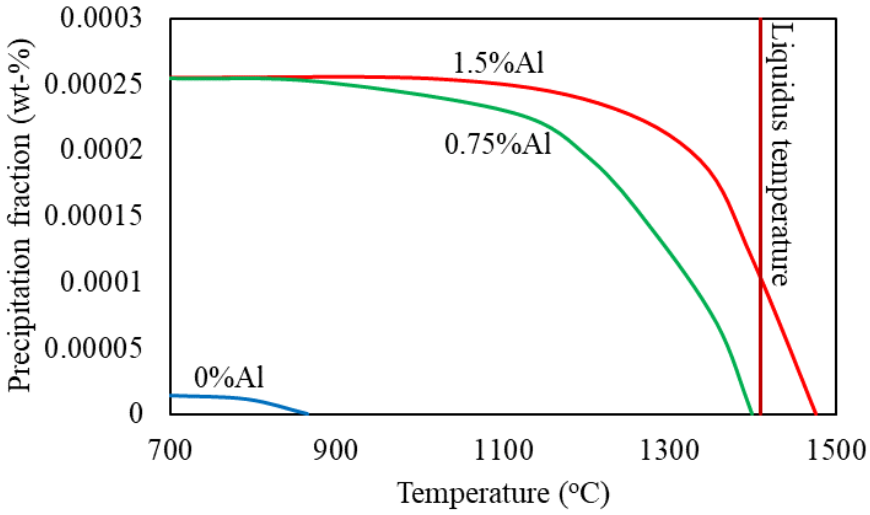

Figure 2-28 The equilibrium phase diagram of TWIP steel with various contents of Al predicted by Thermo-calc software for the base composition: 0.6%C, 0.008%S, 18%Mn and 0.01%N [101].

Furthermore, despite using a lower amount of Al ~0.9% in TWIP steel, Brune et al. [113] observed an increased formation of (AlN) particles leading to poor hot ductility as a result of the higher level of N used, this being 0.0075%.

AlN precipitation is considerably influenced by S content as reported by Kang et al. [16] who studied the AlN precipitation behaviour on hot ductility of TWIP steel with various additions of S. It was observed that the content of S did not influence the hot ductility below 900°C but as the temperature increased up to 1100°C the hot ductility for the very low S-bearing steel, having 0.003%S, significantly improved by 35% (Figure 2-29).

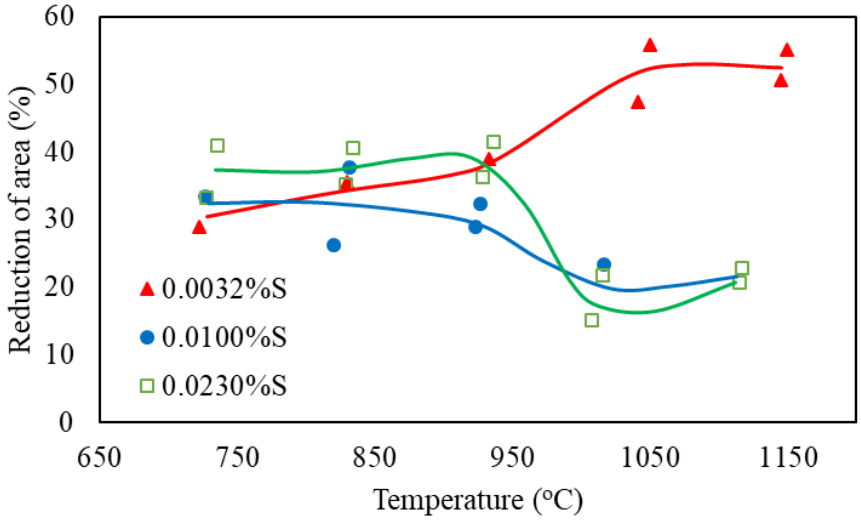

Figure 2-29 Hot ductility curves for three TWIP steels at three S levels for the base composition: 0.6%C, 18%Mn, 0.2%Si, 0.02%P, 1.5%Al and 0.009%N [16].

Indeed, the hot ductility of the higher S-bearing steel deteriorated and this was explained by the morphology and size of the AlN precipitates. AlN has problems in precipitating out in the austenite and precipitation is very sluggish. MnS particles offer themselves as suitable nucleation sites [16]. In all cases, the AlN particles were coarse but were hexagonal in shape and existed mainly in the matrix for the low S-bearing steel and so would not influence the hot ductility. However, the high S-bearing steel resulted in higher volume fraction of AlN particles in the shape of dendritic rods at the dendritic and austenite grain boundaries and this favoured intergranular fracture.

The precipitation of AlN on reheating has been extensively studied but of course is very different to when cooling from 1250°C. Kundu [114] for example investigated the influence of AlN on grain boundary pinning during reheating and the subsequent evolution of the austenite grain structure of HSLA steel. The study showed that AlN precipitates were very effective in refining austenite grain size by pinning the boundaries during reheating. Furthermore, AlN particles were found to be 100% coarser when reheating at a higher temperature of 1150°C in comparison with reheating at 1125°C. Holding time was also examined and showed that extended holding led to further dissolution of AlN particles so that a lower volume fraction was obtained at the extended holding time (Figure 2-30(a)). consequently, grain size was coarsened by ~85% by extending the holding time from 1 to 8 hours, (Figure 2-30(b)) which is associated with the dissolution of the majority of AlN particles while the remaining undissolved particles were too coarse to provide any significant pinning at the boundaries. Therefore, maximising the efficiency of AlN in pinning the boundaries is achieved by reducing both factors; reheating temperature and holding time. However, this is relevant to rolling after casting but not to casting and may not apply to TWIP steels which have with its high Al content a much higher driving force for AlN precipitation. For normal Al levels of 0.02-0.06%Al, AlN precipitates readily on reheating when the phase transformation occurs from α to γ giving numerous nucleation sites but it is very sluggish on cooling from the austenite [16] when fewer sites are available, as is the continuous cast situation. AlN does not precipitate out then unless the concentrations of Al and N are very high.

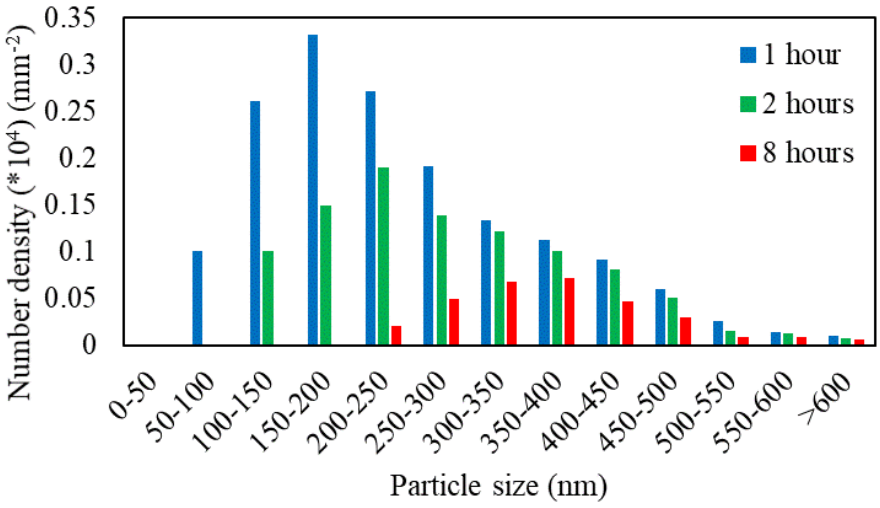

(a)

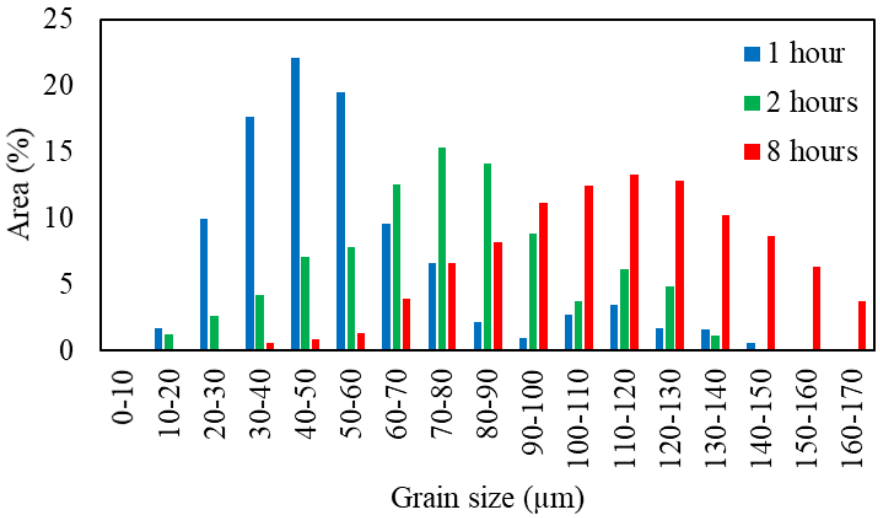

(b)

Figure 2-30 (a) Volume fraction of AlN particles after reheating at 1125°C for 1, 2 and 8 hours, (b) prior austenite grain size distribution after reheating at 1125°C for 1, 2 and 8 hours, for the composition: 0.10%C, 0.4%Mn, 0.005%S, 0.3%Si, 0.017%P, 0.016%Al, 0.02%Nb, 0.001%Ti, 0.3%Ni and 0.008%N [114].

2.4.4 Niobium

The main purpose of Nb addition to steel is to enhance strength at room temperature i.e. TWIP steel exhibits a strength of 800MPa and with Nb the strength increases to 1000MPa [13]. Nb promotes strength through grain refinement, solid solution hardening and precipitation strengthening. However, previous work [57] has shown that adding Nb to a TWIP steel can make hot ductility worse as a result of Nb(CN) precipitation in the matrix and at the austenite grain boundaries, giving low reduction of area values of 10-20% in the temperature range of 700-900°C. Cracks then develop as a consequence of stress and strain concentration at the austenite boundaries caused by grain boundary sliding and hence promoting intergranular

failure. Increasing cooling rate, from 60 to 180°C min^{-1}, led to even worse hot ductility due to the finer Nb(CN) precipitation, making it difficult to cast thin steel slabs without transverse cracking occurring. Comineli et al. [115] examined Ti-Nb microalloyed steels and indicated that a fast cooling rate, ~240°C min^{-1}, resulted in more solute in the matrix for the subsequent strain induced precipitation, giving poor hot ductility. However, the slow cooling rate, ~24°C min^{-1}, provided a longer time for precipitation to occur at higher temperature so making them coarser. Typically, the nose temperature for Nb(CN) precipitation is 950°C [116] and the degree at which Nb(CN) precipitation effects hot ductility is governed by the nitrogen level since these precipitates are rich in N when precipitating in the austenite [57]. It is also important to restrict the Al level to 0.04% in Nb-bearing ferrite/pearlite steel since above this level hot ductility deteriorates and with Nb additions hot ductility can be particularly poor for HSLA steels of peritectic C composition [117].

Earlier work investigating the hot ductility of HSLA steel confirmed that an increase of Nb content was found to deteriorate hot ductility in the austenitic region due to successive Nb(CN) precipitation at the grain boundaries [73]. The static precipitation of Nb(CN) reached a maximum as the temperature decreased below 1000°C. Moreover, by comparing the influence of Nb, Mo and V on dynamic recrystallisation in microalloyed steel, Andrade et al. [118] found that Nb has the highest effectiveness in retarding the onset of recrystallisation. This is attributed to the critical strain required for fracture propagation being low in comparison with the strain needed for recrystallisation to occur. Dynamic recrystallisation was documented to be important to promote maximum dissolution of fine Nb(C,N) precipitates as well as minimising the segregation rate of these elements at the grain boundaries and at the interfaces between the remaining undissolved precipitates and the matrix [119]. Mintz and Arrowsmith [44] have also indicated that Nb additions give worse hot ductility to microalloyed steel as a result of Nb(CN) precipitation at the austenite grain boundaries so encouraging grain boundary sliding leading to intergranular fracture. This behaviour was even enhanced by Al additions giving finer NbCN precipitation and hence pinning the boundaries more effectively. Although Nb was found to be beneficial in strengthening the austenite matrix, this led to stress concentration on the grain boundaries. The influence of Nb on hot ductility is negligible in the presence of either B or Ti, since Nb(C,N) precipitates do not form due to the weaker chemical affinity of Nb compared with both elements, TiN and BN forming instead [120,121].

Banks et al. [122] observed that higher contents of Nb and N contribute further in deteriorating hot ductility in peritectic carbon steels leading to a finer and higher volume fraction of Nb(C,N) particles as observed in Figure 2-31.

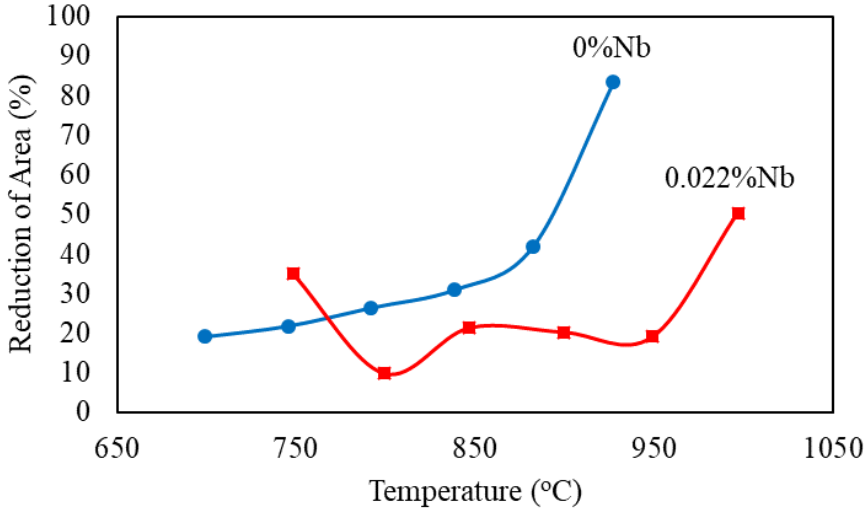

(a)

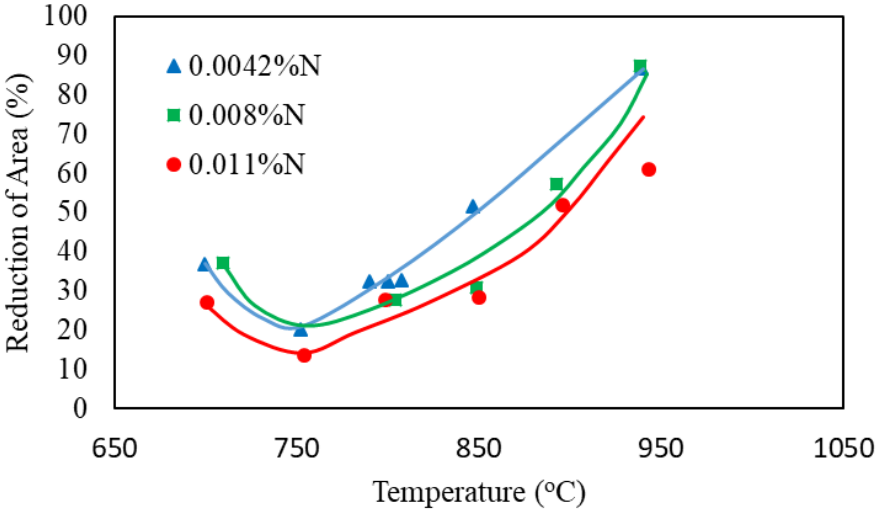

(b)

Figure 2-31 (a) Effect of Nb on hot ductility in high- N steels, (b) effect of N content on the hot ductility of C-Mn-Nb-Al steels [122].

Niobium is preferred over vanadium mainly due to Nb being less soluble in austenite at the temperatures of straightening and rolling stages. Consequently, greater hardening of austenite is achieved leading to a finer microstructure and thus improved properties [123].

Although fine Nb precipitates lead to worse hot ductility at high temperatures, Zhou et al. [124] reported that nano-size Nb precipitates can hinder dislocation recovery by the pinning effect

and thus strengthen the relatively soft austenite matrix, enhancing steel strength at room temperature.

2.4.5 Titanium

Titanium is a very reactive element compared to the other alloying additions. Banks et al. [125] have examined the hot ductility of a Ti–Nb containing peritectic steel under a testing technique which incorporates the primary and secondary cooling cycles to better simulate the industrial cooling cycle. They found that Ti additions are beneficial to hot ductility due to a reduction in the fraction of fine particles meaning that transverse cracking of industrial slabs can be avoided.

The influence of Ti additions on the hot ductility of B and high Al containing TWIP steels under the as casting and reheating conditions have been examined by Kang et al. [15]. The hot ductility was improved and adequate to avoid transverse cracking for the temperatures <950°C due to the combination of Ti with all the N. The best hot ductility was achieved by having the Ti level above the stoichiometric so avoiding the detrimental precipitation of AlN and BN at the boundaries. However, in this work, some of the TiN particles were taken back into solution upon reheating to 1250°C and then re-precipitated out during cooling in a finer form leading to poor hot ductility for temperatures >950°C.

Normally, Nb precipitates in a fine form as particles Nb(C,N) so deteriorating hot ductility [122]. Al additions precipitate as AlN in a different form surrounding the grain surfaces with very thin films which can seriously damage the ductility. However, it has been confirmed that the addition of nitride-forming elements plays a major role in promoting Nb precipitation at higher temperatures [66]. This is because Ti being one of the strongest nitride-forming elements, precipitates at elevated temperatures as coarse TiN particles which then form the nucleating sites for attracting most of the Nb before the straightening operation of the strand takes place [126]. The amount of Ti needed to achieve the maximum hot ductility has been a major question and considerable work has been conducted to identify the optimum Ti additions, In previous work [61], for thick slabs, 0.02%Ti addition was found to be adequate to improve hot ductility in a steel containing 0.023% Nb and 0.009% N.

It is suggested from the literature [127] that the influence of Ti on the hot ductility of N-bearing steel can be beneficial or detrimental depending on the Ti/N ratio. Although they did not identify a specific Ti addition, Liu et al. [127] recommended not to raise Ti/N ratio in austenitic steel more than ~7 to avoid the detrimental effect of Ti(C,N) precipitation at the grain

boundaries and triple junctions leading to weak cohesion between the grains and accelerating crack growth.

Luo et al. [128] found that a high Ti/N ratio in the range of 3 to 6 is detrimental to hot ductility even when a secondary cooling step is included. On the other hand, an improvement was recorded by lowering the Ti/N ratio to ~2.5 as reported by Abushosha et al. [61]. In the former case, the high ratio led to larger volume fraction of fine strain-induced TiN precipitates. However, restricting the Ti/N ratio in the latter case minimised the volume fraction of TiN yet was sufficient to avoid AIN from precipitating out which is reflected by the hot ductility improvement.

The beneficial influence of Ti on allowing its coarse particle size at high temperatures to serve as sites for Nb and Al to precipitate out on cooling also applies to B precipitation as reported by Cho et al. [120]. It was observed that the Ti free B-bearing microalloyed steel had poor hot ductility due to BN precipitating at grain boundaries and weakening them (Figure 2-32). Adding a small amount of Ti, although, did not prevent BN precipitation due to the Ti/N ratio being too low~1.6 but improved hot ductility as the BN precipitation distribution pattern became more homogeneous and concentrated in the matrix rather than boundaries so reducing strain localisation at the boundaries.

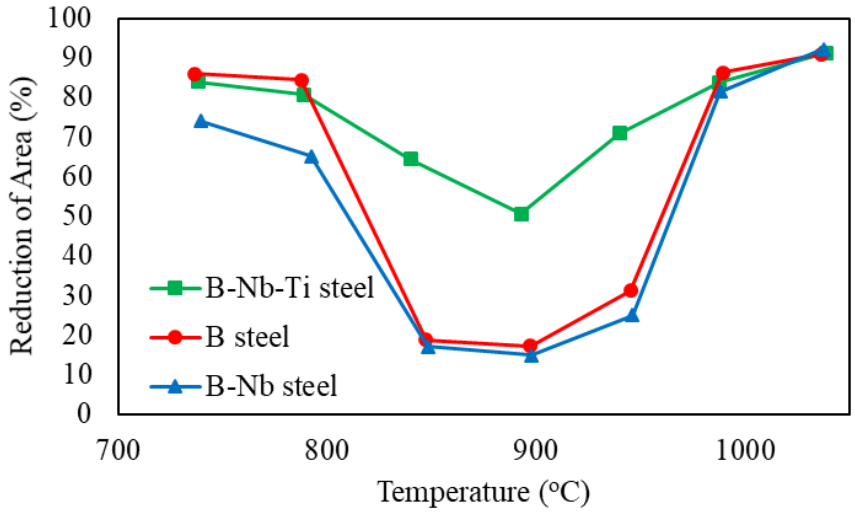

Figure 2-32 Hot ductility of B steel, B-Nb steel and a B-Nb-Ti steel [120].

Unlike niobium and vanadium precipitates, Ti precipitates do not inhibit static recrystallisation since they form at high temperatures and become too coarse to hinder the recrystallisation process [129].

Although most research work [15, 61, 120, 126] has shown a considerable improvement in hot ductility as a function of Ti, Salas-Rayes et al. [130] have reported otherwise. They investigated the internal cavities propagation of TWIP steel under uniaxial loading at high temperature. In the Ti-free steel, cavitation occurred and this led to poor hot ductility causing premature failure during forming. Indeed, the addition of Ti gave higher volume fractions of cavities and resulted in predominantly brittle fracture caused by finer grain-boundary precipitation, so weakening grains cohesion and activating crack growth through grain boundary sliding.

There has been a serious difficulty in simulating the continuous casting process for Ti containing steels to predict transverse cracking in the laboratory [131]. This arises since thermal history has a critical influence on Ti precipitation during solidification and thus influencing precipitation of other elements whose behaviour is affected by Ti such as N, Nb and Al, respectively. During continuous casting, the temperature drops very quickly from the melting point in the mould reaches a minimum and then rises (known as the undercooling step) and this is followed by the temperature falling but at a slower cooling rate (Figure 2-4). As a result, there is a high temperature gradient between the centre and the surface of the strand [125]. It has been extensively shown that the addition of Ti leads to better hot ductility in the presence of the undercooling step [45, 60, 128,132] and this explains the better hot ductility given by the industrially cast steel compared to the laboratory produced steel when there is no undercooling [133]. The main drawback of the simplified hot tensile testing, although being widely used [132], is that the thermal process does not take into consideration the temperature oscillations during casting and rolling, and instead, an average cooling rate is utilised. Therefore, many attempts have been made to apply the *in-situ* melting conditions with a similar cooling cycle, to better simulate the practical continuous casting of the Ti containing steel in the laboratory. This resulted in a better agreement in the hot ductility pattern [41]. Employing *in-situ* melting conditions is desirable to ensure complete resolution of Ti particles since the solubility of Ti increases on increasing temperature (Figure 2-33) [134].

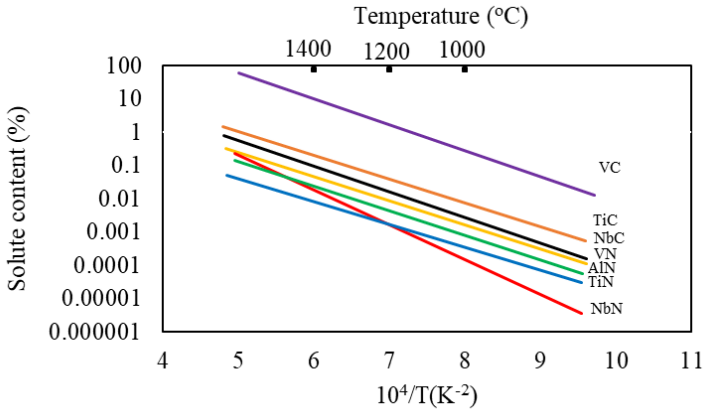

Figure 2-33 Solubility products of nitrides and carbides in austenite as a function of temperature [134].

Carpenter et al. [66] designed a complex thermal pattern to simulate the cooling regime used during continuous casting in a Ti-Nb containing steel after melting. A marked improvement of hot ductility was recorded in comparison with the simplified hot-ductility test which was attributed to the formation of coarser TiN particles, due to slower cooling conditions. Coarsening of Ti particles is guaranteed in this situation as more time is given for particles' growth. Figure 2-34 shows a typical relationship between particle size and %RA. Again, it can be seen that to achieve 40% RA the particle size needs to be greater than about 15nm.

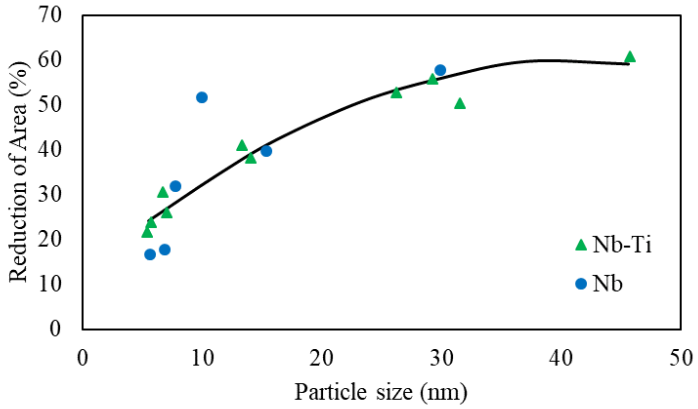

Figure 2-34 %RA as a function of niobium carbonitride precipitate mean diameter in the Nb and Nb-Ti steels in the austenite phase [66].

2.4.6 Vanadium

Vanadium was found to influence hot ductility of steel through VC and VN precipitates at high temperature [135-138]. Although the research work on the effect of V on the hot ductility of TWIP steel is limited, there had been an extensive work on other types of steel, mainly microalloyed steels. The behaviour of V at high temperatures is similar in all types of steel to

a certain extent and literature can help assess the ability of V to control the hot ductility of TWIP steel.

Reyes et al. [135] have examined the influence of a V addition on the hot deformation of TWIP steel in the temperature range of 900-1100°C. Unexpectedly, the addition of V did not show any change in the hot flow behaviour and this was explained by the low formation temperature of VC ~1010°C, according to FactSage thermochemical software and databases. Above this temperature, V remained in a solid solution state, so would have no effect on hot ductility. In case of microstructure, the V-bearing steel was found to exhibit a slightly finer grain size suggesting that V can have some control of the size of the recrystallised grains during hot deformation. Precipitation of VC could be promoted by lowering strain rate, so giving more time for precipitation to occur.

V starts precipitating at a relatively low temperature, ~950°C, compared to Ti and Al. Above this temperature, V is still in solid solution state and the influence of V on hot ductility can be only evident at the temperatures below 950°C, where V could be precipitated [139,140].

Mintz and Abushosha [141] examined the effect of V content (0.01 – 0.1%) on hot ductility of microalloyed steel and observed that higher V additions led to worse hot ductility (Figure 2-37) This was linked to the precipitation behaviour of the VN particles, as a higher volume fraction of precipitation occurs when the V content is increased at a constant N. In comparison with other alloying elements, precipitation of V particles is characterised by its ability to coarsen more rapidly due to its high solubility so is less detrimental to hot ductility [142]. V has also been found to precipitate randomly in the matrix, unlike many other alloying elements which appear at grain boundaries [142].

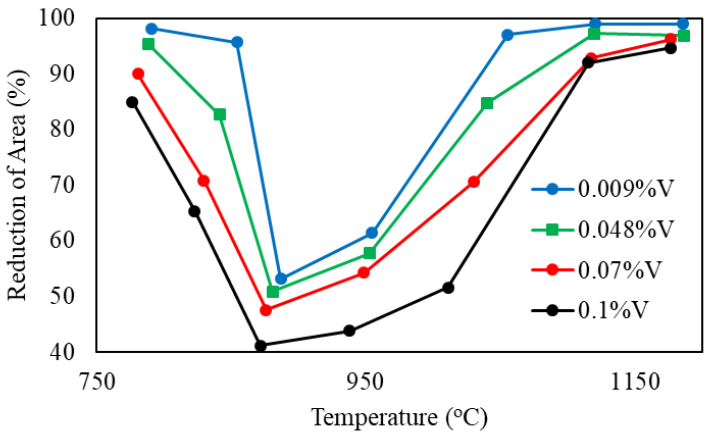

Figure 2-35 Influence of V content on the hot ductility of steel for the base composition: 0.1%C, 1.4%Mn, 0.3%Si, 0.003%S, 0.016%P, 0.03%Al and 0.005%N [141].

Mintz and Arrowsmith [143] have shown that V and Nb behave similarly except that V is less effective due to its high solubility in austenite. Although V is also a nitride forming element, formation of VN is often absent in the presence of Al or Ti as both elements have a higher chemical affinity for N leaving no N to combine with V. It was therefore recommended by Coleman and Wilcox [144] that the detrimental effect of VN could be minimised by the addition of Al to the composition.

The hot ductility of a medium carbon V-bearing steel, ~0.11 wt.%V, was assessed by Lee et al. [145], and showed excellent behaviour in the temperature range 950-1100°C (Figure 2-36). However, the hot ductility fell upon lowering temperature from 950 to 800°C which is above the Ae_3 temperature so the microstructure was fully austenitic. This behaviour was ascribed to V(C,N) precipitation at the austenite grain boundaries. These precipitates were found to be accompanied by precipitate free zones adjacent to austenite grain boundaries. These zones are weak and lead to stress concentration during deformation giving poor ductility. As mentioned earlier, V precipitation starts below 950°C so any improvement above this temperature can not be due to the vanadium addition.

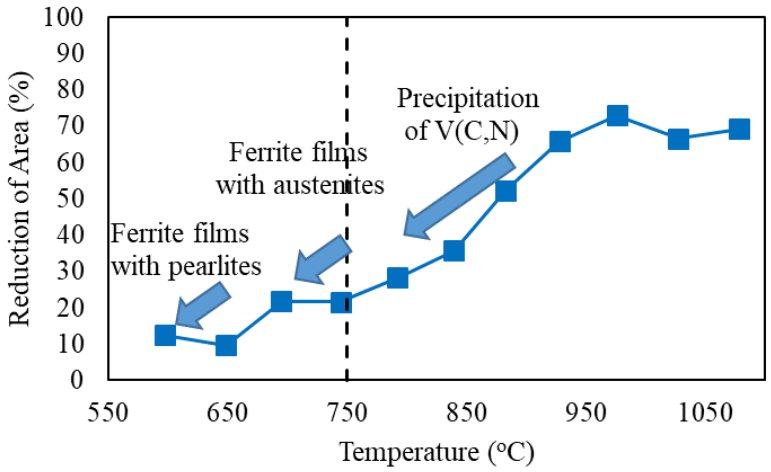

Figure 2-36 Hot ductility behaviour in a medium carbon steel containing vanadium for the base composition: 0.52%C,0.26%Si,1.0Mn,1.1Cr–0.11V–0.019Al [145].

Further examination by TEM at 850°C on the medium carbon steel with vanadium confirmed the presence of V(C,N) precipitates which acted as void nucleation sites at austenite grain boundaries (Figure 2-37). The rapid growth of these voids led to their coalescence and subsequently to intergranular fracture. More published work [141,146] also confirmed the deteriorating influence of V on the hot ductility of steel due to V(C,N) precipitation at austenite grain boundaries which could explain the promotion of grain boundary sliding and the formation of precipitate free zones. It is therefore recommended to straighten the continuous cast strand at temperatures as high as possible in the V-bearing steel to minimise the transverse cracking of the slab which could be caused by the V(C,N) precipitation at lower temperatures.

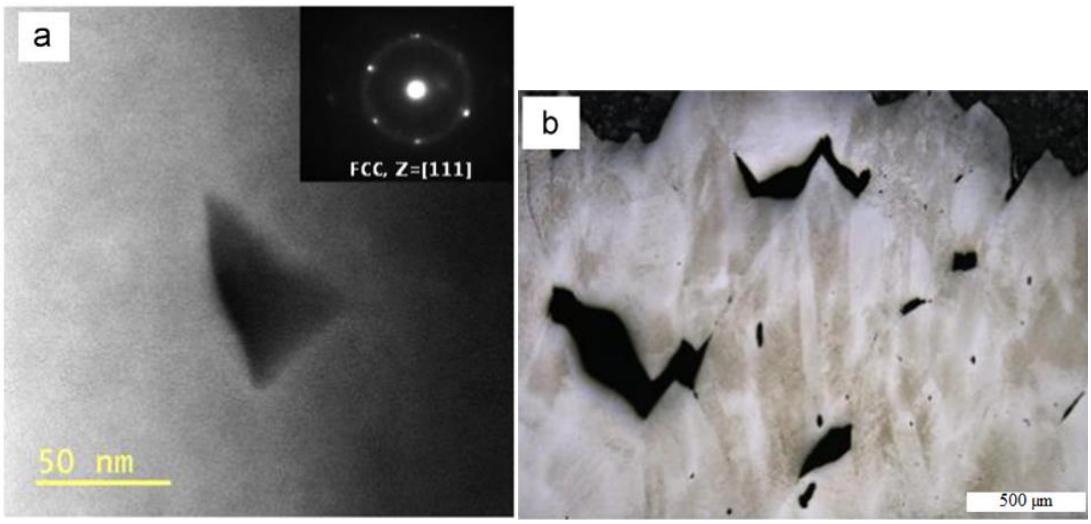

Figure 2-37 Void nucleation sites on V(C,N) precipitates at austenite grain boundaries (a) TEM micrograph, (b) optical micrograph of the fractured sample at 850°C for the base composition: 0.52%C,0.26%Si,1.0Mn,1.1Cr–0.11V–0.019Al [145].

2.4.7 Boron

It has been proved that the detrimental effect of S and P on hot ductility can be prevented by the addition of boron (B), which segregates preferentially to the boundaries and strengthens them [147,148].

The effectiveness of B in improving hot ductility of steel depends mainly on the amount of Ti, and N in the composition as well as the cooling rate as reported by Kang et al. [146] in a TWIP steel containing 0.0025%B. The beneficial influence of B on hot ductility depends on how easily B can segregate to the boundaries and its ability to strengthen them. However, since B is a nitride forming element, it combines with N to form BN which weakens the boundaries leading to poor hot ductility [85]. AlN is in fact more stable than BN but because of boron's smaller atomic size, it diffuses faster to form BN at the expense of AlN [99]. Other compounds such as $Fe_{23}(B,C)_6$ and B_4C can also form but they are less detrimental to hot ductility in comparison to boron-nitride compounds [149]. These particles are coarser and accumulate preferably on MnS and TiN particles and can be found in the matrix and grain boundaries of austenite while their volume fraction increases with the increase of boron content [20]. Therefore, strong nitride forming elements are desired to gain the full potential of B in improving hot ductility [150]. Ti additions allow all the N to combine with Ti to form one of the most thermodynamically stable nitrides [151]. Therefore, BN precipitation is avoided, leaving B to segregate solely to the boundaries and so improve hot ductility, as observed in previous studies [152,153]. In this case, the amount of Ti must be higher than the stoichiometric ratio for TiN of 3.4 (i.e.Ti:N ratio $\geq$ 3.4) [154]. Segregation of B was observed throughout the temperature range 700-1200°C [123], so resulting in a better hot ductility throughout most of this temperature range (Figure 2-38).

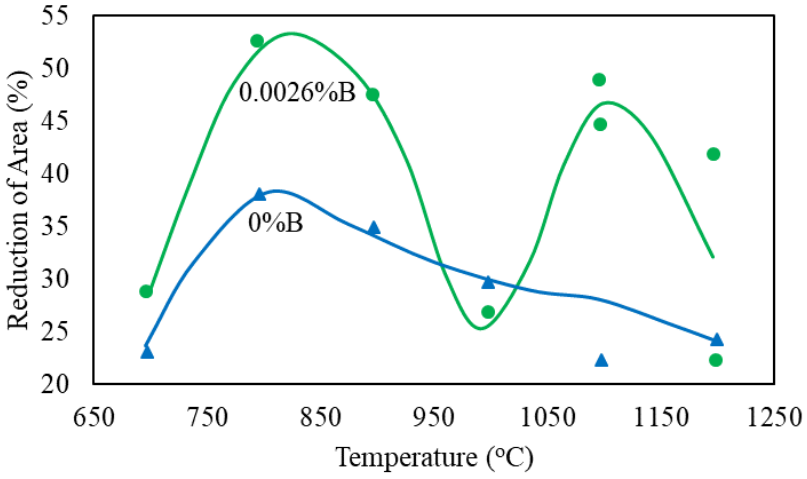

Figure 2-38 Hot ductility of Ti-bearing TWIP steels compared with a similar B-free steel for the base composition: 0.6%C, 18.3%Mn, 0.2%Si, 0.02%P, 1.5%Al and 0.008%N [146].

Chown and Cornish [85] reported that increasing B:N ratio from 0.19 to 0.47% improved the hot ductility in the austenitic phase of a microalloyed steel containing Al. Further improvement was obtained by increasing the B:N ratio to 0.74%, which completely eliminated the hot ductility trough. The poor hot ductility at the low B:N ratio of 0.19 was attributed to the "fine" precipitation of AlN at the grain boundaries and was exacerbated by precipitation of fine (Cu,Fe,Mn)S. Higher B:N ratios minimised the formation of the fine (Cu,Fe,Mn)S precipitates by encouraging co-precipitation of Cu_xS with coarse BN.

The role of cooling rate (18 – 180°C min^{-1}) was also examined as a function of B:N ratio. Generally, in the slower cooling rate range (18 - 72°C min^{-1}), typically experienced by thick slab and bloom, a low B:N ratio of 0.47 was adequate to avoid a ductility trough. However, to avoid the trough, a higher B:N ratio of 0.75 was essential at the high cooling rate of 180°C min^{-1}, associated with thin slab and billet casting [85].

Yamamoto et al. [61] observed that reducing the cooling rate from 20 to 0.1°C/s moved BN precipitation from austenite grain boundaries to within the grain interiors and the nuclei of the MnS inclusions. The worst scenario for good hot ductility in B-bearing steels is the absence of Ti accompanied by the use of fast cooling rates. This induces fine BN precipitation, so reducing the interparticle spacing and allowing cracks to interlink more rapidly, promoting intergranular failure due to microvoid coalescence. This fine precipitation can delay dynamic recrystallisation through the pinning of grain boundaries or pinning of individual dislocations and hence increase the amount of grain boundary sliding [155].

Chipres et al. [156] have also analysed the effect of B contents (0.0029-0.0105wt.%) on the hot ductility of microalloyed steel. Generally, hot ductility improved by increasing the B content due to segregation of boron at austenite grain boundaries, which could give higher resistance to grain boundary sliding [157,158].

B segregation near the boundaries starts at high temperature, when grain boundary sliding is also taking place [157,158]. The detrimental effect of grain boundary sliding is minimised by this segregation so hot ductility improves [159]. Another study by Laha et al. [160] suggested that the hot ductility improvement given by B-bearing steels was due to precipitates in grain interiors and boundaries altering the character of the interface of matrix/precipitates and grain boundary/precipitates in such a way that hinder the formation of micro-cavities and decrease their growth rate significantly.

Mejia et al. [161] studied the hot ductility of a low carbon advanced high strength steels (AHSS) as a function of boron addition. They concluded that the addition of 0.0117%B enhanced the hot ductility significantly throughout the temperature range (650-1150°C) as shown in Figure 2-39.

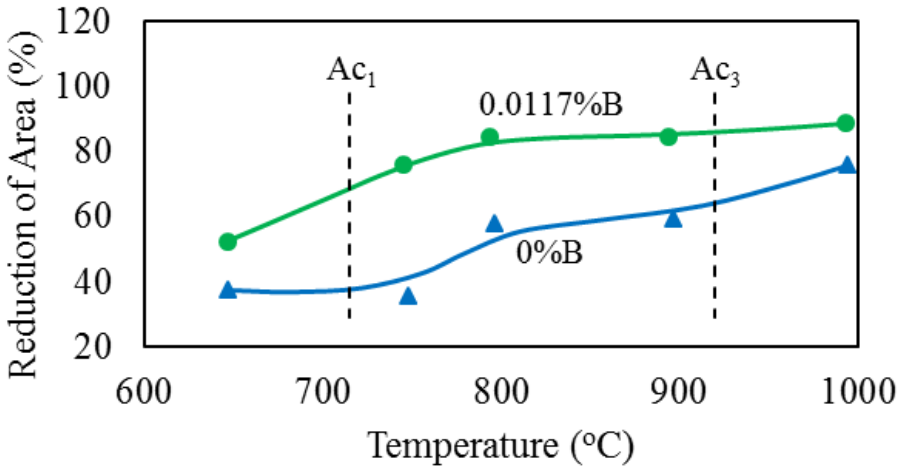

Figure 2-39 Hot ductility curves as a function of boron for the low carbon advanced high strength steels (AHSS) for the base composition: 0.06%C, 0.35%Mn, 0.3%Si, 2.2%Ni, 1.2%Cr, 0.5%Cu, 0.2%V and 0.006%N [161].

The improvement reached a maximum at 750°C but the improvement rate decreased at both temperature ends: low and high temperature ends. At the low-temperature end, this decrease was associated with the presence of inclusions and precipitates, particularly MnS and V(C, N) coupled with voids, which play an important role on the crack nucleation mechanism.

However, the hot ductility improvement at the high-temperature end was due to dynamic recrystallisation and the improvement rate declined due to the grain boundary sliding.

However, Chipres et al. [162] pointed out that B can delay the onset of dynamic recrystallisation without clarifying the cause but it is often observed that most alloying elements reduce the temperature for the start of dynamic recrystallisation. In addition, Lis et al. [149] have shown that boron nitride can supress dynamic recrystallisation of austenite during hot working. In contrast, Mejía et al. [163] pointed out that B and Ti (0.004 and 0.014wt.% respectively) can accelerate dynamic recrystallisation in TWIP steel at the intermediate temperature range (800-900°C) (Figure 2-40) with reduced cavity nucleation and growth during hot working. The finer recrystallised grains can reduce the stress concentration acting on grain boundaries and hence isolate crack propagation [164]. Indeed, stress concentration can weaken the grain boundary whereas at higher temperature, where grain boundary sliding takes place, both mechanisms severely enhance the development of cracks, therefore reducing the elongation to fracture [165].

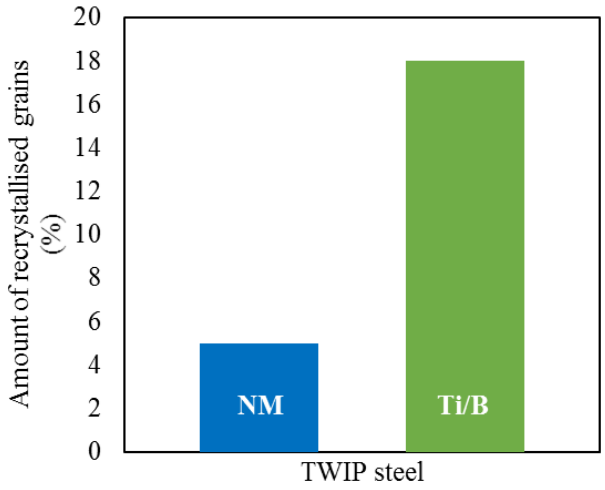

Figure 2-40 Volume fraction of recrystallised grains for not microalloyed (NM) and Ti/B alloyed TWIP steels. B and Ti are 0.004 and 0.014wt.%, respectively for the composition: 0.5%C, 22%Mn, 1.3%Si, 1.5%Al and 0.012%N [163].

However, Campbell [166,167] considered boron to be a beneficial element in reducing transverse cracking during casting through the inhibition of bifilm formation as boron has the capability to lower the melting temperature of the surface oxide in the liquid steel.

2.4.8 Phosphorus

Despite its ability to increase strength, phosphorus (P) is generally considered to be an undesirable impurity in steel as it can give brittle fractures for steels at room temperature.

Phosphorus is well known for its tendency to deteriorate hot ductility through its precipitation as the low melting point iron phosphide phase at grain boundaries which weakens their cohesion and promotes intergranular failure [168].

Segregation kinetics of P to the boundaries is often non-equilibrium and is dependent upon the structure as to whether the primary phase on solidification is austenite or ferrite, the former being more close packed, so more P will be rejected on solidification [169]. Since TWIP steel is austenitic and contains a high C content, it is not surprising that P segregation will always be more intense during solidification, giving more chance for the formation of the deleterious low melting point phosphide phase and this would be expected to be greater in as cast steel where segregation would be more intense.

Suzuki et al. [170] observed the detrimental effect of P only in the carbon steels having C contents higher than 0.25%. The segregation of P is very much influenced by the carbon content and above 0.25%, the melt solidifies as the close packed austenite phase and not the more open δ ferrite (Figure 2.1-23).

In the case of Suzuki et al.'s work, the detrimental effect of P on hot ductility was attributed to the precipitation of P along the dendritic interface which later moved to the austenite grain boundary. Based on these observations, it was recommended to employ a dephosphorisation technique in higher carbon steels to effectively increase hot ductility and produce defect free blooms or slabs on continuous casting. However, later work by Harada et al. [171] showed that intense microsegregation of P at the austenite grain boundaries can occur during solidification even in a low C bearing steel (0.1 - 0.2%C). In contrast, Mintz and Arrowsmith have reported that hot ductility improves in Nb containing HSLA steels by raising P addition from 0.01 to 0.02% in the temperature range (800-1000°C) [44]. The improvement was explained by suggesting that P needs vacant sites to be able to diffuse but Nb(CN) also requires the vacant sites for precipitation. Hence when Nb(CN) precipitates out it reduces the number of vacant sites and so reduces P segregation leading to better hot ductility [172].

However for higher P contents, the low melting point iron phosphide forms [173]. Mintz et al. [173] examined the influence of P contents in the range of 0.01-0.045% on the hot ductility of microalloyed Nb-bearing steel and showed that hot ductility was worse at the higher levels of P. Failure was found to be intergranular in all the P-bearing steels as a result of the formation of films of a low melting point P rich phase and the presence of Nb(CN) at the grain boundaries. Thicker and more continuous films were observed in the higher P containing steels. It is

believed that the P rich films contain the low melting point phase $Fe_3(Mn)P$ or Fe_3P, which solidify at low temperature ~950°C. Indeed, the slight improvement of hot ductility in the low P containing steel was justified by back diffusion of P during the holding time at high temperatures and the slow cooling rate used. More time was given for P to segregate back from the boundaries to the matrix and hence reduces the probability of crack formation and development along the grain boundaries. It was then recommended to restrict P content to 0.01% and slow down the cooling rate after solidification to prevent heterogeneous distribution of P.

These results are in agreement with those reported by Kang et al. [174] who examined the hot ductility of TWIP steel at various P contents (0.01-0.07%). They, observed that hot ductility generally deteriorates as the P content increases, which was accounted for by the segregation of P to the boundaries leading to the formation of the low melting point Fe(Mn) phosphide at the austenite grain boundaries.

Guo et al. [175] have also looked at the influence of P content (0.01-0.06%) on the hot ductility of low alloy steel and reported that the hot ductility trough was widened and deepened at the high P content throughout the temperature range 700-1200°C due to concentrated phosphorus segregation at the austenite grain boundaries.

Therefore, it can be concluded from literature that phosphorus is generally detrimental to hot ductility and should be minimised to the lowest possible level preferably ~0.01%.

2.4.9 Silicon

The information in the literature on the influence of silicon (Si) on the hot ductility of steel is very limited due to the fact that Si content in a typical steel is only in the narrow range of 0.02-0.5%, which is too low to cause any transverse cracking. Nevertheless, electrical steels contain a relatively higher level of Si, which can reach up to 3%, making it difficult to cast this type of steel without cracking [176].

Mintz et al. [176] showed that increasing Si level in a TRIP steel from 0.3 to 1.22% gives lower hot ductility even in the temperature range above Ae_3 in which the structure is fully austenitic (Figure 2-41).

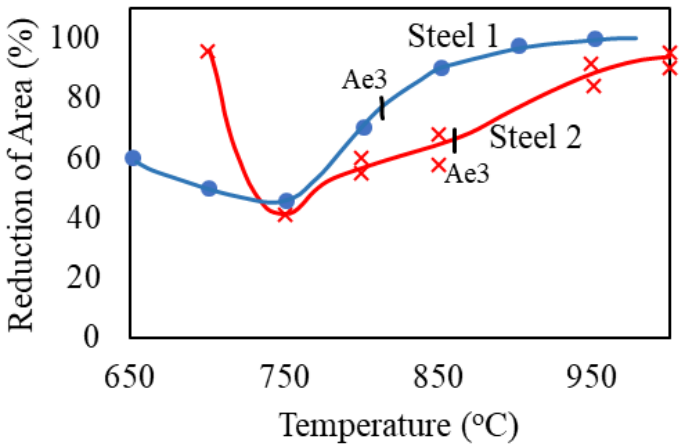

Figure 2-41 Effect of silicon on the hot ductility of C-Mn-Al steel, steel 1 has 0.3%Si and steel 2 has 1.22%Si for the base composition: 0.15%C, 1.45%Mn, 0.30%Si, 0.008%S, 0.003%P, 0.02%Al and 0.06%N [176].

Maehara and Nagamichi [177] have studied the influence of Si on the hot ductility of low carbon steel with particular emphasis on the relationship with Al and N. Generally, increasing either Si or N had a negative effect on hot ductility (Figure 2-42) accompanied by intergranular fracture of austenite. This was attributed to the dynamically enhanced precipitation of the hexagonal close packed (hcp) (Si, Al)N on the austenite grain interiors and boundaries . In the absence of Al, silicon nitride was formed. However, it should be noted that once the N level was below 0.005%N, there is only a small deterioration in ductility (Figure 2-42(a)). In addition, precipitate free zones were present, adjacent to the austenite grain boundaries encouraging strain concentration and leading to microvoid formation and coalescence. In the light of the current work on TWIP steel, the amount of Si does not exceed 0.1% and hence any deleterious influence on hot ductility is minimised.

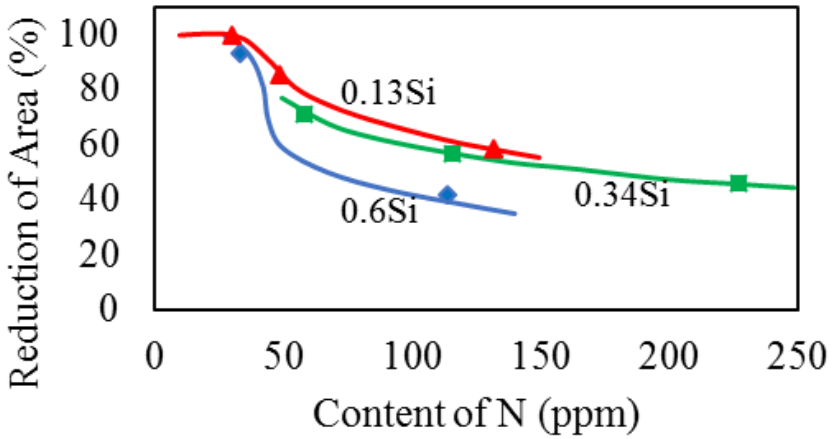

(a)

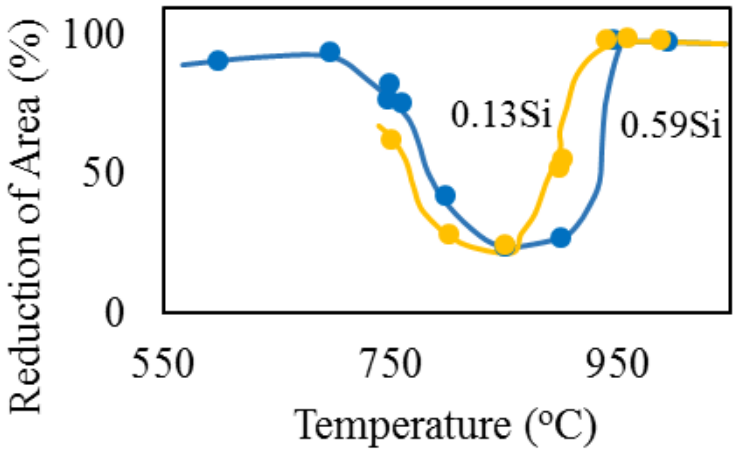

(b)

Figure 2-42 (a) Effect of silicon content on the hot ductility of C-Mn-Al steel, (b) effect of silicon content as a function of nitrogen content on the hot ductility of C-Mn-Al steel for the base composition: 0.1%C, 1.2%Mn, 0.01%P, 0.01%S, 0.03%Al and 0.005%N [177].

3 Literature review: Mechanical properties of hot rolled HSLA steel

3.1 Overview

The superior properties offered by HSLA steel over the former C-Mn steels make them popular in a variety of industrial applications. The most critical properties considered in engineering industry are lower yield strength and impact behaviour. An overview of the main characteristics of these steels and details of their types and their main strengthening mechanisms is illustrated in this section.

3.1.1 Characteristics of HSLA steel

The motivation to develop HSLA steel has been attributed to the following [178]:

- The production cost of HSLA steel is relatively low.
- Weight reduction requirements; especially for the automotive industry. The higher strength of HSLA steel makes it possible to reduce the thickness of steel plates used in vehicle production.
- In the past, higher ultimate tensile strengths in steel could be produced by increasing the carbon content but these steels were difficult to weld, which limited their use in many engineering applications, such as pipe-line which requires both a high yield-strength steel and good weldability. The lower carbon content of HSLA steel facilitates the welding process using the current and basic welding procedures.
- Microstructure and mechanical properties can be controlled easily and cheaply; strength can be enhanced through vanadium and niobium additions as both elements do not react with oxygen during the steel melt processing. These elements can combine with C and N forming nitrides and carbides which can strengthen the steel by grain refinement and precipitation hardening.

3.1.2 Types

HSLA steel can be classified into six main categories based on chemical composition, microstructure and properties [179,180]:

- Ferrite-pearlite steels which contain small amounts of nitride, carbide and carbonitride forming elements, ≤0.1wt.per.cent, for precipitation hardening and grain refinement.
- Pearlitic steels which contain higher contents of carbon to increase the volume fraction of pearlite in the microstructure, and so improve the strength and wear resistance.

- Acicular ferrite steels containing small amounts of carbon, ≤0.05%. The steel offers high yield strength, ~700MPa, good toughness, weldability and formability.
- Weathering steels, containing small additions of specific alloying elements, such as phosphorus and copper to enhance atmospheric corrosion resistance and solid-solution hardening.
- Dual-phase steel; the name indicates their mixed microstructures, which consists of martensite dispersed in a ferritic matrix. The steel has an excellent combination of high tensile strength due to the presence of martensite and good ductility due to the presence of ferrite in the microstructure.
- Inclusion-shape-controlled steels, containing small amounts of the rare-earth elements or titanium, zirconium and calcium in order to control the shape of the sulphide inclusions. The process aims to change sulphide inclusions shape from elongated stringers to small, dispersed, almost spherical globules to improve ductility and toughness.

3.1.3 Strengthening mechanisms

The strengthening mechanisms of HSLA steels can be classified into the following categories [178,179,181]:

- Solid-solution strengthening: dislocation movement during loading is impaired by the presence of interstitial and substitutional solute atoms in a crystal lattice. The resistance to dislocation movement depends on the solubility of the solute atoms of the alloying elements in the steel.
- Grain-boundary strengthening: grain boundaries are effective in obstructing dislocation movement. This leads to higher strengths and the finer grain size limits crack propagation, improving the impact behaviour. Therefore, a finer grain size will increase strength and toughness, simultaneously.
- Dislocation strengthening: the dislocation density on deformation increases as the load increases. Due to the high volume of dislocations induced during loading, dislocation movement is obstructed by other dislocations moving in the opposite direction. The efficiency of this mechanism is governed by the degree of saturation of the structure with dislocations.
- Precipitation strengthening: the high additions of carbide, nitride and sulphide forming elements leads to super-saturation of the solutes at high temperature. Consequently, second-phase particles precipitate out of solution on cooling to room

temperature and form at the matrix and grain boundary. The efficiency of these particles in improving strength depends on their characteristics, such as identity, size, location and volume fraction. However, precipitation must be carefully controlled so that the toughness is not impaired too much.

- Phase-transformation strengthening: steel passes through various phases during heating and cooling. The presence and amount of phases depends on the temperature and alloying composition. Each phase has its own properties. In case of equilibrium cooling of steel, the main phases present are austenite, ferrite and pearlite. The strengthening mechanism depends on the nature of the phases present and their volume fraction.

3.2 Rolling of HSLA steel

Many flat products are produced by rolling, meeting both requirements of reliability and cost effectiveness [182,183]. A typical rolling facility consists of a reheat furnace, sizing press, roughing mill, finishing mill for plate steel and for strip steel, used mainly for car bodies a run-out table and coiler (Figure 3-1) [184].

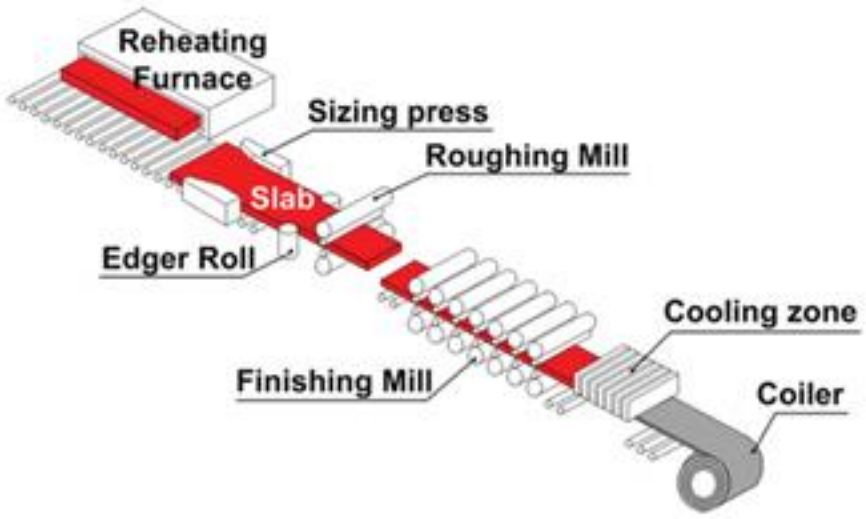

Figure 3-1 Schematic illustration of traditional hot rolling process [184].

The process starts by heating the ingot up to a high temperature in a furnace in order to dissolve all the alloying elements. The ingot is then transferred to the roughing mill which shapes the ingot into a conveniently shaped slab which can then be easily progressively hot rolled to the desired thickness. Due to the reactivity of steel with oxygen during rolling, an oxide scale usually forms on the outer surface of the steel. The rolled plate after cooling down to room

temperature has the scale removed. The cooling rate to room temperature after hot rolling can be optimised to achieve the desired microstructure.

Hot rolling is a simple process and it offers lower production cost in comparison with control rolling. However, microstructure, including grain growth and precipitation morphology, cannot be controlled during this rolling process. After casting the grain size is very coarse and the high finishing temperature approx. 950-1000°C ensures that the grain size remains coarse leading to poor strength and impact behaviour. Intergranular fracture is enhanced in coarse grained structures leading to hot surface cracking of slabs in some HSLA steels and subsequent difficulties when it comes to hot rolling them [185-187]. Because the finishing temperature is so high on hot rolling the resultant grain size is coarse and as such the mechanical properties are poor and this can also be accompanied by an in-complete breakdown of the as cast microstructure. Thus, controlling grain growth behaviour during processing is essential to achieve good hot ductility and the optimum mechanical properties. This can be achieved by control rolling where the finishing temperature can be in the range 800-900°C but not by hot rolling. However, control rolling although more economical requires more complex, advanced equipment and smaller companies cannot afford the initial outlay.

Globally, most small steelmakers still operate on the basis of traditional hot rolling and as already stated with this process, controlling microstructural evolutions during rolling is not possible resulting in poor mechanical properties [188]. In the most advanced control rolling technology, temperature during rolling is continuously controlled such that the austenite grain size is refined and the rolling is interrupted with a hold to allow the plate to attain a lower temperature during the rolling process. Moreover, phase transformation and its consequences such as precipitation behaviour are optimised during cooling of the slab [189]. The refinement of the austenite grain size gives higher area fraction of boundaries, which in turn increases the number of nucleation sites for ferrite grains during transformation. Consequently, the mechanical behaviour is enhanced due to the beneficial effect of the finer ferrite grains [190,191]. A typical schematic representation of various processes taking place during control rolling of C-Mn-Nb steels is illustrated in Figure 3-2.

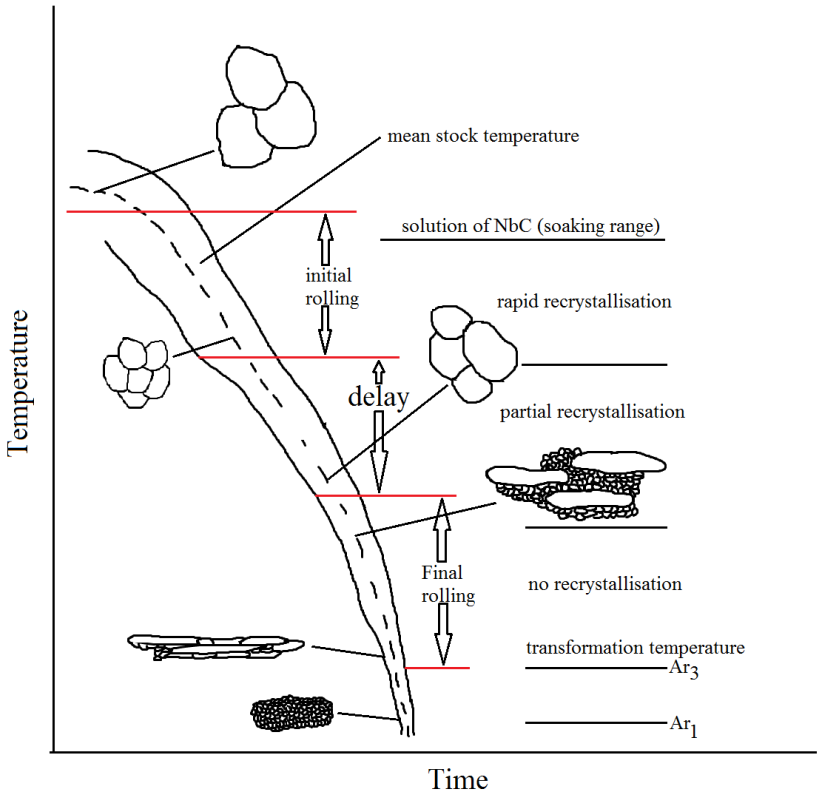

Figure 3-2 Schematic representation of various processes taking place during control rolling of C-Mn-Nb steels [192].

Control rolling normally ends at a temperature slightly higher than Ar_3 (the temperature at which austenite begins to transform to ferrite during cooling) or higher than Ar_1 (the temperature at which transformation of austenite to ferrite or to ferrite and cementite is completed during cooling) but lower than the austenite recrystallisation temperature, T_R. The degree of grain refinement depends on the amount of dislocations and slip bands (localised dislocation slipping in an individual grain) in non-recrystallised austenite [178,180,128]. A higher dislocation density and a greater number of slip bands results in an increase in the nucleation sites during the austenite to ferrite transformation, leading to finer ferrite grain structure [178,180,218]. More advanced control rolling techniques have been developed to better control the recrystallisation process. This is known as dynamic recrystallisation control rolling. In this process, the overall strain is higher with finish rolling while the deformation from pass to pass is accumulated. As a result, the critical strain required to induce dynamic recrystallisation is exceeded and hence a very fine grain size is obtained. Cooling rate in control rolling process generally depends on the desired microstructure. Air cooling is normally used after rolling to obtain ferrite-pearlite structures. However, accelerated rolling is utilised to refine the ferrite grain size and to enrich the rest of the matrix with non-equilibrium phases martensite and/or bainite [178,180,193].

3.3 Factors that influence the mechanical properties

3.3.1 Rolling strain rate

In the 1980s, the hot rolling of steels, such as by hot strip mills, utilised low rolling speeds so that the strain rate of several hundreds per second were attained [194]. As the production technology of metals has been developed over the last two decades, the hot rolling strain rate of a metal billet has considerably increased and can now take place at strain rates of 6000 per second [195]. In general, the strain rates for plate are much slower than for strip steel. As the rolling process starts in the roughing stage, the strain rate is low due to the high thickness of the plate but the strain rate will increase gradually at each pass as the plate becomes thinner until the final pass on the strip mill is attained. The start of the hot rolling range of strain rates is very high compared to that normally used in a tensile test and other laboratory tests are needed to simulate the rolling operation. In tensile tests, the strain rates go only up to a maximum of 1 per second during the test, only the start of the hot rolling range of strain rates and therefore other laboratory tests are needed to simulate the rolling operation. The most favoured has been torsion testing which has given similar results to that given by full scale rolling [196].

Furthermore, Carretero et al. [197] have shown using a Gleeble simulation hot torsion mode equipped with cooling bed and coiling simulation furnace allows not only accurate control of strains, inter-pass times, temperatures and cooling rates for HSLA pipeline steels but also gives enough material for microstructural examination and mechanical testing.

Nevertheless it has been suggested that laboratory hot rolling when possible still provides better simulation of processing constraints and deformation mechanisms than other thermo-mechanical simulators.

The strain rate used during rolling is also variable depending on the rolling temperature. In general higher temperatures enable higher strain rates to be used which in turn influences the austenite grain size and the final grain size and mechanical properties [198]. Suarez et al. [199] applied different strain rates (1 – 8 s^{-1}) in the control rolling of microalloyed steel in the temperature range (1250-900°C) to monitor changes in grain size refinement. Higher strain rates were found to be beneficial in refining the ferrite and bainite grain size, in which the size was refined from 12 to 4μm as the strain rate increased from 1 to 8 s^{-1}. Consequently, both ultimate tensile strength and yield strength showed a gradual improvement while toughness and elongation slightly deteriorated. The improvement was ascribed to grain size refinement

and dislocation hardening. In addition, precipitation strengthening was considerably enhanced at higher strain rates through promoting strain induced precipitation of NbC(N) throughout the matrix and grain boundaries. In addition, the work showed a small increase in both ultimate tensile strength (R_m) and yield strength ($R_{p0.2}$), but a significant drop in impact energy was observed as a function strain rate as presented in Figure 3-3 (a,b). Other work [200] emphasised that it is necessary to dissolve all the NbC(N) during re-heating stage for the best results. Thereafter, NbC(N) precipitation must be precisely controlled during rolling and cooling stages in order to obtain the full potential of the control rolling process and Nb precipitation [200].

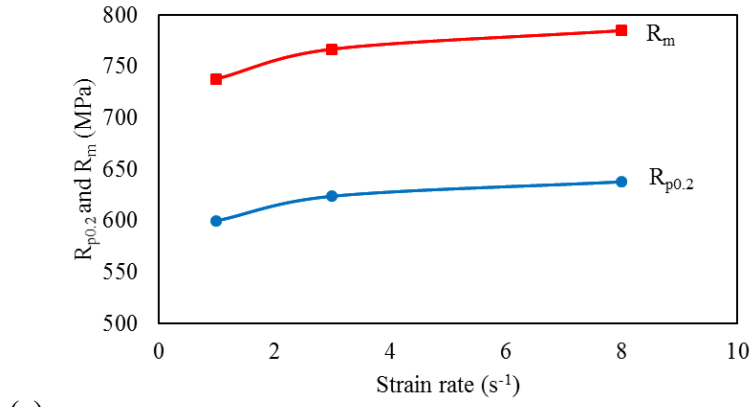

(a)

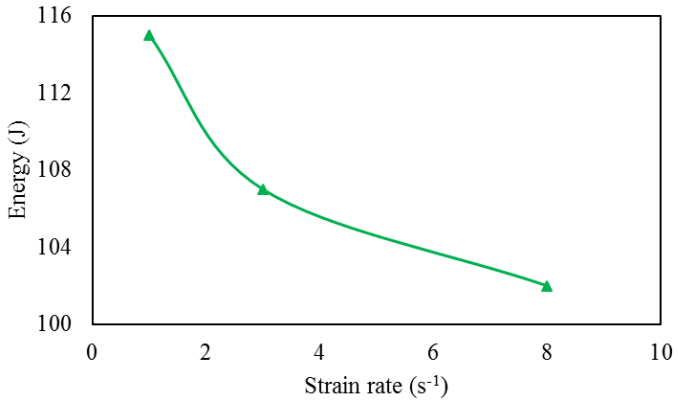

(b)

Figure 3-3 Mechanical properties of control rolled microalloyed steel as a function of strain rate (a) ultimate tensile strength (R_m) and yield strength ($Rp_{0.2}$), (b) Charpy Impact energy for the base composition; 0.044%C, 1.69%Mn, 0.271%Si, 0.0091%P, 0.0016%S, 0.240%Ni, 0.2170%Cu, 0.25%Mo, 0.0310%Al, 0.0554%Nb and 0.014%Ti [200].

Nwachukwu et al. [201] investigated various rolling process parameters on the mechanical performance of hot rolled HSLA steel (St60Mn grade). Rolling strain rate was found to play a critical role in controlling mechanical properties, such as Young's modulus, hardness, elongation, bendability as well as yield strength. Yield strength improved almost steadily on increasing the strain rate from 6.02851 * 10^3 to 6.10388 * 10^3 s^{-1} while toughness deteriorated as shown in Figure 3-4 (a,b). This deterioration was attributed to the presence of internal

stresses, non-uniform dislocation structures and second phase particles which led to coarser grain size and high amount of slippage and as the temperature went up, the grains coarsened and the slippage increased continuously [201].

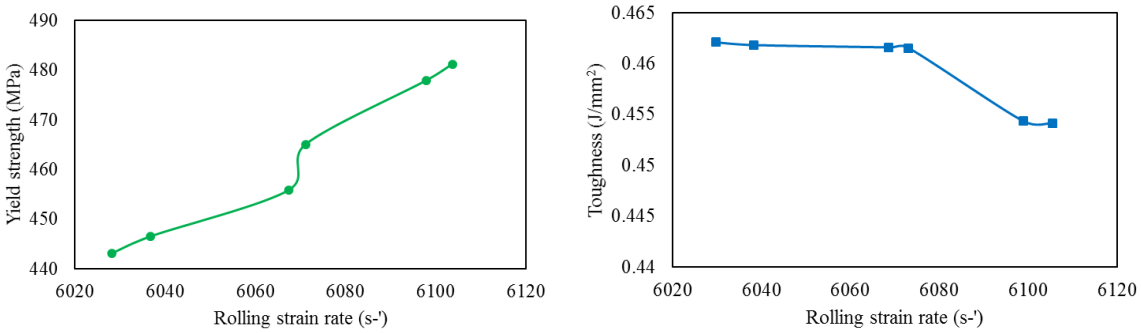

Figure 3-4 Rolling strain rate of hot rolled HSLA steel (St60Mn grade) versus (a) yield strength, (b) toughness for the composition; 0.41%C, 1.12%Mn, 0.24%Si, 0.021%P, 0.008%S, 0.02%Cr, 0.03%Ni, 0.03%Cu and 0.010%N [201].

Similar behaviour was observed by Han et al. [202] who examined the influence of strain rate ($0.0001\text{-}0.01s^{-1}$) at room temperature on the yield strength of a HSLA steel after rolling. They observed a slight increase in the strength as a function of strain rate (Figure 3-5). Generally, the influence of strain rate on the flow stress of metals is not substantial at low temperature but becomes more pronounced as the temperature increases [203].

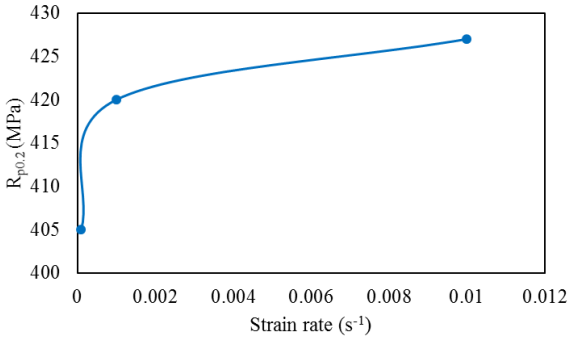

Figure 3-5 Room temperature Yield strength of hot rolled HSLA steel as a function of strain rate for the composition; 0.062%C, 1.2%Mn, 0.020%Si, 0.018%P, 0.006%S, 0.022%Cr, 0.048%Ni, 0.094%Cu, 0.026%Al, 0.008%Ti, 0.003%V and 0.009%N [202].

3.3.2 Strain-induced precipitation

It is well established that carbide and nitride forming elements such as Nb precipitate at the grain boundaries to give grain refinement by inhibiting growth of austenite, leading to a fine microstructure at room temperature [204]. In order to obtain the full potential of these microalloying elements for grain refinement, the control rolling process is used so as to increase the number of nucleation sites and so promote "strain-induced precipitation" [205].

Hong et al. [205] performed hot deformation tests on Nb-bearing HSLA steel (0.085%C and 0.047%Nb) at a strain rate of 10 s^{-1} and observed that strain-induced precipitation started immediately with the test and continued for approximately 16 minutes (Figure 3-6).

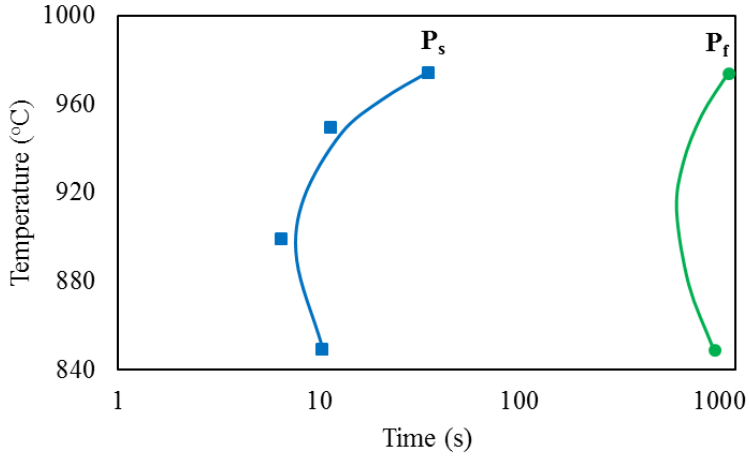

Figure 3-6 The precipitation-time-temperature (PTT) diagram showing the range of strain-induced precipitation of Nb-bearing HSLA steel at a strain rate of 10 s^{-1} with the composition; 0.085%C, 0.30%Si, 1.5%Mn, 0.012%P, 0.003%S, 0.023%Al, 0.047%Nb and 0.004%N, where P_s and P_f donate the start and finish time of the strain-induced precipitation, respectively [205].

Cao et al. [206] examined the influence of Nb content (0.078-0.130%) on strain-induced precipitation behaviour of HSLA steel under various deformation temperatures (925-1000°C). During the re-heating stage, it was observed that Nb did not completely dissolve into the solution in the high Nb-bearing steels. The remaining undissolved Nb precipitates acted as heterogeneous nucleation sites for the strain-induced precipitates. Strain-induced precipitates formed faster at the deformation temperature of 975°C (Figure 3-7). The start time of strain-induced precipitation was found to depend mainly on the supersaturated Nb content (the difference between the dissolved Nb after soaking and the dissolved Nb during deformation at a specific temperature). Higher contents of supersaturated Nb could promote the precipitation process at shorter time, meaning that higher Nb addition can promote strain-induced precipitation, and this effect became more pronounced as temperature continued decreasing (Figure 3-7). However, a high carbon content ≥0.13%C was found to delay the strain-induced precipitation even in the high Nb-bearing steel (Figure 3-7). This is due to the fact that C content can influence the dissolution of NbC(N) during the re-heating process, which affects the kinetics of dissolved Nb and undissolved carbonitride on precipitation [207]. It was also confirmed that the strain-induced precipitates have a stronger effect in delaying static recrystallisation than the solid solution of Nb atoms. However, this effect becomes much

weaker as the size of precipitates gets coarser [206]. In addition, the solubility of NbCN is higher at high soaking temperature, but it decreases as the holding time and deformation increases at lower temperatures, in which the supersaturated Nb will precipitate as NbC and NbC(N).

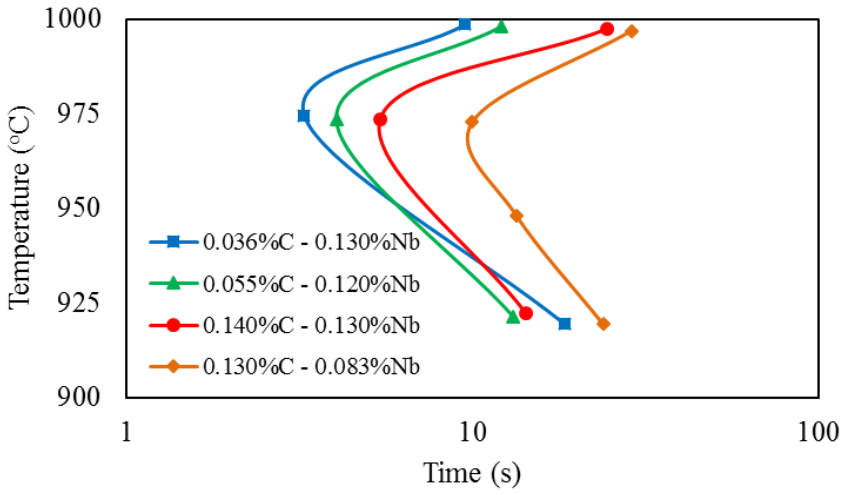

Figure 3-7 The start time of strain-induced precipitation of Nb-bearing HSLA steel at different contents of C and Nb with the base composition; 0.27%Si, 1.7%Mn, 0.014%P, 0.005%S, 0.015%Ti and 0.003%N [206].

3.3.3 Processing Temperature

Temperature is considered as an important factor in controlling the kinetics of metallurgical phenomena during rolling process of HSLA steel, as, for example dynamic recrystallisation is mainly influenced by temperature. Moreover, higher temperatures encourage steel softening during the work hardening effect of rolling so that brittle fracture due to rolling forces is prevented [208,209]. Previous work [210] reported that soaking temperature, drafting schedule, finish rolling and coiling temperatures have major effects in processing of low carbon steel. The main parameters that are influenced are austenitisation, precipitation and recrystallisation behaviour, which strongly affect the final microstructures based on these processes and the way they interact with each other. Therefore, thermal variations can control the microstructural changes and this determines the mechanical behaviour of the final product [208,209].

Finish rolling temperature (FRT)

The final pass during rolling is considered to be the critical step for improving the yield strength and toughness of microalloyed pipelines steels used in the oil and gas industry [211,212]. Therefore, the finish rolling temperature specified depends on chemical composition and desired mechanical properties [210]. Balogun et al. [213] have compared various ranges of

finish rolling temperatures (FRTs) for a conventional microalloyed hot rolled steel. The results showed that the higher the finish rolling temperature is, the lower is the yield strength. In particular, they observed that the optimum mechanical behaviour was achieved within 840 to 860˚C FRT for the steel examined (Figure 3-8). It was also pointed out that FRT is far more important than the temperature at the roughing stand in influencing mechanical properties [214].

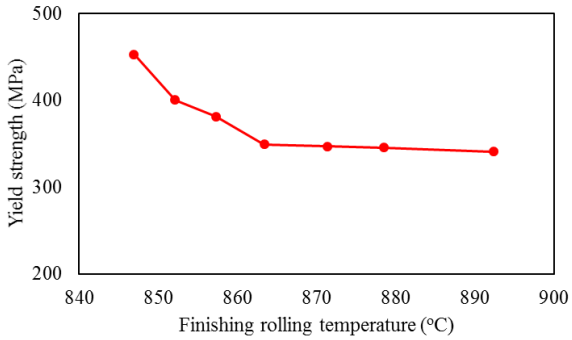

Figure 3-8 The influence of FRT on yield strength of hot rolled HSLA steel with the composition: 0.21 to 0.23%C, 0.20 to 0.25%Si and 0.50 to 0.60%Mn [213].

The previous study is in agreement with recent work by Nwachukwu and Oluwole [201] who investigated the influence of FRT on both yield strength and toughness. The lower the FRT the higher was the yield strength and the better the fracture behaviour. Both properties in HSLA steel (St60Mn grade) at various strain rates are presented in Figure 3-9. Generally, $\gamma \rightarrow \alpha$ transformation should start near the end or immediately after FRT in order to obtain the finest grain size and more homogeneous distribution of ferrite-pearlite phases [215]. However, controlling the FRT is not simple as it is governed mainly by the duration of each rolling cycle and the extent and type of in-process cooling procedure [213].

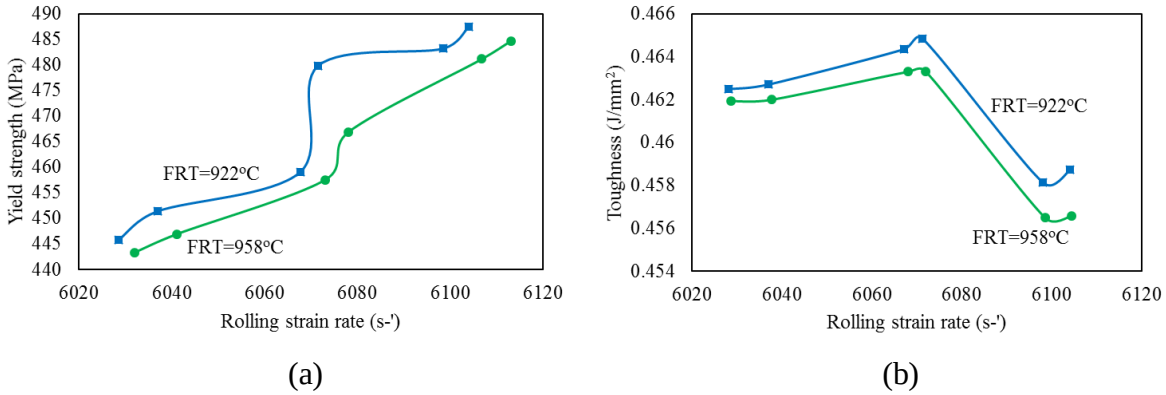

Figure 3-9 The influence of FRT on the mechanical properties of HSLA steel: (a) yield strength, (b) toughness for the composition; 0.41%C, 1.12%Mn, 0.24%Si, 0.021%P, 0.008%S, 0.02%Cr, 0.03%Ni, 0.03%Cu and 0.010%N [201].

Panigrahi [210] provided a more detailed study on the effect of FRT on microstructure and mechanical properties of steel. The study classified FRT into five different categories based on phases present and recrystallisation kinetics. The five FRT categories are: (a) FRT in recrystallised austenite region, (b) FRT in unrecrystallised austenite region, (c) FRT in the middle of recrystallised and unrecrystallised austenite regions, (d) FRT in austenite- ferrite region and (e) FRT in ferrite region.

(a) FRT in the recrystallised austenite region produces a fully recrystallised austenitic structure, which upon transformation provides a recrystallised ferritic structure. Ferrite nucleates on austenite grain boundaries and its grain size depends on the former recrystallised austenitic grain size and the subsequent cooling rate from FRT. The average ferrite grain size, dα, can be estimated using *Equation 6* [210]:

Equation 6

$$d_\alpha = 3.75 + 0.18\, d_\gamma + 1 \times 4\, (dT/dt)^{-1/2}$$

where d_γ represents recrystallised austenite grain size in μm and dT/dt is the average cooling rate in °C s^{-1}.

(b) FRT in unrecrystallised austenite region, which provides elongated austenitic structure with twins and deformation bands in microalloyed steel. Deformation bands form on inhomogeneities which block dislocations on numerous adjacent slip lines resulting in the lateral growth of the band. Therefore, ferrite nucleates intensively on twins and deformation bands as well as the austenite grain boundaries. In microalloyed steel, twins and deformation bands can form when reduction per rolling pass is above 20% in the unrecrystallised austenite region. Hence, finer ferrite grains are obtained in microalloyed steel due to the various nucleation sites available for ferrite upon transformation.

(c) FRT in the middle of recrystallised and unrecrystallised austenite regions, which produces mixed ferrite grain sizes. The mixed ferrite grain sizes, which is caused by inhomogeneous deformation of austenite grains, leads to poor impact toughness.

(d) FRT in austenite- ferrite region provides a mixture of ferrite and pearlite structures. Ferrite can be classified into two types; soft ferrite (recrystallised ferrite) and deformed ferrite (which may recover or recrystallise). As the temperature drops below Ar_3 (the temperature at which austenite begins to transform to ferrite during cooling), ferrite starts nucleating on the austenite grain boundaries. Deformation occurring in the two phase (α+γ) region encourages strain hardening of austenite and ferrite grains. Ferrite nucleates on the deformed austenite grain

boundaries and also on dislocations within the austenite matrix. The strain hardened ferrite can recrystallise to finer grains or can either remain in unrecovered or recovered state. This depends on the chemical composition, temperature and percent reduction per rolling pass. In microalloyed steel, the microalloying elements can retard recrystallisation through stabilising the sub-structure. The growth of newly formed ferrite grains, which grow on austenite grain boundaries, will be hindered by sub-grain boundary walls. Toughness behaviour will depend on the degree of recrystallisation and recovery. Recrystallisation will improve toughness due to the fact that fine ferrite structure is characterised by high angle grain boundaries. Recovery will improve toughness but the presence of too much strain hardened ferrite will lead to a deterioration.

(e) FRT in ferrite region, finish rolling at these temperatures (600-800°C) will increase roll wear, energy consumption. Dynamic recrystallisation is difficult in the ferrite phase. The produced slabs have high elongation and high anisotropy but very low yield strength, typically 180-250MPa.

Re-heating holding time

Gong et al. [216] investigated the influence of holding time (0-100s) during re-heating at 1200°C of HSLA on Nb and Nb-Ti bearing steels (0.03%Nb and 0.02%Ti). The study considered the Nb dissolution kinetics in austenite, and followed precipitation behaviour and grain size evolution. The austenite grain size was found to continue growing steadily with the holding time in the Nb-bearing steel as shown in Figure 3-10 (a). This was explained by a reduction in the pinning effect of NbC and Nb(C,N) on the grain boundaries due to the fact that Nb continually dissolved into the austenite during re-heating (Figure 3-10 (b)), so giving fewer Nb precipitates to pin the boundaries (Figure 3-10 (c)). It is worth mentioning that the rate of grain size coarsening in the Nb-bearing steel was higher than the Nb-Ti-bearing steel (Figure 3-10 (a)). This was attributed to the lower stability of NbC and Nb(C,N) in comparison with the (Ti,Nb)C and (Ti,Nb)(C,N). At the holding time of 100s, most of the Nb has been dissolved into the solution in the Nb-bearing steel while this is not so for the Nb-Ti-bearing steel (Figure 3-10 (b,c)). The re-heating temperature of 1200°C exceeds the equilibrium dissolution temperature of both Nb and C in the Nb-bearing steel which is far lower than the equilibrium dissolution temperature of TiN [217]. Therefore, titanium is often added to HSLA steel to enhance toughness.

Therefore, the addition of Ti in Nb-bearing steel increases the thermodynamic stability of the Nb(CN), thus suppressing the kinetics of dissolution. Furthermore, the size of the Nb precipitates is relevant to the Nb content in solution, the higher amount of Nb dissolved in the solution leading to smaller precipitate size (Figure 3-10 (b,d)).

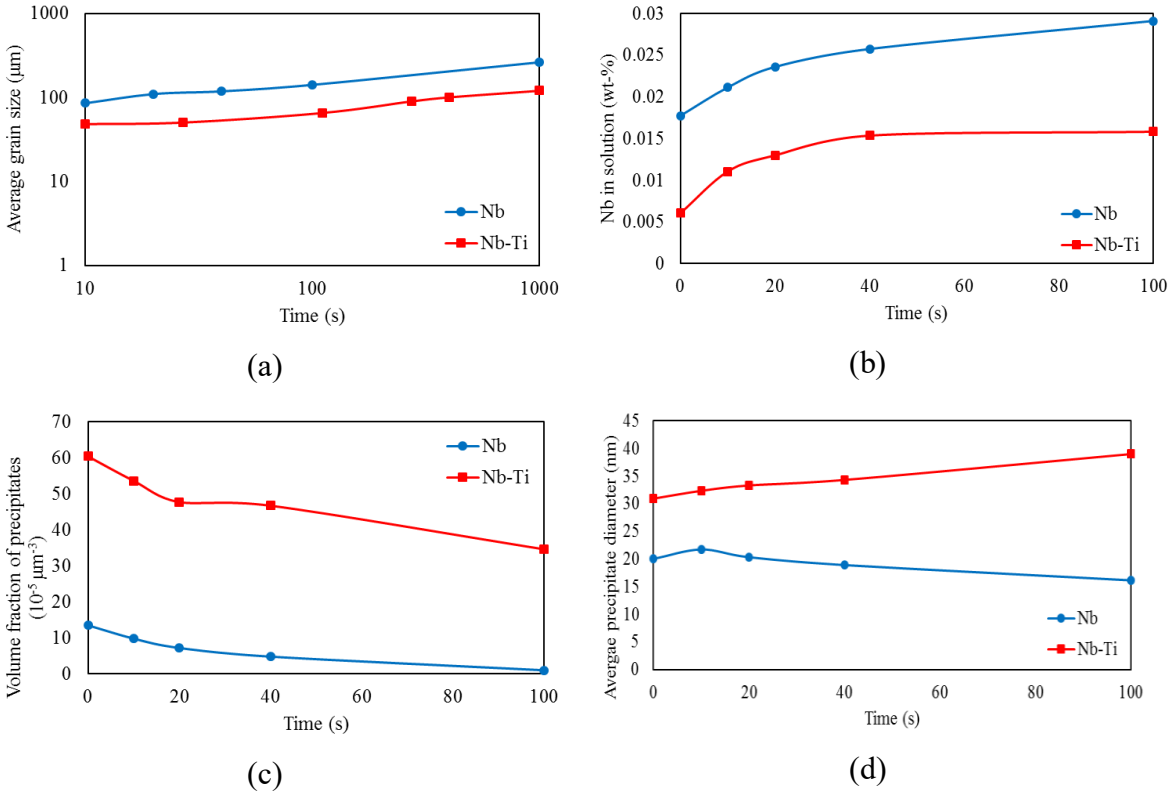

Figure 3-10 Data from carbon extraction replicas results in the Nb and Nb–Ti steels presenting the (a) grain size, (b) amount of Nb in solution, (c) volume fraction of precipitates and (d) diameter of precipitates, under different holding times (0-100s) at 1200°C in HSLA steel with the base composition: 0.06%C, 0.77%Mn, 0.03%Nb, 0.11%Si, 0.016%P and 0.006%N, an additional 0.02%Ti wad added to the Nb-Ti steel[216].

3.3.4 Cooling rate

Mechanical properties of steel are optimised through modifying the alloying composition. The improvement of these properties are obtained mainly through grain refinement and precipitation hardening. Both mechanisms are controlled by cooling rate which in turn influences the microstructure and the precipitation kinetics. Currently, there is a strong interest in the role of cooling rate in controlling the microstructure and mechanical behaviour of industrial processed steel [218]. Therefore, there have been extensive research work aimed at understanding the relationship between cooling rate, microstructure and mechanical properties.

Previous work [219] investigated the influence of cooling rate (180-900°C min^{-1}) on the microstructure and mechanical behaviour of a commercial microalloyed forging steel

(30MSV6). During rolling after cooling at 180°C min^{-1}, the as-received ferrite-pearlite microstructure changed to acicular ferrite (Figure 3-11 (a)). As the cooling rate increased (420-900°C min^{-1}), the acicular ferrite microstructure was replaced by bainite and martensite microstructures (Figure 3-11 (b,c)).

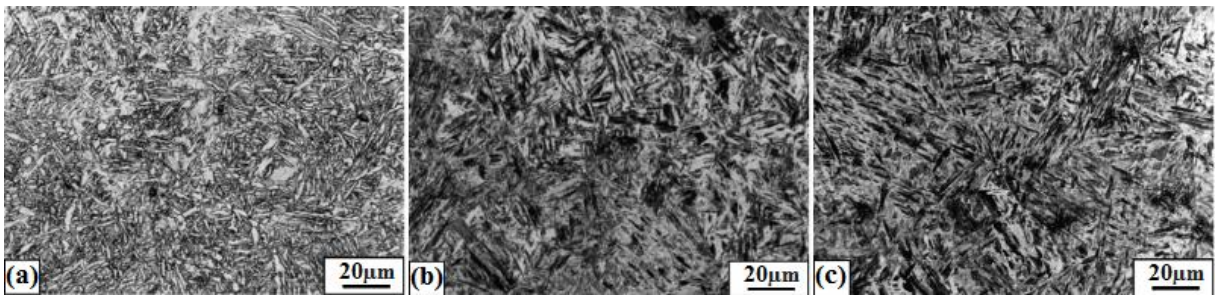

Figure 3-11 Microstructures of samples of a microalloyed steel at different cooling rates (a) 180°C min-1, (b) 420°C min^{-1} and (c) 900°C min^{-1}, for the composition: 0.3%C, 1.54%Mn, 0.54%Si, 0.011%P, 0.079%S, 0.22%Cr, 0.08%Ni, 0.23%Cu, 0.01%Mo, 0.016%Al, 0.017%Ti and 0.013%N [219].

The yield strength and ultimate tensile strength were found to increase steadily with increased cooling rate as shown in Figure 3-12 (a). However, both elongation and toughness deteriorated gradually as the cooling rate increased (Figure 3-12 (b,c)). The improvement in strength and deterioration in toughness were attributed to the formation of brittle phases; bainite and martensite, whose formation enhances strength at the expense of ductility and impact behaviour.

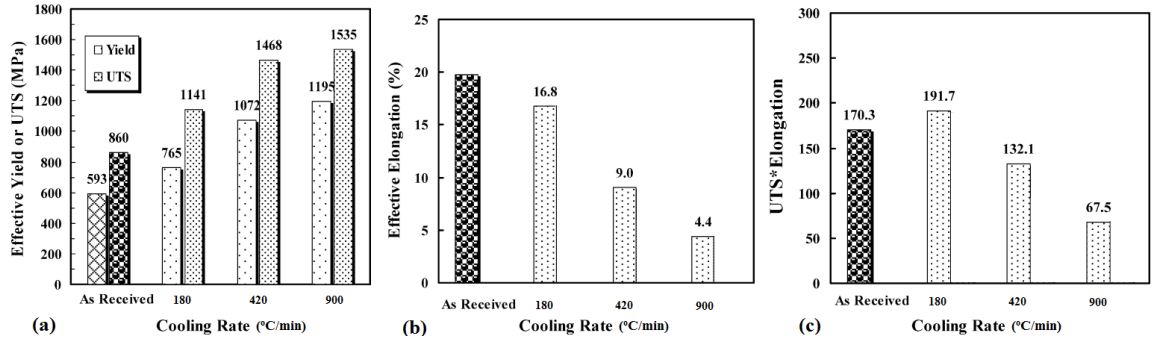

Figure 3-12 Effect of cooling rate on (a) yield strength and ultimate tensile strength, (b) elongation and (c) toughness, represented by the product of ultimate tensile strength by elongation for the composition: 0.3%C, 1.54%Mn, 0.54%Si, 0.011%P, 0.079%S, 0.22%Cr, 0.08%Ni, 0.23%Cu, 0.01%Mo, 0.016%Al, 0.017%Ti and 0.013%N [219].

Ceschini et al. [220] studied the strength and impact behaviour of a microalloyed carbon steel as a function of cooling rate (42 and 450°C min^{-1}), after hot rolling. They observed that the slower cooling rate led to a larger prior austenite grain size, ~24µm. In addition, the final microstructure was a mixture of pearlite surrounded by pro-eutectoid ferrite, which forms at

the boundaries of prior austenite grains, and bainite. The faster cooling rate refined the prior austenite grain size to ~17 µm and induced a mixed microstructure consisting of acicular ferrite and martensite. Interestingly, with the faster cooling rate, the steel showed an improvement in both properties; strength and impact toughness, simultaneously (Figure 3-13). The characteristics of inclusions such as size and distribution were found to be similar in both steels, so other microstructural features were considered for the interpretation. The higher impact toughness exhibited by the faster cooling rate steel was correlated to the refined microstructure and more importantly to the formation of acicular ferrite. This acicular ferrite nucleates intragranularly with a random orientation, which deflects the path of crack propagation and hence increases the resistance to crack propagation [221], leading to improved strength and toughness.

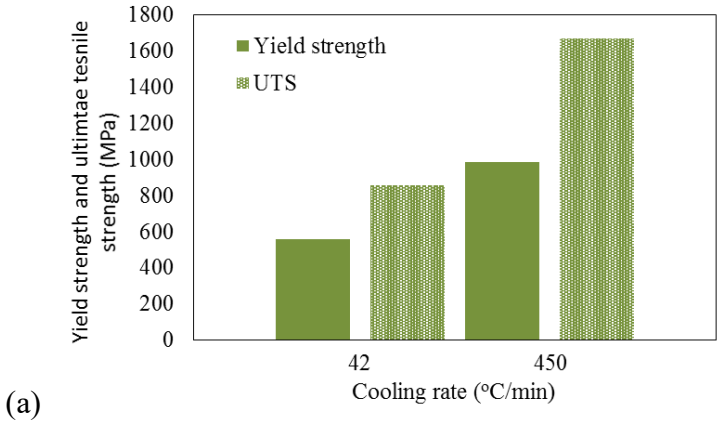

(a)

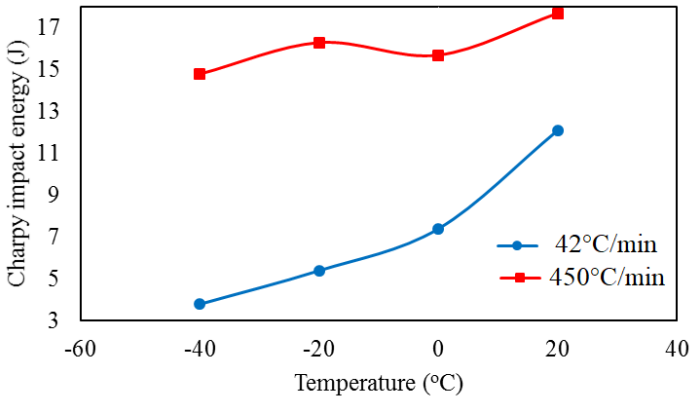

(b)

Figure 3-13 Influence of cooling rate on (a) yield strength and ultimate tensile strength, (b) Charpy impact energy for the chemical composition: 0.33%C, 1.55%Mn, 0.25%Si, 0.007%P, 0.002%S, 0.35%Cr, 0.09%Ni, 0.018%Al, 0.018%Ti, 0.1%V and 0.0052%N [220].

Recent work by Equbal et al. [222] have noted that the cooling rate has a considerable influence on the microstructure and mechanical behaviour of a commercial medium carbon forging steel (AISI 1035 grade) at room temperature. The work utilised three different cooling techniques;

normal air cooling, ~18°C min^{-1}, forced air cooling, ~30°C $min^{-1}$and oil quenching, ~480°C min^{-1}. The microstructure was found to be ferrite-pearlite for all the cooling rates. However, the grain size and the volume fraction of phases varied dramatically with respect to cooling condition. A finer grain size was obtained by increasing the cooling rate (Figure 3-14 (a)), due to the fact that faster cooling rates lower the Ae_3 and Ae_1 transformation temperatures, and hence ferrite-pearlite grains have less time to grow [223]. Microstructural analysis indicated that the volume fraction of pearlite increases on increasing the cooling rate, at the expense of ferrite (Figure 3-14 (b)). This behaviour is normally correlated with the effect of cooling rate on the coalescence and growth rate of ferrites [220].

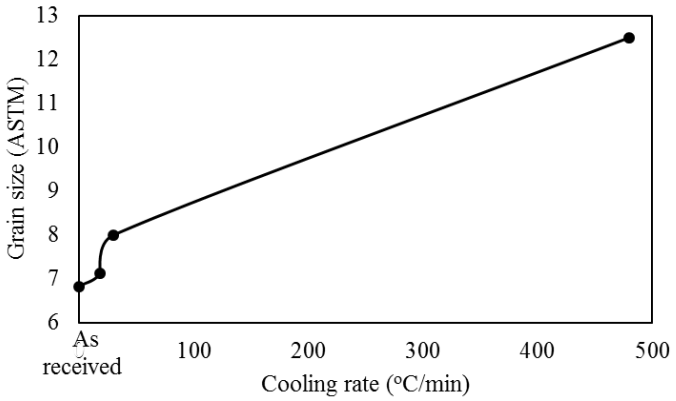

(a)

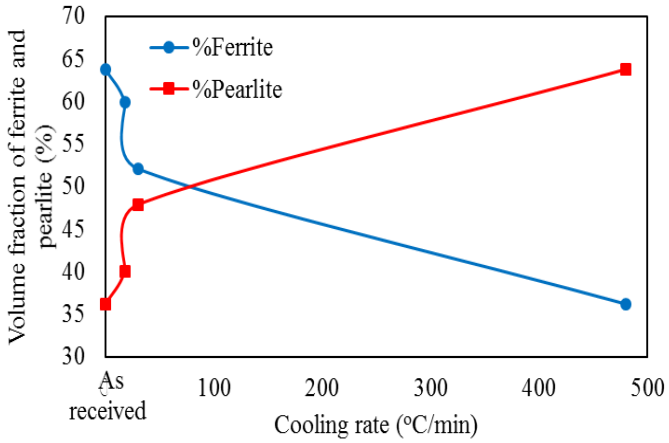

(b)

Figure 3-14 The effect of cooling rate on medium carbon forging steel as a function of (a) grain size, (b) ferrite and pearlite volume fraction for the following composition: 0.32%C, 0.79%Mn, 0.25%Si, 0.02%P, 0.01%S and 0.028%Al [222].

This microstructure variation accounts for the significant changes in strength and impact behaviour as shown in Figure 3-15. Faster cooling rates were anticipated to give higher yield strength and ultimate tensile strength (Figure 3-15 (a)). However, there is a corresponding deterioration in impact behaviour and percentage elongation as the cooling rate increases

(Figure 3-15 (b)), probably due to the formation of finer and harder phases leading to poor ductility.

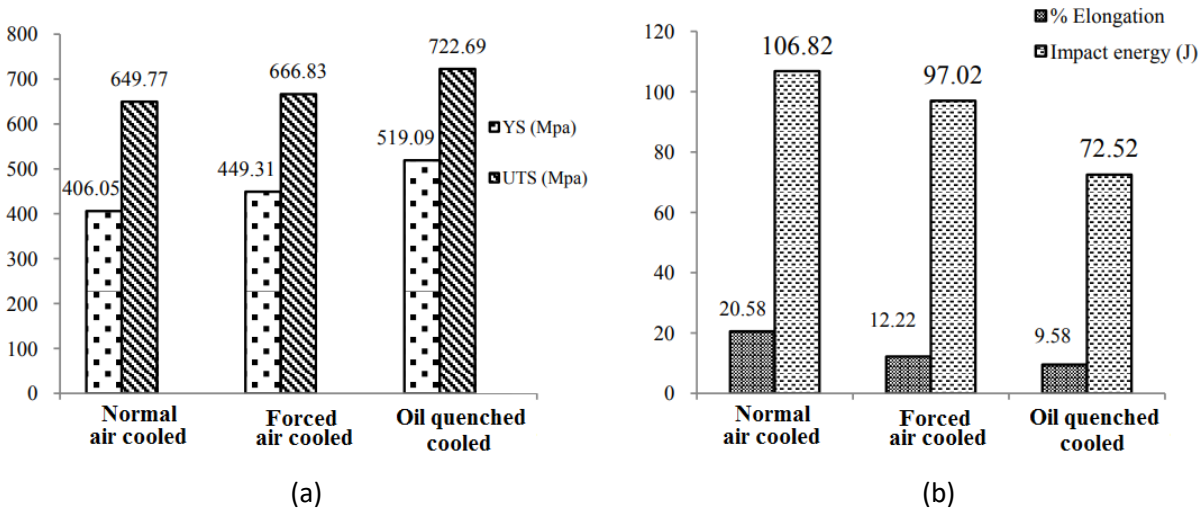

Figure 3-15 The effect of cooling rate on medium carbon forging steel as a function of (a) yield strength and ultimate tensile strength, (b) elongation and impact energy for the following composition: 0.32%C, 0.79%Mn, 0.25%Si, 0.02%P, 0.01%S and 0.028%Al [222].

3.3.5 Grain size

At elevated temperatures and particularly in the austenite phase, grains grow rapidly, and it is necessary to control this growth to optimise the mechanical properties. Therefore, HSLA steel is commonly alloyed with carbide and nitride forming elements which precipitate preferably at the grain boundaries. During dynamic recrystallisation, precipitates pin down the boundaries and prevent further growth leading to finer grains. In addition to chemical composition, processing parameters play a vital role in the microstructural refinement. Therefore, HSLA steel exhibits a high degree of grain refinement, giving a higher level of yield strength in comparison with plain C-Mn steel.

Much research work has been carried out to understand the grain structure and growth behaviour at the austenite phase. It is observed that grains start to grow quickly upon the complete transformation into austenite as a single phase [224]. The influence of bcc-stabilising elements on the range of austenitic phase is shown in Figure 3-16.

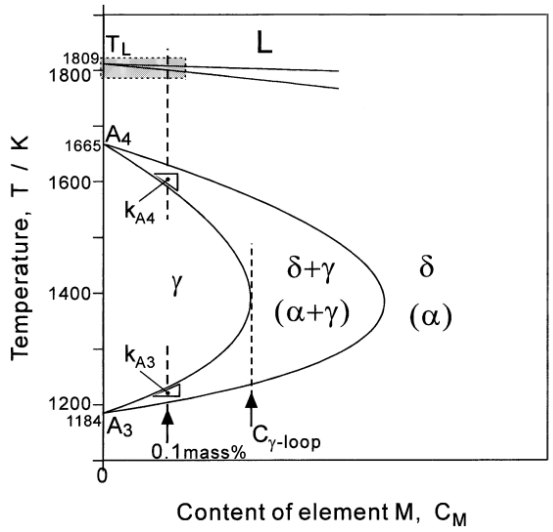

Figure 3-16 Schematic phase diagram of a Fe–M binary alloy (bcc-stabilising elements) binary alloy, where M is the alloying element showing that as the amount increases the γ loop narrows and the Ae_3 transformation temperatures increases [225].

It is observed that the stabilising elements narrow down the austenitic phase into a closed region which gets wider toward the iron rich side. As the content of the bcc-stabilising elements increases, the Ae_3 (the temperature at which austenite begins to transform to ferrite during cooling at equilibrium) increases. Moreover, the Ae_4 (the temperature at which delta-ferrite transforms to austenite during cooling at equilibrium) decreases, further limiting the range of the austenite phase. The most influential bcc-stabilising elements and their effect on stabilisation are presented in Table 3-1. k_{A3} and k_{A4} are the transformation gradients, temperature per unit content, , which are relatively high for Al. Thus, Al is considered as a strong bcc-stabiliser, raising Ae_3 and lowering Ae_4, and thus suppressing the austenitic grain growth.

Table 3-1 Influence of bcc-stabilising elements for the Fe-0.1mass%M binary alloy, where M is the alloying element [225].

Element	Al	Be	Cr	Mo	P	Si	Ti	V	W
k_{A4}	-81	-750	-1.5	-46	-550	-52	-140	-80	-30
k_{A3}	+140	+190	-16	+38	+340	+77	+180	+92	+9

k_{A4} Gradient of transformation temperature per unit content from liquid to austenite.

k_{A3} Gradient of transformation temperature per unit content from austenite to ferrite.

In the austenitic phase, the microstructure development and grain growth are mainly dependant on the alloying composition and the content of each element [226]. Furthermore, cooling rate is prominent in grain refinement since faster cooling rates generally give less time for grains

growth and thus giving finer microstructure [227]. It is important to mention that the cooling rate speed is often restricted to avoid the formation of lower transformation products.

The nature of grain growth can be classified into two types; normal grain growth which gives a uniform grain size distribution while abnormal grain growth gives a random grain size distribution (a mixture of coarse and fine grains). Many researchers have investigated grain growth behaviour as a response to chemical composition and processing parameters due to its considerable influence on the properties. Cotterill and Mould [228] studied the relationship between precipitation and grain growth at different temperatures. They concluded that heating materials up to the dissolution temperature of precipitates produces abnormal grains while heating up to a temperature higher than the dissolution temperature of precipitates gives normal grain growth. However, heating to a temperature lower than the dissolution temperature of precipitates gave the highest degree of grain refinement.

The solubility temperature of niobium carbonitrides was predicted by Rios [229] to be in the range of 1000-1300°C depending on the Nb content and this assumption was also observed experimentally by Tokizane [230] as shown in Figure 3-17.

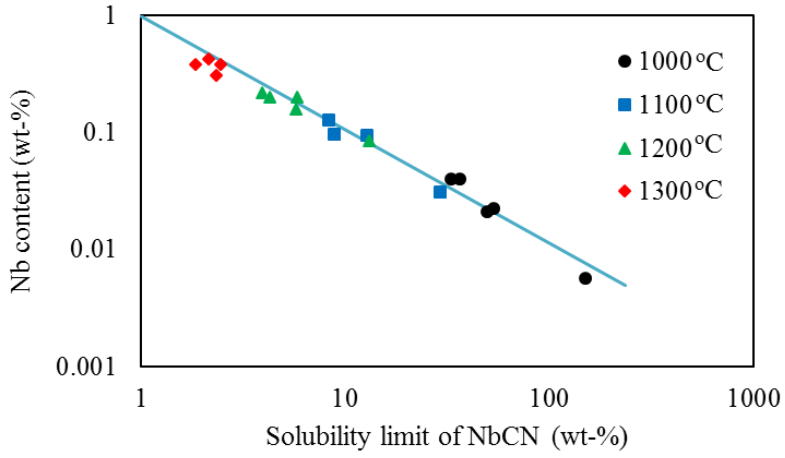

Figure 3-17 Predicted (continuous line) and experimental (symbols) solubility temperature data of NbCN at different Nb contents (wt-%) [229,230].

Further work conducted by Fernández et al. [231], estimating the solubility of NbC and NbN to be 1073°C and 1338°C, respectively. In addition, the work established a relationship between solubility of precipitates and grain growth behaviour. The work also showed that abnormal grain growth is enhanced by the dissolution of the precipitates. A similar observation was pointed out by Danon et al. [232] who observed abnormal grain growth in the Nb-bearing steel in a critical austenitization temperature range of (1000-1100°C). This phenomenon was absent

in the Nb free steel under the same experimental conditions. This was attributed to the initial austenite grain size distribution and austenite grain size growth which is affected by the pinning force of Nb-rich particles. It was also confirmed that heating rate plays a major role on the austenite grain size distribution as the fraction of coarse abnormal grains increases on increasing heating rate [232].

3.4 Influence of alloying elements on the mechanical properties

HSLA steel commonly contains small amounts of phosphorus, silicon and sulphur. Sulphur and phosphorus segregate to the boundaries leading to poor toughness and giving rise to the low melting point iron phosphide phase, which can cause cracking. Manganese is always added to attract all the sulphur as MnS and raise the melting point. For better strength and toughness, other alloying elements such as niobium are added to precipitate as NbC for significant precipitation strengthening. Since grain refinement plays a dominant role, aluminium is added to precipitate as AlN so as to give finer microstructure.

3.4.1 Carbon

Carbon is one of the most critical alloying elements in steels due to its considerable influence on microstructure and properties. It is well established that strength is proportionally related to carbon content, as the ultimate tensile strength increases markedly with increasing carbon content above 0.3%C (Figure 3-18). This is attributed mainly to the increase in pearlite content with C content. Moreover, carbon in solution contributes to the strength by interacting with dislocations but only a very small amount is ever present as the solubility of C in ferrite is normally very low. Furthermore, carbon plays a vital role in combining with carbide forming elements such as Nb, Ti, Mo and V and hence strength is enhanced by precipitation hardening [233].

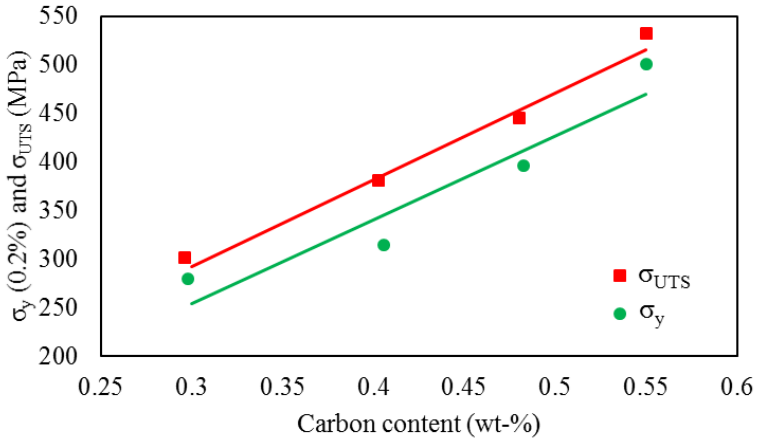

Figure 3-18 Carbon content as a function of yield stress (σ_y) and ultimate tensile stress (σ_{UTS}) the base composition; 0.18%Si, 0.78%Mn and0.18%Cr [233].

Balogun et al. [213] examined the influence of carbon concentration (0.16 – 0.3%C) on the yield strength of HSLA steel. The yield strength remained constant despite increasing the carbon content from 0.16 to 0.22% (Figure 3-19). However, as the content exceeded this range, strength started to improve and reached a maximum at the highest carbon content of 0.6%C.

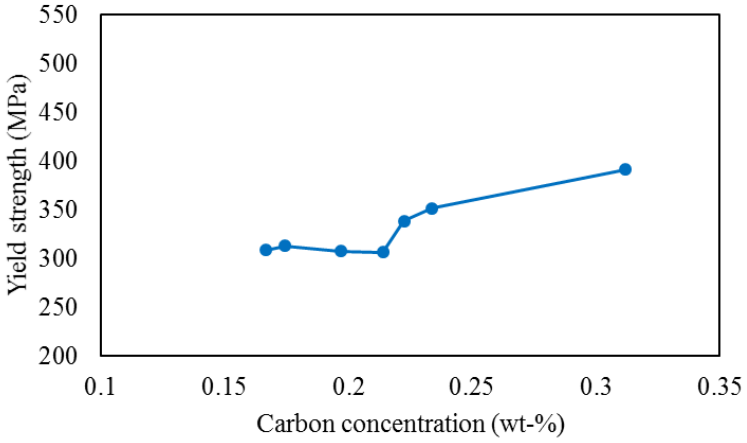

Figure 3-19 Influence of carbon content on the yield strength of hot rolled HSLA steel with the composition: 0.21 to 0.23%C, 0.20 to 0.25%Si and 0.50 to 0.60%Mn [213].

However, a high carbon content has been shown to alter the microstructure markedly forming lower transformation products such as martensite and bainite leading to poor impact performance. Zheng et al. [234] evaluated the influence of carbon content at very low concentrations between 0.004-0.034wt-% on the microstructure, strength and impact toughness of hot rolled and air cooled stainless steel. They observed a continuous improvement in strength with increasing the carbon content (Figure 3-20 (a)) accompanied by a deterioration in the

impact toughness (Figure 3-20 (b)). This was accredited to a reduction in the ferrite volume fraction, this being replaced by martensite (Figure 3-20 (c)).

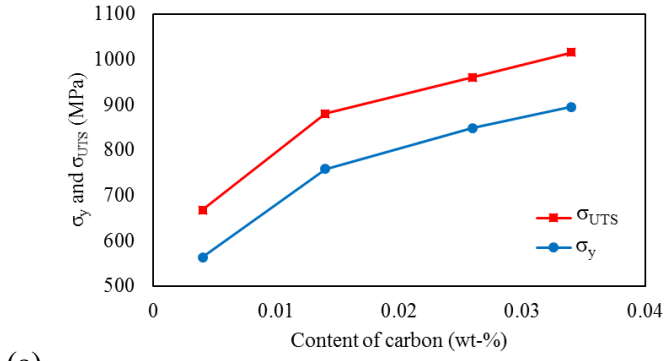

(a)

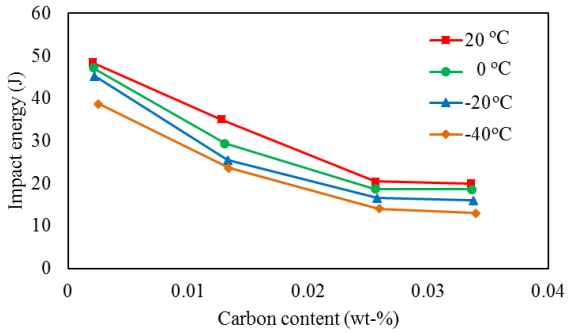

(b)

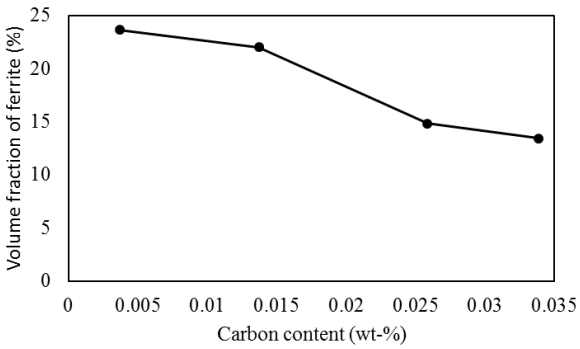

(c)

Figure 3-20 Influence of carbon content on (a) ultimate tensile strength and yield strength, (b) impact energy tested at different temperatures, (c) volume fraction of ferrite of hot rolled steel with the composition: 0.004-0.034%C, 0.01%N, 0.01%S, 0.012%P, 0.3%Si, 1.6%Mn, 12.5%Cr, 0.78%Ni and 0.33%Ti [234].

Alkan et al. [235] have also studied the influence of the volume fraction and morphology of ferrite on toughness of hot rolled steel. They pointed out that the ferrite volume fraction is directly proportional to toughness. The more ferrite that is present the higher the impact energy. This was for the Charpy specimens tested at a variety of test temperatures (Figure 3-21). However, it was confirmed that the thickness of ferrite did not have a significant influence on toughness.

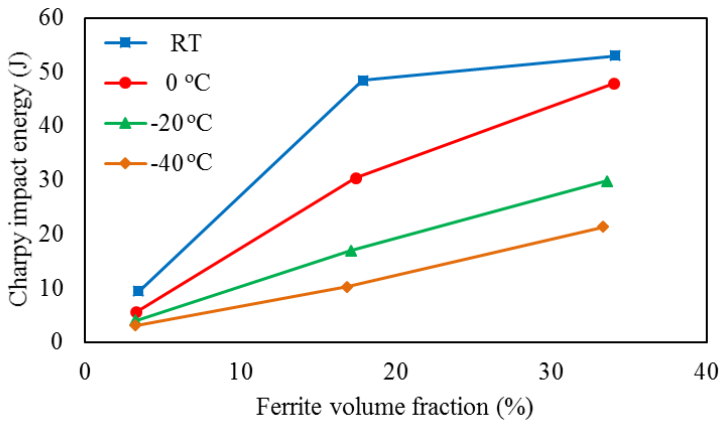

Figure 3-21 Influence of ferrite volume fraction on Charpy impact energy at various temperatures for hot rolled steel with the composition: 0.028%C, 0.1%Nb, 0.015%N, 0.02%P, 0.3%Si, 0.3%Mn, 12.5%Cr, 1.75%Ni and 0.16%Ti [235].

Gladshtein et al. [236] conducted a comprehensive study on the influence of ferrite-pearlite microstructure on low alloy steel properties including strength and impact behaviour. The examined steels were processed differently with carbon contents in the range 0.028-0.84wt-%. The heat treatment was designed to control the volume fraction of phases. It was found that the volume fraction of pearlite had a striking effect on steel deformation and failure behaviour. Strength was found to improve gradually with the increase of pearlite content but at the expense of the impact strength. This behaviour became more pronounced as the pearlite content exceeded 20 vol-. A significant deterioration in impact transition temperature was observed on increasing the pearlite content to ~63% (Figure 3-22).

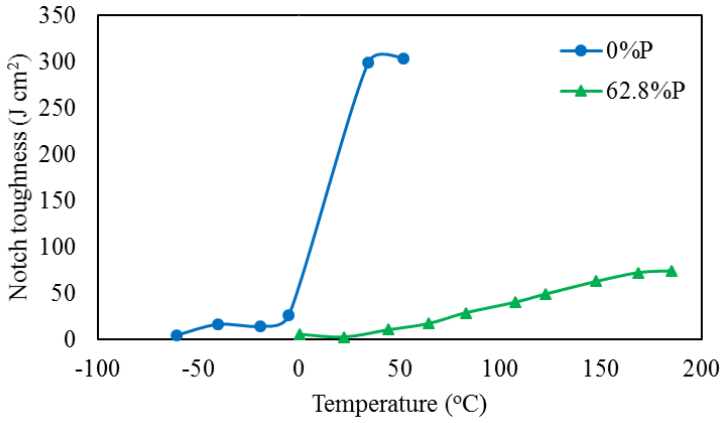

Figure 3-22 The effect of pearlite content (P) on the impact strength of low alloy steel at various temperatures with the composition: 0.57%Mn, 0.25%Si, 0.004%S, 0.004%P, 0.007%Cr, 0.008%%Ni, 0.005%Cu and 0.034%Al, 0.028%C for 0%P steel and 0.50%C for 62.8%P steel [236].

The main microstructural features affected by the carbon content are summarised below.

Phases in the microstructure

The microstructure of HSLA steels consists mainly of ferrite and pearlite. Each of these phases has its own properties. Therefore, the volume fraction of each phase contributes significantly in altering the mechanical properties of the steel. Ferrite is soft in nature and hence increasing its content in the microstructure enhances ductility. Pearlite consists of a lamellar of ferrite and cementite which is rich in carbon and this makes it harder and more brittle at room temperature. Increasing the carbon content, raises the volume fraction of pearlite in the microstructure at the expense of ferrite. Initially, cracks initiate in cementite plates during deformation then extend through the pearlite colonies. Subsequently, cracks extend from the pearlite colonies into adjacent ferrite grains, leading to brittle fracture [237].

Characteristics of cementite

The morphology and volume fraction of cementite in pearlite has a major effect on ductility in low alloy steel [238]. In high carbon containing steels, cementite forms as thick and continuous plates but changes to dispersed, discontinuous and thinner ones upon reducing the carbon content. This is attributed to the lack of carbon in the pearlite colony leading to the formation of degenerate pearlite which enhances ductility. In addition, more space becomes available for the soft ferrite to form in the pearlite colony at the expense of the brittle cementite, giving better ductility, owing to the lower carbon content [238].

The size of the pearlite grains plays a dominant role in controlling the ductility of steel through the thickness of cementite [239]. Coarse pearlite size deforms inhomogeneously leading to strain concentration in narrow slip bands [240]. The thick cementite of coarse pearlite provides poor ductility under impact loading, leading to immediate fracture without prior deformation. This behaviour is ascribed to a shear cracking process which at a later stage develops into cleavage type cracks [241]. On the other hand, thin cementite in fine pearlite offers a better level of ductility and necks down into fragments under impact loads, giving ductile fracture [242,243]. Other work [244] has reported that the refinement of the pearlite colony size enhances ductility due to higher area fraction of boundaries which act as obstacles to brittle crack propagation.

Prior austenite grain size and interlamellar spacing of the pearlite

Bae et al., [245] investigated the influence of microstructural features, such as prior austenite grain size and interlamellar spacing of the pearlite on the ductility of pearlitic steels at carbons in the range of 0.52 – 0.82wt-%. They observed that the size of prior austenite grain and interlamellar spacing increased considerably with increase in carbon content leading to worse ductility. Although interlamellar spacing is affected markedly by the carbon content, cooling rate was reported to have a stronger effect, in which increasing the cooling rate from 100 - 1000°C min^{-1} was found to reduce the interlamellar spacing considerably [244].

Formation of lower transformation products

High carbon additions enhance the formation of lower transformation products, such as martensite and bainite [246]. These phases are undesirable when considering ductility but can be beneficial for applications requiring high levels of strength without considering ductility.

Previous work [25] investigated the influence of carbon content (0.02-0.1%) on aluminium bearing hot rolled plain C-Mn steels. It was observed that the addition of the highest carbon content ~0.1% with the presence of aluminium encouraged martensite formation leading to poor ductility. Therefore, it was recommended to reduce the carbon content to 0.02% in order to accommodate a higher level of Al without martensite being formed [26].

Grain boundary carbides

Grain boundary carbides act as preferred sites for crack initiation, propagation and coalescence leading to poor ductility and impact behaviour [247]. This behaviour was found to be associated with the presence of carbide forming elements, such as Nb which is a strong carbide forming element [248]. The degree to which carbides influence ductility depends on their thickness and volume fraction and they have a big in influence on impact performance and brittle fracture [249]. Most of the thermomechanical processing techniques lack the capability of hindering the formation of grain boundary carbides. However, the characteristics of carbides, i.e. size and volume fraction, can be controlled through carbon content and processing parameters [248].

Previous work has reported that the grain boundary carbides can be refined by the addition of a high Al content ~0.2%Al, which is found to be effective in the improvement of the impact performance of HSLA steels [26].

Reaction of carbon with manganese and silicon

Most steels are alloyed with various amounts of manganese and silicon. In the constitutional equilibrium Fe-C diagram, approx. 0.8%C is present at the eutectoid composition. Mn and Si reduce the carbon content for the eutectoid, (the eutectoid is at 0.6%C when 1.4%Mn is present) and this increases the amount of proeutectoid cementite and reduces the volume fraction of ferrite in the microstructure [237]. The formation of an increased amount of pearlite, pearlite being deleterious to impact behaviour is more than compensated for by Mn giving additional grain refinement and in the case of Si by reducing the C that segregates to the boundaries and locks the dislocations. However, the addition of silicon to very high carbon steels (0.8wt-%C) is reported to retard the formation of the network of the continuous grain-boundary cementite film which is present when silicon is absent [250]. Therefore, steels at the hypereutectoid range have a better than expected combination of high strength and impact behaviour through the addition of silicon.

Low carbon containing steels, among all steels, are chosen for their good ductility, weldability and impact behaviour. However, the strength level in these steels is not sufficient to meet the growing demands for high strength steels in the rapidly developing industry. Therefore, alternative alloying elements are being explored to compensate for this poor strength.

3.4.2 Aluminium

Aluminium is added to HSLA steel primarily to provide grain refinement by the formation of stable AlN at high temperatures. However, both strength and toughness can be improved by microalloying additions of Al [251]. Al is a well-known nitride forming element as it precipitates as AlN preferably at the grain boundary due to the volumetric misfit between the matrix and the AlN particles [252,253]. Finer grains are obtained, as AlN pins the austenite grain boundaries after recrystallisation, preventing any further growth so enhancing the room temperature strength and toughness [254,255]. It must be taken into account that the removal of N by Al eliminates the solid solution strengthening of N [254]. However, the solid solution strengthening of N is smaller in comparison to the considerable benefit of the finer-grain microstructure on the mechanical properties given by AlN precipitation pinning the grain boundaries [255]. Militzer et al. [256] have shown a significant increase in grain size from 40um to 200um on eliminating any AlN precipitation by dissolving all the AlN in solution during hot rolling of A36 steel (0.038%C, 0.30%Mn, 0.040%Al and 0.0052%N). They also

found that the maximum allowable temperature for AlN precipitation is 1100°C, beyond this temperature all the AlN will dissolve in solution so eliminating any grain size refinement.

In addition, the amount of N in solution must be minimised as any excessive content can dissolve in ferrite resulting in a higher level of embrittlement in the absence of adequate Al content.

3.4.3 Niobium

Micro-additions of Nb play a crucial role in improving the metallurgical and mechanical properties of HSLA steel by solid solution strengthening, precipitation hardening and grain refinement [257]. The kinetic segregation of Nb is much greater compared to that of aluminium [258]. Precipitation of Nb as carbonitrides, NbC and Nb(CN) is an important phenomenon affecting the microstructure and hence the corresponding mechanical properties. Nb carbonitrides precipitate and hinder recrystallisation of austenite, through pinning forces exerted by the precipitates on the grain boundaries, leading to a finer and heterogeneous microstructure at room temperature [259]. The control of Nb precipitation behaviour is substantial, as yield strength is highly affected by the size and volume fraction of Nb precipitates. Due to the combined contribution of both solid solution and precipitation strengthening, researchers find it difficult to quantify the relative contribution of each mechanism [260]. Among the carbonitrides forming elements Nb, V and Ti, niobium carbonitrides were found to be the most stable especially at the lower temperature range of austenite as calculated by Thermo Calc (Figure 3-23).

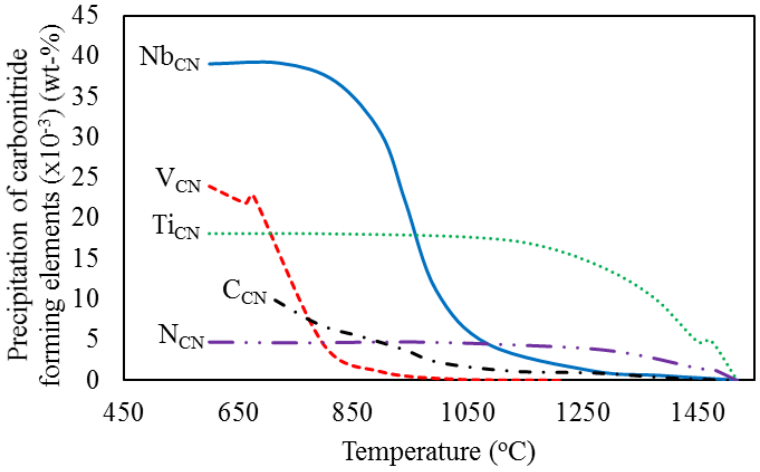

Figure 3-23 The stability of carbonitride forming elements (Nb, Ti, V) at 600–1600°C [259].

In the past, higher amounts of carbon were added to steel to increase strength, but this improvement came at the expense of other properties such as toughness. Therefore, it was

necessary to find alternative elements that can balance properties such as vanadium, titanium and niobium. Among the before mentioned elements, the addition of Nb was found to be more beneficial to improve strength without necessarily effecting toughness [261], and therefore less carbon is needed to avoid toughness deterioration. Nb has the maximum efficiency to weight ratio and a small amount (typically 0.01-0.04) is adequate to obtain the desired properties [261]. Nb lowers the austenite to ferrite transformation temperature and thus influences microstructure and precipitation behaviour [261].

Sally et al. [262] have studied the effect of Nb content on the transformation behaviour from austenite to ferrite under hot rolling conditions. It was concluded that the Nb-bearing steel had a slower transformation rate compared to the Nb free steel and hence increasing the amount of Nb reduces the transformation rate. It has been reported that Nb retards carbon diffusivity rate during the austenite to ferrite transformation [263]. It has been also suggested [188,216,205] that carbide–forming elements such as Mo, Nb and V retard the diffusion of carbon during the transformation from austenite to ferrite.

3.4.4 Phosphorus

Phosphorus is an undesirable impurity which causes embrittlement in steels and it exists naturally in steel scrap. In the processing of HSLA steel, the amount of phosphorus is kept to a minimum, typically 0.004%, to avoid poor toughness from the segregation of P to the grain boundaries and weakening them. Previous work [264] showed that increasing P level by 0.3wt-% raised the ITT drastically by 200°C due to P segregation to grain boundaries. However, phosphorus in low concentration can enhance corrosion resistance and solid solution hardening, 1wt-% of P increases the strength by 690MPa [264]. The maximum allowable P content depends mainly on the steel application as shown in Table 3-2. Typically, P levels are kept below 0.05%, except for weathering steel since here the main property considered is corrosion resistance which is considerably enhanced by P but at the expense of toughness [264].

Table 3-2 Maximum limit of P content in different commercial steels [264].

Steel	Grade	P content (wt-%)
High strength steel	WEL-TEN 50	≤ 0.035
	WEL-TEN 60	≤ 0.040
	WEL-TEN 80	≤ 0.040
Non-tempered steel	HSB 50	≤ 0.050
Tempered steel	U.S.S.T-1	≤ 0.040
	Ducol W-30	≤ 0.050
Weathering steel	ASTM A242	≤ 0.150

Since high amounts of P exist in the recycled steels and it is too expensive to minimise their content, many efforts have been made to maximise the benefits and minimise the harms of P. A special thermo-mechanical process, known as cross rolling, is utilised to obtain the maximum potential of phosphorus and minimise the detrimental influence a higher P content so as to improve toughness and strength [90]. The process involves refining the grains to increase the grain boundary area and hence P is distributed across a wider area, and its density is minimised.

Moreover, Yoshida et al. [265] reported that P was beneficial in enhancing austenite grain refinement. This was attributed to the phosphorus being the strongest bcc-stabiliser, having very high transformation gradients temperature per unit content, giving a higher Ae_3 and lower Ae_4 temperatures (Table 3-1).

Grain refinement by thermo-mechanical treatment improves both strength and toughness in the high phosphorus steels, using the novel process or the cross rolling [189]. Thus, the harmful effects of phosphorus can be suppressed.

3.4.5 Manganese and sulphur

Sulphur is one of the most undesirable non-metallic impurities and it is present naturally as part of the ingredients of steel making. It is only added to steel to improve machinability as MnS inclusions helps to break off the turnings. To remove S from steel, particularly to the very low value industry is demanding is very costly.

Rudyuk, et al. [266] investigated the influence of sulphur concentration on the microstructure and mechanical properties of hot rolled low alloy steel. As the sulphur content increased from 0.030 to 0.055%, the yield strength increased significantly by almost 50%, much greater than the increase in the ultimate tensile strength. However, toughness deteriorated considerably, the ITT increasing by ~25°C, which was attributed to the increased size and volume fraction of sulphide inclusions. It was also observed that these inclusions were elongated and existed only in the matrix for the low S-bearing steel while for the high S-bearing steel some inclusions were also found in the grain boundary leading to considerable embrittlement. The fracture condition was mixed, having regions of both intergranular and transgranular fracture, but upon increasing the S concentration, the transgranural failure was the dominant mode indicating embrittlement. Despite the great advantages of S being beneficial in improving yield strength, it is always essential to minimise its concentration to maintain good impact performance [266].

Manganese is added to steel composition in order to form MnS inclusions aiming to avoid the detrimental effects of S. Several research studies have been conducted over the years and found

that MnS inclusions are beneficial in retarding grain growth but the extent of their effectiveness is based on their characteristics; morphology and distribution. An early work by Kiessling and Lange [267] categorised the morphology of MnS generally into three types; randomly distributed spherical sulphides, grain boundary sulphides and angular sulphides. Avdušinović and Gigović [268] carried out a deeper analysis on the morphology and distribution of MnS inclusions at various temperatures in low carbon steel. The morphology of the inclusions followed a very similar trend at all temperatures (Figure 3-24 (a)). As the temperature increased to 1350°C the inclusions coarsened but above this temperature, the size followed an unsteady manner and random behaviour was observed (Figure 3-24 (b)).

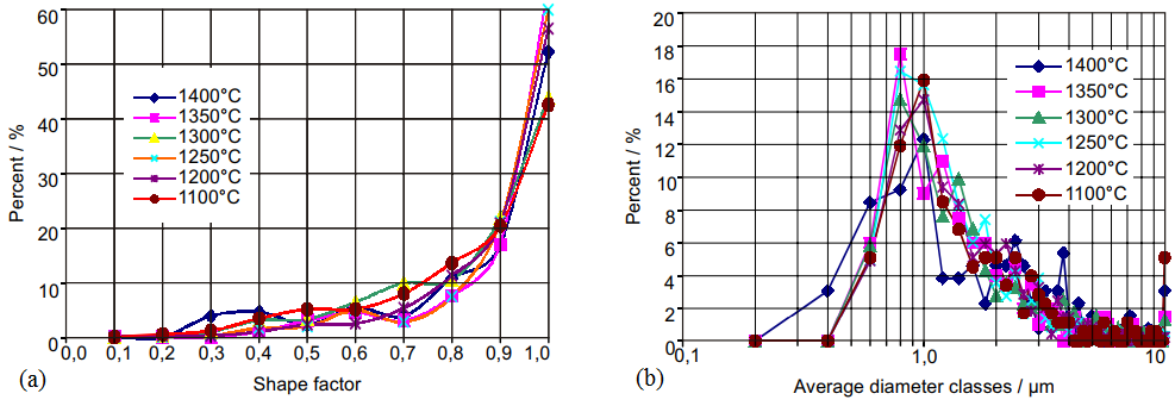

Figure 3-24 MnS inclusions in low carbon steel at various temperatures showing their (a) shape factor, (b) area represented by the diameter for the following composition: 0.11%C, 0.31%Si, 0.35%Mn, 0.011%P and 0.015%S [268].

4 Experimental, results and discussion of TWIP steel

4.1 Experimental

4.1.1 Composition

The steels were cast as 50 kg vacuum melts and air cooled to room temperature. The base composition for all the TWIP steels was 0.6%C, 0.1%Si, 18%Mn, 0.01%N and 1.5%Al. P and S levels were low for all steels, ~0.01 and 0.005%, respectively. The boron level was the same as has been used previously ~ 0.002–0.003% [146,174]. The composition of the steels examined (wt-%) are given Table 4-1. Whereas, previous work had been concentrated on low N levels, the present work was carried out to explore the influence of high N (0.01%) on the hot ductility on these boron treated TWIP steels more in keeping with electric arc furnace N levels.

The Ti/N ratio for the stoichiometric composition for TiN is 3.4. In the present instance, three steels with different Ti/N ratios were examined. The Ti/N ratio was low for steel 1, close to stoichiometric Ti/N ratio for steels 2 and greater than that of stoichiometry for steel 3. Once there is sufficient Ti to combine with all the N, it is likely that very little N will go back into solution on reheating to 1250°C so the condition for steels 2 and 3 will probably remain close to that present when melted. Reheating was, therefore, chosen rather than melting, but this does put a limit on the applicability of the results to the continuous casting operation.

Steel 1, (Table 4-1), is the base composition with a Ti level of 0.019% and 0.009%N, whose hot ductility curve was to be used for comparison purposes. Steels 2 is made at the stoichiometric composition for TiN. Steel 3 was well in excess of the stoichiometric Ti/N ratio for TiN.

Table 4-1 Composition of TWIP steels chosen for examination, wt-%.

Steel	Ti/N	C	Si	Mn	P	S	Al	Ti	Nb	B	N
1	2.1	.60	.09	18.2	.009	.003	1.57	.019	.031	.0027	.009
2	3	.60	.09	18.2	.009	.003	1.55	.030	.032	.0028	.010
3	6.8	.60	.10	18.0	.010	.006	1.50	.075	.032	.0028	.011

4.1.2 Tensile specimens

Tensile specimens, 120 mm in length and 10 mm in diameter, were machined from the as-cast ingot and tested using a Gleeble. For each temperature, two tensile specimens were tested and the average value of reduction of area (%RA) taken. After casting, the ingot was stripped from

its mould and air cooled. The position in the ingot where the tensile specimens were taken from and their dimensions are shown in Figure 4-1.

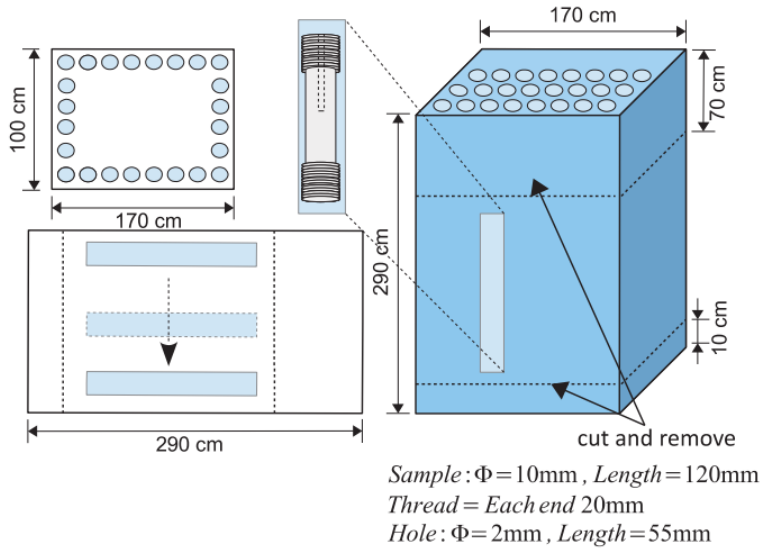

Figure 4-1 Schematic diagram showing the dimensions and position of the tensile specimens in the original ingot.

4.1.3 Hot tensile testing

The Gleeble 3500 Digital Control System has been used to perform the hot tensile testing to control thermal and mechanical test variables simultaneously (Figure 4-2). Electrical resistance heating technology was employed to give a uniform temperature across the sample. An R type thermocouple (platinum/platinum-13% rhodium) was inserted inside the samples to give signals for accurate feedback control of specimen temperatures. This set-up provides the versatility that is necessary to simulate the straightening operation in continuous casting. The hot ductility tests were performed according to POSCO standard that has been utilised to evaluate the cracking behaviour of TWIP steel. Ideally, to simulate the continuous casting and straightening operation more closely, 'in situ melting' should be used and two cooling rates, a fast cooling rate for the primary cooling, followed by a slower cooling rate for the secondary cooling, should be incorporated [269]. However, obtaining a satisfactory tensile specimen on in-situ melting, free of porosity and choosing silica tubing, which does not react with the Ti present in the steel, encounters serious practical difficulties. Before embarking on this melting route, the advantages of melting over 're-heating' to 1250°C, need to be weighed up carefully in advance. The cooling rate to room temperature for the region in the ingot corresponding to where the tensile specimens were taken from is slow ~1°C min^{-1}. However, the tensile samples after machining were heated at 150°C min^{-1} to 1250°C, held 3 min and cooled at a faster cooling rate, 12°C min^{-1} down to the test temperatures in the range 1100 to 700°C. The three

steels, were also cooled at 60°C min^{-1} to study the effect of cooling rate on the hot ductility. After holding for 30s, the tensile samples were strained to failure using a strain rate of 3×10^{-3} s^{-1}. The strain rate used in the tensile test is chosen to be the same as that undergone in the straightening operation. The temperature profile is shown in detail in Figure 4-3.

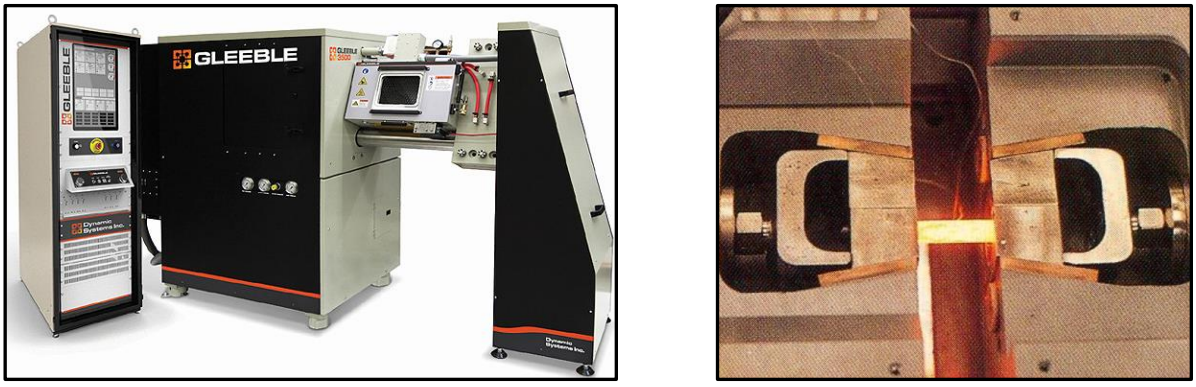

(a) (b)

Figure 4-2 (a) Layout of Gleeble 3500, (b) arrangement for the hot ductility test.

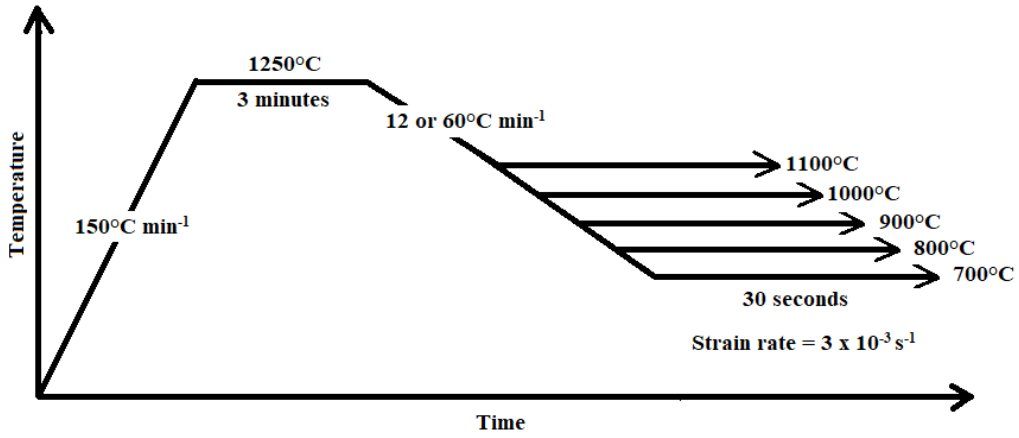

Figure 4-3 Schematic diagram of heating and cooling programme.

4.1.4 Evaluation of hot ductility

The percent reduction of area (%RA) has been used extensively to evaluate hot ductility in most of the previous literature surveys [41]. Hot ductility curves were produced by tensile testing at elevated temperatures after cooling from the solution treated temperature. Normally, the hot ductility curves are obtained by measuring the percent reduction in area (%RA) at fracture using *Equation 3*:

Equation 3

$$\%\mathrm{RA} = \frac{\text{Decrease in area}}{\text{Original area}} = \frac{D_i^2 - D_f^2}{D_i^2}$$

where D_i is the initial diameter before the test and D_f represents the final diameter after fracture. Both values were measured in the laboratory by digital Vernier Calipers.

For the current samples, the equation is modified slightly by subtracting 2^2 from the denominator to account for the 2mm drilled hole in each sample used to accommodate the thermocouple, (*Equation 7*).

Equation 7

$$\%\text{RA} = \frac{\text{Decrease in area}}{\text{Original area}} = \frac{D_i^2 - D_f^2}{D_i^2 - 2^2}$$

The %RA was recorded and then plotted against the test temperature to obtain the hot ductility curves. The higher the %RA value is, the less likely the steel will be prone to transverse cracking during continuous casting. Generally, 40% is adequate to avoid transverse cracking [40].

4.1.5 Metallography

Preparation of samples

Once a tensile sample had failed, it was immediately gas quenched with argon to preserve the microstructure. Thereafter, one half of each sample was cut along the longitudinal axis. The samples were then mounted in epoxy resin and cured. Mechanical preparation was then used to prepare the samples for microscopic examinations. Firstly, the samples were ground using the following silicon carbide (SiC) pads in the order 240, 400 and 600grit, the latter being the finest. The samples were then polished using diamond suspensions with 6um followed by 1um diamond paste. While moving from one pad to another, the surface of each sample was washed and wiped with absolute ethanol then finally dried. At this stage, the samples had a mirror surface without any scratches or foreign matter for clear microscopic examinations. Finally, the samples were etched using picric acid to show the detailed microstructure for subsequent microscopic examinations.

Optical microscopy

Optical microscopy (OM) was carried out on longitudinal sections from the necked down region of the fractured tensile specimens. OM was used to monitor the microstructure evolution as a function of testing temperature, composition and cooling rate. The changes in grain size and cracking behaviour were also evaluated.

Scanning electron microscope

Scanning electron microscope (SEM) examinations were made on sections taken close to the point of fracture. SEM was used to evaluate the precipitates and inclusions more closely by evaluating their morphology, size, volume fraction and location. Examinations were carried out using FEG-SEM equipped with EDX system for deeper analysis of the particles. The spatial resolution of the microscope was <50nm at 20kV accelerating voltage.

Transmission electron microscope

Transmission electron microscope (TEM) examinations were made on sections taken close to the point of fracture. The carbon extraction replicas were mounted on nickel grids. Examinations were carried out using JEM-2100F Jeol Field Emission Transmission Electron Microscope (FE-TEM).

4.2 Results

4.2.1 Hot ductility curves

The hot ductility curves of the examined TWIP steels at a cooling rate of 12°C min^{-1} with different Ti/N ratios in the temperature range (700-1100°C) are shown in Figure 4-4 (See Appendix A for the detailed hot ductility measurements). In general, it is observed that both steels with low and medium Ti/N ratios have a RA over 40% in the temperature range (700-1000°C) while the steel with high Ti/N ratio achieved >40%RA for the entire temperature range (700-1100°C).

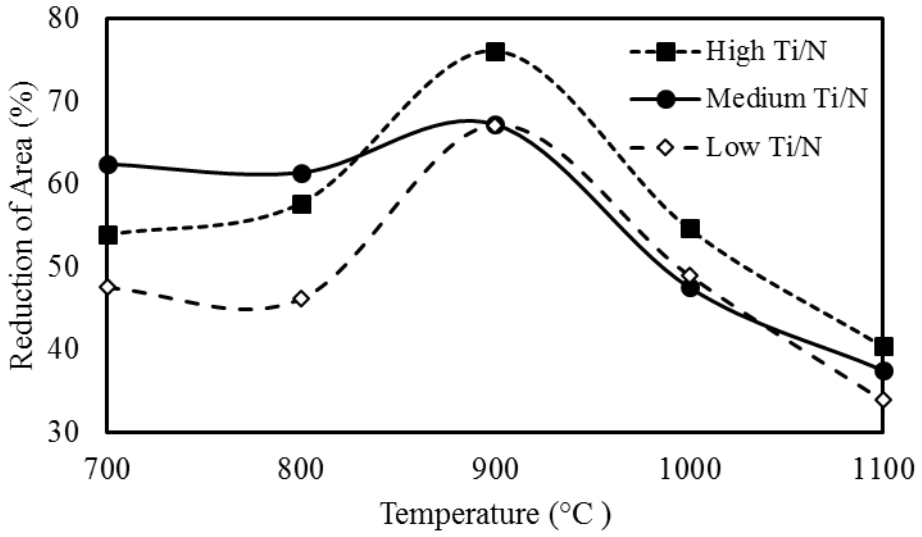

Figure 4-4 The hot ductility of the examined TWIP steels with different Ti/N ratios at various temperatures.

Upon cooling from 1100 to 900°C, the hot ductility of the steels with low and medium Ti/N ratios is similar. However, as the temperature drops further the medium Ti/N ratio bearing steel maintains its ductility steadily while the ductility of the low Ti/N ratio bearing steel deteriorates sharply but still above the 40% limit.

The high Ti/N ratio bearing steel gave the best ductility among all the examined steels in the temperature range (900-1100°C). As the temperature drops further, the ductility drops but is still higher than the base steel though slightly below the medium Ti/N ratio bearing steel.

It is also observed that the maximum ductility for all the examined steels was attained at 900°C and the minimum ductility at 1100°C.

In order to evaluate the cracking behaviour of TWIP steel based on the plate thickness, as is the case in slab and billet, the effect of cooling rate was also considered in the current work. The hot ductility of three steels with different Ti/N ratios were further examined at the following cooling rates 12°C min^{-1} and 60°C min^{-1} (Figures 4-5 to 4-7).

In general, fast cooling rate gave better hot ductility for all the examined steels, independent of the Ti/N ratio (Figures 4-4 to 4-7). The improvement in ductility is insignificant and estimated to be around 10% on average. Since all three steels behaved in a similar manner toward the cooling rate, only one steel, steel 3, was selected for further microscopic examination at both cooling rates.

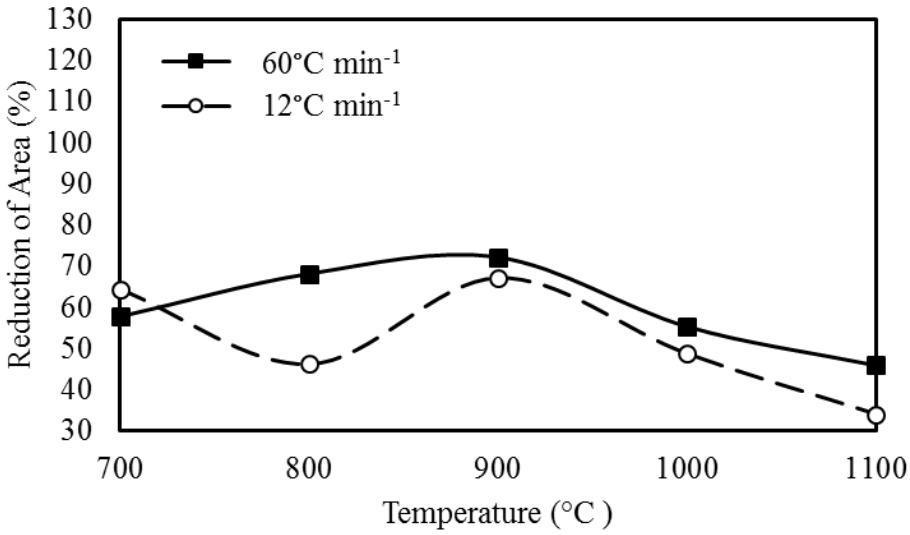

Figure 4-5 The hot ductility of TWIP steel with low Ti/N ratio at 12 and 60°C min^{-1}.

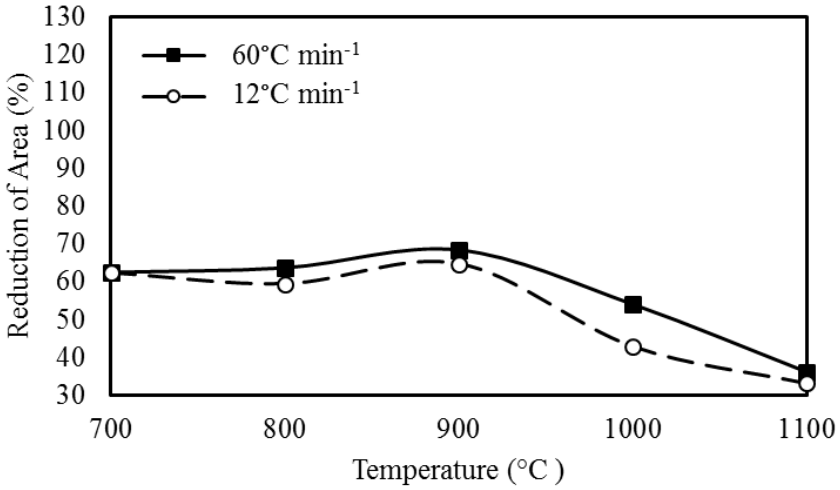

Figure 4-6 The hot ductility of TWIP steel with medium Ti/N ratio at 12 and 60°C min^{-1}.

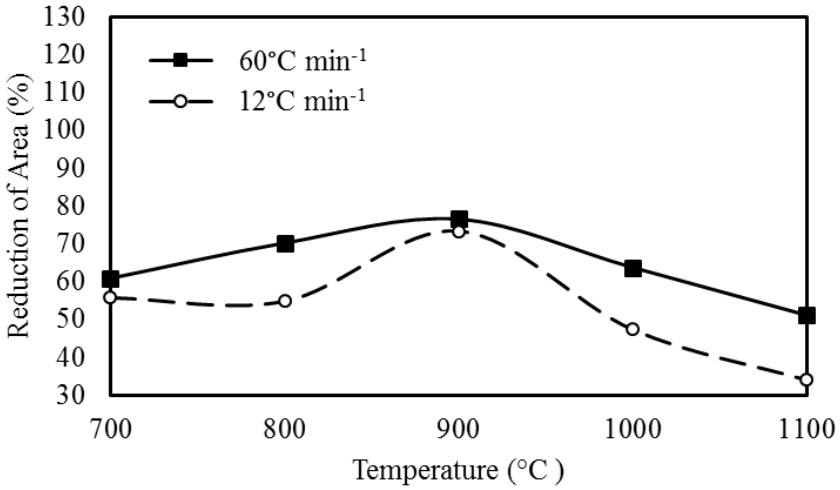

Figure 4-7 The hot ductility of TWIP steel with high Ti/N ratio at 12 and 60°C min^{-1}.

4.2.2 Optical micrographs

Since all the three examined steels behave in a similar manner, in which the hot ductility improves when lowering the temperature from 1000 to 900°C then deteriorates when lowering the temperature further to 800°C, one steel was chosen for further optical microscopic examination, the high Ti/N steel, in the temperature range (800-1000°C) in order to investigate the grain size evolution and its relation to hot ductility. Analysis of grain size evolution was based on the optical micrographs shown in Figures 4-8 (a-c). The grain size is coarse in size and is estimated to be ~600μm at 1000°C (Figures 4-8a). As the temperature drops to 900°C, the grains exhibit a high degree of refinement due to the onset of dynamic recrystllisation (Figures 4-8b). It is observed that dynamic recrystallisation is more active at the regions close to fracture. Moreover, intergranular cracks are observed to be present intensively near the point

of necking (Figures 4-8 (a,b)). As the temperature continues decreasing from 900 to 800°C, the recrystallised grains grow and the microstructure becomes coarser again (Figures 4-8c).

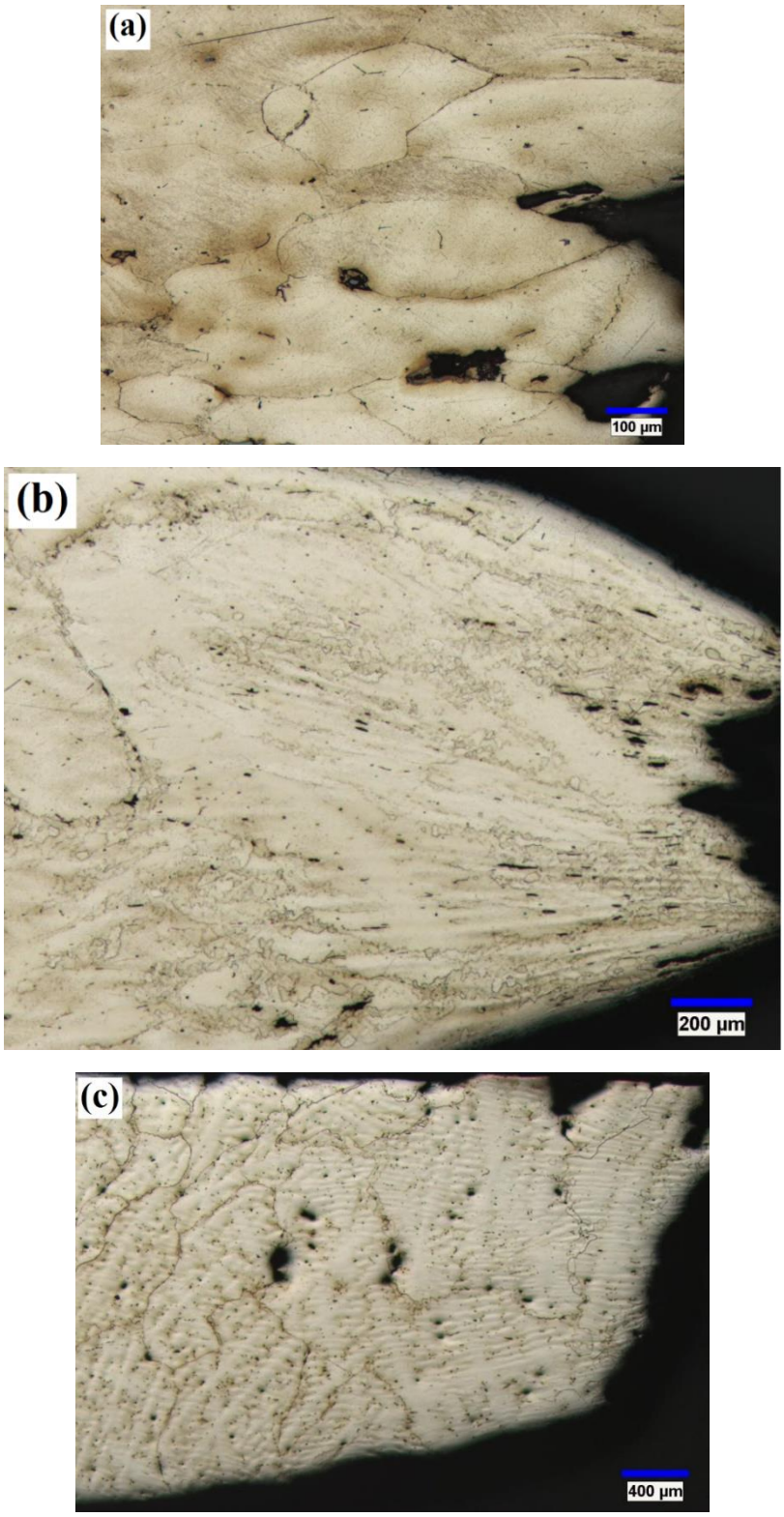

Figure 4-8 Optical micrographs of the high Ti/N bearing steel (a) examined at 800°C showing coarse grain with no dynamic recrystallisation, (b) examined at 900°C showing dynamic recrystallisation which is enhanced at the heavily deformed regions close to the neck, (c) examined at 1000°C showing coarse grain with no dynamic recrystallisation.

4.2.3 SEM micrographs

The SEM micrographs of the low and high Ti/N steels cooled at 12°C min^{-1} with the corresponding EDS analysis spectrums are presented in Figures 4-9 and 4-10, respectively. It is observed that Se is presented in some of the analysis spectrums. The addition of Se was needed in order to add and control the required level of Mn through an electrolysis technique, which uses Se as an electrolyte medium. Moreover, the Au peak is present due to the gold coating used on the sample surface to supply conductivity during SEM examination.

The main compounds detected in the low Ti/N steel were AlN and MnS. Both were found to be attached to each other and were located in the matrix (Figure 4-9). AlN is very sluggish in precipitating out but the presence of MnS in the matrix provides ideal nucleation sites for AlN precipitates [16]. Some TiN particles were also detected but their low volume fraction was very low.

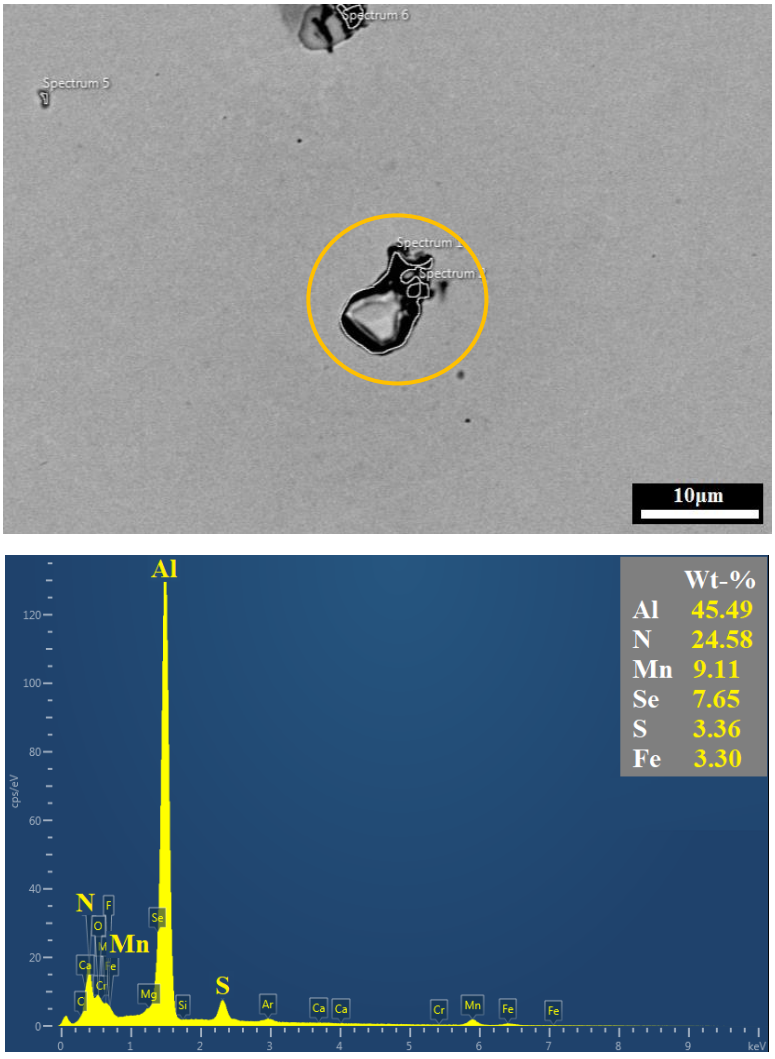

Figure 4-9 SEM micrograph of the low Ti/N steel at 800°C with the analysis spectrum showing the presence of AlN on MnS particles (AlN is black and MnS is grey in colour).

In the high Ti/N steel, the main particles found were TiN and NbN. Occasionally both compounds were to found to be attached together (Figures 4-10). Although AlN precipitates were present, their volume fraction was very low in comparison with the former steel.

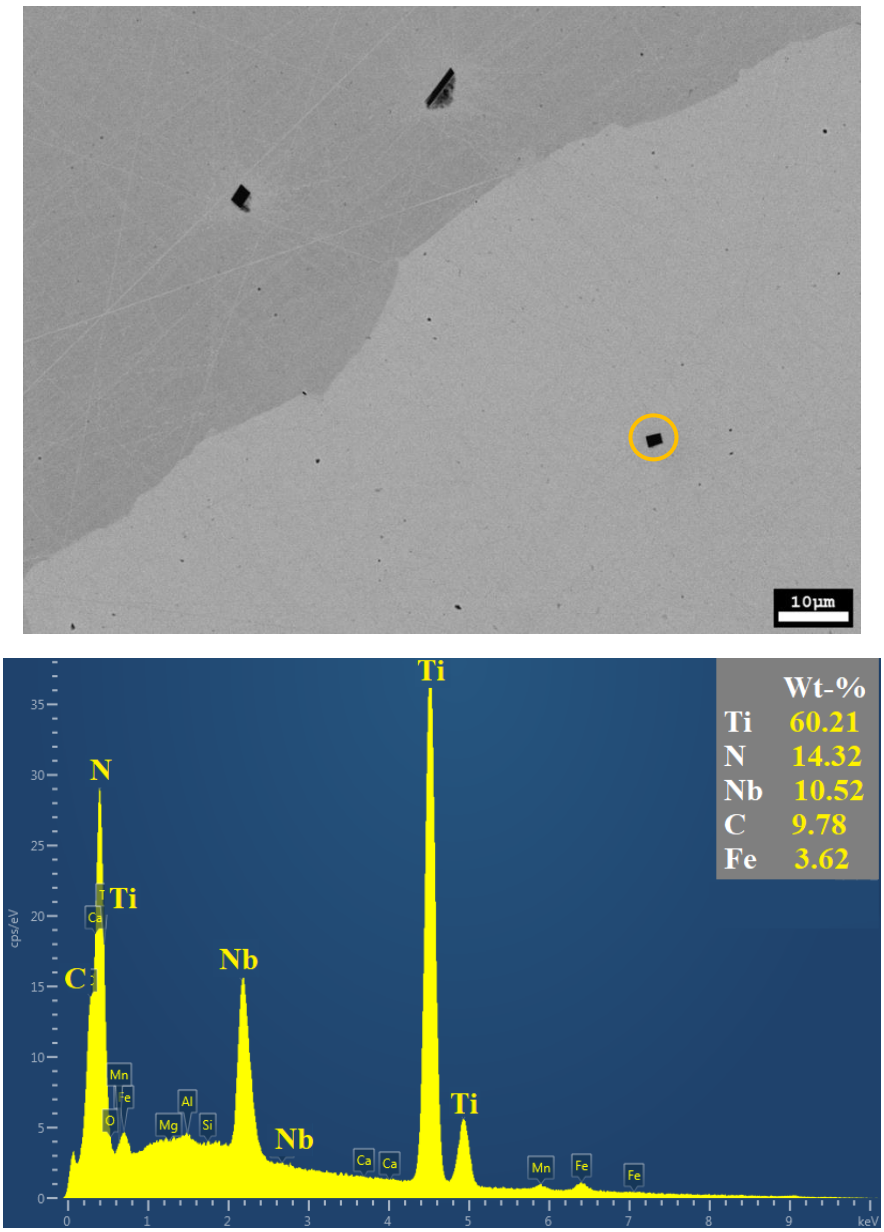

Figure 4-10 SEM micrograph of the high Ti/N steel at 800°C with the analysis spectrum showing the presence of Ti-Nb nitride particles.

4.2.4 TEM micrographs

The TEM micrographs of the low and high Ti/N steels cooled at 12°C min^{-1} with the corresponding EDS analysis spectrums are presented in Figures 4-11 and 4-12, respectively. It is also observed that Ni is presented in the analysis spectrums because of the Ni grids used to support the replicas. It is worth mentioning that N is a very light element and not always detected and its presence at times have to be assumed when nitride formers are detected on the spectrums.

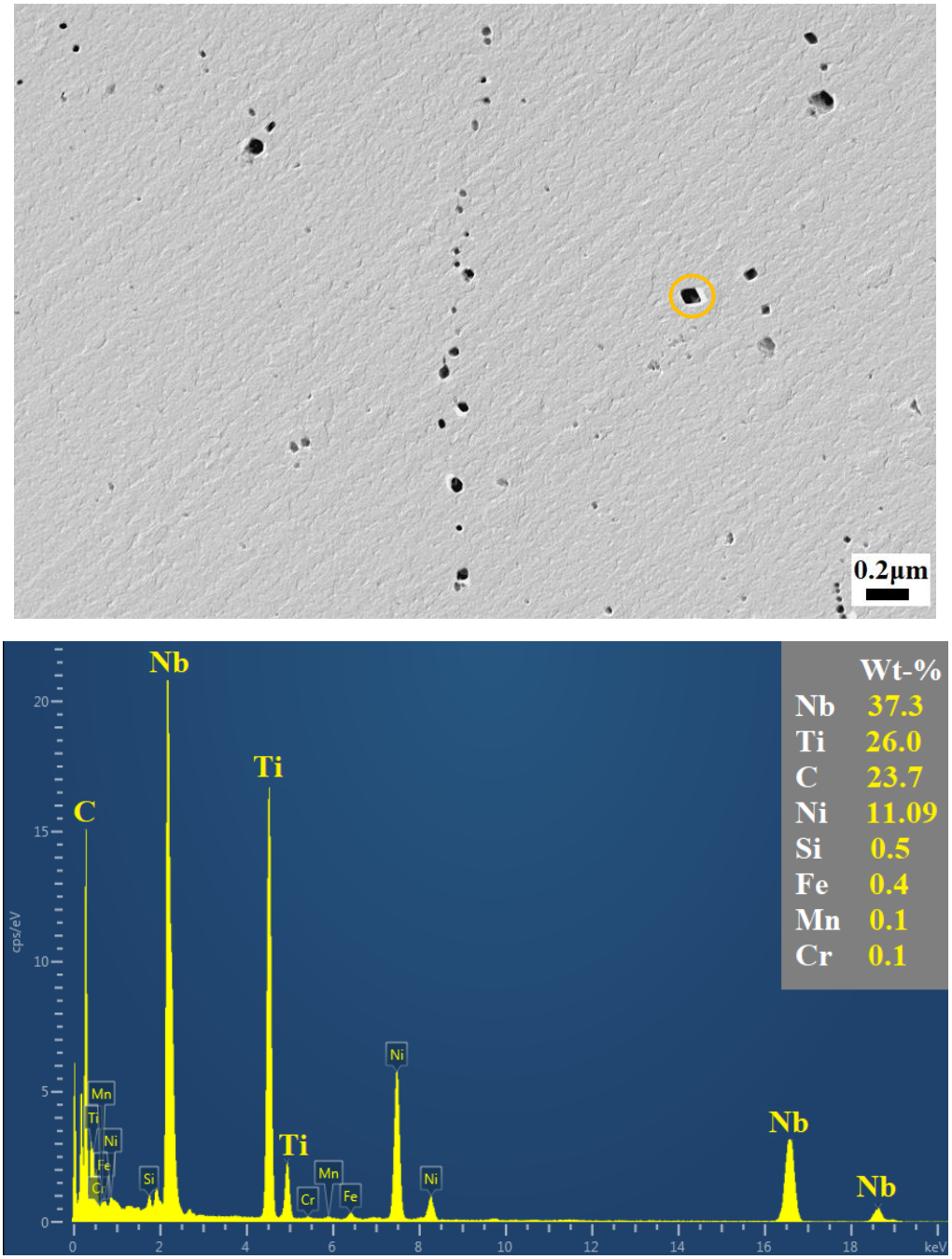

Figure 4-11 TEM micrograph of the low Ti/N bearing steel at 800°C with the analysis spectrum showing the presence of Nb-Ti carbonitrides.

Both steels show Nb-Ti 'nitrides' but their volume fraction was much higher in the high Ti/N steel as shown in Figure 4-12. In the low Ti/N ratio, the weight percentage content of Nb in the precipitate was found to be approximately 50% higher than Ti content, as shown in the spectrum of Figure 4-11. However, the weight percentage content of Ti in precipitates of the high Ti/N steel was enhanced considerably. The Ti level was ~100% higher than the Nb content, as shown in the spectrum of Figure 4-12.

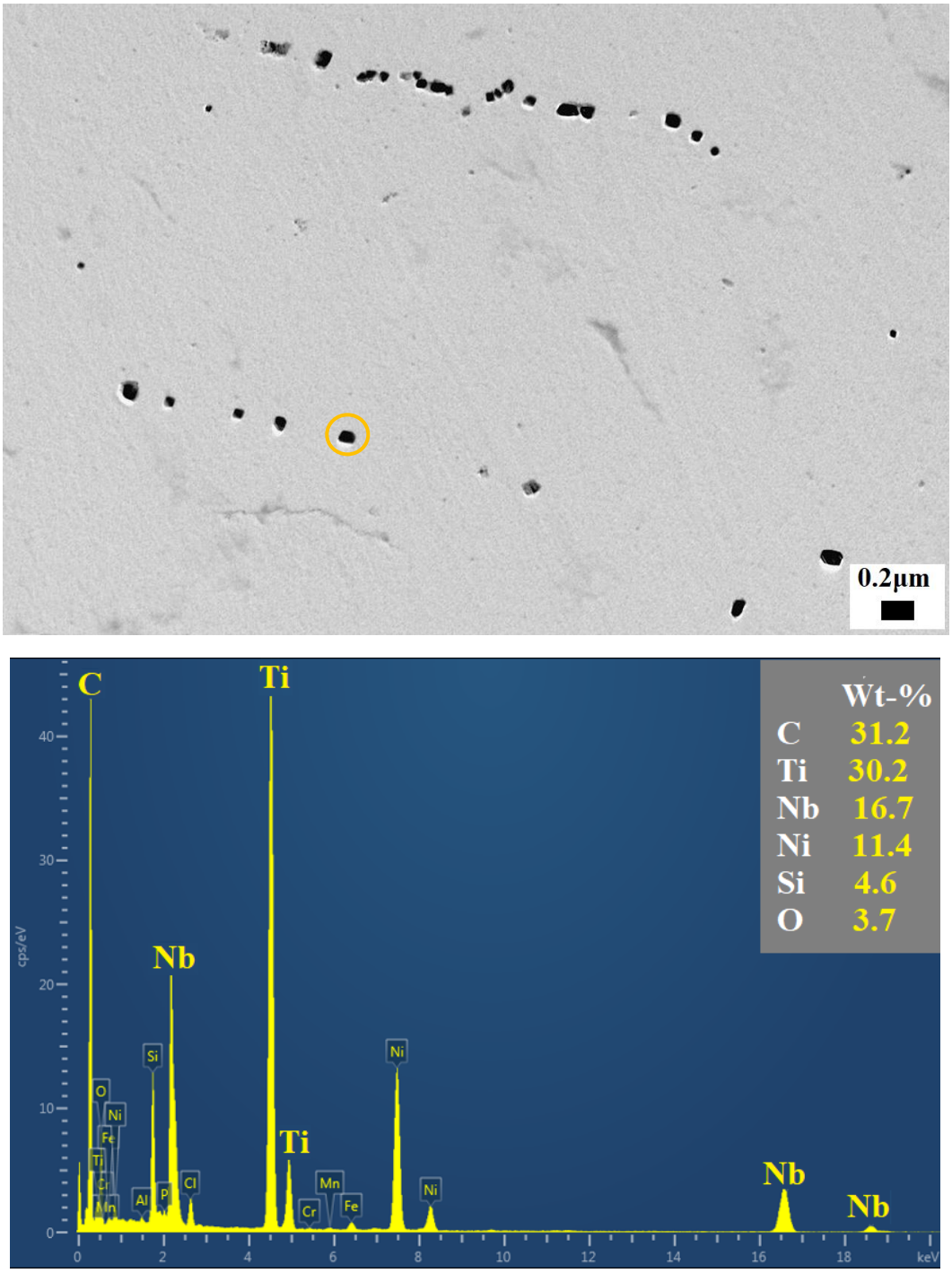

Figure 4-12 TEM micrograph of the high Ti/N bearing steel at 1000°C with the analysis spectrum showing the presence of Ti-Nb carbonitrides.

4.2.5 Cooling rate

Typical SEM photographs of the high Ti/N steel at both cooling rates (12 and 60°*C min*$^{-1}$) at 800°C are shown in Figures 4-13 and 4-14, respectively. At both cooling rates, the majority of the particles are located within the matrix. In general, the size of the particles is coarser at the slow cooling rate (Figure 4-13).

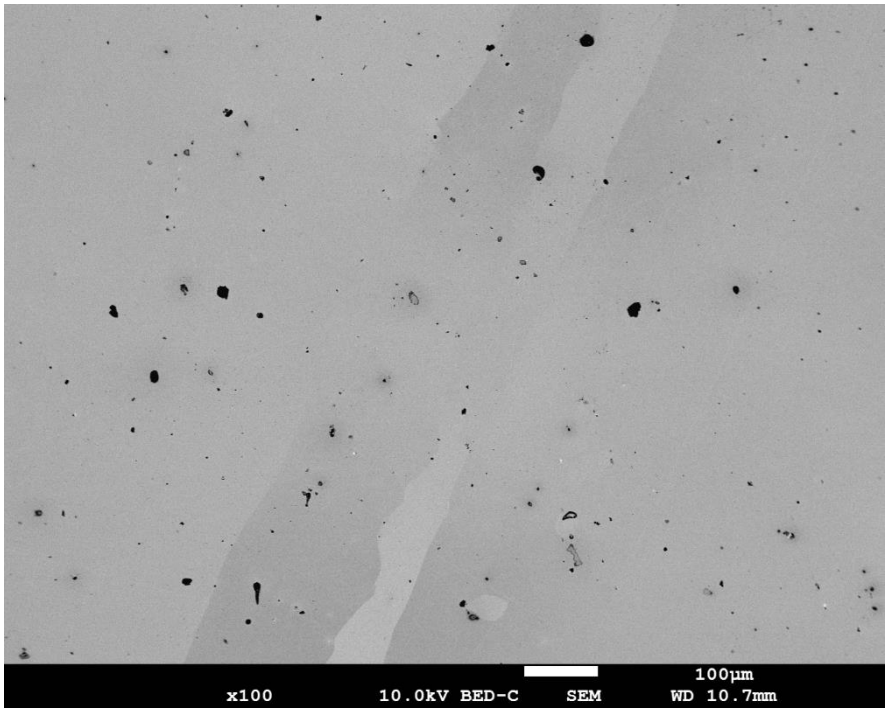

Figure 4-13 SEM micrograph of the high Ti/N bearing steel at 800°C at 12°C min^{-1}.

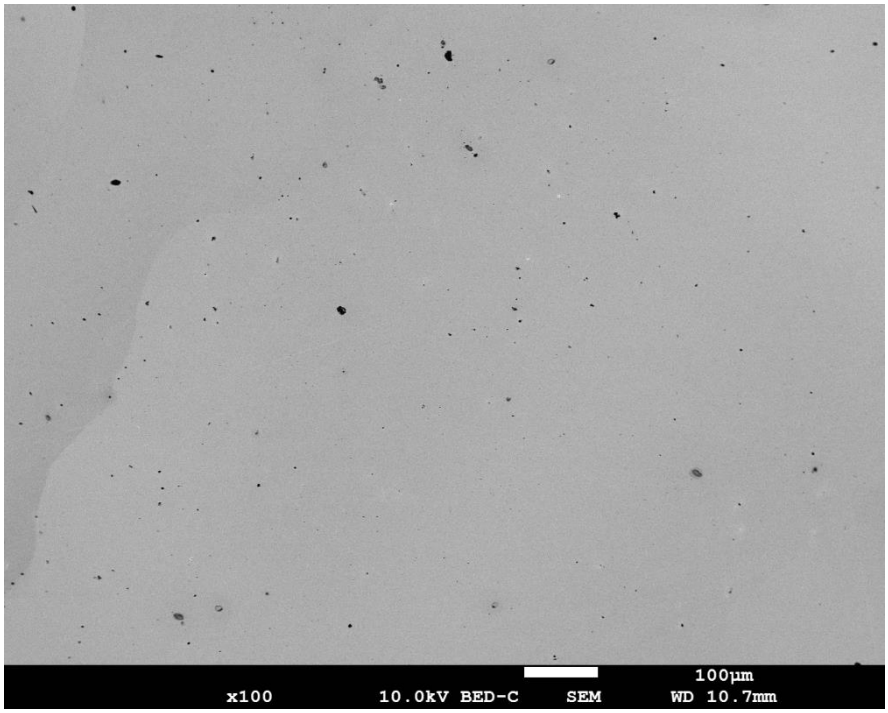

Figure 4-14 SEM micrograph of the high Ti/N bearing steel at 800°C at 60°C min^{-1}.

4.2.6 Fracture surface analysis

The fracture surfaces for the medium Ti/N ratio steel (steel 2) tested for the temperature range 900-1100°C at the cooling rate 12°C min^{-1} are shown in Figures 4-15 to 4-17. In general, various modes of fracture can be observed from these SEM figures. At 1100°C, intergranular grain boundary sliding is the main mode of fracture indicating brittle failure (Figure 4-15). As the temperature drops to 1000°C, a mixture of fracture modes is observed as shown by grain boundary sliding and ductile voiding, the latter indicating ductile fracture (Figure 4-16). At 900°C, the fracture behaviour shifts dramatically to a ductile mode, as shown in Figure 4-17, where ductile voiding is dominant.

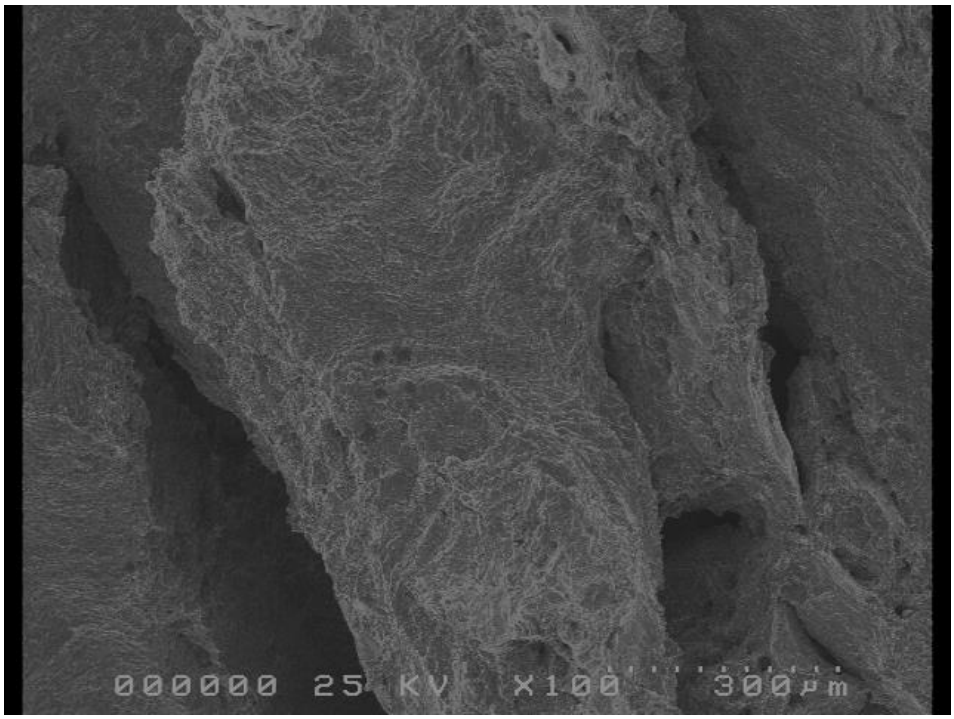

Figure 4-15 Fracture behaviour of the medium Ti/N bearing steel at 1100°C.

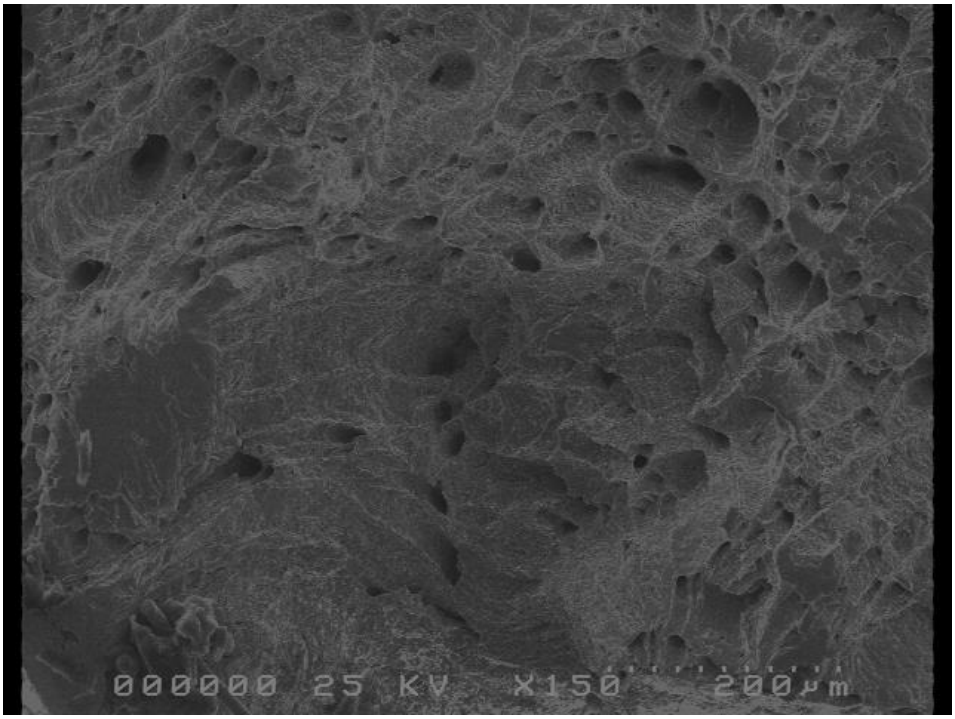

Figure 4-16 Fracture behaviour of the medium Ti/N bearing steel at 1000°C.

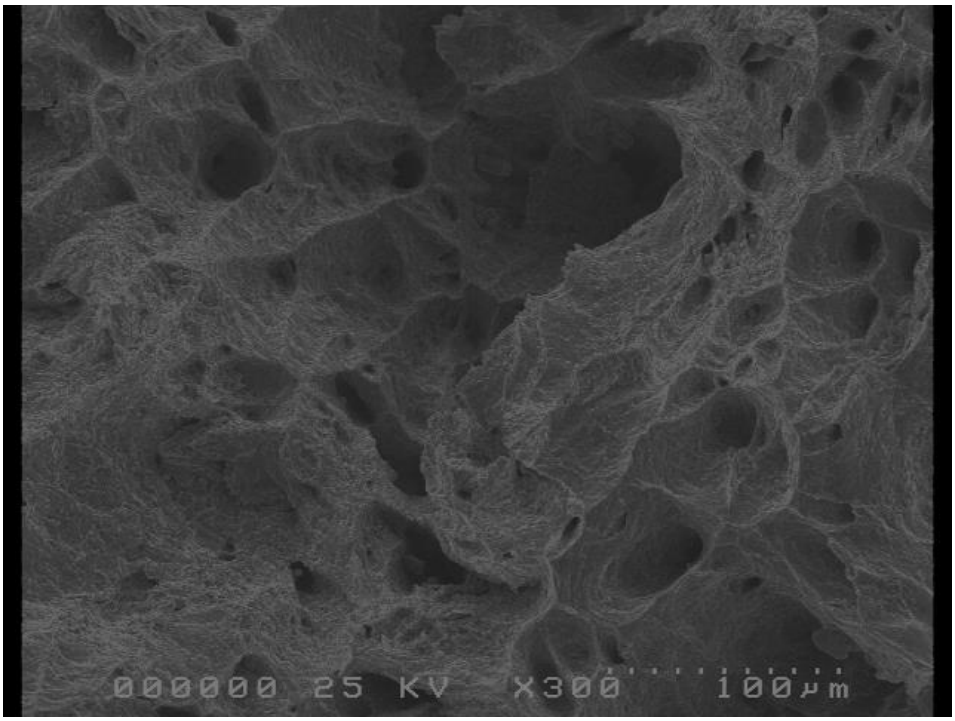

Figure 4-17 Fracture behaviour of the medium Ti/N ratio steel at 900°C.

4.3 Discussion

4.3.1 Role of alloying elements

Previous work [20] showed that a combination of Al and Nb in HSLA steel encourages transverse cracking during casting. This was ascribed to the inter-granlur mode of failure due to the detrimental precipitation of AlN at the austenite grain boundaries. Al behaves in a similar manner when added to TWIP steel by encouraging inter-granular fracture [16]. The addition of Nb is beneficial to strength but detrimental to hot ductility due to the formation of Nb(CN). Both elements (Al and Nb) are nitride formers and it is necessary to avoid the formation of both compounds AlN and Nb(CN) to maintain good ductility in B containing steels.

Ti is also a nitride forming element but is not as detrimental to ductility as Al and Nb provided the TiN is coarse. Therefore, Ti is normally added when Al and Nb are present to in the steel to attract all the N from solution and only form TiN. This addition must be accompanied by a slow cooling rate <25 C min^{-1}, to allow TiN particles to coarsen and avoid any deterioration in ductility [41]. To make B effective, removing the N [146] is always required to allow it to segregate to the boundaries and strengthen them to obstruct inter-granular cracking.

During solidification, most of the N would be attracted to Ti to form coarse TiN particles, which act as nucleation sites for NbC precipitation [270]. Consequently, most of the NbC particles precipitate on the coarse TiN particles by the time the temperature reaches 1200°C during solidification [270]. Therefore, the detrimental fine precipitation of Nb(CN) is avoided, and in its place coarse Nb(CN) and TiN particles are obtained in the temperature range of the straightening stage as shown in Figures 4-11 and 4-12. A previous study [271] showed that increasing the amount of N increases the onset temperature for Nb(CN) precipitation and hence provides coarser particles.

Extensive work has been carried out successfully to reduce transverse cracking in Nb containing HSLA steels but not eliminating it. Therefore, further processing is always required and that includes scarfing the surface to remove surface cracks and trimming the edges to remove edge cracks, creating a considerable amount of scrap.

TWIP steels can be heavily alloyed with nitride formers that include Al, Nb, Ti and B to enhance specific properties. Therefore, there is always a great competition for N but Ti has the highest affinity to N among all the other nitride formers.

4.3.2 Analysis of the results

The hot ductility curves shown in Figure 4-4 can be analysed based on the optical micrographs shown in Figure 4-8(a-c). The improvement of the hot ductility, as the temperature drops from 1000 to 900°C, is associated with the onset of dynamic recrystallisation. It is shown to be more active in the region of the tensile specimen which is necking down to failure (Figure 4-8b). As the temperature goes down to 800°C, dynamic recrystallisation becomes less active and the grains coarsen further so (Figure 4-8c), and so ductility falls (Figure 4-4).

The marked deterioration of ductility from 900 to 1100°C could be attributed to the behaviour of B [15]. At elevated temperatures, >900°C, B has less tendency to segregate to the boundaries, and so there is more chance for inter-granular fracture to occur [15]. Therefore, the deterioration of ductility at the higher temperature end of the curves, >900°C, (Figure 4-4) is ascribed to the reduction of B segregation to the boundaries, grain boundary sliding which increases as a function of temperature and the absence of dynamic recrystallisation. Moreover, although full solidification under equilibrium conditions takes place at ~1270°C, liquid films can be present at the austenite grain boundaries at lower temperatures and their volume fraction increases as a function of temperature [272].

In order to evaluate the influence of Nb on the hot ductility, the current steels are compared with previous work on Nb free TWIP steels of otherwise similar composition. The previously examined steels were cooled at 60°C min^{-1} and so the current steels with the same cooling rate are used for comparison. The full composition of the current steels (1, 2 and 3) and previous work steels (4, 5 and 6) [174] is listed in Table 4-2. Moreover, the values of Ti/N ratio and [Ti][N] product were used to evaluate their influence on hot ductility.

Table 4-2 Compositions examined (wt-%) for Nb-free TWIP steels (4,5,6) in previous work [174] and the current containing TWIP steels (1,2,3).

Steel	C	Si	Mn	P	S	Al	Ti	Nb	B	N	Ti/N	[Ti][N] $\times 10^{-4}$
1	.60	.09	18.2	.009	.003	1.57	.019	.031	.0027	.009	2.1	1.71
2	.60	.09	18.2	.009	.003	1.55	.030	.032	.0028	.010	3	3
3	.60	.10	18.0	.010	.006	1.50	.075	.032	.0028	.011	6.8	8.25
4	0.55	0.07	17.6	0.019	0.0014	1.44	0.098	-	0.0017	0.009	10.9	8.8
5	0.62	0.30	18.2	0.007	0.006	1.50	0.105	-	0.0026	0.0073	14.4	7.7
6	0.60	0.30	18.2	0.019	0.005	1.50	0.100	-	0.0027	0.0068	14.7	6.8

The hot ductility curves for these steels at the temperature range (700-1100°C) are presented in Figure 4-18. It is obvious that as the N content and the [Ti][N] product increase the hot ductility improves. Furthermore, the addition of Nb actually improves the hot ductility. In the

presence of Ti, NbC particles are encouraged to precipitate out onto the Ti-rich particles at higher temperatures, resulting in coarser NbC and TiN particles and better ductility.

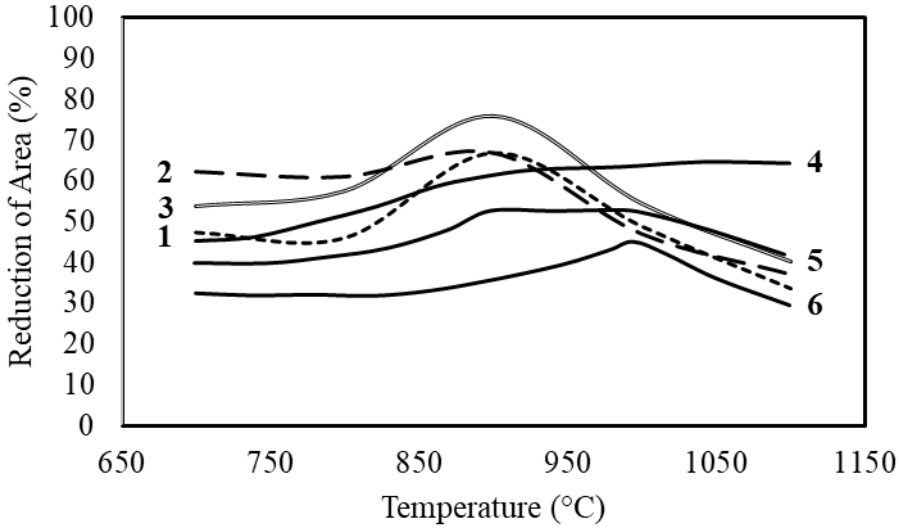

Figure 4-18 Hot ductility curves for Nb and Nb-free TWIP steels, cooled at 60°C min^{-1}.

It is observed that the [Ti][N] gives a better measure of hot ductility than the Ti/N ratio. It is worth mentioning that the straightening operation in continuous casting takes place in the temperature range 800-1000°C. In this range, the difference in ductility between the low and the medium Ti/N steels (steels 1 and 2) is very small but the high Ti/N steel (steel 3) gives the best ductility.

The hot ductility curves of the Nb free steels (steels 4, 5 and 6) varies markedly and so it is easier to identify the differences (Figure 4-18). It is observed that there is a direct relation between the [Ti][N] product and the hot ductility, in which increasing the [Ti][N] product (Table 4-2) leads to better ductility (Figure 4-18). This is related to the precipitation temperature, in which higher [Ti][N] product has the benefit of encouraging precipitation at higher temperatures and so the particles coarsen, leading to better ductility

In the current work, it is interesting that the low Ti/N steel (steel 1 < stoichiometric) did not show any detrimental AlN precipitation close to or at the boundaries. Alternatively, AlN precipitation was mainly in the matrix, which is not detrimental to ductility, so avoiding inter-granular fracture. At this high level of N, a higher volume fraction of AlN is present which has a detrimental influence on ductility. However, there is also a coarsening of particles which has a beneficial effect on ductility and this has the greatest effect.

4.3.3 Inter-granular and transgranular failure

Hot ductility in the austenitic phase depends on ease of crack formation and linking up of cracks along the grain boundaries. Inter-granular fracture is very common in steels but alloying the current TWIP steel with B was beneficial in keeping the failure trans-granular, and so giving good ductility.

Inter-granular failure, when the RA is less than 40%, is enhanced by the presence of fine particles along the boundary. Less distance becomes available between the particles, which facilitates the crack propagation along the boundary from one particle to another. Moreover, the finer particle distribution at the boundary at high temperatures (1000-1100°C) can delay or pin the grain boundary movement encouraging grain boundary sliding as shown in Figure 4-15, which explains the deterioration of the hot ductility at the higher temperature end of the curves in Figure 4-4.

In trans-granular failure, the fracture is governed by void nucleation. In this case, coarser particles in the matrix are considered detrimental for ductility because void nucleation is easier with coarse particles and vice versa [273]. With coarse particles, the cavities that are formed are deeper around the particles making it easier to join up and give trans-granular failure.

It is worth mentioning that it is not possible to eliminate the formation of grain boundary cracks. However, the development of these cracks is prevented by dynamic recrystallisation moving the boundary away from the cracks as finer recrystallised grains are produced (Figure 4-8b). In this way inter-granular failure does not take place. In this case, trans-granular failure takes over and the ductility becomes dependant on the ease of cracks linking up in the matrix. The cracks in the matrix then elongate into cavities and link up with cracks formed in the boundary and provide a mixed inter-granular and trans-granular failure as shown in Figure 4-16.

Previous work [274] confirmed that trans-granular failure is controlled by microvoid coalescence around the inclusions in the matrix. However, inter-granular failure is dependent on the dynamic recrystallisation and the amount of grain boundary sliding. The latter is the most critical operation that controls crack development and the greater it is, the longer are the cracks and the worse is the ductility (Figures 4-4 and 4-15).

Normally, cracks start forming at the grain boundaries so inter-granular failure contributes considerably toward failure behaviour. In this case, coarse precipitation is beneficial because it provides a longer distance between the particles, making it more difficult for cracks to link up. Moreover, coarse precipitation encourages dynamic recrystallisation and retards grain

boundary sliding, which is opposite to fine precipitation. Once the development of inter-granular failure is avoided, trans-granular failure takes over and having finer precipitation in the matrix can provide further improvement to ductility.

There is always a balancing act on the hot ductility behaviour depending on the precipitation characteristics e.g. size and volume fraction. The TiN precipitates can be coarsened to enhance ductility by increasing the content of Ti or N. However, this coarsening effect will be also accompanied by an increase in the precipitate volume fraction which is detrimental to ductility [60]. Previous work [60] showed that the increasing the Nb addition in a Ti containing steel resulted in coarser particles but without improving the hot ductility because of the higher volume fraction of precipitation which offset any benefits to ductility.

4.3.4 Influence of cooling rate

Increasing the cooling rate from 12 to 60°C min^{-1} was shown to improve the hot ductility for all the examined steels (steels 1, 2 and 3) independent of the Ti/N ratio as shown in Figures 4-4 to 4-7. This improvement can be analysed based on the SEM micrographs shown in Figures 4-13 and 4-14. The improvement of the hot ductility at the fast cooling rate is associated with a refinement of the particle size (see Figures 4-13 and 4-14 for comparison). Generally, it is expected that the particles will be finer at faster cooling rates because there is less time given for these particles to grow. For inter-granular failure, finer particle distribution normally results in early failure and poor ductility. However, when trans-granular failure is dominant, finer particle size will be beneficial to ductility. Indeed, previous work [275] on HSLA steel showed that increasing the cooling rate from 12 to 60°C min^{-1} lead to worse ductility because inter-granular fracture was the dominant mode of failure. Therefore, the influence of cooling rate on hot ductility can vary depending on the mode of failure.

4.3.5 Influence of reheating to 1250°C

In the current work, steel samples were examined in the laboratory using hot tensile tests to simulate the continuous casting process to assess the likelihood of transverse cracking. In continuous casting, the steel is heated to the meting temperature, 1420°C. However, the steel samples in the current work were re-heated to only 1250°C due to the technical difficulties in reaching such a high temperature ~1420°C during the tests. This difference in thermal history must be considered to interpret the results in relation to the continuous cast process. Upon re-heating to 1250°C, some of the N combined with Ti as TiN is taken back into solution. The amount of of N that goes back into solution at 1250°C can be predicted using the solubility

equation derived by Wada and Pehlke [152]. The results on the presently examined steels are given in Table 4-3.

Equation 8

$$Log\ (wt\text{-}\%Ti)(wt\text{-}\%N)total = -14400/T + 4.94 \qquad where\ T\ is\ in\ K.$$

Table 4-3 Nitrogen in solution at 1250°C from solubility equations for TiN (wt-%).

Steel	Ti/N ratio	Ti	Total N	N_2 in solution
1	2.1	0.019	0.009	0.0052
2	3.0	0.030	0.010	0.0037
3	6.8	0.075	0.011	0.0008

The solubility equation of Leslie et al. [276] for steels with 1.5% Al free of Ti, shows that no N will be taken back into solution at 1250°C from the AlN precipitates. It is, therefore, unlikely that any of the N will go back into solution on re-heating in any of the current TWIP steels containing both Al and Ti, so that precipitation pattern is consistent in both cases (melting and re-heating).

In regards to MnS precipitation, the solubility equation for MnS [277] shows that no sulphur will be taken back into solution at 1250°C due to the high Mn content.

Equation 9

$$Log\ [Mn][S] = -14855/T + 6.82$$

Grain size is mainly affected by phase transformation but in the current austenitic TWIP steel no phase change will take place on re-heating and so the grain size will be similar to that given by the as-cast condition.

SEM and EDS analysis have been conducted in order to analyse the precipitates present in the current TWIP steels based on the Ti/N ratio. In the low Ti/N ratio (steel 1), there is a high amount of AlN forming and this is because of the lack of sufficient Ti to combine with all the N.

In the case of the high Ti/N ratio (steel 3), AlN precipitates are not present and only Ti-Nb-rich particles are observed as shown in Figure 4-10. Therefore, it can be understood that Ti first combines with the N and any N remaining in solution, as for steel 1, ends up combined with the Al.

4.3.6 The role of S in influencing the hot ductility

A previous study [278] found that the segregation of S to the austenite grain boundaries is detrimental to the hot ductility. Another investigation [279] showed that precipitation of AlN to the grain boundaries can pin them and makes it easier for S to segregate to the boundaries. Reducing the S content in the composition was found to improve ductility even with the presence of high volumes of AlN precipitation. Recent work [280] has examined the role of a low S content, ~0.0005%, in influencing the hot ductility of TWIP steel with a similar processing conditions to the current work and observed very good ductility throughout the temperature range (700-1000°C). AlN precipitates are found to be always attached to MnS particles as shown in Figure 4-9. The MnS particles act as nucleation sites for AlN precipitation and so having a low S level will restrict the sites available for AlN to precipitate out. This lack of sites reduces the volume fraction of AlN precipitates and restricts their presence to the matrix rather than the boundaries [16]. Generally, a high Mn content with low sulphur level [281] has been shown to restrict the MnS precipitation to the matrix so avoiding the detrimental precipitation at the grain boundaries. In fact, eliminating the S from the steel will result in the production of crack-free steel but this is commercially not possible yet [280].

5 Experimental, results and discussion of hot rolled HSLA steel

5.1 Experimental

5.1.1 Composition

Laboratory vacuum melts were produced as 22kg ingots with the composition analysis given in Table 5-1. The base composition was ~0.06% C, 0.5% Si, 1.4% Mn. Steel H1 is of similar composition to steel H2 but is a ”normal” low Al (0.02-0.04%Al) plain C-Mn steel and will be used for comparison purposes to confirm or otherwise whether a high Al addition is beneficial to impact performance. In general, AlN is very sluggish in precipitating out in austenite and does not precipitate out during rolling and so does not influence grain size [282]. Most of the previous investigations have focused on low Al containing steels, ~0.02%Al, where AlN does not precipitate out during rolling. Increasing the Al content in the current work aims to encourage precipitation of AlN, as the driving force for precipitation becomes higher and thus Al can remove some or all the N from solution. N in solution has a detrimental effect on the impact behaviour of steels because it increases the ITT [283]. The removal of 0.001N% from solution has been shown to reduce the ITT by 2.75°C in plain C–Mn steels [283]. Impact behaviour has been shown, according to previous studies, to be improved by the addition of Al [26], the optimum being observed at 0.16%Al, and so this level was used for steel H2 [23,24].

In order to reach the strength level of control rolled steels an addition of Nb has been made to enhance the strength by precipitation hardening and grain refinement. Nb is normally added in the range 0.015-0.03% for strengthening and 0.018%Nb has been chosen for steel H3.

The C content has been kept low at ~0.06% so as to minimise the likelihood of formation of lower transformation products, bainite and martensite. Silicon is added to steels to increase strength without deteriorating the impact behaviour. Commercially, the Si addition is normally set at 0.3% but a recent study [26] has shown that a further improvement in strength without influencing the impact behaviour can be made by increasing the addition to 0.5%. The beneficial influence of Si on strength was reported previously to give a solid solution strengthening of 80MPa on adding 1%Si [284]. Therefore, the contribution of Si for the all the examined steels in the current work would be estimated to give an additional strength of ~40MPa and ~10°C reduction in ITT.

The carbon solubility in ferrite at room temperature is very low, ~0.001%. When the carbon precipitates out on cooling to room temperature it can come out in various forms depending on

the carbon content and cooling rate. If the cooling rate is rapid the carbon cannot get to the boundaries, alternatively it precipitates as cementite in the form of pearlite. At a high cooling rate, the carbon gets frozen in solution and forms colonies of martensite. In case of the current low C steels, 0.06%C, under normal cooling conditions (air cooling), the majority of the carbon would be expected to precipitate out easily in the form of cementite and at the boundaries. Carbides are brittle in nature and they provide the nucleation sites for crack initiation and propagation [285], so the finer they are the better is the impact behaviour.

Both Al and Nb have a major role on the development of grain boundary carbides and thus impact behaviour. Al contributes to slowing down the diffusion rate of carbon at the grain boundaries [23]. In earlier work, Al was reported to lower the pearlite start transformation temperature this being the temperature the carbides first form so giving less time for carbides to develop at the boundaries [285]. However, in the case of low Al additions (≤0.02%), the transformation temperature is higher and most of the C precipitates out as carbides at the grain boundaries resulting in thicker carbides.

Extra care was taken during the design of the alloying composition and heat treatment to avoid the formation of the lower transformation products in the microstructure. The additions of both Al and Nb were restricted and the cooling rate through the transformation was reduced by working at a thicker plate.

Nb is a strong carbide forming element, so encouraging the formation of NbCN precipitates [286]. The solubility of Nb depends mainly on the amount of Nb added to the composition. Increasing this amount leads to a subsequent rise in the dissolution temperature [287]. In the current work, the solubility temperature of Nb was predicted previously by Thermo-Calc to be ~1200°C [259]. Therefore, the re-heating temperature in the current work was set to ~1250°C in order to ensure a complete dissolution of all the Nb particles.

Steels H1 and H3 are of similar composition to steels H4 and H5, respectively, but the former plates were rolled to 15mm gauge and the latter two to 30mm thickness followed by air cooling. The cooling rates for 15 and 30mm air cooled plates are 33°C min^{-1} and 17°C min^{-1}, respectively. The slower cooling rate of the thicker plate may be helpful in avoiding the lower transformation products. The increase in finishing thickness to 30mm meant that the ingot size had to be increased to 60kg to ensure that sufficient deformation was available to break down the as cast structure.

Steels C1 and C2 are of similar composition to steels H1 and H2, respectively, but H-steel plates were processed by hot rolling while the C-steel plates were control rolled so that comparisons could be made.

Table 5-1 Composition wt-%, rolling condition and cooling rate of the HSLA steels chosen for examination.

Steel	Rolling condition	Cooling rate (°C min^{-1})	C	Mn	Si	S	P	Nb	Al	N
H1	HR*	33	0.051	1.4	0.46	0.0043	0.005	-	0.02	0.009
H2	HR	33	0.06	1.4	0.47	0.0045	0.005	-	0.16	0.007
H3	HR	33	0.056	1.39	0.46	0.0046	0.005	0.018	0.16	0.006
H4	HR	17	.061	1.39	.49	.0046	.004	-	.022	.007
H5	HR	17	.062	1.38	.49	.0041	.004	0.018	.17	.007
C2	CR+	33	0.06	1.4	0.47	0.0045	0.005	-	0.16	0.007
C3	CR	33	0.056	1.39	0.46	0.0046	0.005	0.018	0.16	0.006

HR*: hot rolling, CR+: control rolling.

5.1.2 Rolling

After casting, the ingots were soaked at 1250°C in a furnace and then rolled, finish rolling at 950°C and 900°C, for the hot and control rolled plate plates, respectively. The hot rolling was carried out to give 15mm and 30mm thick plates, the cooling rates being 33 and 17°C min^{-1}, respectively. The control rolling was carried out also to give only 15mm thick plates, the cooling rate being 33°Cmin^{-1}. The temperature and heating time used was sufficient to ensure dissolution of all the carbides and the nitrides. The steel was then taken out of the furnace and rolled. Since the hot steel reacts with oxygen in the air, an oxide scale formed on the outer surface of the steel and this scale was removed before entering the mill using a hammer to avoid deterioration of the surface quality. The ingot was rolled by a powerful four-roll mill having two back up rolls and two smaller working rolls. The rolling schedules for the hot and control rolling are presented in Figures 5-1 and 5-2, respectively. The steel plates were then left to cool in air as shown in Figure 5-3 (See Appendix B for the detailed rolling schedule of the HSLA steels examined).

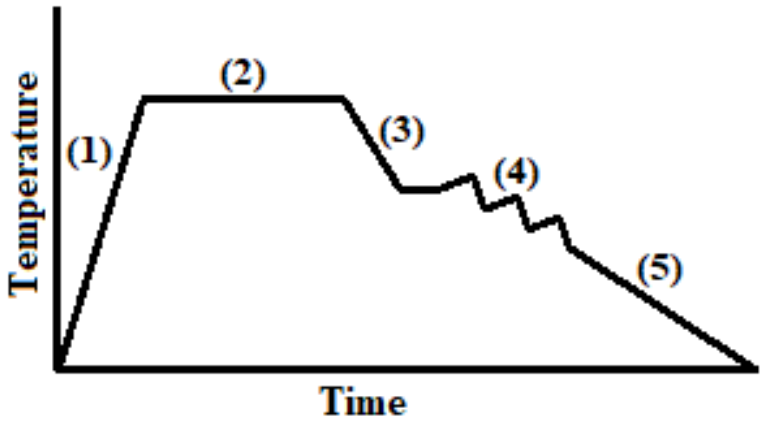

Figure 5-1 Schematic diagram of the hot rolling process: 1) Heating from room temperature to soaking temperature 1250°C; 2) Held at soaking temperature for 20 mins; 3) Gap time to receiving the billet from the furnace to the mill; 4) Deformed at temperatures generally in the range 1100°C to 950°C; 5) The plates were then air cooled after rolling to the desired thickness.

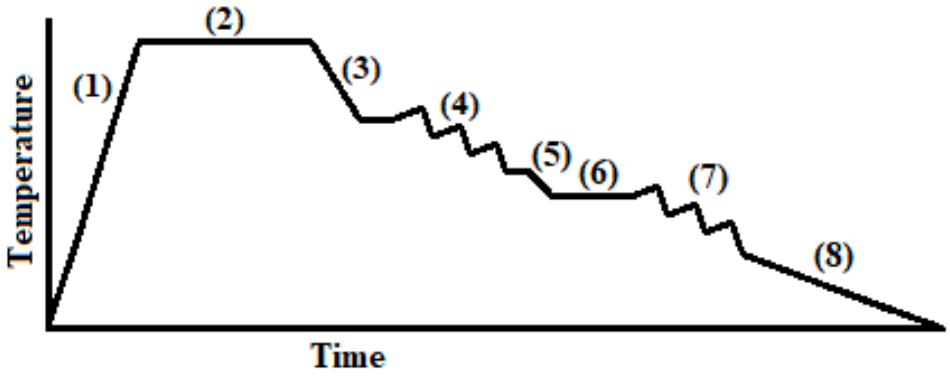

Figure 5-2 Schematic diagram of the control rolling process: 1) Heating from room temperature to soaking temperature 1250°C; 2) Held at soaking temperature for 20 mins; 3) Gap time to receiving the billet from the furnace to the mill; 4) Deformed at temperatures generally in the range 1100°C to 1030°C; 5) Lowering the temperature to 950°C; 6) Held at this temperature; 7) Deformed at temperatures generally in the range 950°C to 900°C; 8) The plates were then air cooled after rolling to the desired thickness.

5.1.3 Charpy impact test

Standard Charpy V-notch impact samples were machined from the rolled plates in the rolling direction (Figure 5-3). The samples were prepared for the Charpy impact V-notch test based on the ISO 148-1 standard. Specimens were 55.60mm in length and 10.06mm in width and all specimens were notched in an identical way as shown in Figure 5-4. Controlling the temperature of each sample was achieved by immersing the specimen into constant temperature baths of liquid nitrogen and iso-pentane for 30 minutes. The specimens were then removed from the bath and rapidly transferred to a sample holder in the impact testing machine and impact tested (Figure 5-5). The values of the impact energy absorbed by the samples were

monitored using the software Zwick/Roell. This process was repeated for each sample over a range of temperatures to establish the impact transition curve.

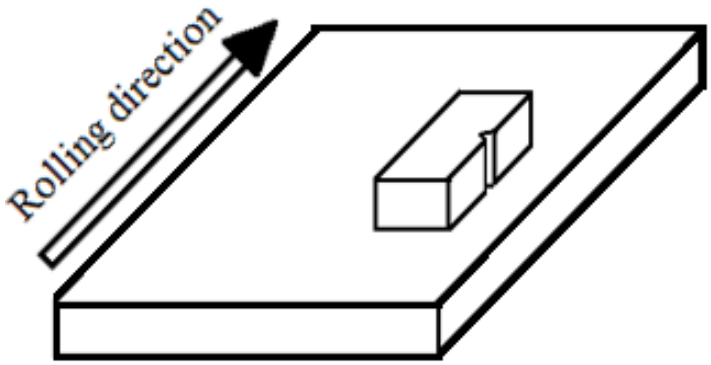

Figure 5-3 Schematic diagram of the impact specimen orientation relative to the rolling direction of the plate.

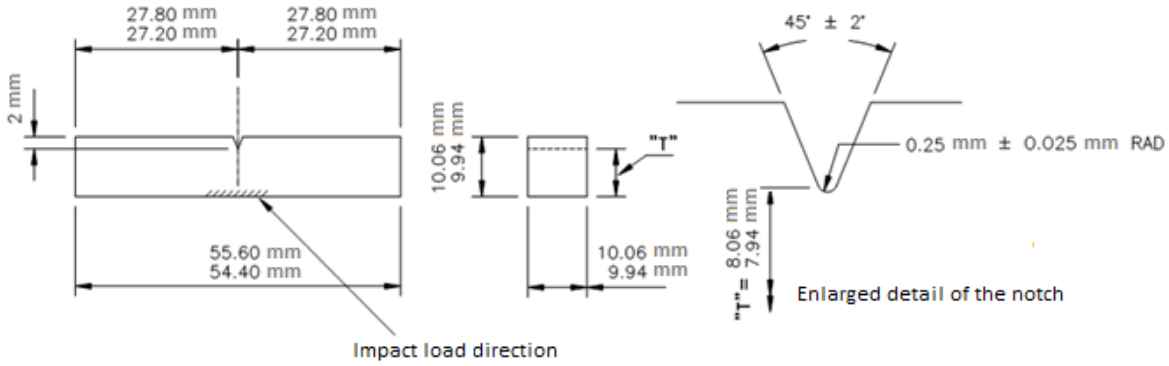

Figure 5-4 Detailed dimensions of the impact test specimens.

Figure 5-5 Charpy Impact testing machine.

5.1.4 Tensile test

Duplicate tensile specimens were machined from the plates in the transverse direction (Figure 5-6a) and tested to fracture on an Instron tensile machine under static loading conditions at a cross head speed of 0.025 cm min^{-1}. The tensile test was carried out according to ISO 6892-1 standard at room temperature using a tensile testing machine supplied by DMG universal machines (Figure 5-6b). The samples had a 55mm gauge length and were 10mm in diameter (Figure 5-7). Strain gauges were connected to the samples to record the strain data during the test. The stress-strain curve was monitored using Bluehill software.

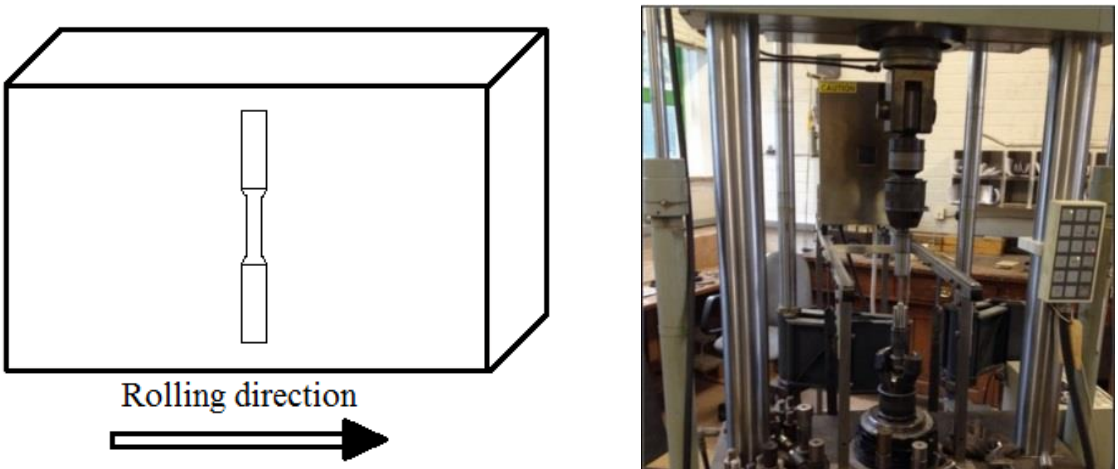

(a) (b)

Figure 5-6 (a) Schematic diagram of the tensile specimen orientation relative to the rolling direction of the plate.(b) Instron tensile testing machine supplied by DMG universal machines.

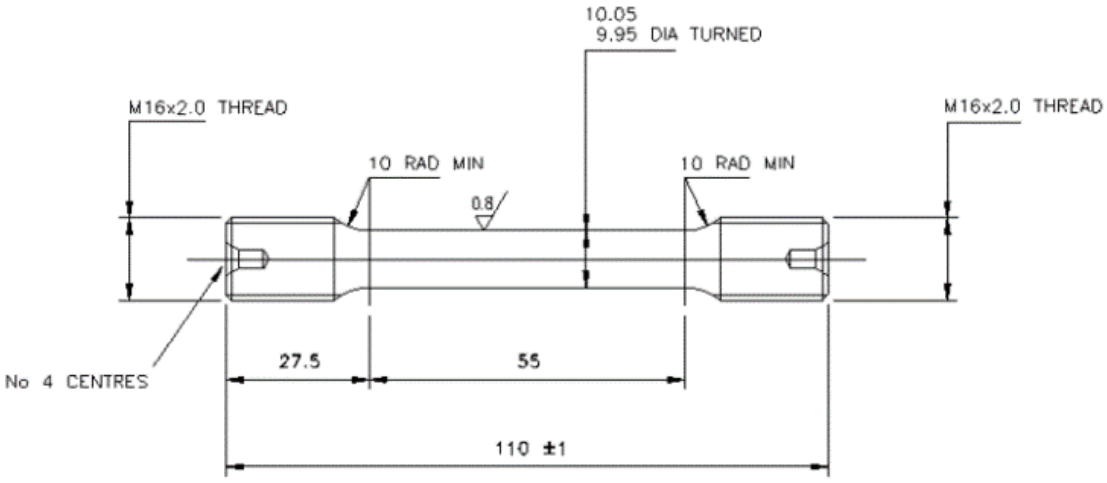

Figure 5-3 Detailed dimensions of the tensile test specimens.

5.1.5 Metallography

Preparation of samples

One broken Charpy specimen showing a fully brittle fracture was taken at each composition and cooling rate for further analyses of the microstructure. The surface to be examined was the face opposite to the notch. The samples were then ground and polished according to the schedule shown in Table 5-2. On moving from one pad to another, the surface was cleaned with washing up liquid then sprayed with absolute ethanol and finally dried. At this stage, the samples had a mirror surface finish without any scratches or foreign matter for clear microscopic examination. Finally, the samples were etched using 2%nital (2%nitric acid with 98%ethanol by volume) to show the detailed microstructure.

Table 5-2 Preparation steps of samples for metallographic examination (stages 1-4).

Stage	Surface	Abrasive / Size	Load (N)	Rotation	Base Speed (rpm)	Time (min)
1	CarbiMet	120 to 320 grit SiC water cooled	30	Clockwise	300	Until Plane
2	UltraPad	9um MetaDi Supreme Diamond	30	Anticlockwise	150	5:00
3	TriDent	3um MetaDi Supreme Diamond	30	Clockwise	150	3:00
4	ChemoMet	0.05um MasterPrep Alumina	30	Anticlockwise	150	2:00

Optical microscopy

Optical microscopy (OM) examinations were carried out to analyse the microstructure as a function of composition and cooling rate. The volume fraction of the phases present was measured by the point counting method while grain size was measured by the linear intercept method. The grain boundary carbide density was measured by counting the number of grain boundary carbides in a 20 mm linear traverse.

Scanning electron microscope

Scanning electron microscope (SEM) examinations were performed to analyse the microstructure as a function of composition and cooling rate. Examinations were carried out using FEG-SEM and the spatial resolution of the microscope was <50nm at 20kV accelerating voltage. The SEM was used to measure the thickness of the grain boundary carbides. The thickness of 100 carbides was measured for each sample and the average value was taken.

5.2 Results

5.2.1 Mechanical properties

Influence of increasing Al content from 0.02 to 0.16%

The lower yield strength results of the 0.02%Al and 0.16%Al steels are shown in Figure 5-7. The Al content did not noticeably influence the lower yield strength. Indeed, the 0.02%Al steel gave a slightly higher strength, ~12MPa, which is equivalent to 4% increase. (See Appendix B for the detailed tensile measurements).

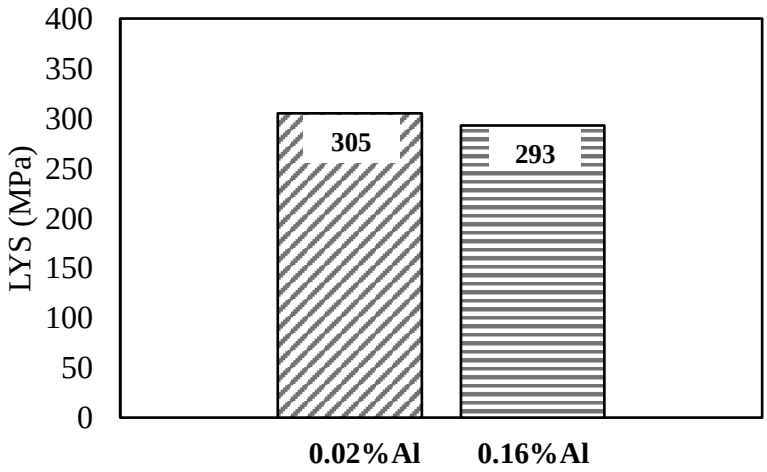

Figure 5-4 Lower yield strength of the 0.02%Al and 0.16%Al steels.

The Impact transition curves of the 0.02%Al and 0.16%Al steels are shown in Figure 5-8. Increasing the Al content gave a considerable improvement in impact behaviour, reducing the 27J, impact transition temperature (ITT) from -50 to -90°C. (See Appendix B for the detailed impact energy measurements).

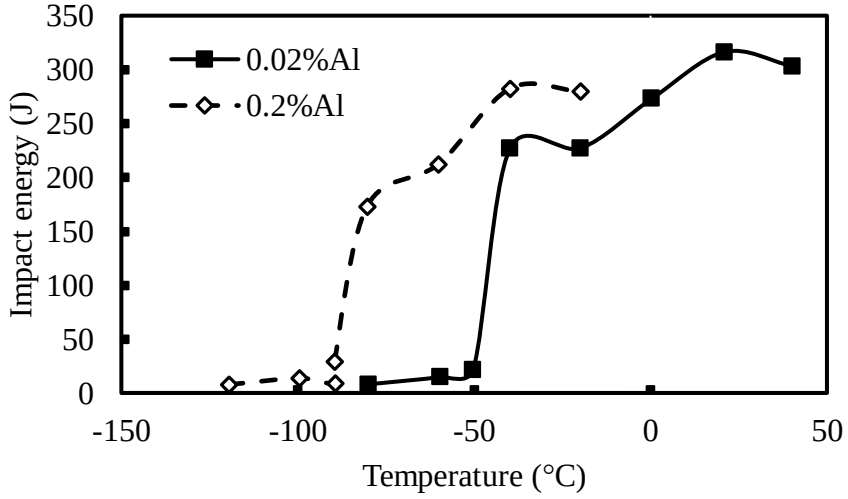

Figure 5-5 Impact energy of the 0.02%Al and 0.16%Al steels at various temperatures.

Influence of 0.018%Nb addition to the 0.16%Al steel

The lower yield strength results of the Nb free and 0.018%Nb containing steels are shown in Figure 5-9. The lower yield strength was significantly enhanced by the addition of Nb, in which the strength increased by 92MPa, which is equivalent to ~30% increase.

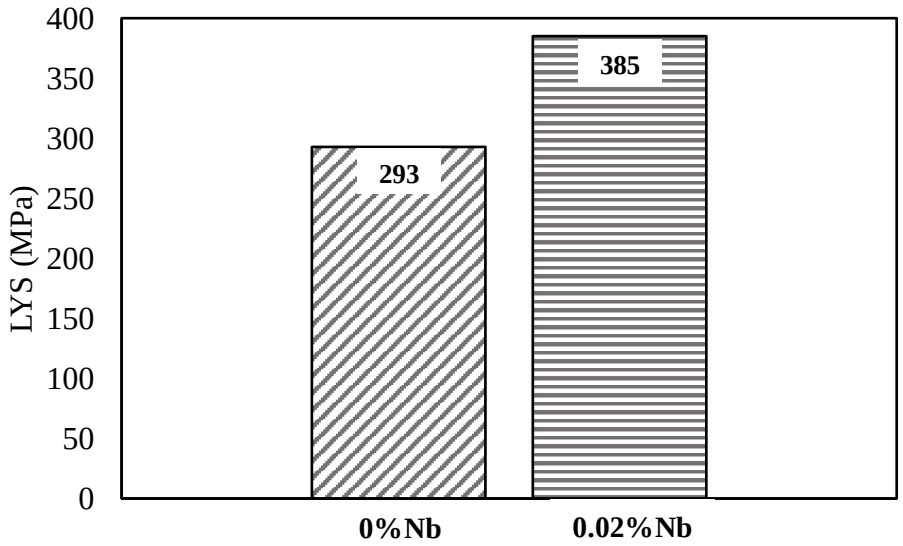

Figure 5-6 Lower yield strength of the Nb free and 0.018%Nb steels.

The Impact transition curves of the Nb free and 0.018%Nb containing steels are shown in Figure 5-10. The addition of Nb led to a marked deterioration in impact behaviour, increasing the 27J, ITT from -90 to -30°C.

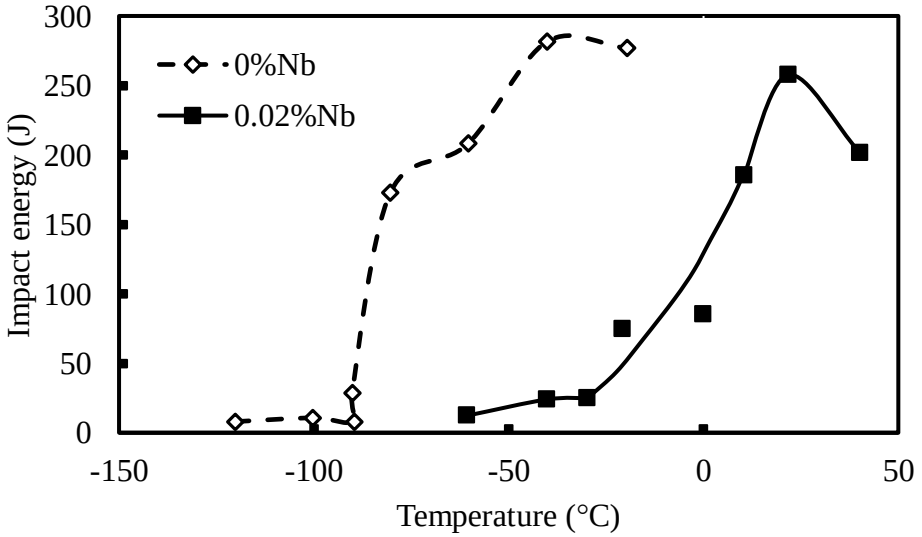

Figure 5-7 Impact energy of the Nb free and 0.018%Nb steels at various temperatures.

Influence of cooling rate on the 0.02%Al steel

The lower yield strength results of the 0.02%Al steel at both cooling rates (33 and 17°C min^{-1}) are shown in Figure 5-11. Reducing the cooling rate was found to reduce the lower yield strength by ~10%.

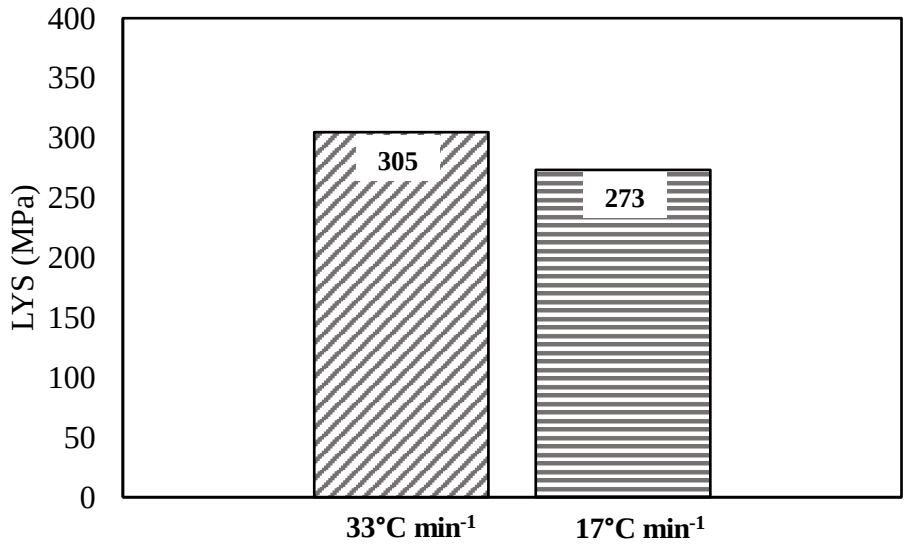

Figure 5-8 Lower yield strength of the 0.02%Al steel at both cooling rates (33 and 17°C min^{-1}).

The Impact transition curves of the 0.02%Al steel at both cooling rates (33 and 17°C min^{-1}) are shown in Figure 5-12. Reducing the cooling rate led to a small improvement of impact behaviour, the 27J, ITT decreasing by a small amount from -50 to -60°C.

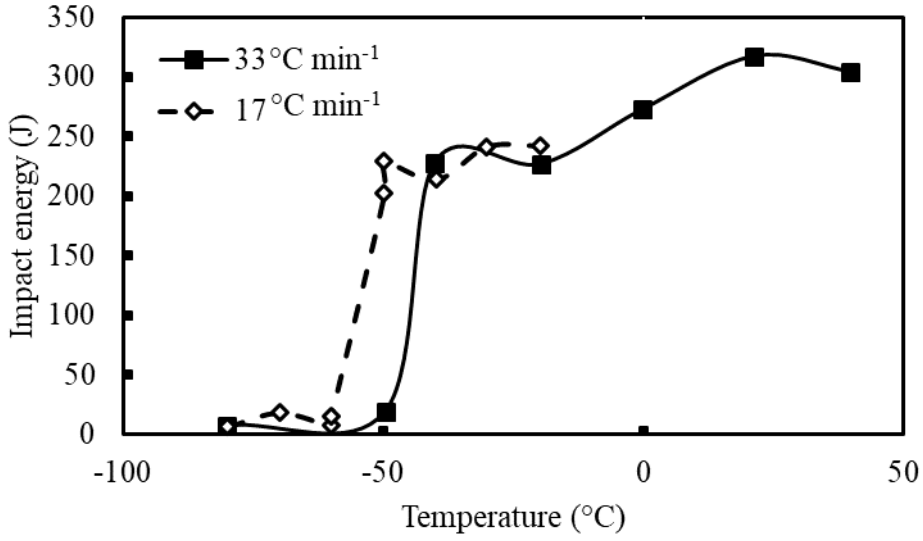

Figure 5-9 Impact energy of the 0.02%Al steel at both cooling rates (33 and 17°C min^{-1}) at various temperatures.

Influence of cooling rate on the 0.018%Nb containing steel

The lower yield strength results of the 0.018%Nb containing steel at both cooling rates (33 and 17°C min^{-1}) are shown in Figure 5-13. Again, reducing the cooling rate was found to reduce the lower yield strength by ~10%.

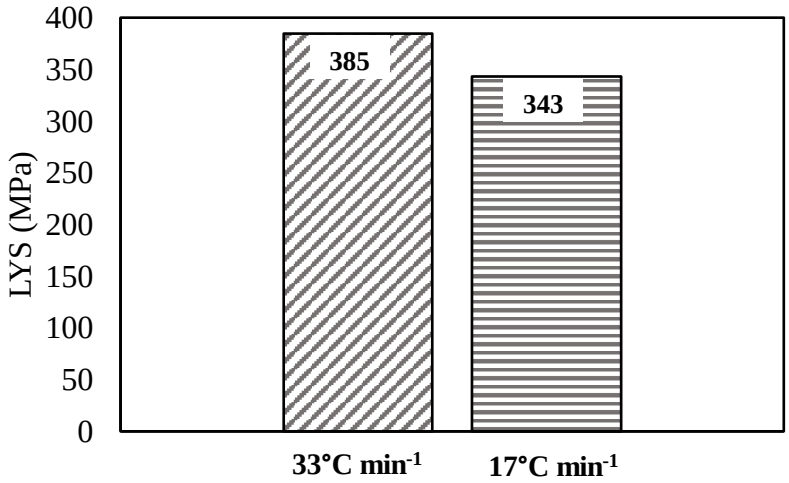

Figure 5-10 LYS of the 0.018%Nb steel at both cooling rates (33 and 17°C min^{-1}).

The Impact transition curves of the 0.018%Nb containing steel at both cooling rates (33 and 17°C min^{-1}) are shown in Figure 5-14. Despite the scatter shown at the lower temperature end at the slower cooling rate, impact behaviour is generally better on slower cooling, the 27J impact ITT decreasing from -30 to -40°C.

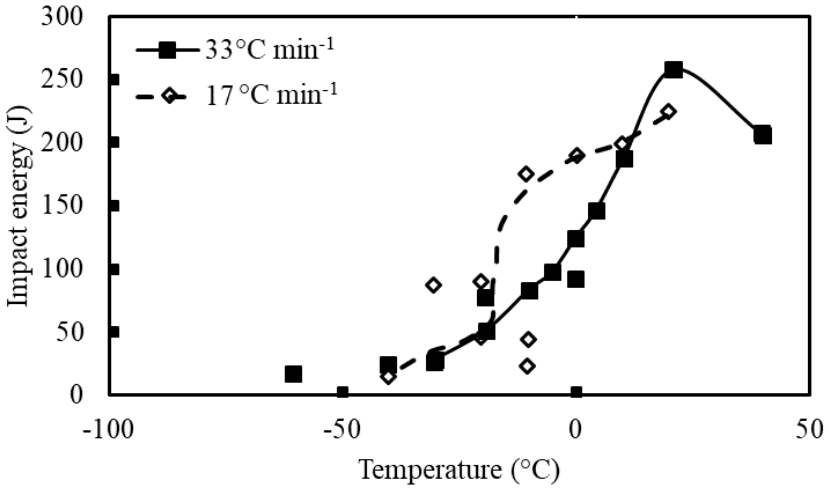

Figure 5-11 Impact energy of the 0.018%Nb steel at both cooling rates (33 and 17°C min^{-1}).

Both steels (0.02%Al and 0.018%Nb) showed a very similar response to cooling rate independent of the composition, the slower cooling rate giving a 10% lower yield strength and a decrease in 27J, ITT of 10°C.

Influence of control rolling on the 0.16%Al steel

The Impact transition curves of the hot and control rolled 0.16%Al steels are shown in Figure 5-15. Both steels exhibit very similar impact energy throughout the entire temperature range -20 to -120°C, and both have a 27J, ITT of ~-90°C.

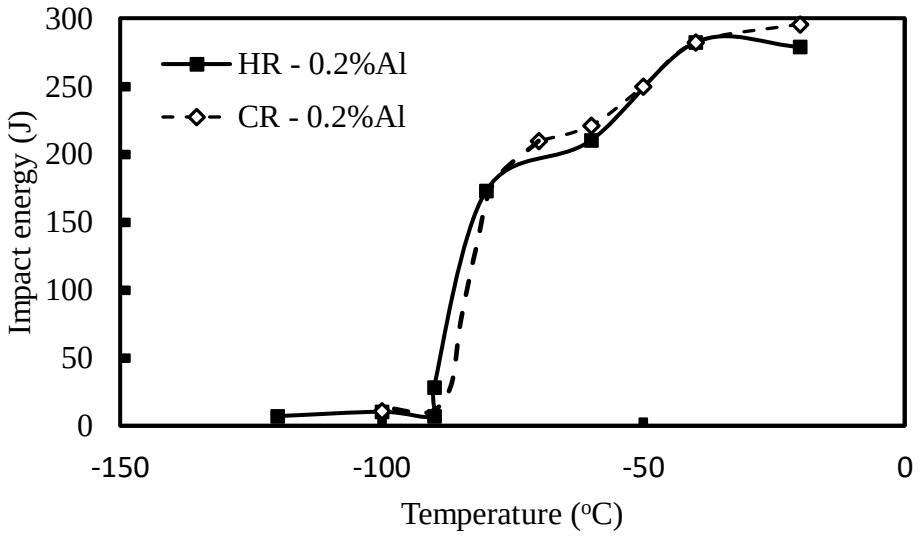

Figure 5-12 Impact energy curves of the hot and control rolled 0.16%Al steels.

Influence of control rolling on the 0.018%Nb containing steel

The Impact transition curves of the hot and control rolled 0.018%Nb containing steels are shown in Figure 5-16. Both steels behave in a similar manner in the temperature range 40-20°C but as the temperature drops further, control rolling was found to be effective in increasing the impact energy and lowering the 27J, ITT from -30°C to -75°C.

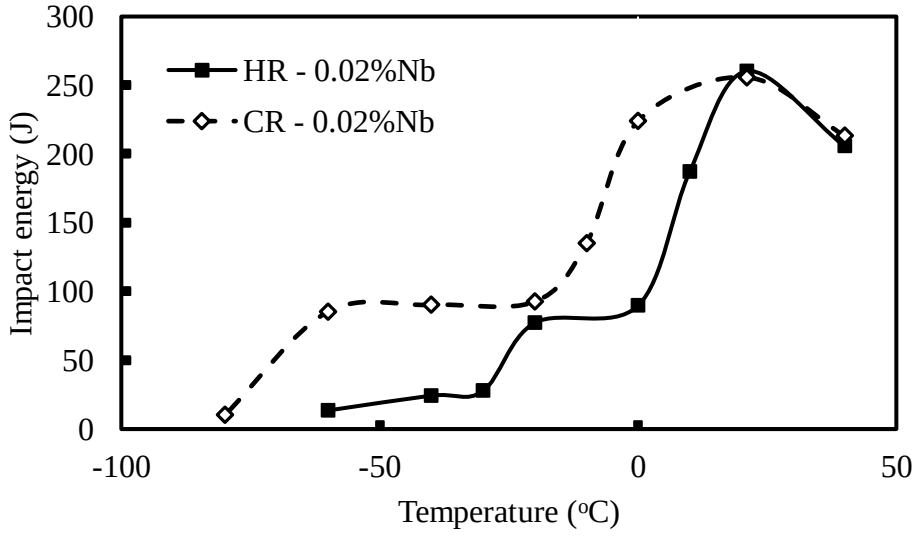

Figure 5-13 Impact energy curves of the hot and control rolled 0.018%Nb containing steels.

5.2.2 Optical micrographs

Influence of increasing Al content from 0.02 to 0.16%

The microstructures of the hot rolled 0.02%Al and 0.16%Al steels are shown in Figures 5-17 and 5-18, respectively. The phases present in both steels are ferrite and pearlite. Increasing the Al content from 0.02 to 0.16%Al raised the volume fraction of pearlite significantly from 5 to 8%. The grain sizes were found to be 6.4 and 6.5$mm^{-1/2}$ for the 0.02%Al and 0.16%Al steel, respectively, which is not significantly different.

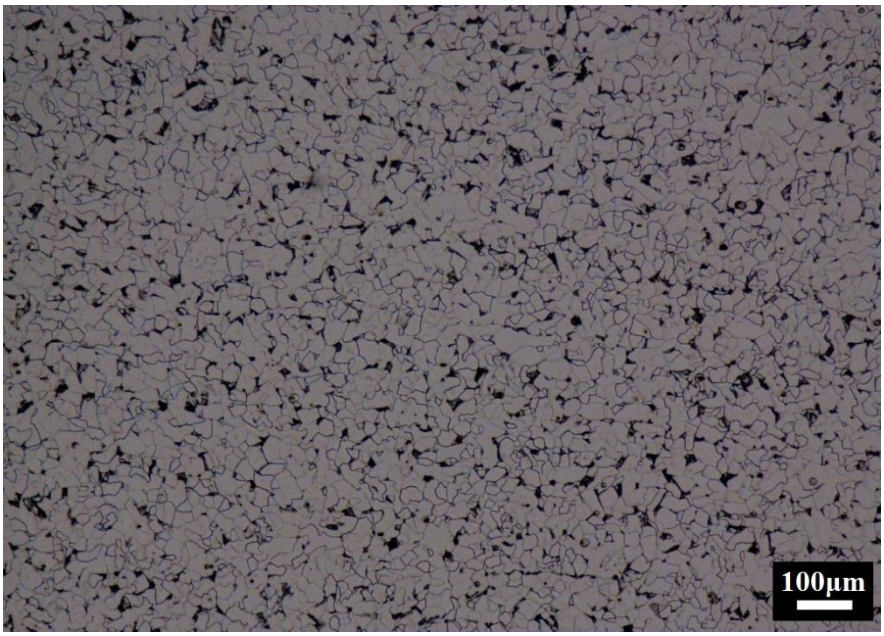

Figure 5-14 Optical microstructure of the hot rolled 0.02%Al steel at 33°C min^{-1}.

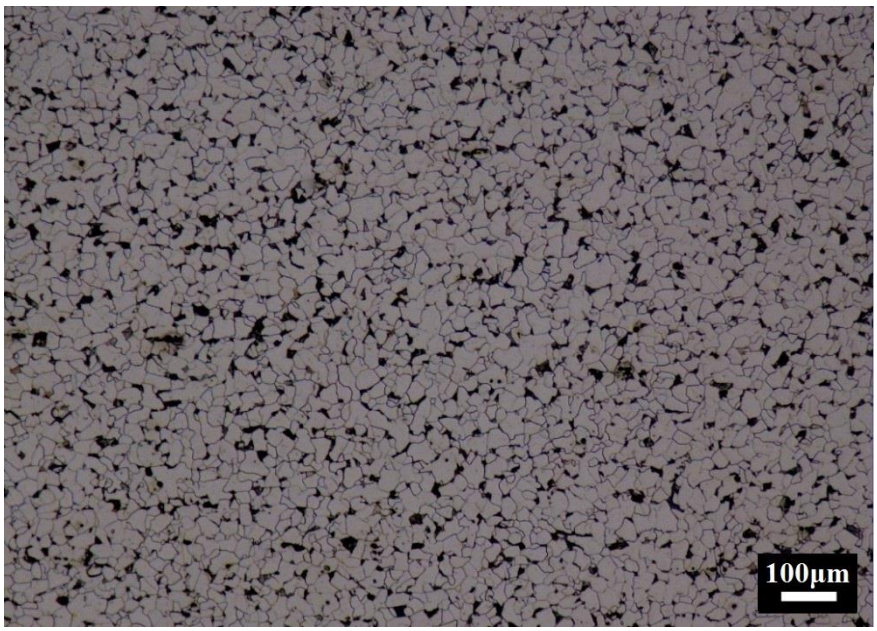

Figure 5-15 Optical microstructure of the hot rolled 0.16%Al steel at 33°C min^{-1}.

Influence of 0.018%Nb addition to the 0.16%Al steel

The microstructure of the hot rolled 0.018%Nb containing steels is shown in Figure 5-19. The volume fraction of pearlite decreased from 8 to 4% by the addition of 0.018%Nb (Table 5-3, see Figures 5-18 and 5-19 for comparison). This addition also changed the grain size distribution from a homogeneous to a heterogeneous distribution (a mixture of fine and coarse grains) but overall the grain size was refined from 6.5 to 8.2$mm^{-1/2}$ by the Nb addition.

Influence of cooling rate on the 0.02%Al steel

The microstructure of the hot rolled 0.02%Al steel at the slower cooling rate (17°C min^{-1}) is shown in Figure 5-20. Only ferrite and pearlite phases were present in the microstructure at both cooling rates Nb (Table 5-3, see Figures 5-17 and 5-20 for comparison). Lowering the cooling rate did not affect the grain size distribution but slightly coarsened the grain size from 6.4 to 6.1$mm^{-1/2}$.

Figure 5-16 Optical microstructure of the hot rolled 0.02%Nb containing steel at 33°C min^{-1}.

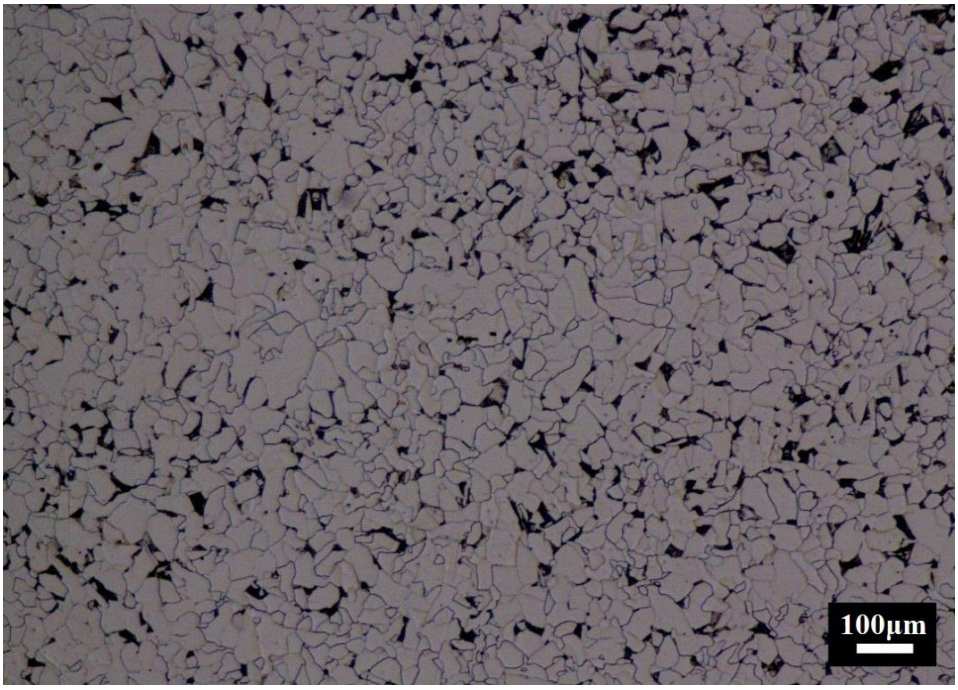

Figure 5-17 Optical microstructure of the hot rolled 0.02%Al steel at 17°C min^{-1}.

Influence of cooling rate on the 0.018%Nb containing steel

The microstructure of the hot rolled 0.018%Nb containing steel at the slower cooling rate (17°C min^{-1}) is shown in Figure 5-21. Again, no significant effect was observed on the volume fraction of phases (Table 5-3, see Figures 5-19 and 5-21 for comparison). The grain size distribution was similar in both steels but reducing the cooling rate coarsened the grain size from 8.2 to 7.4mm$^{-1/2}$.

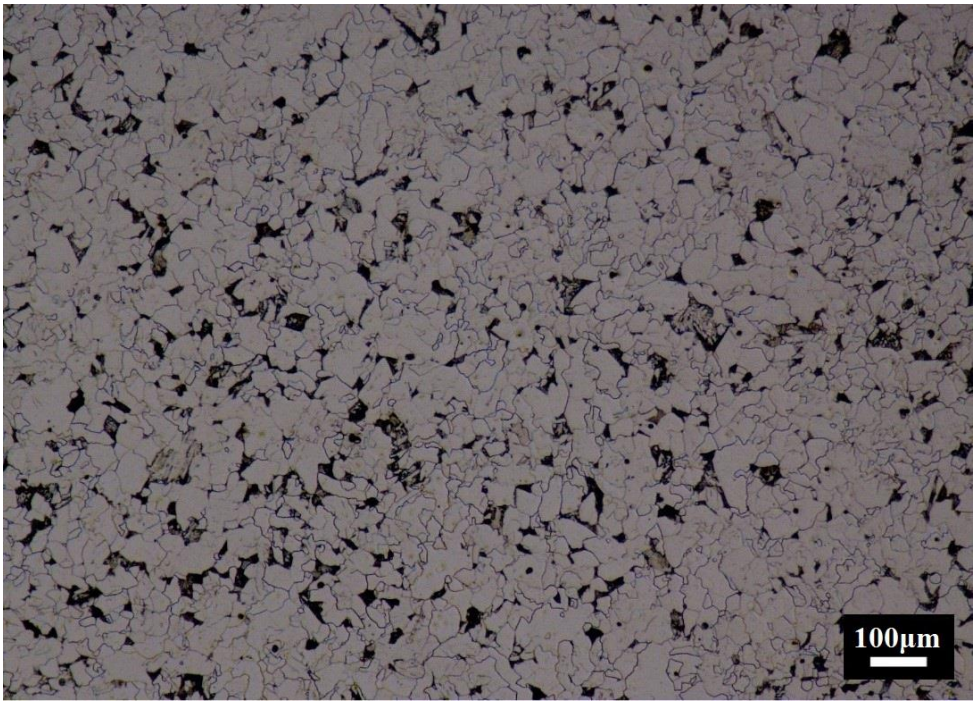

Figure 5-18 Optical microstructure of the hot rolled 0.018%Nb containing steel at 17°C min^{-1}

Influence of control rolling on the 0.16%Al steel

The microstructure of the control rolled 0.16%Al steel is shown in Figure 5-22. Only ferrite and pearlite phases were present in the microstructure for both rolling conditions, hot rolling and control rolling (Table 5-3). The control rolling condition did not have any influence on the pearlite volume fraction nor the grain size (the slight refinement from to 6.5 to 6.6$mm^{-1/2}$is not significan).

Influence of control rolling on the 0.018%Nb containing steel

The microstructure of the control rolled 0.018%Nb steel is shown in Figure 5-23. Only ferrite and pearlite phases were present in the microstructure for both rolling conditions, hot rolling and control rolling (Table 5-3, see Figures 3.3-19 and 3.3-23 for comparison). The control rolling condition was found to increase the pearlite volume fraction from 4 to 5 (not significant), with a small grain size refinement from 8.2 to 8.4$mm^{-1/2}$.

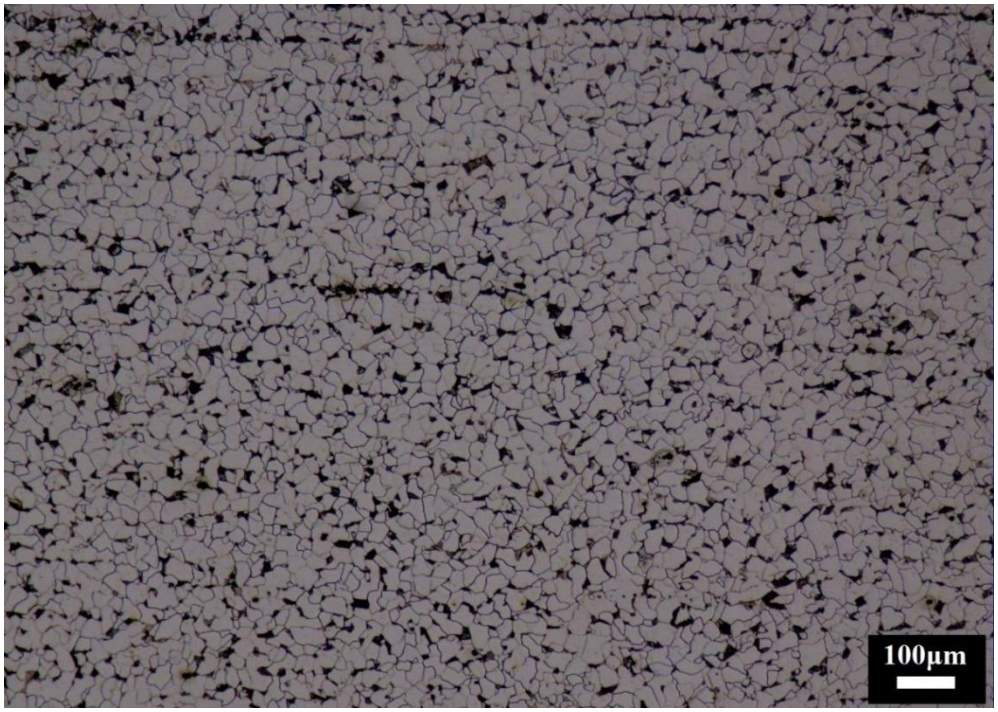

Figure 5-19 Optical microstructure of the control rolled 0.16%Al steel at 33°C min^{-1}.

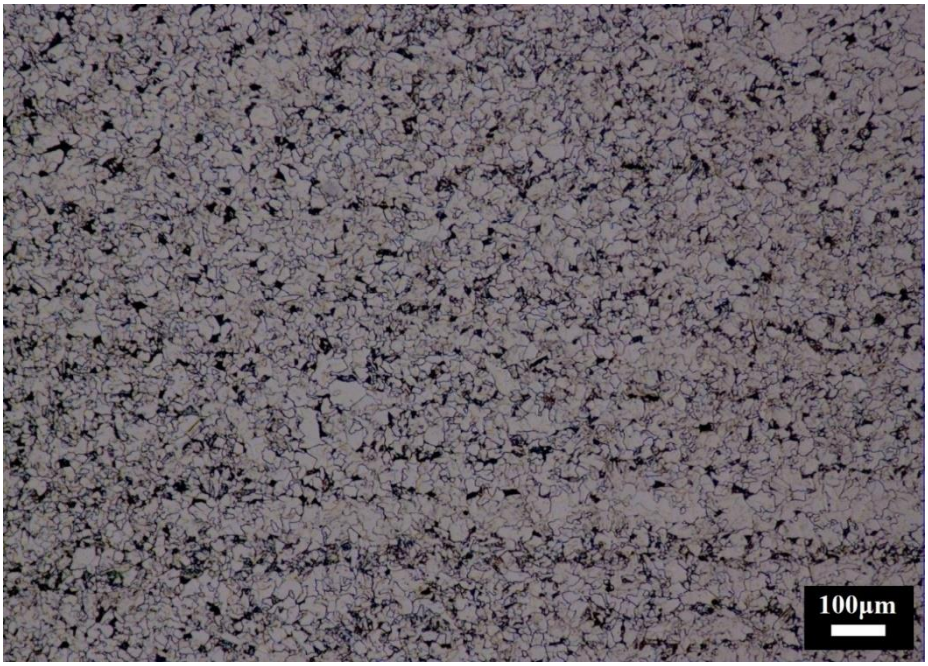

Figure 5-20 Optical microstructure of the control rolled 0.018%Nb containing steel at 33°C min^{-1}.

Detection of Widmanstätten ferrite by optical microscope

A feature of these steels was the presence of Widmanstätten ferrite in most of the steels particularly after hot rolling as well as lower transformation products. Widmanstätten ferrite is normally recognised by the ferrite lenticular islands that appear in the pearlite colonies. However, optical micrographs often show teeth (saw) like structures which probably indicate the early stages of the development of the Widmanstätten structure. The structure was detected in all the examined steels and a typical structure is shown in Figure 5-24.

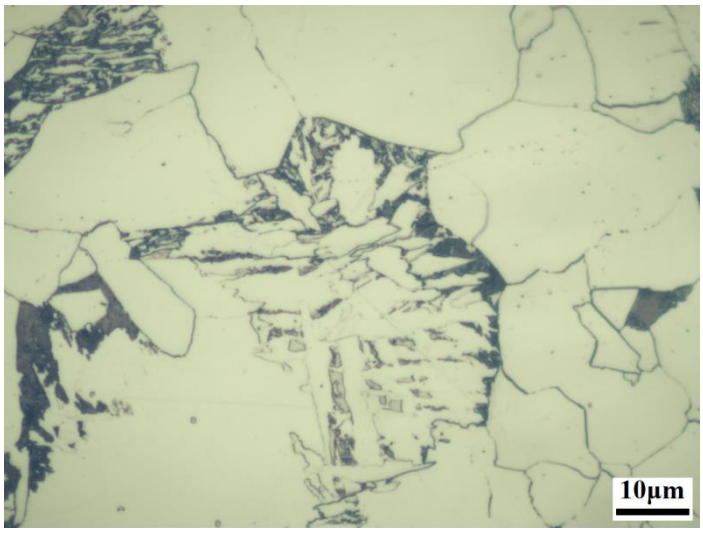

Figure 5-21 A typical optical micrograph of Widmanstätten ferrite in the 0.018%Nb steel at 17°C min^{-1}.

The 0.018%Nb containing steel, H3 had the highest volume fraction of Widmanstätten ferrite while the 0.16%Al steel, H2 had the lowest volume. Generally, increasing the cooling rate gave a higher volume fraction of Widmanstätten ferrite. Optical micrographs showing examples of teeth or saw cuts are presented in Figure 5-25 (a,b) and SEM micrographs in Figure 5-25 (c).

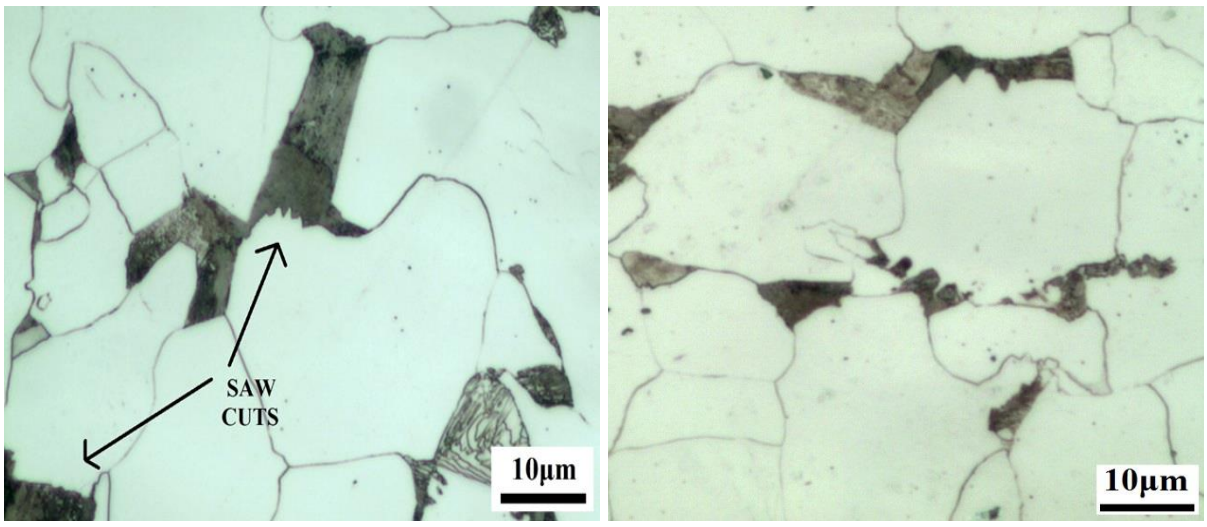

(a) (b)

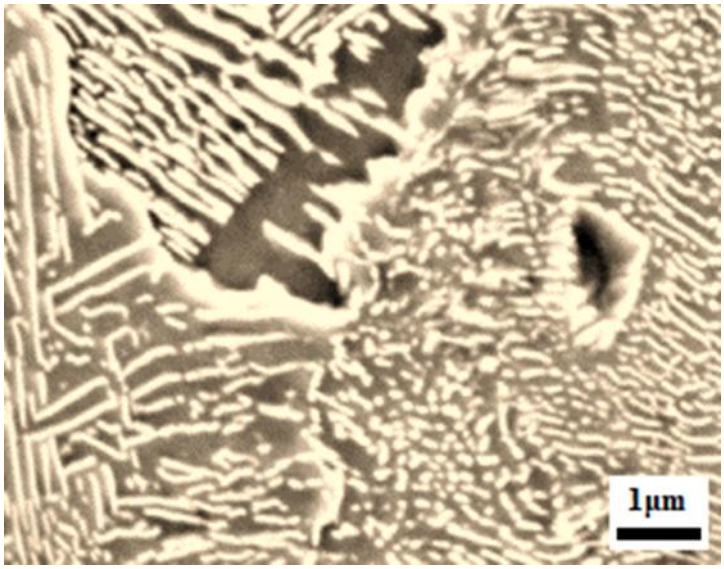

(c)

Figure 5-22 (a) OM photo showing teeth or saw cuts in the hot rolled 0.02%Al steel (40X), (b) OM photo showing teeth or saw cuts in the hot rolled 0.16%Al steel (40X), (C) SEM photo showing the teeth projecting into the transgranular Widmanstätten ferrite.

The importance of Widmanstatten ferrite can be seen when the volume fraction is plotted against the 27J ITT (Figure 26).

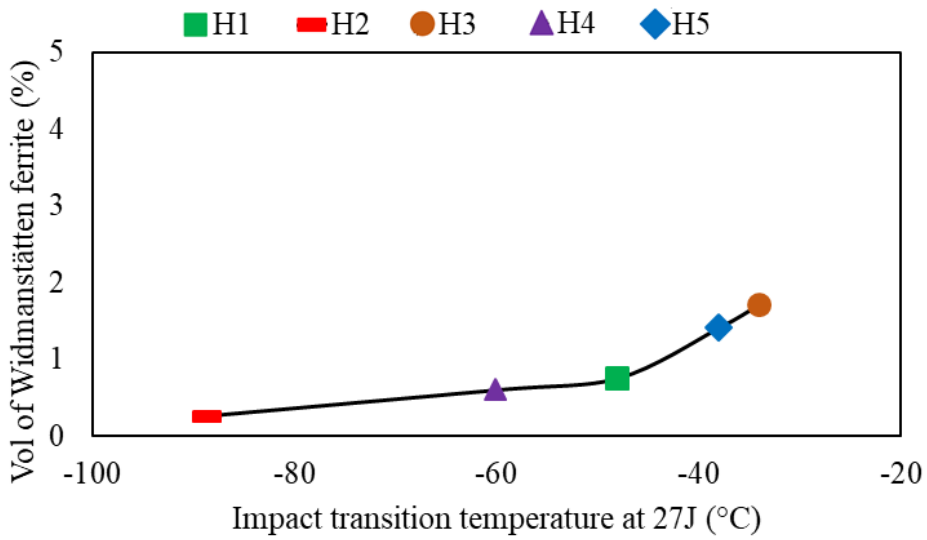

Figure 5-23 Volume fraction of Widmanstätten ferrite plotted against the 27J ITT

5.2.3 Scanning electron microscope

Influence of increasing Al content from 0.02 to 0.16% in Nb free steels, steels H1 and H2, respectively

The SEM micrographs of the 0.02%Al (steel H1) and 0.16%Al (steel H2) are shown in Figures 5-27 and 5-28, respectively. Carbides were detected in both steels at the grain boundaries. Increasing the Al content refined the grain boundary carbide thickness, slightly from 0.25 to 0.21µm and the carbide density decreased from 16.2 to 14.1N mm^{-1}.

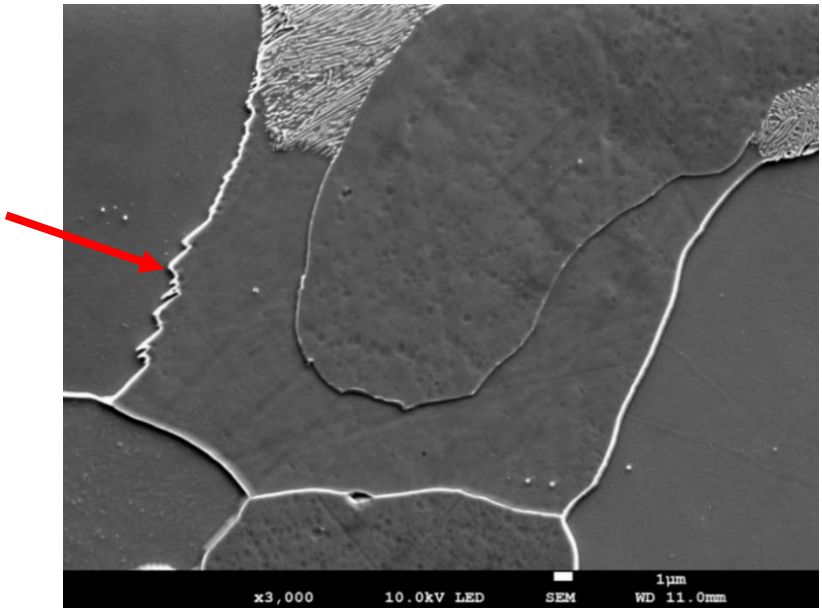

Figure 5-24 SEM micrograph of the hot rolled 0.02%Al steel (H1), with grain boundary carbides and an arrow pointing at serrated boundary indicating an attempt of forming Widmanstatten ferrite.

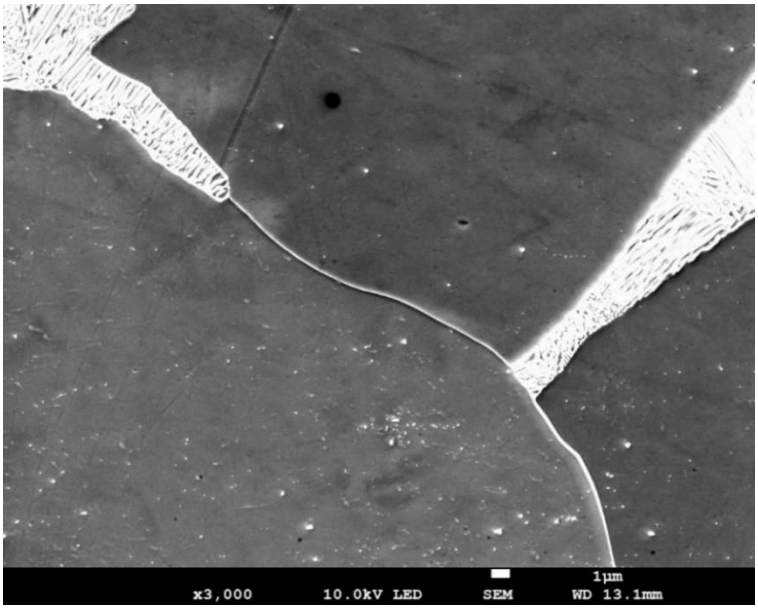

Figure 5-25 SEM micrograph of the hot rolled 0.16%Al steel (H2), showing thinner grain boundary carbides.

Influence of 0.018%Nb addition to the 0.16%Al steel, steel H3

The SEM micrograph of the hot rolled 0.018%Nb containing steel, steel H3 is shown in Figure 5-29. It is observed that adding 0.018%Nb significantly altered the density and more importantly the thickness of the grain boundary carbides (Table 5-3, see Figures 5-28 and 5-29) for comparison). The Nb addition coarsened the carbides from 0.21 to 0.3µm and increased their density from 14.1 to 18.9N mm^{-1}.

Influence of cooling rate on the 0.02%Al steel, steels H1 and steel H4

The SEM micrograph of the hot rolled 0.02%Al steel, H4 at the slower cooling rate (17°C min^{-1}) is shown in Figure 5-30. Reducing the cooling rate is shown to slightly coarsen the grain boundary carbides from 0.25 to 0.27um and also reduced their density slightly from 16.2 to 15.4N mm^{-1}, (Table 5-3, see Figures 5-27 and 5-30 for comparison).

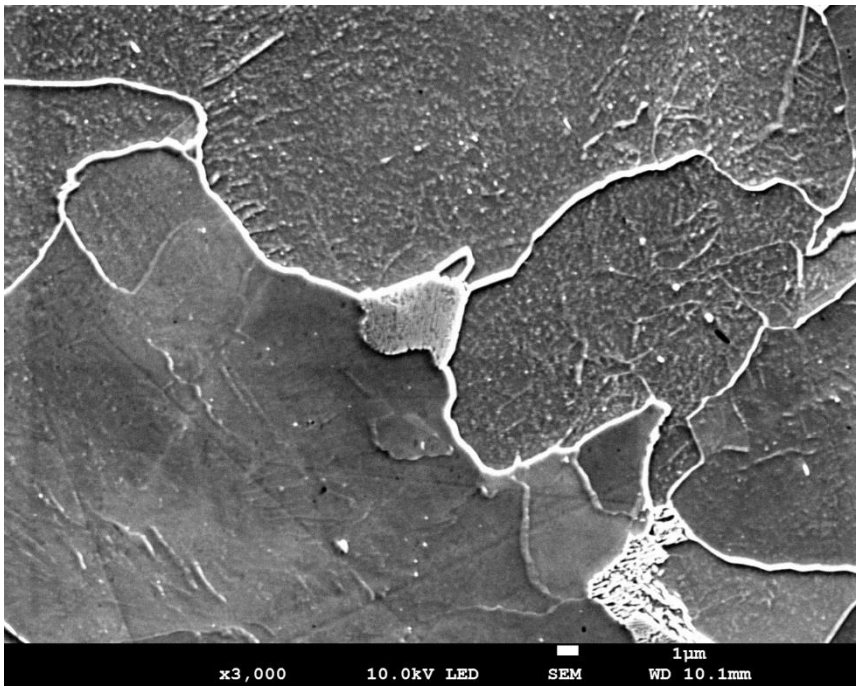

Figure 5-26 SEM micrograph of the hot rolled 0.018%Nb containing steel (H3), showing grain boundary carbides.

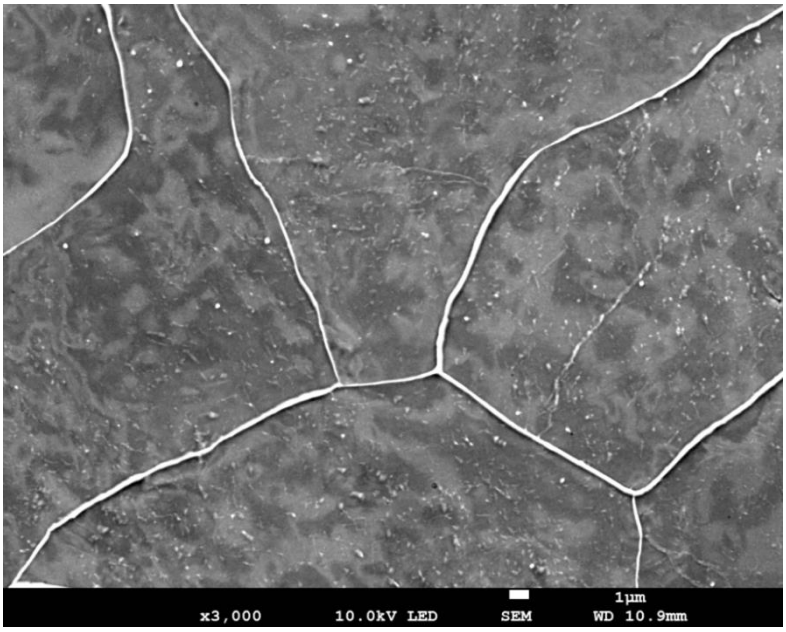

Figure 5-27 SEM micrograph of hot rolled 0.02%Al steel at 17°C min^{-1} (H4), with grain boundary carbides.

Influence of cooling rate on the 0.018%Nb containing steel, steels H3 and H5

The SEM micrograph of the hot rolled 0.018%Nb containing steel at the slower cooling rate (17°C min^{-1}), steel H5, is shown in Figure 5-31. Again, the slower cooling rate thickened the grain boundary carbides only slightly from 0.30 to 0.32um and reduced their density from 18.9 to 17.1N mm^{-1}, (Table 5-3, see Figures 5-29 and 5-31 for comparison).

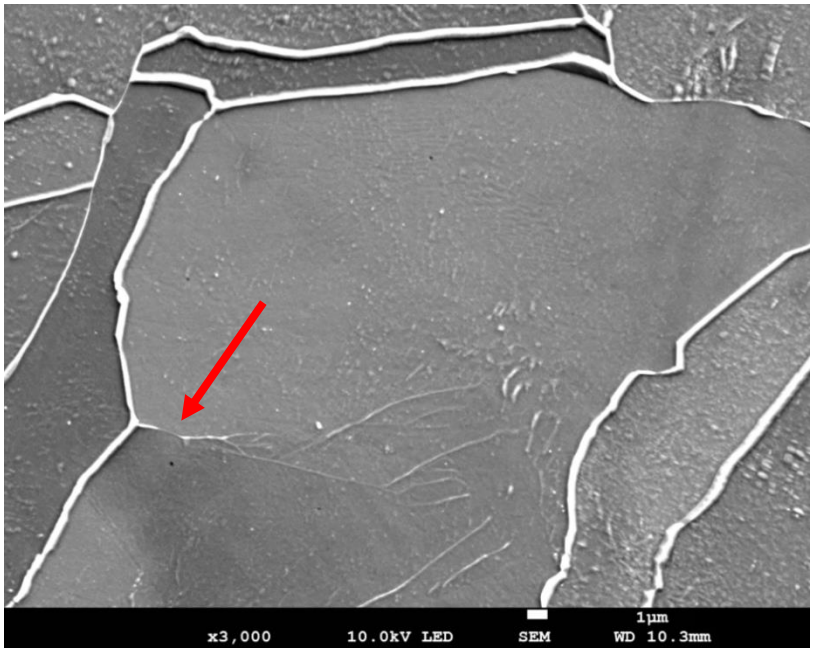

Figure 5-28 SEM micrograph of the hot rolled 0.018%Nb containing steel at 17°C min^{-1} (H5), showing extensive coverage of the grain boundaries with carbides. An arrow pointing at carbides precipitating from the grain boundary to the matrix.

Influence of control rolling on the 0.16%Al steel, steel C2

The SEM micrograph of the control rolled 0.16%Al steel is shown in Figures 5-32. The control rolling condition had only a small influence on the grain boundary carbide thickness and density, being 0.20um and 14.3N mm^{-1}, respectively (Table 5-3, see Figures 3.3-28 and 3.3-32 for comparison).

Influence of control rolling on the 0.018%Nb containing steel, steel C3

The SEM micrograph of the control rolled 0.018%Nb containing steel is shown in Figures 5-33. The control rolling condition was found to reduce the grain boundary carbide thickness markedly from 0.30 to 0.23um associated with an increase in the carbide density from 18.9 to 21.8N mm^{-1}, (Table 5-3, see Figures 5-29 and 5-33 for comparison).

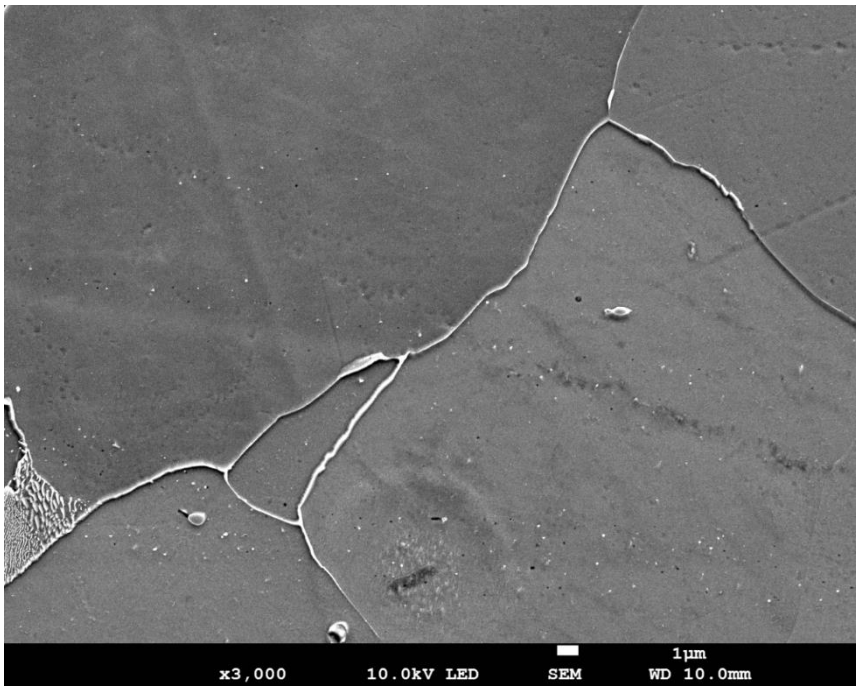

Figure 5-29 Optical microstructure of the control rolled 0.16%Al Nb free steel at 33°C min^{-1} (C2).

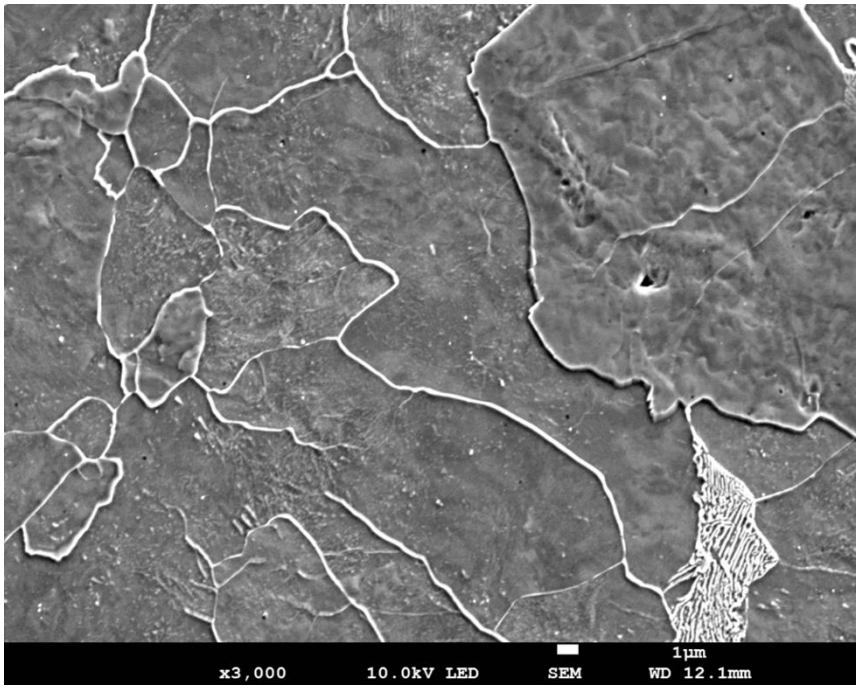

Figure 5-30 Optical microstructure of the control rolled 0.018%Nb containing steel at 33°C min^{-1}, (C3).

Detection of AlN precipitates in the 0.16% Al, Nb free steel, steel H2

A typical SEM photograph of the AlN precipitates in the 0.16%Al steel, steel H2 is shown in Figure 5-34. It was observed that AlN precipitates are normally attached to MnS particles and found adjacent to grain boundaries.

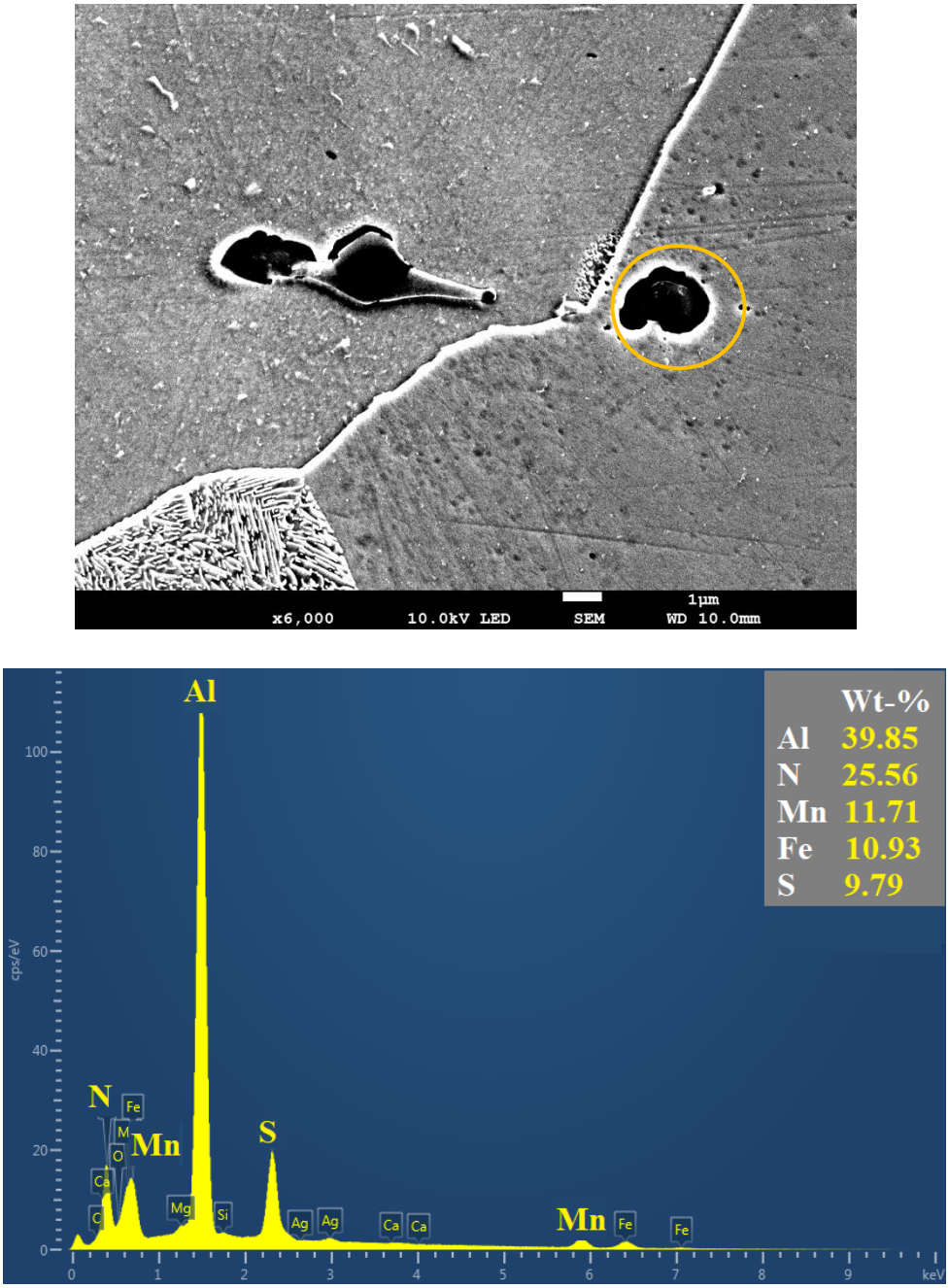

Figure 5-31 SEM micrograph of the 0.16%Al steel (H2), showing typical AlN precipitates presented by the EDS analysis spectrum confirming the presence of AlN and MnS particles.

Influence of 0.018%Nb addition on the pearlite colonies of the 0.16%Al steel, steel H3

A typical pearlite colony in the 0.16%Al steel, steel H2 is shown in Figure 5-35. However, the addition of 0.018%Nb, steel H2 reduced the volume fraction of pearlite significantly (Table 5-3, Figure 5-36). In addition, the plate carbides in the pearlite of the 0.16%Al steel appear more complete and straight and aligned in set, crystallographic oriented directions. However, the plate carbides in the 0.018%Nb containing steel, steel H3 do not not have a uniform shape and they do not follow any specific pattern.

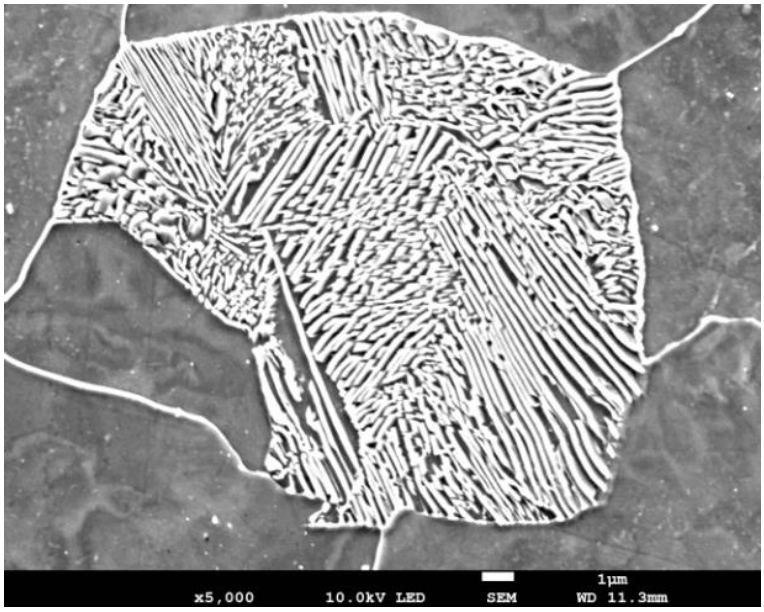

Figure 5-32 SEM micrograph of 0.16% Al (free Nb) steel (H2), showing a typical pearlite colony.

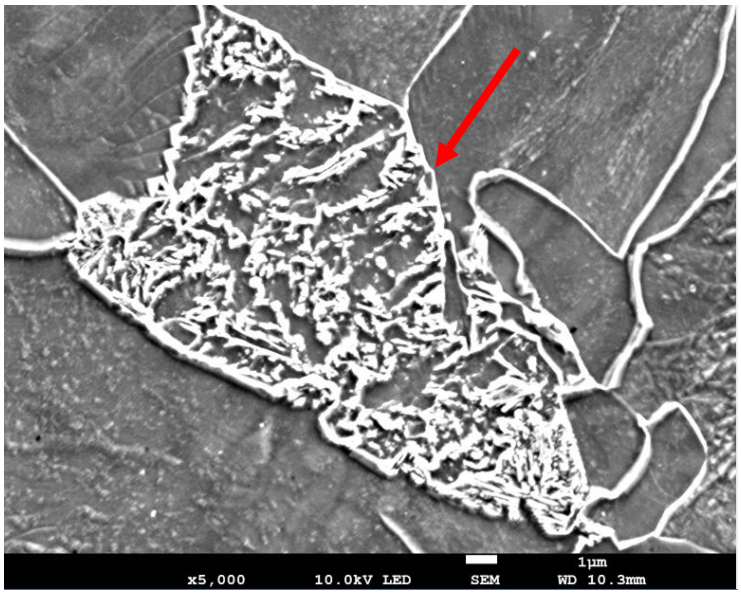

Figure 5-33 SEM micrograph of the 0.018%Nb containing steel (H3), showing a "pearlite colony" which has partially transformed to other phases. Note the saw cut boundary and presence of Widmanstätten ferrite (under the arrow).

Detection of Widmanstätten ferrite by SEM

Widmanstätten ferrite was observed under the SEM. Typical micrographs of Widmanstätten structures are shown in Figures 5-37 and 5-38 for the 0.018%Nb containing steel, steel H5 at 17°C min^{-1}.

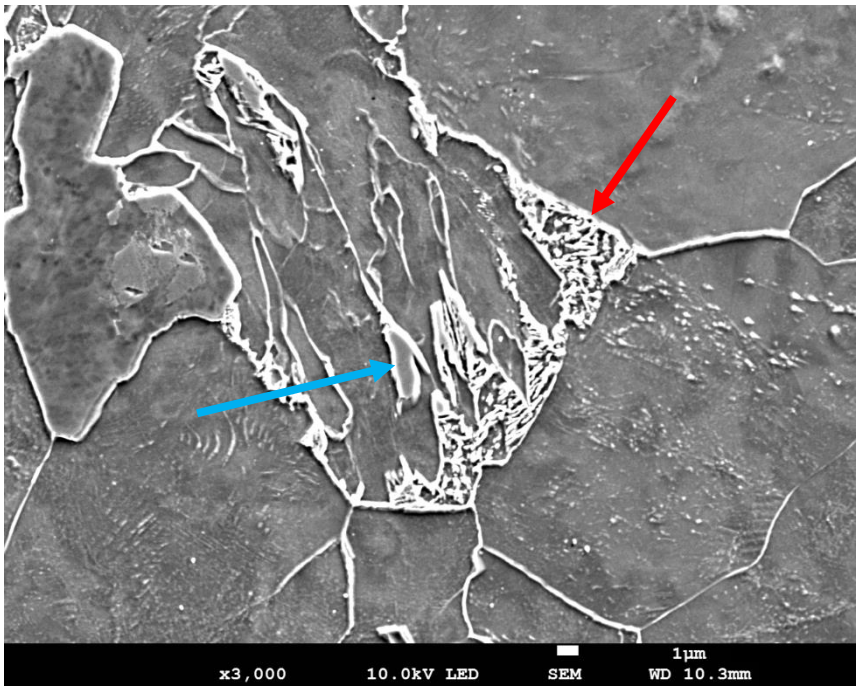

Figure 5-34 SEM micrograph of the 0.018%Nb containing steel at 17°C min^{-1} (H5), showing Widmanstätten ferrite (in red arrow) and M-A constituents (in blue arrow).

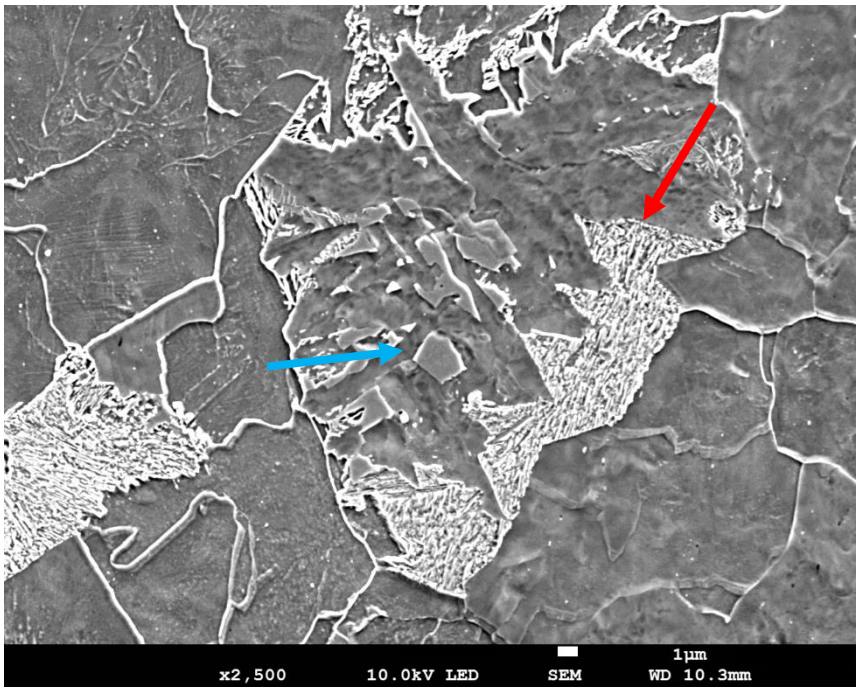

Figure 5-35 SEM micrograph of the 0.018%Nb containing steel at 17°C min^{-1} (H5), showing Widmanstätten ferrite (in red arrow) and M-A constituents (in blue arrow).

5.2.4 Analysis of the optical and SEM micrographs

The optical and SEM micrographs were analysed thoroughly for all the examined steels in order to obtain the following data; average grain size, volume fraction of phases, thickness and density of grain boundary carbides (Table 5-3).

Table 5-3 Summary of the analysis of the optical and SEM micrographs.

Steel	Nb	Al	Plate thickness (mm)	Cooling rate (°C min^{-1})	Grain size ($mm^{-1/2}$)	Ferrite volume fraction (%)	Pearlite volume fraction (%)	Widman-stätten ferrite volume fraction (%)	Grain boundary carbide thickness (µm)	Grain boundary carbide density (N mm^{-1})
H1	-	0.02	15	33	6.4	95.2	4.8	0.75	0.25	16.2
H2	-	0.16	15	33	6.5	92.1	7.9	0.3	0.21	14.1
H3	0.018	0.16	15	33	8.2	95.9	4.1	1.7	0.30	18.9
H4	-	0.02	30	17	6.1	95.4	4.6	0.6	0.27	15.4
H5	0.018	0.16	30	17	7.4	96	4.0	1.4	0.32	17.1
C2	-	0.20	15	33	6.7	92.3	7.7	0.25	0.20	14.3
C3	0.018	0.16	15	33	8.9	95	5	1.3	0.23	21.8

5.3 Discussion.

5.3.1 Influence of increasing Al content from 0.02 to 0.16%, steels H1 and H2

The 0.02%Al (H1) and 0.16%Al (H2) steels showed a similar level of strength despite the large difference in Al content. Indeed, the 0.02%Al steel gave a small improvement in strength over the 0.16%Al steel by around 12MPa as shown in Figure 5-7.

Precipitation of AlN

The lower yield strength of the 0.02%Al bearing steel is slightly higher than the 0.16%Al bearing steel (Figure 5-7). This can be ascribed to the presence of N in the solid solution, rather than precipitating as AlN, so contributing to strength improvement [283]. However, this improvement in strength was associated with a marked deterioration in impact behaviour, the ITT was found to be -50 and -90°C for the 0.02%Al and 0.16%Al steels respectively, as shown in Figure 5-8.

There is no grain refinement from the 0.16%Al addition**.** AlN was however found in the 0.16% Al steel (H2) so some N was taken out of solution (Figure 5-34). The interstitial hardening by 1%N is ~5000MPa [283], so a complete removal of 0.008%N in the 0.16%Al steel would be expected to lead to a decrease in strength by ~40MPa but the amount actually removed is not clear.

The solid solution hardening by Al would account for 14MPa (1%Al increases strength by 70MPa so 0.16% Al increases strength by 14MPa). In addition, the 0.16%Al steel contains a higher volume fraction of pearlite, ~8%, in comparison with the 0.02%Al steel, ~5%. Pearlite is known to enhance strength (1% pearlite increases the yield strength by 1.5MPa so this would mean an increase of strength of 5MPa) so the higher it is in the microstructure, the higher is the strength level. Therefore, both factors, the solid solution hardening by Al and pearlite volume fraction, contribute to narrowing down the strength difference due to Al precipitation**.** However, this suggests that only 0.004%N is taken out of solution for the 0.16%Al (H2) steel.

The removal of 0.004%N in the current 0.16%Al steel due to AlN precipitation should reduce the ITT by ~12°C [283]. This is much lower than the actual value 40^{o}C and the good impact behaviour is accounted for by the refinement in the grain boundary carbides and a reduction in the volume fraction of Widmanstätten ferrite (WF), 0.75 to 0.30%.

Grain boundary carbides

The carbon solubility in ferrite at room temperature is very low, ~0.001%. When the carbon precipitates out on cooling to room temperature it can come out in various forms depending on the carbon content and cooling rate. If the cooling rate is rapid the carbon cannot get to the boundaries, alternatively it precipitates as cementite in the form of pearlite. At a high cooling rate, the carbon gets frozen in solution and forms colonies of martensite. In case of the current low C steels, 0.06%C, under normal cooling conditions (air cooling), the majority of the carbon would be expected to precipitate out easily in the form of cementite and at the boundaries.

Al and Nb have a considerable influence on the development of carbides during precipitation. Increasing the Al content from 0.02 to 0.16% refined the grain boundary carbides thickness from 0.25 to 0.21μm and reduced the carbide density from 16.2 to 14.1N mm^{-1} (Figures 5-27 and 5-28). This would result in the ITT decreasing by 8ºC if the normal vector for thickness $173t^{1/2}$ is used. Carbides are brittle in nature and they provide the nucleation sites for crack initiation and propagation [285], so the finer they are, the better is the impact behaviour as shown in the 0.16%Al steel (Figure 5-8). However, this is insufficient to account for the better properties and again the reduction in the WF may contribute.

Formation of pearlite

It is observed that the 0.16%Al steel gave a higher volume fraction of pearlite, ~8%, in comparison with the 0.02%Al steel, ~5% (Table 5-3). The increase in pearlite volume fraction in the 0.16%Al steel was found to be associated with the refinement of grain boundary carbides (Table 5-3). Pearlite supplies the grain boundary with carbides, so there is a direct relationship between the volume fraction of pearlite colonies and the amount of grain boundary carbides [285]. The finer and fewer grain boundary carbides in the 0.16%Al steel indicates that a smaller number of carbides were supplied by pearlite in comparison with the 0.02%Al steel.

A previous investigation [26] showed that the addition of 0.1%C to hot-rolled low-alloy steel containing 0.16%Al would give an average pearlite volume fraction of ~20%. In addition, the combination of 0.1%C and 0.16%Al was found to encourage the formation of the lower transformation products, bainite and martensite [26]. In the present work, the carbon addition was restricted to 0.06% in order to prevent the formation of lower transformation products and to promote ferrite formation and limit the volume fraction of pearlite. Such an arrangement has provided ferritic–pearlitic microstructure (Figures 5-17 and 5-18).

The effect of pearlite volume fraction on ITT of hot rolled steels can be estimated using *Equation 10* [282]:

Equation 10

$$ITT\ °C = 18(\%P)^{1/3}$$

where %P is the pearlite volume fraction.

The low volume fraction of pearlite in the current 0.16%Al steel, ~8%, in comparison with the previous work, ~20%, is beneficial to impact behaviour, preventing the increase of ITT due to the reduced volume fraction of the harder carbide phase [288] as shown in Table 5-4.

Table 5-4 The influence of carbon content on pearlite volume fraction and ITT for the current steels (H1-0.02%Al and H2- 0.16%Al) and previous steels with the higher volume fraction (P-0.02%Al and P2-0.16%Al) [26].

Steel	C (%)	Al (%)	Nb (%)	Pearlite volume fraction (%)	Increase of ITT (°C)
H1	0.06	0.02	-	5	30
P1 [26]	0.11	0.02	-	20	49
H2	0.06	0.16	-	8	36
P2 [26]	0.11	0.16	-	19	48

However, this improvement would be accompanied by a reduction in LYS, since the LYS of ferrite-pearlite steels decreases gradually on reducing the volume fraction of pearlite [289]. This deterioration in strength is affected significantly by the cooling rate, combination of a fast cooling rate and a high volume of pearlite leads to very much lower strengths (Figure 5-39). However, the current steels were air cooled and thus only a very slight deterioration in LYS is expected.

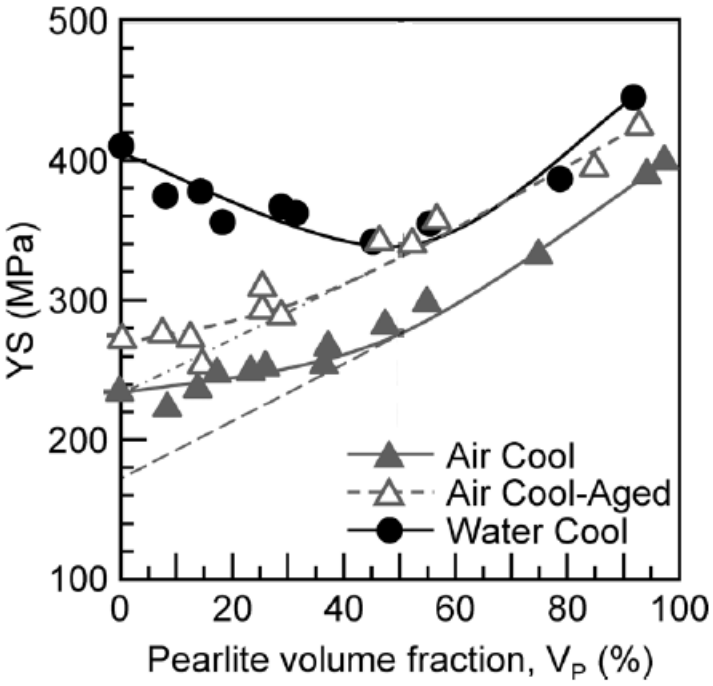

Figure 5-36 Effect of pearlite volume fraction on the yield strength of ferrite-pearlite steels [289].

Despite the fact that Al has the advantage of reducing the amount of WF, removing N from solution and refining the grain boundary carbides, the Al content should always be restricted because higher additions, <0.16%Al favour the formation of martensite, which in turn deteriorates the impact behaviour and results in preyielding so giving a lower LYS [25]. Therefore, the addition of 0.16%Al is recommended to achieve the optimum balance in strength and impact behaviour.

5.3.2 Influence of 0.018%Nb addition to the 0.16%Al steel, steels H2 and H3

The previous discussion showed that increasing Al content from 0.02 to 0.16% in hot rolled HSLA steel improves impact behaviour without impairing strength. Further work has been conducted to explore whether further improvement could be obtained by the addition of Nb. Adding 0.018%Nb to the 0.16%Al steel was found to give a considerable improvement in strength (Figure 5-9). The 0.018%Nb steel achieved the highest strength level among all tested steels, obtaining a 100MPa increase in LYS in comparison with the Nb free steel. The considerable improvement in strength is observed to be associated with a high degree of grain size refinement as shown in Figure 5-19.

Despite the great advantage of Nb addition on the strength, Nb caused the impact behaviour to markedly deteriorate, increasing the ITT from -90 to -30°C (Figure 5-10). Despite the absence of martensite and bainite in the optical microstructure the impact behaviour still deteriorated

considerably. This is because Nb encourages the formation of WF. WF is very dependent on grain size and one of the problems with Nb is that it has a mixed grain size and the coarser grains favour the production of WF.

Precipitation of NbCN

Initially, NbCN dissolves during the homogenisation stage, generally at 1250°C as shown in Figure 5-40, [290] but NbCN has the lowest solubility among all the metal carbides [291]. Therefore, as the temperature drops and during the hot rolling process, supersaturated Nb precipitates out from solution leading to the formation of NbCN at the lattice defects such as dislocations and also at grain boundaries due to the mismatch between Fe matrix and NbCN. This behaviour has the advantage of preventing excessive grain growth (Figure 5-19). NbCN is very effective in retarding grain boundary movement through pinning during hot rolling [292]. During cooling, the new ferrite phase nucleates on the austenite grain boundaries. Due to the considerable grain size refinement of the Nb steel, nucleation of the ferrite phase is encouraged due to the availability of a higher fraction of boundaries [293]. Therefore, more nucleation sites prior to transformation become available and so transformation occurs more readily at a higher temperature.

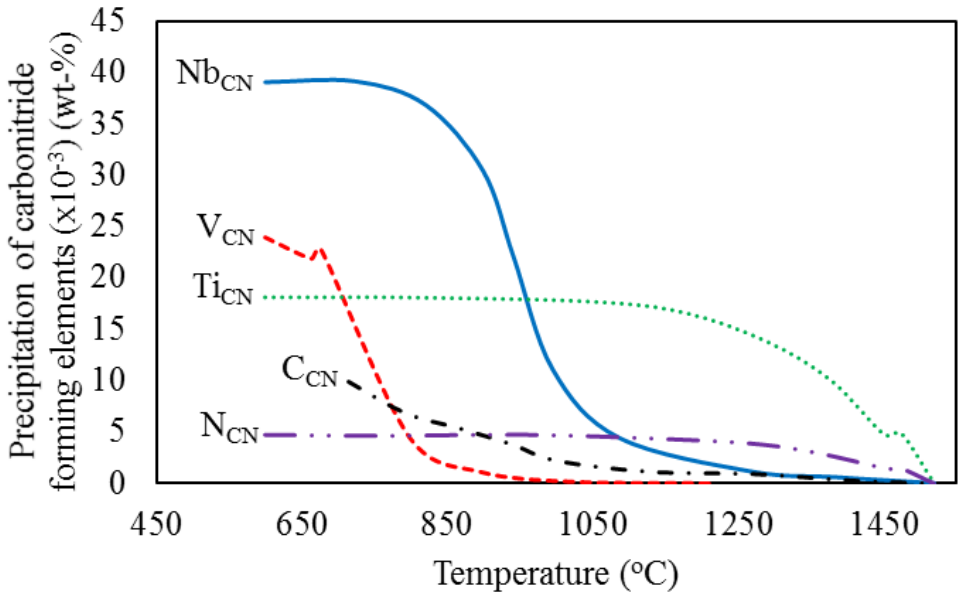

Figure 5-37 The stability of carbonitride forming elements (Nb, Ti, V) at 600–1600°C [259].

Grain boundary carbides

Generally, transformation temperature has a considerable effect on carbide development, in which higher transformation temperature would give more time for carbides to grow and thicken [293]. Therefore, Nb steel is found to have the finest grain size as well as the highest carbide thickness and density among all the examined steels (Table 5-3).

The increase in the grain boundary carbide thickness and density in the Nb steel is found to be associated with a significant change in the morphology of pearlite. Firstly, the addition of Nb reduced the volume fraction of pearlite from 8% to the half ~4% (Table 5-3). Secondly, the pearlite colonies in the Nb free steel are found to be saturated with cementite (Figure 5-35). However, the addition of Nb reduced the volume fraction of cementite considerably (Figure 5-36). Another observation is that plate carbides in the Nb free steel appear to be more tidy and uniform and are arranged crystallographically in lines of set orientation. However, the plate carbides in the Nb steel do not have a uniform shape and they are not following a specific pattern. The reduction of pearlite volume fraction and cementite density in the pearlite colonies can account for the significant increase in the grain boundary carbide thickness and density of the Nb steel.

Cracks start at carbides along the grain boundary, this being the preferred site for cleavage crack propagation. The thickness of these carbides controls the initiation and propagation of cracks along the boundary. The thicker carbides, as the case in the Nb steel, speed up the cracks development and make it easier for cracks to link up, not really so in the case of transgranular brittle failure but is so for intergranular, leading to final fracture and thus poor impact behaviour. However, it is worth mentioning that the change in carbide thickness from 0.2 to 0.32um, by the addition of Nb, will cause the ITT to increase by about 20°C but the further increase in ITT is caused by the formation of LTPs and WF.

Despite the fact that a higher degree of grain size refinement can be obtained by increasing the Nb level, coarser carbides are induced at the boundaries leading to poorer impact behaviour. A change in carbide thickness from 0.21um (H2) to the Nb containing steel (H3) would account for 16^{o}C. However, the Nb encourages WF and lower transformation products making the impact behaviour far worse.

The carbon content in the current work was kept lower, ~0.06%, in comparison with previous work [26] due to the fact that a combination of high contents of carbon and aluminium/niobium

would lead to the formation of lower transformation products leading to poor impact behaviour [26]. However, at low carbon levels transformation occurs at higher temperatures as indicated in the iron-carbon phase diagram (Figure 5-41), so lower carbon contents result in coarser grain boundary carbides due to the wider window available for carbide growth. However, this would only give a relatively small increase in ITT.

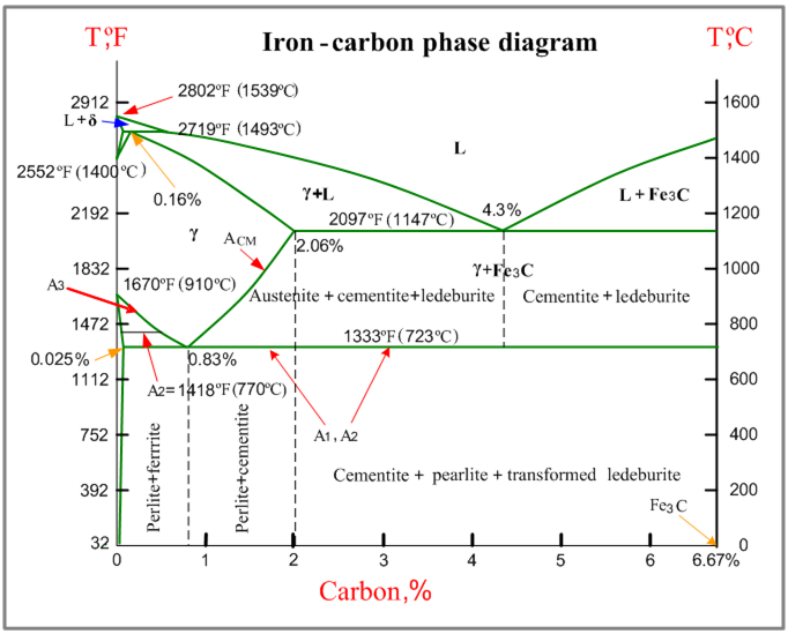

Figure 5-38 Iron-carbon phase diagram [294].

Grain size distribution

An abnormal grain structure (a mixture of coarse and fine grains) was only observed in the Nb steel (Figure 5-19). The degree of refinement depends mainly on the size of NbCN particles. During cooling, the size of these particles increases and since slow cooling rates were used in the present work, more time was given for the NbCN particles to grow. When the particle size exceeds a critical level, the pinning effect becomes weaker, resulting in a further growth of the grains [293]. Due to the size variation of NbCN particles, particular grains are allowed to grow preferably faster than the others and thus abnormal grain microstructure is obtained [295]. The WF only formed in the coarse grains.

5.3.3 Influence of Widmanstätten ferrite

Widmanstätten ferrite was observed in the examined steels but the Nb steel obtained the highest volume fraction while the 0.16%Al steel had the lowest fraction (Table 5-3), a typical Widmanstätten structure is shown in Figures 5-24 and 5-25. The teeth observed under the SEM

(Figures 5-37 and 5-38) represent the side plates of the formed Widmanstätten ferrite [296]. Widmanstätten ferrite plates nucleate on the interface between austenite and ferrite grains as reported in previous work [297]. It is clear that the carbon built up at the tips of the ferrite needles during cooling so favouring carbide formation. Due to the low carbon content in the currents steels, 0.06%, the pearlite reaction often ends early because the front runs out of carbon, resulting in carbide sheets of the pearlite colonies separated by the ferrite.

Generally, hypoeutectoid steels having Widmanstätten ferrite are characterised by poor impact behaviour and low ductility in comparison with regular ferrite/pearlite structures [298]. The current work shows that as the volume of WF increases, the ITT increases (Figure 5-26). Carbides are brittle and they provide the nucleation sites for crack initiation and propagation [285] but the teeth like carbides have a higher tendency to break more easily than normal carbides to initiate the crack for brittle failure. The strong pearlite is separated by weak ferrite patches along which crack can propagate more readily due to the lack of any support such as a grain boundary or another pearlite lamellar to break up crack propagation.

Lu S et al. [299] pointed out that a small addition of Nb, ~0.02wt.%, increases the amount of Widmanstätten ferrite at the expense of pro-eutectoid ferrite. Widmanstätten ferrite forms because of the coarse austenite grain size and the cooling rate being fast enough. Generally, the increase of Widmanstätten ferrite content enhances strength but lowers the impact energy while the increase of pro-eutectoid ferrite content enhances impact behaviour [299]. Therefore, the high volume fraction of Widmanstätten ferrite formed by Nb addition in the present work is an additional factor that contributed to the strength improvement (Figure 5-9) and deterioration of impact behaviour (Figure 5-10). Subsequently, the 0.16%Al steel, having the lowest volume fraction of Widmanstätten ferrite, shows the best impact behaviour among all the examined steels (Figure 5-26). Further processing through annealing is effective in eliminating Widmanstätten structure but the main objective of the current work was to optimise the mechanical properties on hot rolling.

5.3.4 Influence of cooling rate

The current work has also examined the influence of cooling rate on the microstructure and mechanical properties of the 0.02%Al steel and 0.018%Nb steel (Table 5-3). Reducing the cooling rate from 33 to 17°C min^{-1} was found to reduce the LYS for both steels (Figures 5-11 and 5-13) but improve the impact behaviour slightly (Figures 5-12 and 5-14).

Cooling rate is a very critical parameter in controlling microstructural features and hence properties. Reducing the cooling rate gave a coarser grain size for the 0.02%Al steel (Figure 5-20) and also for the 0.018%Nb steel (Figure 5-21). Grains are known to grow rapidly in the austenitic phase so the faster cooling rate gives less time for grains to grow [224].

Development of grain boundary carbides

Coarser carbides were obtained by lowering the cooling rate for the 0.02%Al steel (Figure 5-30) and also for the 0.018%Nb steel (Figure 5-31). Fast cooling rates are effective in lowering the transformation temperature (austenite to ferrite) and as a result, less time becomes available for carbides to grow during transformation [300]. The finer grain size obtained at the fast cooling rate, by giving less opportunity for carbides to accumulate at the boundary through providing a higher fraction of boundary, also contributes in the carbide refinement.

In order to analyse the kinetics of carbides formation and growth, it is important to understand the phenomenon behind their origin and early stages of development. Based on SEM micrographs (Figures 5-35 and Figure 5-36), grain boundary carbides are not isolated but often attached to the pearlite colonies. This indicates that these carbides originate from pearlite and their subsequent development depends significantly on the former pearlite reaction and so pearlite acts a feedstock for grain boundary carbides. Both, carbide plates within the pearlite colony and the carbides at the boundary of the pearlite contribute to feeding the grain boundary with carbides [285]. As the carbides precipitate from the pearlite colonies to the grain boundaries, the refinement of these carbides depends significantly on the duration of pearlite transformation. A lower transformation temperature, as is the case for the fast cooling rate 33°C min^{-1}, is expected to give finer grain boundary carbides due to the smaller period available for carbides to precipitate out of pearlite [285]. Carbides are often found attached to the pearlite colonies, so the size and volume fraction of pearlite grains are of importance. Refinement of austenite grain size at the fast cooling rate will sequentially refine both the ferrite and pearlite grain size. In this case, finer pearlite colonies are obtained which result in thinner and denser carbides at the boundaries for the 0.02%Al steel (Figure 5-27) and also for the 0.018%Nb steel (Figure 5-29).

The role of thermal history based on the austenitising temperature in influencing carbides should be considered [300]. This is due to the fact that higher austenitising temperatures will result in coarser austenite grain size [224]. Coarse grain size reduces the transformation temperature which could lead to a refinement of the grain boundary carbides. Offsetting this is

that a coarser austenite grain size leads to a coarser ferrite grain size which would give coarser carbides.

Widmanstätten ferrite

Reducing the cooling rate is found to be associated with having less amount of Widmanstätten ferrite for the 0.02%Al steel and also for the 0.018%Nb steel (Table 5-3). Previous work [301] has also concluded that the volume fraction of Widmanstätten ferrite increases with increasing the cooling rate. At faster cooling rates, less time is available for diffusion of the equilibrium pro-eutectoid ferrite. Instead, non-equilibrium ferrite develops easily in the form of a Widmanstätten pattern. Independent of the composition, the improvement of lower yield strength and the deterioration of impact behaviour, for both steels 0.02%Al and 0.018%Nb at the faster cooling rate 33°C min^{-1}, is associated with an increase in the volume fraction of Widmanstätten ferrite (Figure 5-26).

The refinement of grain size and grain boundary carbides at fast cooling rate was expected to give better impact behaviour. However, the formation of higher volume fraction of Widmanstätten ferrite at this cooling rate is found to eliminate any beneficial effects of refinement of grain size and grain boundary carbides.

5.3.5 Influence of control rolling

Control rolling has been shown to improve the impact behaviour of the 0.018%Nb steel (Figure 5-16). The improvement in the steel has been shown to be associated with a refinement in grain size and a refinement in carbide thickness and a reduction in the volume fraction of Widmanstätten ferrite (Table 5-3). In control rolling, the steel plate is rolled below the non-recrystalisation temperature, which creates a high density of dislocations. During transformation, ferrite nucleates preferably at these dislocations, so a finer ferrite grain size is achieved. Upon refinement of grain size, carbide thickness was shown to be thinner and denser due to the higher area fraction of grain boundary available for carbide to precipitate on, so less chance is available for carbides to accumulate at the boundaries (Figure 5-33). Generally, finer grain sizes are more resistant to the formation of lower transformation products like bainite and martensite and particularly Widmänstatten ferrite. Therefore, the improvement of impact behaviour (-30°C to -75°C, ITT) can be ascribed to the decrease of carbide thickness (0.30 to 0.23μm) and Widmänstatten ferrite (1.7 to 1.3%) as a result of grain size refinement (8.2 to 8.9$mm^{-1/2}$). Removal of N must also form part of any improvement in ITT. Moreover, the

decrease in carbide thickness was found to be associated with an increase in pearlite volume fraction (4 to 5%) due to the fact that pearlite supplies the grain boundary with carbides.

Control rolling had no influence on the impact behaviour of the 0.16%Al steel (Figure 5-15). The microstructural measurements, including grain size and carbide thickness (Figures 5-22 and 5-32), did not vary for both conditions; hot and control rolling (Table 5-3). Although there was a considerable improvement in the properties of the 0.018%Nb steel on control rolling, the 0.16% Al steel was not influenced by the rolling condition. Al is very effective in suppressing grain boundary carbide development and the formation of Widmänstatten ferrite in the hot rolling condition. Therefore, it should not be assumed that there is no improvement in impact behaviour on control rolling. In fact, Al enhanced the impact behaviour of the hot rolled steel so that it reached the low ITT levels pertaining to the control rolled steel. Among all the examined steels, the 0.16%Al steel was found to give the finest grain boundary carbides and the lowest level of Widmänstatten ferrite and this gave the lowest ITT at 27J.

6 Conclusions and futue work

6.1 Conclusions

6.1.1 Hot ductility of TWIP steel

- The effect of Ti/N content ratio on the hot ductility of the Nb-containing, high Al, high N, TWIP steels was examined. For the Ti/N ratio, range examined of 2.1 to 6.8, the hot ductility was good >40% RA in the straightening temperature range 800–1000°C, indicating that such steels can be processed by continuous casting without the formation of transverse cracks. Previous work has shown that when the RA value exceeds 40% no cracking occurs [42].

- The high ductility has been shown previously to be due to the presence of boron [161]. The addition of 0.003%B enhances the hot ductility of TWIP steel by B segregating to the austenite grain boundaries and strengthening them. However for atomic B to segregate unimpededly without combining with N first to form a nitride before reaching the boundaries, all the free N must first be removed. Ti is normally added to achieve this and the stoichiometric Ti/N ratio of at least 3.4 is required.

- To achieve this high ductility of ≥ 40% the Ti/N ratio should not only meet the stoichiometric ratio of 3.4 but should also produce a sufficiently coarse enough TiN particle size to not influence the hot ductility. This is where the high N content has the advantage over a low N content. The driving force for precipitation to take place is given by the product of [Ti][N] and the higher this is the higher is the temperature at which the precipitation occurs and so the coarser will be the precipitation with the potential of better hot ductility.

- The comparatively small difference in the hot ductility for the steels examined, indicate for these steels there is no point in exceeding the stoichiometric Ti/N ratio of 3.4. Even below this ratio, a Ti/N ratio of 2.2 was adequate and this may be because the high Al content can remove the remaining free N as a coarse AlN precipitation.

- Previous work [66] has shown that the TiN precipitates are excellent sites for Nb(CN) to precipitate out on. As TiN forms at high temperature ~1450°C, the further precipitation of Nb(CN) on cooling on top of the original TiN

particles leads to a coarser conglomerate precipitation that enhances ductility. Removing the Nb from solution in this way avoids the very fine detrimental to ductility, dynamically induced precipitate of NbCN, which occurs during the straightening operation.

- AlN has been shown to precipitate preferentially at the austenite boundaries rather than in the matrix and this is the most detrimental place for favouring intergranular fracture and poor ductility. It has also been shown to precipitate out on MnS inclusions. Reducing the S content to 0.005% results in a low volume fraction of MnS inclusions encouraging transgranular ductile failure. The MnS nucleation sites are now mainly in the matrix and the AlN precipitates as coarse hexagonal particles with little influence on ductility [154].

- The maximum improvement in hot ductility was attained at 900°C in all the examined TWIP steels. This improvement is due to dynamic recrystallisation being able to occur resulting in the coarse austenite grain size being refined. Dynamic recrystallisation in these steels is more active in the region of the tensile specimen which has necked down to failure. Dynamic recrystallisation does not normally occur during the straightening operation because the strain involved in the bending operation, 1-2%, is too small. Ductility in these steel is nevertheless good enough to avoid cracks even without dynamic recrystallisation.

- Because the ductility was so good transgranular failure rather than intergranular failure occurred and because of this a faster cooling rate was more beneficial as finer particles are formed which give better ductility as ductile voiding is very much reduced.

6.1.2 Yield strength and impact behaviour of hot rolled HSLA steel

- The aim of the present work to develop a hot rolled steel having a lower yield strength between 350 and 400MPa to replace control rolled steels of similar strength levels and more importantly to have similar impact behaviour has not been fulfilled.

- Adding 0.16%Al, to a hot rolled plain C-Mn steel resulted in a substantial improvement in impact behaviour, the 27J ITT being 40°C lower. An excellent 27J ITT of -90°C was obtained but returned the same lower yield stress of ~300MPa as the plain C-Mn steel.

- Adding Nb to increase the yield strength by grain refinement and precipitation hardening was successful in achieving the required strength ~400MPa but the ITT was much worse than expected, (-30°C). Generally, it is found that an increase in strength by 100MPa to attain the desired strength level of 400MPa, should have given rise to an increase in ITT of 25 to 50°C resulting for the Nb containing steel in an ITT of -40 to -65°C not the -30°C given in this work

- The deterioration in impact behavior of the Nb containing hot rolled steel is caused partly by the formation of thicker grain boundary carbides and partly by the presence of a higher volume fraction of Widmanstätten ferrite accompanied by the presence of MA. In contrast, the 0.16%Al containing steel which had given excellent impact behaviour had no MA and was relatively free of Widmanstätten ferrite. Its better impact behaviour over a plain C-Mn steel is ascribed to refinement of the grain boundary carbides and removal of N from solution as AlN.

- Independent of the composition, all the hot rolled steels show a similar response to cooling rate, the slower cooling rate ,17°C min^{-1}, giving a 10% reduction in yield strength and a decrease in ITT of 10°C in comparison with the fast cooling rate, 33°C min^{-1}. The reduction in strength and improvement in ITT was ascribed to the slower cooling rate resulting in a coarser precipitation of Nb(CN). The changes in grain boundary carbide thickness on altering the cooling rate were too small to have any influence on the impact behaviour.

- In contrast to hot rolling, control rolling improved the impact behaviour of the Nb containing steel (reducing the ITT from -30 to -75°C) due to grain refinement. Precipitation hardening by Nb(CN) also raised the strength to ~400MPa leading to an excellent combination of mechanical properties. Of great importance to the present examination is that the grain refinement prevented the formation of Widmanstätten ferrite and MA, so that the benefit from adding Al to Nb containing steel could be observed. If therefore one can prevent the formation of MA and Widmanstätten ferrite then achieving the original aim of achieving a strength level of 400MPa and an ITT of -50^{o}C in hot rolled steels should be possible.

6.2 Future work

6.2.1 Hot ductility of TWIP steel

- It may not be necessary to achieve the stoichiometric Ti/N ratio, ~3.4, for TiN, as the high Al level seems sufficient to remove all the N from solution as AlN. The Ti is only being added to remove the N so the atomic boron can segregate unimpededly to the grain boundaries. However, an equally important factor is that this removal of N by Ti for the cooling rates examined also occurs without influencing the hot ductility as the TiN particles formed are very coarse. Whether the AlN is needed to coarsen the TiN is not known. A high Al content (1-2%) is required to meet the properties so from any commercial development this will always be a prime requirement. If Ti is not required this will obviously reduce cost. The present work indicates that for these high N steels (0.01%N) even if Ti is required a Ti/N ratio of 2.2 is enough to give RAs $\geq$ 40%, the value required to avoid cracking. This means a Ti addition of 0.02% should be sufficient. The hot ductility of a steel with an even lower Ti/N ratio of 1, eg.0.01%Ti should be examined as well as a steel with no Ti.

- In order to meet the high strength often required in these steels at room temperature a Nb addition has to be made, Nb as with Al causes problems with cracking during straightening. In the case of Nb, the strain on straightening allows the NbCN to precipitate dynamically on dislocations and so is a very fine precipitation favouring intergranular failures. It is possible therefore that the Ti may be needed to produce these coarse TiN particle during casting so as to allow the Nb to precipitate out on them and thus give good hot ductility. The Nb will go back into solution when heated to the start rolling temperature and will thus be able to promote grain refinement on rolling and subsequently precipitation hardening by precipitating as NbCN in a fine form on cooling so conferring the high strength required at room temperature.

- The high N level and Al level in solution during solidification on casting will result in a high product of [Al][N] which would encourage precipitation to occur at a higher temperature and so give a coarser precipitation. This may account for it not seeming to be detrimental to hot ductility as is found in low Al, (0.02-0.04%), containing steel. The low S level also contributes to this improvement.

There is no doubt that a thorough replica examination is required to identify all the precipitates, their compositions, size and morphology. However, a high Ti addition is necessary to encourage the NbC to come out at a high temperature and coarsen more rapidly so not to have any detrimental effect on ductility. Further work is needed to explore these possibilities.

6.2.2 Yield strength and impact behaviour of hot rolled HSLA steel

- The work has shown that although the initial concept of improving the impact behaviour by adding a high Al addition is beneficial, when Nb is added to strengthen the steel, very small amounts of Widmanstätten ferrite and lower transformation products, particularly MA appear. These are so detrimental to the impact behaviour that any benefit from adding Al is obscured.

- On the academic side, the relative roles of WF and MA need to be explored. WF is a high temperature product whereas MA is a lower transformation product. Although they have similarities, they are very different. Specimens with varying small amounts (for example, 0% to a maximum 5% volume fraction) of WF with no MA and MA with no WF need to be tested and the impact/strength behaviour obtained. This would give us some idea as to which was worse, MA which is most likely or WF and how much can be accepted before the impact performance deteriorates. This would then make it easier to engineer the alloying composition and find out which elements are most susceptible to forming these detrimental products. Al for example favours higher temperature products like WF whilst Nb favours the lower temperature products MA. However, Al does not produce a precipitation hardener.

- For any further commercial development of the properties of hot rolled steels, it is clear that Nb at a 0.018% level, cannot be used because with the coarse grain size present in hot rolled steels both WF and MA still form.

- It is possible that a lower Nb level of 0.005-0.01% will give some strengthening but avoid MA and WF. Strength may possibly be further increased by having a Nb/V combination for example, 0.01%Nb, 0.02%V, V being less hardenable than Nb.

References

1. Matlock, D.K. and Speer, J.G., 2009. Third generation of AHSS: microstructure design concepts. In *Microstructure and texture in steels* (pp. 185-205). Springer, London.
2. Wagoner, R.H., Lim, H. and Lee, M.G., 2013. Advanced issues in springback. *International Journal of Plasticity*, *45*, pp.3-20.
3. UCI Department of Chemistry [online] Available at: https://www.chem.uci.edu/~lawm/263%202.pdf [Accessed 30 October 2019].
4. Smallman, R.E., Dillamore, I.L. and Dobson, P.S., 1966. The measurement of stacking fault energy. *Le Journal de Physique Colloques*, *27*(C3), pp.C3-86.
5. Monsalve, A., Barbieri, F.D., Gómez, M., Artigas, A., Carvajal, L., Sipos, K., Bustos, O. and Pérez-Ipiña, J., 2015. Mechanical Behavior of a Twip Steel (Twinning Induced Plasticity). *Matéria (Rio de Janeiro)*, *20*(3), pp.653-658.
6. Lee, Y.K. and Choi, C., 2000. Driving force for γ→ ε martensitic transformation and stacking fault energy of γ in Fe-Mn binary system. *Metallurgical and Materials Transactions A*, *31*(2), pp.355-360.
7. Saeed-Akbari, A., Imlau, J., Prahl, U. and Bleck, W., 2009. Derivation and variation in composition-dependent stacking fault energy maps based on subregular solution model in high-manganese steels. *Metallurgical and Materials Transactions A*, *40*(13), pp.3076-3090.
8. Frommeyer, G., Brüx, U. and Neumann, P., 2003. Supra-ductile and high-strength manganese-TRIP/TWIP steels for high energy absorption purposes. *ISIJ international*, 43(3), pp.438-446.
9. Piercea, D.T., Jiménezc, J.A., Bentleyd, J., Raabee, D., Oskaya, C. and Wittiga, J.E., 2014. The influence of manganese content on the stacking fault and austenite/e-martensite interfacial energies in Fe–Mn–(Al–Si) steels investigated by experiment and theory. *Acta Materialia*, *68*, pp.238-253.
10. Vercammen, S., Blanpain, B., De Cooman, B.C. and Wollants, P., 2004. Cold rolling behaviour of an austenitic Fe–30Mn–3Al–3Si TWIP-steel: the importance of deformation twinning. *Acta Materialia*, 52(7), pp.2005-2012.
11. Rhodes, C.G. and Thompson, A.W., 1977. The composition dependence of stacking fault energy in austenitic stainless steels. *Metallurgical Transactions A*, *8*(12), pp.1901-1906.

12. Qi-Xun, D., An-Dong, W., Xiao-Nong, C. and Xin-Min, L., 2002. Stacking fault energy of cryogenic austenitic steels. *Chinese Physics*, *11*(6), p.596.

13. Kwon, O., Kim, S., Cho, J., Kwak, W. and Kim, G., 2007, June. Development of TWIP steel for automotive application, Posco, Korea. In *Proceedings 3rd International Steel Conference on New Developments in Metallurgical Process Technologies (METEC InSteelCon) S* (pp. 690-697).

14. De Cooman, B.C., Chin, K.G. and Kim, J., 2011. High Mn TWIP steels for automotive applications. In *New trends and developments in automotive system engineering*. InTech.

15. Kang, S.E., Banerjee, J.R., Maina, E.M. and Mintz, B., 2013. Influence of B and Ti on hot ductility of high Al and high Al, Nb containing TWIP steels. *Materials Science and Technology*, 29(10), pp.1225-1232.

16. Kang, S.E., Banerjee, J.R. and Mintz, B., 2012. Influence of S and AlN on hot ductility of high Al, TWIP steels. *Materials Science and Technology*, 28(5), pp.589-596.

17. Kang, S.E., Tuling, A., Banerjee, J.R., Gunawardana, W.D. and Mintz, B., 2011. Hot ductility of TWIP steels. *Materials Science and Technology*, 27(1), pp.95-100.

18. Xue, Q., Benson, D., Meyers, M.A., Nesterenko, V.F. and Olevsky, E.A., 2003. Constitutive response of welded HSLA 100 steel. *Materials Science and Engineering: A*, *354*(1), pp.166-179.

19. Liu, Z.K., 2004. Thermodynamic calculations of carbonitrides in microalloyed steels. *Scripta Materialia*, *50*(5), pp.601-606.

20. Mintz, B. and Crowther, D.N., 2010. Hot ductility of steels and its relationship to the problem of transverse cracking in continuous casting. *International Materials Reviews*, *55*(3), pp.168-196.

21. Konstrukcijska, V.M.H., 2011. High-strength low-alloy (HSLA) steels. *Materiali in tehnologije*, *45*(4), pp.295-301.

22. Stephens, R.I., 1982. *Fatique and Fracture Toughness of Five Carbon Or Low Alloy Cast Steels at Room Or Low Climatic Temperatures*. Carbon and Low Alloy Technical Research Committee, Steel Founders' Society of America.

23. Mintz, B., 2003. The influence of Al on the mechanical properties of hot rolled steel plates. In *Materials Science Forum* (Vol. 426, pp. 1219-1223). Trans Tech Publications Ltd., Zurich-Uetikon, Switzerland.

24. Mintz, B., Williamson, A., Su, H. and Morrison, W.B., 2007. Influence of nitride formers on strength and impact behaviour of hot rolled steel. *Materials science and technology*, *23*(1), pp.63-71.
25. Mintz, B., Gunawardana, W.D. and Su, H., 2008. Al as solid solution hardener in steels. *Materials Science and Technology*, *24*(5), pp.596-600.
26. Mintz, B., Gunawardana, W.D. and Su, H., 2008. Influence of Al on strength and impact behaviour of hot rolled plain C–Mn steels. *Materials Science and Technology*, *24*(5), pp.601-606.
27. Wojcik, T. and Kozeschnik, E., 2017. Influence of NbC-Precipitation on Hot Ductility in Microalloyed Steel-TEM Study and Thermokinetic Modeling. In *Materials Science Forum* (Vol. 879, pp. 2107-2112). Trans Tech Publications.
28. Maehara, Y., Nakai, K., Yasumoto, K. and Mishima, T., 1988. Hot Cracking of Low Alloy Steels in Simulated Continuous Casting-Direct Rolling Process. *Transactions of the Iron and Steel Institute of Japan*, *28*(12), pp.1021-1027.
29. Klinkenberg, C., Kintscher, B., Hoen, K. and Reifferscheid, M., 2017. More than 25 Years of Experience in Thin Slab Casting and Rolling Current State of the Art and Future Developments. S*teel Research International*, *88*(10), p.1700272.
30. Zarandi, F. and Yue, S., 2004. Failure mode analysis and a mechanism for hot-ductility improvement in the Nb-microalloyed steel. *Metallurgical and Materials Transactions A*, *35*(12), pp.3823-3832.
31. Novak, J.S., Moro, L., Benasciutti, D. and De Bona, F., 2018. Accelerated cyclic plasticity models for FEM analysis of steelmaking components under thermal loads. *Procedia Structural Integrity*, 8, pp.174-183.
32. Ma, F.J., Wen, G.H., Tang, P., Yu, X., Li, J.Y., Xu, G.D. and Mei, F., 2010. Causes of transverse corner cracks in microalloyed steel in vertical bending continuous slab casters. *Ironmaking & Steelmaking*, *37*(1), pp.73-79.
33. Mizuno, H., Esaka, H., Shinozuka, K. and Tamura, M., 2008. Analysis of the crystallization of mold flux for continuous casting of steel. *ISIJ international*, *48*(3), pp.277-285.
34. Yu, H.L. and Liu, X.H., 2010. Longitudinal crack on slab surface at straightening stage during continuous casting using finite element method. *Journal of Central South University of Technology*, *17*(2), pp.235-238.
35. Yao, C.G., Yuan, S.Q., Chen, L., Wang, Z.J., Wang, H.L. and Jing, L.L., 2011. Research of Transverse Corner Crack and Optimization of Concasting Process for

Bloom of Peritectic Steel Q235D. In *Advanced Materials Research* (Vol. 284, pp. 1115-1119). Trans Tech Publications.

36. Yang, X., Zhang, L., Lai, C., Li, S., Li, M. and Deng, Z., A Method to Control the Transverse Corner Cracks on a Continuous Casting Slab by Combining Microstructure Analysis with Numerical Simulation of the Slab Temperature Field. S*teel Research International*, p.1700480.
37. Takeuchi, E. and Brimacombe, J.K., 1985. Effect of oscillation-mark formation on the surface quality of continuously cast steel slabs. *Metallurgical Transactions B*, *16*(3), pp.605-625.
38. Matsumiya, T., 2006. Recent topics of research and development in continuous casting. *ISIJ international*, *46*(12), pp.1800-1804.
39. Arıkan, M.M., 2015. Hot ductility behavior of a peritectic steel during continuous casting. *Metals*, *5*(2), pp.986-999.
40. Mintz, B., 1996. Importance of Ar3 temperature in controlling ductility and width of hot ductility trough in steels, and its relationship to transverse cracking. *Materials Science and Technology*, *12*(2), pp.132-138.
41. Jansto, S.G., 2015. Hot ductility characterization of industrially cast microalloyed steels, *in 46th Steelmaking* August 17th-21st, 2015, Rio de Janeiro, RJ, Brazil, pp.542-551.
42. Mintz, B., 1999. The influence of composition on the hot ductility of steels and to the problem of transverse cracking. *ISIJ international*, 39(9), pp.833-855.
43. Liu, G.X. and Dahl, W., 1989. The influence of temperature and strain rate on the stress-strain behaviour of "in-situ solidified" steel during tensile test. *Steel Research*, *60*(5), pp.221-229.
44. Mintz, B. and Arrowsmith, J.M., 1979. Hot-ductility behaviour of C–Mn–Nb–Al steels and its relationship to crack propagation during the straightening of continuously cast strand. *Metals technology*, 6(1), pp.24-32.
45. Abushosha, R., Comineli, O. and Mintz, B., 1999. Influence of Ti on hot ductility of C–Mn–Al steels. *Materials science and technology*, *15*(3), pp.278-286.
46. Mintz, B., Yue, S. and Jonas, J.J., 1991. Hot ductility of steels and its relationship to the problem of transverse cracking during continuous casting. *International Materials Reviews*, 36(1), pp.187-217.

47. Spradbery, C. and Mintz, B., 2005. Influence of undercooling thermal cycle on hot ductility of C–Mn–Al–Ti and C–Mn–Al–Nb–Ti steels. *Ironmaking & steelmaking*, 32(4), pp.319-324.
48. Banks, K.M., Bentley, A.P. and Koursaris, A., 2000. Precipitation model for predicting hot ductility behaviour in microalloyed steels. In *42 nd Mechanical Working and Steel Processing Conference* (pp. 329-340).
49. Vedani, M., Ripamonti, D., Mannucci, A. and Dellasega, D., 2008. Hot ductility of microalloyed steels. *METALLURGIA ITALIANA*, *5*, p.19.
50. Landheer, H., 2010. *Nucleation of ferrite in austenite: The role of crystallography* (Doctoral dissertation, TU Delft, Delft University of Technology).
51. Mintz, B. and Cowley, A., 2006. Deformation induced ferrite and its influence on the elevated temperature tensile flow stress–elongation curves of plain C–Mn and Nb containing steels. *Materials science and technology*, *22*(3), pp.279-292.
52. Nguyen, T.D., Sawada, K., Kushima, H., Tabuchi, M. and Kimura, K., 2014. Change of precipitate free zone during long-term creep in 2.25 Cr–1Mo steel. *Materials Science and Engineering: A*, 591, pp.130-135.
53. Rösler, J., Harders, H. and Baeker, M., 2007. Mechanical behaviour of engineering materials: metals, ceramics, polymers, and composites. *Springer Science & Business Media.*
54. Xu, K. and Thomas, B.G., 2009, May. Prediction of Grain Size, Precipitation and Crack Susceptibility in Continuous Casting. In *AISTech 2009 Steelmaking Conference Proceeding* (Vol. 1, p. 12).
55. Lan, P., Tang, H. and Zhang, J., 2016. Hot ductility of high alloy Fe–Mn–C austenite TWIP steel. *Materials Science and Engineering*: *A*, 660, pp.127-138.
56. Abushosha, R., Ayyad, S. and Mintz, B., 1998. Influence of cooling rate and MnS inclusions on hot ductility of steels. *Materials science and technology*, 14(3), pp.227-235.
57. Kang, S.E., Tuling, A., Lau, I., Banerjee, J.R. and Mintz, B., 2011. The hot ductility of Nb/V containing high Al, TWIP steels. *Materials Science and Technology*, 27(5), pp.909-915.
58. Zhang, Z.L., Lin, Q.Y. and Yu, Z.S., 2000. Non-equilibrium intergranular segregation in ultra low carbon steel. *Materials science and technology*, 16(3), pp.305-308.

59. Karlsson, L., Norden, H. and Odelius, H., 1988. Overview no. 63 Non-equilibrium grain boundary segregation of boron in austenitic stainless steel—I. Large scale segregation behaviour. *Acta Metallurgica*, 36(1), pp.1-12.

60. Comineli, O., Abushosha, R. and Mintz, B., 1999. Influence of titanium and nitrogen on hot ductility of C–Mn–Nb–Al steels. *Materials Science and Technology*, 15(9), pp.1058-1068.

61. Yamamoto, K., Suzuki, H.G., oono, Y., noda, N. and inoue, T., 1987. Formation mechanism and prevention method of facial cracks of continuously cast steel slabs containing boron. *Tetsu-to-Hagane*, 73(1), pp.115-122.

62. Cho, K.C., Mun, D.J., Kang, M.H., Lee, J.S., Park, J.K. and Koo, Y.M., 2010. Effect of thermal cycle and nitrogen content on the hot ductility of boron-bearing steel. *ISIJ international*, 50(6), pp.839-846.

63. Deng, J., Lin, Y.C., Li, S.S., Chen, J. and Ding, Y., 2013. Hot tensile deformation and fracture behaviors of AZ31 magnesium alloy. *Materials & Design*, 49, pp.209-219.

64. Mišičko, R., Longauerová, M., Vojtko, M., Konrádyová, J. and Fedáková, S.A., 2015. Effect of Strain Rate on Hot Ductility of Low Carbon Steel. *Acta Metallurgica Slovaca*, 21(2), pp.94-101.

65. Großeiber, S., Ilie, S., Poletti, C., Harrer, B. and Degischer, H.P., 2012. Influence of Strain Rate on Hot Ductility of a V-Microalloyed Steel Slab. *Steel Research International*, 83(5), pp.445-455.

66. Carpenter, K., Dippenaar, R. and Killmore. C., 2009. Hot Ductility of Nb- and Ti-Bearing Microalloyed Steels and the Influence of Thermal History. *Metallurgical and Materials Transactions A·* 40(A), pp.573-580.

67. Wang, Z., Meng, Q., Qu, M., Zhou, Z., Wang, B. and Fu, W., 2016. Effect of Strain Rate on Hot Ductility Behavior of a High Nitrogen Cr-Mn Austenitic Steel. *Metallurgical and Materials Transactions A*, 47(3), pp.1268-1279.

68. Fares, M.L., Darsouni, A. and Le Coze, J., 2015. Comparing the Hot Ductility Behaviour of Low-Carbon Microalloyed Nb-V-Ti Steels During Two Thermal Cycling Routes: Solutionizing and Precipitation Treatments. *Steel research international*, 86(9), pp.1090-1103.

69. Wang, Z., Sun, S., Wang, B., Shi, Z., Zhang, R. and Fu, W., 2014. Effect of grain size on dynamic recrystallization and hot-ductility behaviors in high-nitrogen CrMn austenitic stainless steel. *Metallurgical and Materials Transactions A, 45*(8), pp.3631-3639.

70. Mintz, B., Abushosha, R. and JJ, J., 1992. Influence of dynamic recrystallisation on the tensile ductility of steels in the temperature range 700 to 1150°C. *ISIJ international*, 32(2), pp.241-249.
71. Ozturk, U., Cabrera, J.M. and Calvo, J., 2017. High-Temperature Deformation of Inconel 718PlusTM. *Journal of Engineering for Gas Turbines and Power*, *139*(3), p.032101.
72. Crowther, D.N. and Mintz, B., 1986. Influence of grain size on hot ductility of plain C–Mn steels. *Materials science and technology*, 2(9), pp.951-955.
73. Ouchi, C. and Matsumoto, K., 1982. Hot ductility in Nb-bearing high-strength low-alloy steels. *Transactions of the iron and steel institute of Japan*, 22(3), pp.181-189.
74. Schmidt, I. and josefsson, A., 1974. Scand., J. *Metallurgy*, *3*, pp.193-199.
75. Crowther, D.N. and Mintz, B., 1986. Influence of grain size and precipitation on hot ductility of microalloyed steels. *Materials science and technology*, 2(11), pp.1099-1105.
76. Moon, S.C. and Dippenaar, R., 2004. The Effect of Austenite Grain Size on Hot Ductility of Steels. In *MS&T 2004 Conference Proceedings, Nueva Orleans, EEUU* (pp. 675-684).
77. Offerman, C. and Dacker, C., 1997. Way to avoid transverse cracking by surface temperature control. *Continuous Casting*, *8*, pp.149-153.
78. Abushosha, R., Vipond, R. and Mintz, B., 1991. Influence of sulphur and niobium on hot ductility of as cast steels. *Materials science and technology*, 7(12), pp.1101-1107.
79. Evans, H.E., 1969. Effect of grain size on the hot ductility of steels, *Met. Sci. J*, 3, pp.33.
80. Crowther, D.N. and Mintz, B., 1986. Influence of carbon on hot ductility of steels. *Materials science and technology*, 2(7), pp.671-676.
81. Sellars, C.M. and Tegart, W.M., 1966. Relationship between strength and structure in deformation at elevated temperatures. *Mem Sci Rev Met*, *63*(9).
82. Sankar, J., Hawkins, D. and McQueen, H.J., 1979. Behaviour of low-carbon and HSLA steels during torsion-simulated continuous and interrupted hot rolling practice. *Metals Technology*, 6(1), pp.325-331.
83. Mintz, B. and Mohamed, Z., 1989, March. Intergranular failure in micro-alloyed steels and its relationship to carbon content. In *ICF7*, Houston (USA).
84. Mohamed, Z., 1995. Hot Ductility of Directly Cast Steels with Different Carbon Contents, 8, pp.167-181.

85. Chown, L.H. and Cornish, L.A., 2008. Investigation of hot ductility in Al-killed boron steels. *Materials Science and Engineering: A*, 494(1), pp.263-275.
86. Kalinenko, A., Kusakin, P., Belyakov, A., Kaibyshev, R. and Molodov, D.A., 2017. Microstructure and Mechanical Properties of a High-Mn TWIP Steel Subjected to Cold Rolling and Annealing. *Metals*, *7*(12), p.571.
87. Nokhrina, O.I. and Rozhihina, I.D., 2015. Manganese concentrate usage in steelmaking. In IOP Conference Series: *Materials Science and Engineering* (Vol. 91, No. 1, p. 012044). IOP Publishing
88. Wieder, R.K. and Lang, G.E., 1986. Fe, Al, Mn, and S chemistry of Sphagnum peat in four peatlands with different metal and sulfur input. *Water, Air, and Soil Pollution*, 29(3), pp.309-320.
89. Nakama, K., Haruna, Y., Nakano, J. and Sridhar, S., 2009. The effect of alloy solidification path on sulfide formation in Fe–Cr–Ni alloys. *ISIJ international*, 49(3), pp.355-364.
90. Kang, M.H., Lee, J.S., Koo, Y.M., Kim, S.J. and Heo, N.H., 2014. Correlation between MnS precipitation, sulfur segregation kinetics, and hot ductility in C-Mn steel. *Metallurgical and Materials Transactions A*, 45(12), pp.5295-5299.
91. Hosseini, S.B., Temmel, C., Karlsson, B. and Ingesten, N.G., 2007. An in-situ scanning electron microscopy study of the bonding between MnS inclusions and the matrix during tensile deformation of hot-rolled steels. *Metallurgical and Materials Transactions A*, 38(5), pp.982-989.
92. Temmel, C., Ingesten, N.G. and Karlsson, B., 2006. Fatigue anisotropy in cross-rolled, hardened medium carbon steel resulting from MnS inclusions. *Metallurgical and materials Transactions A*, 37(10), pp.2995-3007.
93. Keh, A.S. and Van Vlack, L.H., 1956. Microstructure of Iron-Sulfur Alloys. *JOM*, 8(8), pp.950-958.
94. Oikawa, K., Ohtani, H., Ishida, K. and Nishizawa, T., 1995. The control of the morphology of MnS inclusions in steel during solidification. *ISIJ international*, 35(4), pp.402-408.
95. Sun, W.P., Militzer, M. and Jonas, J.J., 1992. Strain-induced nucleation of MnS in electrical steels. *Metallurgical and Materials Transactions A*, 23(3), pp.821-830.
96. Abushosha, R., Ayyad, S. and Mintz, B., 1998. Influence of cooling rate on hot ductility of C-Mn-AI and C-Mn-Nb-AL steels. *Materials science and technology*, 14(4), pp.346-351.

97. Kizu, T. and Urabe, T., 2009. Hot ductility of sulfur-containing low manganese mild steels at high strain rate. *ISIJ international*, 49(9), pp.1424-1431.

98. Steenken, B., Rezende, J.L.L. and Senk, D., 2017. Hot ductility behaviour of high manganese steels with varying aluminium contents. *Materials Science and Technology*, 33(5), pp.567-573.

99. Wilson, F.G. and Gladman, T., 1988. Aluminium nitride in steel. *International Materials Reviews*, 33(1), pp.221-286.

100. Lückl, M., Wojcik, T., Povoden-Karadeniz, E., Zamberger, S. and Kozeschnik, E., 2017. Co-Precipitation Behavior of MnS and AlN in a Low-Carbon Steel. *Steel research international.*

101. Liu, H., Liu, J., Wu, B., Shen, Y., He, Y., Ding, H. and Su, X., 2017. Effect of Mn and Al contents on hot ductility of high alloy Fe-xMn-C-yAl austenite TWIP steels. *Materials Science and Engineering: A*, 708, pp.360-374.

102. Cabanas, N., Penning, J., Akdut, N. and De Cooman, B.C., 2006. High-temperature deformation properties of austenitic Fe-Mn alloys. *Metallurgical and Materials Transactions A*, 37(11), pp.3305-3315.

103. Banks, K.M., Tuling, A.S. and Maubane, D.R.N., 2017. Roughing of Thick, Coarse-grained High-temperature-processing Steels Processed via Compact Strip Production. *ISIJ International*, *57*(9), pp.1586-1594.

104. Comineli, O., Juuti, T. and Aranas, C., 2017. The Importance of MnS Inclusions on Hot Shortness of Cu-Containing Steels. *Steel research international*, 88(10), pp.1-12.

105. Kim, J.M. and Park, J.K., 2017. On the AlN precipitation and grain refinement in the Al (N)-added medium C–Mn steels. *Philosophical Magazine Letters*, 97(8), pp.320-327.

106. Vedani, M., Dellasega, D. and Mannuccii, A., 2009. Characterization of grain-boundary precipitates after hot-ductility tests of microalloyed steels. *ISIJ international*, 49(3), pp.446-452.

107. Kalisz, D. and Rzadkosz, S., 2013. Modeling of the formation of AlN precipitates during solidification of steel. *Archives of Foundry Engineering*, 13(1), pp.63-68.

108. Zambrano, O.A., 2016. Stacking Fault Energy Maps of Fe–Mn–Al–C–Si Steels: Effect of Temperature, Grain Size, and Variations in Compositions. *Journal of Engineering Materials and Technology*, 138(4), p.041010.

109. Liu, H., Liu, J., Michelic, S., Wei, F., Zhuang, C., Han, Z. and Li, S., 2016. Characteristics of AlN inclusions in low carbon Fe–Mn–Si–Al TWIP steel produced by AOD-ESR method. *Ironmaking & Steelmaking*, 43(3), pp.171-179.

110. Liu, H., Liu, J., Michelic, S.K., Shen, S., Su, X., Wu, B. and Ding, H., 2016. Characterization and Analysis of Non-Metallic Inclusions in Low-Carbon Fe–Mn–Si–Al TWIP Steels. *Steel research international*, 87(12), pp.1723-1732.

111. Yin, H., 2006. Inclusion characterization and thermodynamics for high-Al advanced high-strength steels. *Iron & steel technology*, 3(6), pp.64-73.

112. Kaushik, P., Lowry, M., Yin, H. and Pielet, H., 2012. Inclusion characterisation for clean steelmaking and quality control. *Ironmaking & Steelmaking*, 39(4), pp.284-300.

113. Brune, T., Senk, D., Walpot, R. and Steenken, B., 2015. Hot ductility behavior of boron containing microalloyed steels with varying manganese contents. *Metallurgical and Materials Transactions B*, 46(3), pp.1400-1408.

114. Kundu, A., 2014. Austenite Grain Boundary Pinning during Reheating by Mixed AlN and Nb (C, N) Particles. *ISIJ international*, 54(3), pp.677-684.

115. Comineli, O., Luo, H., Liimatainen, H.M. and Karjalainen, L.P., 2005. Influence of Cu alloying on hot ductility of C-Mn-Al and Ti-Nb microalloyed steels. *Revista de metalurgia*, 41(I), p.407.

116. Dastur, Y.N. and Leslie, W.C., 1981. Mechanism of work hardening in Hadfield manganese steel. *Metallurgical and Materials transactions A*, 12(5), pp.749-759.

117. Tuling, A., Banerjee, J.R. and Mintz, B., 2011. Influence of peritectic phase transformation on hot ductility of high aluminium TRIP steels containing Nb. *Materials Science and Technology*, 27(11), pp.1724-1731.

118. Andrade, H.L., Akben, M.G. and Jonas, J.J., 1983. Effect of molybdenum, niobium, and vanadium on static recovery and recrystallization and on solute strengthening in microalloyed steels. *Metallurgical Transactions A*, 14(10), pp.1967-1977.

119. Mintz, B. and Abushosha, R., 1992. Effectiveness of hot tensile test in simulating straightening in continuous casting. *Materials science and technology*, 8(2), pp.171-178.

120. Cho, K.C., Mun, D.J., Koo, Y.M. and Lee, J.S., 2011. Effect of niobium and titanium addition on the hot ductility of boron containing steel. *Materials Science and Engineering: A*, 528(10), pp.3556-3561.

121. Turkdogan, E.T., 1989. Causes and effects of nitride and carbonitride precipitation during continuous casting. *Iron Steelmaker*, 16(5), p.61-75.

122. Banks, K.M., Tuling, A. and Mintz, B., 2011. The influence of N on hot ductility of V-, Nb-, and Nb-Ti-containing steels using improved thermal simulation of continuous casting. *Journal of the Southern African Institute of Mining and Metallurgy*, 111(10), pp.711-716.

123. Gómez, M., Medina, S.F. and Quispe, A., 2003, January. Evolution of austenite microstructure and precipitation state during hot rolling of a Nb-microalloyed steel. In *Materials Science Forum* (Vol. 426, No. 432, pp. 1535-1540).

124. Zhou, W., Guo, H., Xie, Z., Wang, X. and Shang, C., 2013. High strength low-carbon alloyed steel with good ductility by combining the retained austenite and nano-sized precipitates. *Materials Science and Engineering: A*, 587, pp.365-371.

125. Banks, K.M., Tuling, A. and Mintz, B., 2011. Influence of V and Ti on hot ductility of Nb containing steels of peritectic C contents. *Materials Science and Technology*, 27(8), pp.1309-1314.

126. Suzuki, K.I., Miyagawa, S., Saito, Y. and Shiotani, K., 1995. Effect of microalloyed nitride forming elements on precipitation of carbonitride and high temperature ductility of continuously cast low carbon Nb containing steel slab. *ISIJ international*, 35(1), pp.34-41.

127. Liu, H., Liu, J., Wu, B., Su, X., Li, S. and Ding, H., 2017. Influence of Ti on the Hot Ductility of High-manganese Austenitic Steels. *High Temperature Materials and Processes*, 36(7), pp.725-732.

128. Luo, H., Karjalainen, L.P., Porter, D.A., Liimatainen, H.M. and Zhang, Y., 2002. The influence of Ti on the hot ductility of Nb-bearing steels in simulated continuous casting process. *ISIJ international*, 42(3), pp.273-282.

129. Medina, S.F., Quispe, A. and Gómez, M., 2015. Precipitation model in microalloyed steels both isothermal and continuous cooling conditions. *Revista de Metalurgia*, 51(4), pp.10-3989.

130. Salas-Reyes, A.E., Mejía, I. and Cabrera, J.M., 2016. Effect of Ti microaddition on cavitation behavior during uniaxial hot-tensile of Fe-22Mn-1.5 Al-1.3 Si-0.5 C austenitic TWIP steel. *MRS Online Proceedings Library Archive*, 1812, pp.123-128.

131. Banks, K.M., Tuling, A., Klinkenberg, C. and Mintz, B., 2011. Influence of Ti on hot ductility of Nb containing HSLA steels. *Materials Science and Technology*, 27(2), pp.537-545.

132. Maehara, Y., Yasumoto, K., Tomono, H., Nagamichi, T. and Ohmori, Y., 1990. Surface cracking mechanism of continuously cast low carbon low alloy steel slabs. *Materials Science and Technology*, 6(9), pp.793-806.

133. Mintz, B., 2000. Influence of nitrogen on hot ductility of steels and its relationship to problem of transverse cracking. *Ironmaking & steelmaking*, 27(5), pp.343-347.

134. Aronsson, B., 1969. Steel Strengthening Mechanisms, *Climax Molybdenum Company Symposium*, Eilert Printing Co. Inc.

135. Reyes, F., Calvo, J., Cabrera, J.M. and Mejía, I., 2012. Effect of V on hot deformation characteristics of TWIP steels. *Steel research international*, 83(4), pp.334-339.

136. Salas-Reyes, A.E., Mejía, I., Bedolla-Jacuinde, A., Boulaajaj, A., Calvo, J. and Cabrera, J.M., 2014. Hot ductility behavior of high-Mn austenitic Fe–22Mn–1.5 Al–1.5 Si–0.45 C TWIP steels microalloyed with Ti and V. *Materials Science and Engineering: A*, 611, pp.77-89.

137. Ryan, N.D. and McQueen, H.J., 1990. Comparison of dynamic softening in 301, 304, 316 and 317 stainless steels. *High Temperature Technology*, 8(3), pp.185-200.

138. McQueen, H.J. and Jonas, J.J., 1984. Recent advances in hot working: fundamental dynamic softening mechanisms. *Journal of Applied Metalworking*, 3(3), pp.233-241.

139. Perrard, F. and Scott, C., 2007. Vanadium precipitation during intercritical annealing in cold rolled TRIP steels. *ISIJ international*, 47(8), pp.1168-1177.

140. Akben, M.G., Weiss, I. and Jonas, J.J., 1981. Dynamic precipitation and solute hardening in AV microalloyed steel and two Nb steels containing high levels of Mn. *Acta Metallurgica*, 29(1), pp.111-121.

141. Mintz, B. and Abushosha, R., 1993. Influence of vanadium on hot ductility of steel. *Ironmaking and Steelmaking* (UK), 20(6), pp.445-452.

142. Maugis, P. and Gouné, M., 2005. Kinetics of vanadium carbonitride precipitation in steel: A computer model. *Acta materialia*, *53*(12), pp.3359-3367.

143. Mintz, B. and Arrowsmith, J.M., 1980. Hot working and forming processes. *Met. Soc. Book*, (264), p.99.

144. Coleman, T.H. and Wilcox, J.R., 1985. Transverse cracking in continuously cast HSLA slabs–influence of composition. *Materials Science and Technology*, 1(1), pp.80-83.

145. Lee, C.H., Park, J.Y., Chung, J., Park, D.B., Jang, J.Y., Huh, S., Kim, S.J., Kang, J.Y., Moon, J. and Lee, T.H., 2016. Hot ductility of medium carbon steel with vanadium. *Materials Science and Engineering: A*, 651, pp.192-197.

146. Kang, S.E., Banerjee, J.R., Tuling, A.S. and Mintz, B., 2014. Influence of B on hot ductility of high Al, TWIP steels. *Materials Science and Technology*, 30(4), pp.486-494.

147. Liu, C.T., White, C.L. and Horton, J.A., 1985. Effect of boron on grain-boundaries in Ni3Al. *Acta Metallurgica*, 33(2), pp.213-229.

148. Song, S.H., Faulkner, R.G. and Flewitt, P.E.J., 1999. Effect of boron on phosphorus-induced temper embrittlement. *Journal of materials science*, 34(22), pp.5549-5556.

149. Lis, A., Lis, J., Kolan, C. and Knapiński, M., 2010. Effect of strain rate on hot ductility of C-Mn-B steel. *Journal of Achievements in Materials and Manufacturing Engineering*, 41(1-2), pp.26-33.

150. Shen, Y. and Hansen, S.S., 1997. Effect of the Ti/N ratio on the hardenability and mechanical properties of a quenched-and-tempered C-Mn-B steel. *Metallurgical and Materials Transactions A*, 28(10), pp.2027-2035.

151. Ghali, S.N., El-Faramawy, H.S. and Eissa, M.M., 2012. Influence of boron additions on mechanical properties of carbon steel. *Journal of Minerals and Materials Characterization and Engineering*, 11(10), p.995.

152. Wada, H. and Pehlke, R.D., 1985. Nitrogen solubility and nitride formation in austenitic Fe-Ti alloys. *Metallurgical and Materials Transactions B*, 16(4), pp.815-822.

153. Cameron, T.B. and Morral, J.E., 1980. Boron in Steel: *Proc. Int. Symp. Boron Steels.*

154. Qaban, A., Mintz, B., Kang, S.E. and Naher, S., 2017. Hot ductility of high Al TWIP steels containing Nb and Nb-V. *Materials Science and Technology*, 33(14), pp.1645-1656.

155. Lücke, K. and Detert, K., 1957. A quantitative theory of grain-boundary motion and recrystallization in metals in the presence of impurities. *Acta Metallurgica*, 5(11), pp.628-637.

156. López-Chipres, E., Mejía, I., Maldonado, C., Bedolla-Jacuinde, A. and Cabrera, J.M., 2007. Hot ductility behavior of boron microalloyed steels. *Materials Science and Engineering: A*, 460, pp.464-470.

157. Hannerz, N.E., 1985. Critical hot plasticity and transverse cracking in continuous slab casting with particular reference to composition. *Transactions of the Iron and Steel Institute of Japan*, 25(2), pp.149-158.

158. Zarandi, F. and Yue, S., 2006. The effect of boron on hot ductility of Nb-microalloyed steels. *ISIJ international*, 46(4), pp.591-598.

159. Lagerquist, M. and Lagneborg, R., 1972. Influence of boron on the creep properties of austenitic steels. *Aktiebolaget Atomenergi*, Stockholm.

160. Laha, K., Kyono, J., Kishimoto, S. and Shinya, N., 2005. Beneficial effect of B segregation on creep cavitation in a type 347 austenitic stainless steel. *Scripta Materialia*, 52(7), pp.675-678.

161. Mejía, I., Bedolla-Jacuinde, A., Maldonado, C. and Cabrera, J.M., 2011. Hot ductility behavior of a low carbon advanced high strength steel (AHSS) microalloyed with boron. *Materials Science and Engineering: A*, 528(13-14), pp.4468-4474.

162. López-Chipres, E., Mejía, I., Maldonado, C., Bedolla-Jacuinde, A., El-Wahabi, M. and Cabrera, J.M., 2008. Hot flow behavior of boron microalloyed steels. *Materials Science and Engineering: A*, 480(1), pp.49-55.

163. Mejía, I., Salas-Reyes, A.E., Calvo, J. and Cabrera, J.M., 2015. Effect of Ti and B microadditions on the hot ductility behavior of a High-Mn austenitic Fe–23Mn–1.5 Al–1.3 Si–0.5 C TWIP steel. *Materials Science and Engineering: A*, 648, pp.311-329.

164. Mejía, I., Altamirano, G., Bedolla-Jacuinde, A. and Cabrera, J.M., 2014. Modeling of the hot flow behavior of advanced ultra-high strength steels (A-UHSS) microalloyed with boron. *Materials Science and Engineering: A*, 610, pp.116-125.

165. Hurtado-Delgado, E. and Morales, R.D., 2001. Hot ductility and fracture mechanisms of a C-Mn-Nb-Al steel. *Metallurgical and materials transactions B*, 32(5), pp.919-927.

166. Campbell, J., 2017. Discussion of "Investigation of Oxide Bifilms in Investment Cast Superalloy IN100 Parts I and II". *Metallurgical and Materials Transactions A*, 48(10), pp.5151-5153.

167. Campbell, J., 2017. Melting, remelting, and casting for clean steel. *Steel research international*, 88(1), pp.1-13.

168. Rege, J.S., Hua, M., Garcia, C.I. and Deardo, A.J., 2000. The segregation behavior of phosphorus in Ti and Ti+ Nb stabilized interstitial-free steels. *ISIJ international*, 40(2), pp.191-199.

169. Adams, C. J., 1971. National Open Heart Basic Oxygen Steel *Conf. Proc*, 54, pp.290–302.

170. Suzuki, H.G., Nishimura, S. and NAKAMURA, Y., 1984. Improvement of hot ductility of continuously cast carbon steels. *Transactions of the Iron and Steel Institute of Japan*, 24(1), pp.54-59.

171. Harada, S., Tanaka, S., Misumi, H., Mizoguchi, S. and Horiguchi, H., 1990. A formation mechanism of transverse cracks on CC slab surface. *ISIJ international*, 30(4), pp.310-316.

172. Ohmori, Y. and Maehara, Y., 1984. Precipitation of NbC and hot ductility of austenitic stainless steels. *Transactions of the Japan Institute of Metals*, 25(3), pp.160-167.

173. Mintz, B., Cowley, A., Talian, C., Crowther, D.N. and Abushosha, R., 2003. Influence of P on hot ductility of high C, Al, and Nb containing steels. *Materials science and technology*, 19(2), pp.184-188.

174. Kang, S.E., Banerjee, J.R., Tuling, A. and Mintz, B., 2014. Influence of P and N on hot ductility of high Al, boron containing TWIP steels. *Materials Science and Technology*, 30(11), pp.1328-1335.

175. Guo, A.M., Wang, Y.H., Shen, D.D., Yuan, Z.X. and Song, S.H., 2003. Influence of phosphorus on the hot ductility of 2.25 Cr1Mo steel. *Materials Science and Technology*, 19(11), pp.1553-1556.

176. Mintz, B., Tuling, A. and Delgado, A., 2003. Influence of silicon, aluminium, phosphorus and boron on hot ductility of TRansformation Induced Plasticity assisted steels. *Materials Science and Technology*, 19(12), pp.1721-1726.

177. Maehara, Y. and Nagamichi, T., 1991. Effects of silicon and nitrogen on hot ductility of low carbon steels. *Materials at High Temperatures*, 9(1), pp.30-34.

178. Gladman, T., 1997. The Physical Metallurgy of Microalloyed Steels, Univ. *Press Cambridge*.

179. Bhadeshia, H. and Honeycombe, R., 2017. *Steels: microstructure and properties*. Butterworth-Heinemann.

180. Adamczyk, J., 2006. Development of the microalloyed constructional steels. *Journal of Achievements in materials and Manufacturing Engineering*, *14*(1-2), pp.9-20.

181. Pickering, F.B., 1978. *Physical metallurgy and the design of steels*. Applied Science Publishers.

182. Kobayashi, Y., Iwasaki, S., Nakazato, K., Hibaru, T., Kuroda, S., Sakuma, N., Yoshida, N. and Nagai, K., 2008. Evolution of Columnar γ Grain in Low Carbon Steel and Its Refinement by Additional Elements in Thin Slab Casting Simulator. *ISIJ International*, *48*(3), pp.344-349.

183. Watanabe, T., 2002. Overview of near-net-shape continuous casting for steel sheet. *Tetsu-to-hagane*, *88*(3), pp.107-116.

184. Lee, K., Han, J., Park, J., Kim, B. and Ko, D., 2015. Prediction and control of front-end curvature in hot finish rolling process. *Advances in Mechanical Engineering*, *7*(11), p.1687814015615043.

185. Yasumoto, K., Maehara, Y., Ura, S., Ura, S. and Ohmori, Y., 1985. Effects of sulphur on hot ductility of low-carbon steel austenite. *Materials Science and Technology*, *1*(2), pp.111-116.

186. Kohno, T., Shima, T., Kuwabara, T., Mizogucht, S., Yamamoto, T., Misumi, H. and Tsuneoka, A., 1982. The Metallographical Characteristics and the Formation Mechanism of Longitudinal Surface Cracks in CC Slabs. *Tetsu-to-Hagané*, *68*(13), pp.1764-1772.

187. Ohmori, Y. and Kunitake, T., 1983. Effects of austenite grain size and grain boundary segregation of impurity atoms on high temperature ductility. *Metal science*, *17*(7), pp.325-332.

188. Biswas, S.K., Chen, S.J. and Satyanarayana, A., 1997. Optimal temperature tracking for accelerated cooling processes in hot rolling of steel. *Dynamics and Control*, *7*(4), pp.327-340.

189. Lamberterie, B., 2006. Recent evolutions and trends in the steel rolling industry-Inaugural speech of the 9th International Steel Rolling Conference. *Revue de Métallurgie*, *103*(7-8), pp.311-318.

190. Zhao, M.C., Yang, K. and Shan, Y., 2002. The effects of thermo-mechanical control process on microstructures and mechanical properties of a commercial pipeline steel. *Materials Science and Engineering: A*, *335*(1-2), pp.14-20.

191. Ghosh, A., Das, S., Chatterjee, S., Mishra, B. and Rao, P.R., 2003. Influence of thermo-mechanical processing and different post-cooling techniques on structure and properties of an ultra low carbon Cu bearing HSLA forging. *Materials Science and Engineering: A*, *348*(1-2), pp.299-308.

192. Yuan, S.Q., Liang, G.L. and Zhang, X.J., 2010. Interaction between elements Nb and Mo during precipitation in microalloyed austenite. *Journal of Iron and Steel Research, International*, *17*(9), pp.60-63.

193. Phaniraj, M.P., Behera, B.B. and Lahiri, A.K., 2005. Thermo-mechanical modeling of two phase rolling and microstructure evolution in the hot strip mill: Part I. Prediction of rolling loads and finish rolling temperature. *Journal of Materials Processing Technology*, *170*(1-2), pp.323-335.

194. Elwazri, A.M., Yue, S. and Wanjara, P., 2005. Effect of prior-austenite grain size and transformation temperature on nodule size of microalloyed hypereutectoid steels. *Metallurgical and Materials Transactions A*, *36*(9), p.2297.

195. Craven, A.J., He, K., Garvie, L.A.J. and Baker, T.N., 2000. Complex heterogeneous precipitation in titanium–niobium microalloyed Al-killed HSLA steels—I.(Ti, Nb)(C, N) particles. *Acta Materialia*, *48*(15), pp.3857-3868.

196. Baird, J.D. and Preston, R.R., 1973. Processing and properties of low carbon steel. *Mechanical Working of Steel I, Metallurgical Society of AIME, New York*, pp.1-46.

197. Zajac, S., Siwecki, T., Hutchinson, B. and Attlegård, M., 1991. Recrystallization controlled rolling and accelerated cooling for high strength and toughness in V-Ti-N steels. *Metallurgical Transactions A*, *22*(11), pp.2681-2694.

198. Lee, Y., Choi, S. and Hodgson, P.D., 2002. Integrated model for thermo-mechanical controlled process in rod (or bar) rolling. *Journal of materials processing technology*, *125*, pp.678-688.

199. Suarez, M.A., Alvarez, O., Alvarez-Pérez, M.A., Herrera, R., Zorrilla, C., Valdez, S. and Juárez-Islas, J.A., 2012. The effect of grain refinement on the mechanical properties of a micro alloyed steel. *Revista mexicana de física*, *58*(5), pp.417-421.

200. Choquet, P., Fabregue, P., Giusti, J., Chamont, B., Pezant, J.N. and Blanchet, F., 1990. Mathematical modelling of hot rolling of steel. *CIM, Montreal, Canada*.

201. Nwachukwu, P.U. and Oluwole, O.O., 2017. Effects of rolling process parameters on the mechanical properties of hot-rolled St60Mn steel. *Case Studies in Construction Materials*, *6*, pp.134-146.

202. Han, K., Van Tyne, C.J. and Levy, B.S., 2005. Effect of strain and strain rate on the Bauschinger effect response of three different steels. *Metallurgical and Materials Transactions A*, *36*(9), pp.2379-2384.

203. Osakada, K., 1997. Effects of strain rate and temperature in forming processes of metals. *Le Journal de Physique IV*, *7*(C3), pp.C3-XXXVII.

204. Show, B.K., Veerababu, R., Balamuralikrishnan, R. and Malakondaiah, G., 2010. Effect of vanadium and titanium modification on the microstructure and mechanical properties of a microalloyed HSLA steel. *Materials Science and Engineering: A*, *527*(6), pp.1595-1604.

205. Hong, S.G., Kang, K.B. and Park, C.G., 2002. Strain-induced precipitation of NbC in Nb and Nb–Ti microalloyed HSLA steels. *Scripta materialia*, *46*(2), pp.163-168.

206. Cao, Y.B., Xiao, F.R., Qiao, G.Y., Huang, C.J., Zhang, X.B., Wu, Z.X. and Liao, B., 2012. Strain-induced precipitation and softening behaviors of high Nb microalloyed steels. *Materials Science and Engineering: A*, *552*, pp.502-513.

207. Cao, Y.B., Xiao, F.R., Qiao, G.Y., Zhang, X.B. and Liao, B., 2011. Quantitative research on effects of Nb on hot deformation behaviors of high-Nb microalloyed steels. *Materials Science and Engineering: A*, *530*, pp.277-284.

208. Richard, S., 2001. Method for controlling the temperature of steel on a continuous hot rolling mill. *Metallurgical Transaction B*, *22*, pp.121-128.

209. Pereloma, E.V., Crawford, B.R. and Hodgson, P.D., 2001. Strain-induced precipitation behaviour in hot rolled strip steel. *Materials Science and Engineering: A*, *299*(1-2), pp.27-37.

210. Panigrahi, B.K., 2001. Processing of low carbon steel plate and hot strip—an overview. *Bulletin of Materials Science*, *24*(4), pp.361-371.

211. Muszka, K., Hodgson, P.D. and Majta, J., 2009. Study of the effect of grain size on the dynamic mechanical properties of microalloyed steels. *Materials Science and Engineering: A*, *500*(1-2), pp.25-33.

212. Nemat-Nasser, S. and Guo, W.G., 2005. Thermomechanical response of HSLA-65 steel plates: experiments and modeling. *Mechanics of Materials*, *37*(2-3), pp.379-405.

213. Balogun, S.A., Lawal, G.I., Sekunowo, O.I. and Adeosun, S.O., 2011. Influence of finishing temperature on the mechanical properties of conventional hot rolled steel bar. *Journal of Engineering and Technology research*, *3*(11), pp.307-313.

214. Laasraoui, A. and Jonas, J., 2007. Prediction of temperature distribution, flow stress and microstructure during the multipass hot rolling of steel plate and strip. *ISIJ international*, *31*(1), pp.95-105.

215. Kothe, A., Richter, J., Guth, A., Musgen, B. and Baumgardt, H., 1993. Structure/Property Relationships In Hsla Steel With Low-Carbon And Manganese And Increased Silicon Content. *Journal de Physique IV*, *3*(C 7), pp.101-104.

216. Gong, P., Palmiere, E.J. and Rainforth, W.M., 2015. Dissolution and precipitation behaviour in steels microalloyed with niobium during thermomechanical processing. *Acta Materialia*, *97*, pp.392-403.

217. Palmiere, E.J., Garcia, C.I. and De Ardo, A.J., 1994. Compositional and microstructural changes which attend reheating and grain coarsening in steels containing niobium. *Metallurgical and Materials Transactions A*, *25*(2), pp.277-286.

218. Ndaliman, M.B., 2006. An assessment of mechanical properties of medium carbon steel under different quenching media. *AU JT*, *10*(2), pp.100-104.

219. Rasouli, D., Asl, S.K., Akbarzadeh, A. and Daneshi, G.H., 2008. Effect of cooling rate on the microstructure and mechanical properties of microalloyed forging steel. *Journal of materials processing technology*, *206*(1-3), pp.92-98.

220. Ceschini, L., Marconi, A., Martini, C., Morri, A. and Di Schino, A., 2013. Tensile and impact behaviour of a microalloyed medium carbon steel: Effect of the cooling condition and corresponding microstructure. *Materials & Design*, *45*, pp.171-178.

221. Sarma, D.S., Karasev, A.V. and Jönsson, P.G., 2009. On the role of non-metallic inclusions in the nucleation of acicular ferrite in steels. *ISIJ international*, *49*(7), pp.1063-1074.

222. Equbal, M.I., Alam, P., Ohdar, R., Anand, K.A. and Alam, M.S., 2016. Effect of Cooling Rate on the Microstructure and Mechanical Properties of Medium Carbon Steel. *International Journal of Metallurgical Engineering*, *5*(2), pp.21-24.

223. Kaynar, A., Gündüz, S. and Türkmen, M., 2013. Investigation on the behaviour of medium carbon and vanadium microalloyed steels by hot forging test. *Materials & Design*, *51*, pp.819-825.

224. Maruyama, T., Kudoh, M. and Itoh, Y., 2000. Effects of carbon and ferrite-stabilizing elements on austenite grain formation for hypo-peritectic carbon steel. *Tetsu-to-Hagané*, *86*(2), pp.86-91.

225. Yoshida, N., Umezawa, O. and Nagai, K., 2003. Influence of phosphorus on solidification structure in continuously cast 0.1 mass% carbon steel. *ISIJ international*, *43*(3), pp.348-357.

226. Maehara, Y., Yasumoto, K., Sugitani, Y. and Gunji, K., 1985. Effect of carbon on hot ductility of as-cast low alloy steels. *Tetsu-to-Hagané*, *71*(11), pp.1534-1541.

227. Yan, H.Q., Wu, K.M., Wang, H.H., Li, L., Yin, Y.Q. and Wu, N.C., 2014. Effect of fast cooling on microstructure and toughness of heat affected zone in high strength offshore steel. *Science and Technology of Welding and Joining*, *19*(4), pp.355-360.

228. Cotterill, P. and Mould, P.R., 1976. *Recrystallization and grain growth in metals* (Vol. 183). London: Surrey University Press.

229. Rios, P.R., 1988. Expression for solubility product of niobium carbonitride in austenite. *Materials science and technology*, *4*(4), pp.324-327.

230. Tokizane, M., 1968. K, Yamaguchi, E. Sumaru and Y. Nakazima. *Tetsu-to-Hagan~(J. Iron Steel Inst. Jpn.)*, *54*, pp.763-776.

231. Fernández, J., Illescas, S. and Guilemany, J.M., 2006. Effect of microalloying elements on the austenitic grain growth in a low carbon HSLA steel. *Materials Letters*, *61*(11), pp.2389-2392.

232. Danon, A., Servant, C., Alamo, A. and Brachet, J.C., 2003. Heterogeneous austenite grain growth in 9Cr martensitic steels: influence of the heating rate and the austenitization temperature. *Materials Science and Engineering: A*, *348*(1), pp.122-132.

233. Calik, A., Duzgun, A., Sahin, O. and Ucar, N., 2010. Effect of carbon content on the mechanical properties of medium carbon steels. *Zeitschrift für Naturforschung A*, 65(5), pp.468-472.

234. Zheng, H., Ye, X.N., Li, J.D., Jiang, L.Z., Liu, Z.Y., Wang, G.D. and Wang, B.S., 2010. Effect of carbon content on microstructure and mechanical properties of hot-rolled low carbon 12Cr–Ni stainless steel. *Materials Science and Engineering: A*, *527*(27-28), pp.7407-7412.

235. Alkan, G., Chae, D. and Kim, S.J., 2013. Effect of δ ferrite on impact property of hot-rolled 12Cr–Ni steel. *Materials Science and Engineering: A*, *585*, pp.39-46.

236. Gladshtein, L.I., Larionova, N.P. and Belyaev, B.F., 2012. Effect of ferrite-pearlite microstructure on structural steel properties. *Metallurgist*, *56*(7-8), pp.579-590.

237. Samuels, L.E., 1999. *Light microscopy of carbon steels*. Asm International.

238. Houin, J.P., Simon, A. and Beck, G., 1981. Relationship between structure and mechanical properties of pearlite between 0.2% and 0.8% C. *Transactions of the Iron and Steel Institute of Japan*, *21*(10), pp.726-731.

239. Miller, L.E. and Smith, G.S., 1970. Tensile properties in carbon steels. *J. Iron Steel Inst*, (11), pp.998-1005.

240. Porter, D.A., Easterling, K.E. and Smith, G.D.W., 1978. Dynamic studies of the tensile deformation and fracture of pearlite. *Acta metallurgica*, *26*(9), pp.1405-1422.

241. Park, Y.J. and Bernstein, I.M., 1979. The process of crack initiation and effective grain size for cleavage fracture in pearlitic eutectoid steel. *Metallurgical Transactions A*, *10*(11), pp.1653-1664.

242. Nam, W.J. and Bae, C.M., 1995. Void initiation and microstructural changes during wire drawing of pearlitic steels. *Materials Science and Engineering: A*, *203*(1-2), pp.278-285.

243. Dollar, M., Bernstein, I.M. and Thompson, A.W., 1988. Influence of deformation substructure on flow and fracture of fully pearlitic steel. *Acta Metallurgica*, *36*(2), pp.311-320.

244. Gladman, T., McIvor, I.D. and Pickering, F.B., 1972. Some aspects of the structure-property relationships in high-C ferrite-pearlite steels. *J. Iron Steel Inst.*, *210*(12), pp.916-930.

245. Bae, C.M., Lee, C.S. and Nam, W.J., 2002. Effect of carbon content on mechanical properties of fully pearlitic steels. *Materials science and technology*, *18*(11), pp.1317-1321.

246. Sun, J.J., Liu, Y.N., Zhu, Y.T., Lian, F.L., Liu, H.J., Jiang, T., Guo, S.W., Liu, W.Q. and Ren, X.B., 2017. Super-strong dislocation-structured high-carbon martensite steel. *Scientific reports*, *7*(1), p.6596.

247. Gutiérrez, I., 2014. Effect of microstructure on the impact toughness of high strength steels. *Revista de Metalurgia*, *50*(4).

248. Fujita, N. and Bhadeshia, H.K.D.H., 2001. Modelling precipitation of niobium carbide in austenite: multicomponent diffusion, capillarity, and coarsening. *Materials Science and Technology*, *17*(4), pp.403-408.

249. Mintz, B. and Campbell, P., 1989. Growth of grain boundary carbides in C–Mn steels. *Materials science and technology*, *5*(2), pp.155-161.

250. Han, K., Edmonds, D.V. and Smith, G.D.W., 2001. Optimization of mechanical properties of high-carbon pearlitic steels with Si and V additions. *Metallurgical and Materials Transactions A*, *32*(6), pp.1313-1324.

251. Mintz, B., Wilcox, J.R. and Crowther, D.N., 1986. Hot ductility of directly cast C–Mn–Nb–Al steel. *Materials science and technology*, *2*(6), pp.589-594.

252. Cheng, L.M., Hawbolt, E.B. and Meadowcroft, T.R., 2000. Dissolution and Coarsening of Aluminum Nitride Precipitates in Low Carbon Steel—Distribution, Size and Morphology. *Canadian metallurgical quarterly*, *39*(1), pp.73-86.

253. Chávez-Alcalá, J.F., Rodríguez-Reyes, A., Navarrete-Ramos, E.G., Dorantes-Rosales, H.J., Saucedo-Muñoz, M.L. and López-Hirata, V.M., 2001. Microstructural characterization of precipitation in an isothermally aged Nb-containing microalloyed steel. *ISIJ international*, *41*(12), pp.1532-1534.

254. Gladman, T., 1994. Aluminium for grain size control. *Heat Treatment of Metals (UK)*, *21*(1), pp.11-14.

255. Speich, G.R., Cuddy, L.J., Gordon, C.R. and DeArdo, A.J., 1984. Phase transformations in ferrous alloys. *TMS-AIME, Warrendale, PA, pp, 341*.

256. Militzer, M., Hawbolt, E.B., Meadowcroft, T.R. and Giumelli, A., 1996. Austenite grain growth kinetics in Al-killed plain carbon steels. *Metallurgical and Materials Transactions A*, *27*(11), pp.3399-3409.

257. Sobral, M.D.C., Mei, P.R. and Kestenbach, H.J., 2004. Effect of carbonitride particles formed in austenite on the strength of microalloyed steels. *Materials Science and Engineering: A*, *367*(1), pp.317-321.

258. Davis, C.L., 2006. The effect of microalloy precipitates on final product mechanical properties. *Transactions of the Indian Institute of Metals*, *59*(5), pp.695-710.

259. Hong, S.G., Jun, H.J., Kang, K.B. and Park, C.G., 2003. Evolution of precipitates in the Nb–Ti–V microalloyed HSLA steels during reheating. *Scripta materialia*, *48*(8), pp.1201-1206.

260. Yan, P. and Bhadeshia, H.K.D.H., 2015. Austenite–ferrite transformation in enhanced niobium, low carbon steel. *Materials Science and Technology*, *31*(9), pp.1066-1076.

261. Pichler, A., Hebesberger, T., Traint, S., Tragl, E., Kurz, T., Krempaszky, C., Tsipouridis, P. and Werner, E., 2006. Advanced high strength thin sheet grades: Improvement of properties by microalloying assisted microstructure control. In *International Symposium on Niobium Microalloyed Sheet Steel for Automotive Applications* (pp. 245-74).

262. Sally, P., Andrew, R., Geoff, W. and Rachel, T., 2011. Effect of Niobium on Transformations from Austenite to Ferrite in Low Carbon Steels. In *Proceedings of the*

6th International Conference on High Strength Low Alloy Steels (HSLA Steels' 2011)(I).

263. Eldis, G.T. and Hagel, W.C., 1977. Effects of Microalloying on the Hardenability of Steel. *Hardenability Concepts with Applications to Steel*, pp.397-420.

264. Hanamura, T., Yamashita, T., Umezawa, O., Torizuka, S. and Nagai, K., 2002. Improvement of strength-and-toughness balance of recycled steel through ultrarefinement of grain size. *Journal of Advanced Science*, *13*(3), pp.179-182.

265. Yoshida, N., Umezawa, O. and Nagai, K., 2004. Analysis on refinement of columnar γ grain by phosphorus in continuously cast 0.1 mass% carbon steel. *ISIJ international*, *44*(3), pp.547-555.

266. Lamberterie, B., 2006. Recent evolutions and trends in the steel rolling industry-Inaugural speech of the 9th International Steel Rolling Conference. *Revue de Métallurgie*, *103*(7-8), pp.311-318.

267. Kiessling, R. and Lange, N., 1966. Non-metallic inclusions in steel.

268. Avdušinović, H. and Gigović, A., 2005. The morphology and distribution of MnS in low carbon steel. *Metalurgija*, *44*(2), pp.151-154.

269. Banks, K.M., Tuling, A. and Mintz, B., 2012. Influence of thermal history on hot ductility of steel and its relationship to the problem of cracking in continuous casting. *Materials Science and Technology*, *28*(5), pp.536-542.

270. Turkdogan, E.T., 1987. Causes and effects of nitride and carbonitride pre-cipitation in HSLA steels in relation to continuous casting‖ Kenne-dy W. In *Steelmaking Conference Proceedings. New York: AIME* (Vol. 399).

271. Subramanian, S.V., Shima, S. and Ocampo, G., 1985. The Effect of Nitrogen Content on the Evolution of Precipitates and on the Processing of Ti--Nb Bearing HSLA Steel Slabs. *HSLA Steels: Metallurgy and Applications*, pp.151-161.

272. Thermfact and GTT-technologies, Thermomechamical software and database package. Available at: https:/www.factsage.com [Accessed 30 October 2019].

273. Canale, L.D.C.F., Totten, G.E. and Mesquita, R.A. eds., 2008. *Failure analysis of heat treated steel components*. ASM international.

274. Mintz, B., Shaker, M. and Crowther, D.N., 1997. Hot ductility of an austenitic and a ferritic stainless steel. *Materials science and technology*, *13*(3), pp.243-250.

275. Abushosha, R., Vipond, R. and Mintz, B., 1991. Influence of titanium on hot ductility of as cast steels. *Materials Science and Technology*, *7*(7), pp.613-621.

276. Leslie, W.C., Rickett, R.L., Dotson, C.L. and Walton, C.S., 1954. Solution and precipitation of aluminum nitride in relation to the structure of low carbon steels. *Transactions of the American Society for Metals*, *46*, pp.1470-1499.

277. Turkdogan, E.T., Ignatowicz, S. and Pearson, J., 1955. The solubility of sulphur in iron and iron-manganese alloys. *J. Iron Steel Inst*, *180*(8), pp.349-354.

278. Osinkolu, G.A., Tacikowski, M. and Kobylanski, A., 1985. Combined effect of AIN and sulphur on hot ductility of high purity iron-base alloys. *Materials science and technology*, *1*(7), pp.520-525.

279. Osinkolu, G.A. and Kobylanski, A., 1997. Hot tensile deformation of ultra high purity iron base alloys containing Al, N, S on cooling to test temperatures. *Scripta materialia*, *36*(10).

280. Wang, Y.N., Yang, J., Wang, R.Z., Xin, X.L. and Xu, L.Y., 2016. Effects of Non-metallic Inclusions on Hot Ductility of High Manganese TWIP Steels Containing Different Aluminum Contents. *Metallurgical and Materials Transactions B*, *47*(3), pp.1697-1712.

281. Lankford, J.W., 1972. Some considerations of strength and ductility in the continuous-casting process. *Metallurgical Transactions*, *3*(6), pp.1331-1357.

282. Mintz, B., 2003. The influence of Al on the mechanical properties of hot rolled steel plates. In Materials Science Forum (Vol. 426, pp. 1219-1223). Trans Tech Publications Ltd., Zurich-Uetikon, Switzerland.

283. Mintz, B., 1973. Influence of Si and N on the Impact Properties of As-Rolled Mild and C-Mn Steels. J. Iron Steel Inst., 211(6), pp.433-439.

284. Mintz, B. and Turner, P.J., 1978. The influence of silicon on the impact and tensile properties of steels. Metallurgical Transactions A, 9(11), pp.1611-1617.

285. Mintz, B., Tajik, S. and Vipond, R., 1994. Influence of microalloying additions on thickness of grain boundary carbides in ferrite–pearlite steels. Materials science and technology, 10(2), pp.89-96.

286. Wilmes, S. and Zwick, G., 2002. Effect of niobium and vanadium as an alloying element in tool steels with high chromium content. The Use of Tool Steels: Experience and Re-search, 1, pp.227-243.

287. Annan, K.A., Siyasiya, C.W. and Stumpf, W.E., 2015. The influence of niobium content on austenite grain growth in microalloyed steels. Journal of the Southern African Institute of Mining and Metallurgy, 115(10), pp.973-980.

288. Mintz, B., Tajik, S. and Vipond, R., 1994. Influence of microalloying additions on thickness of grain boundary carbides in ferrite–pearlite steels. Materials Science and Technology, 10(2), pp.89-96.

289. Mizuno, R., Matsuda, H., Funakawa, Y. and Tanaka, Y., 2010. Influence of Microstructure on Yield Strength of Ferrite-Pearlite Steels. Tetsu to Hagane-Journal of the Iron and Steel Institute of Japan, 96(6), pp.A414-A423.

290. Baker, T.N., 2016. Microalloyed steels. Ironmaking & Steelmaking, 43(4), pp.264-307.

291. Olasolo, M., Uranga, P., Rodriguez-Ibabe, J.M. and López, B., 2011. Effect of austenite microstructure and cooling rate on transformation characteristics in a low carbon Nb–V microalloyed steel. Materials Science and Engineering: A, 528(6), pp.2559-2569.

292. KA, A. and HJ, K., 2007. The influence of niobium microalloying on austenite grain coarsening behavior of Ti-modified SAE 8620 steel. ISIJ international, 47(2), pp.307-316.

293. Wei, S. and Lu, S., 2012. Effects of multiple normalizing processes on the microstructure and mechanical properties of low carbon steel weld metal with and without Nb. Materials & Design, 35, pp.43-54.

294. Callister Jr, W.D. and Rethwisch, D.G., 2012. Fundamentals of Materials Science and Engineering: an integrated approach. John Wiley & Sons.

295. Razzak, M.A., Perez, M., Sourmail, T., Cazottes, S. and Frotey, M., 2014. Preventing abnormal grain growth of austenite in low alloy steels. ISIJ international, 54(8), pp.1927-1934.

296. Bhadeshia, H. K. D. H., (2000) Widmanstatten Ferrite in Part II Course C9, Alloys, Materials Science & Metallurgy, [online] Available at: https://www.phase-trans.msm.cam.ac.uk/2000/C9/lecture7.pdf [Accessed 30 October 2019].

297. Phelan, D. and Dippenaar, R., 2004. Widmanstätten ferrite plate formation in low-carbon steels. *Metallurgical and Materials Transactions A*, *35*(12), pp.3701-3706.

298. Grewal, R., Aranas Jr, C., Chadha, K., Shahriari, D., Jahazi, M. and Jonas, J.J., 2016. Formation of Widmanstätten ferrite at very high temperatures in the austenite phase field. Acta Materialia, 109, pp.23-31.

299. Lu, S., Wei, S., Li, D. and Li, Y., 2010. Effects of heat treatment process and niobium addition on the microstructure and mechanical properties of low carbon steel weld metal. Journal of Materials Science, 45(9), pp.2390-2402.

300. Coll Ferrari, M.T., 2015. Effect of austenitising temperature and cooling rate on microstructures of hot-work tool steels (Doctoral dissertation, University West).

301. Bodnar, R.L. and Hansen, S.S., 1994. Effects of austenite grain size and cooling rate on Widmanstätten ferrite formation in low-alloy steels. Metallurgic and Materials Transactions A, 25(4), pp.665-675.

APPENDIX

Appendix A

Summary of the recorded hot ductility measurements of the TWIP steels examined are given in Tables A1-A6.

Table A1 The TWIP steel with low Ti/N ratio (steel 1) cooled at 12°C min^{-1}.

Temperature (°C)	D_i (mm)	D_f (mm)	RA (%)
700	10	5.24	47.6
800	10	5.39	46.1
900	10	3.3	67
1000	10	5.11	48.9
1100	10	6.59	34.1

Table A2 The TWIP steel with medium Ti/N ratio (steel 2) cooled at 12°C min^{-1}.

Temperature (°C)	D_i (mm)	D_f (mm)	RA (%)
700	10	3.74	62.6
800	10	3.86	61.4
900	10	3.27	67.3
1000	10	5.27	47.3
1100	10	6.24	37.6

Table A3 The TWIP steel with high Ti/N ratio (steel 3) cooled at 12°C min^{-1}.

Temperature (°C)	D_i (mm)	D_f (mm)	RA (%)
700	10	4.62	53.8
800	10	4.24	57.6
900	10	2.39	76.1
1000	10	4.51	54.9
1100	10	5.94	40.6

Table A4 The TWIP steel with low Ti/N ratio (steel 1) cooled at 60°C min^{-1}.

Temperature (°C)	D_i (mm)	D_f (mm)	RA (%)
700	10	4.17	58.3
800	10	3.18	68.2
900	10	2.71	72.9
1000	10	4.46	55.4
1100	10	5.37	46.3

Table A5 The TWIP steel with medium Ti/N ratio (steel 2) cooled at 60°C min^{-1}.

Temperature (°C)	**D_i (mm)**	**D_f (mm)**	**RA (%)**
700	10	3.7	63
800	10	3.6	64
900	10	3.15	68.5
1000	10	4.55	54.5
1100	10	6.33	36.7

Table A6 The TWIP steel with high Ti/N ratio (steel 3) cooled at 60°C min^{-1}.

Temperature (°C)	**D_i (mm)**	**D_f (mm)**	**RA (%)**
700	10	3.93	60.7
800	10	2.99	70.1
900	10	2.32	76.8
1000	10	3.64	63.6
1100	10	4.87	51.3

Appendix B

Summary of the rolling schedule of the HSLA steels examined are given in Tables B1-B3

Table B1 The hot rolled HSLA steels cooled at 33°C min^{-1}.

		Temperature (°C)		
Pass No	**Aim Gauge (mm)**	**H1**	**H2**	**H3**
0	75			
1	65	1106	1105	1069
2	55	1035	1039	986
3	45	1062	1045	1055
4	35	1016	1018	1025
5	25	1049	1032	1029
6	20	997	993	982
7	15	1011	1008	993
FRT		957	953	945

Soaking temperature: 1250°C. Final thickness: 15mm.

Table B2 The hot rolled HSLA steels cooled at 17°C min^{-1}.

		Temperature (°C)	
Pass No	**Aim Gauge (mm)**	**H4**	**H5**
0	150		
1	130	1081	1130
3	90	1078	1080
5	70	1068	1073
7	50	1011	1052
9	FRT (30)	973	950

Soaking temperature: 1250°C. Final thickness: 30mm.

The temperatures at passes 2, 4, 6, 8 and 10 could not be measured because the Pyrometer was defective.

Table B3 The control rolled HSLA steels cooled at 33°C min^{-1}.

		Temperature (°C)	
Pass No	**Aim Gauge (mm)**	**C2**	**C3**
0	75		
1	65	1094	1095
2	55	1030	
3	45	1045	1026
Held at 950°C			
4	35	952	954
5	25	970	942
6	20	940	922
7	15	938	932
FRT		911	891

Soaking temperature: 1250°C. Final thickness: 15mm.

Summary of the recorded tensile measurements of the HSLA steels examined is presented in Table B4.

Table B4 The tensile properties of the HSLA steels examined.

	H1	**H2**	**H3**	**H4**	**H5**	**C2**	**C3**
Mod E (MPa)	406	211	210	195	202	205	218
Reh (MPa)	793	336	351	314	364	316	423
Rel (MPa)	770	293	305	273	343	288	389
Rm (MPa)	1078	448	310	437	499	442	534

Summary of the recorded impact energy measurements of the HSLA steels examined is presented in Tables B5-B11.

Table B5 The impact energy measurements of the H1 steel at various temperatures

Temperature (°C)	**Energy (J)**
40	302.9
21	315.3
0	272.9
-20	227.2
-40	226.6
-50	20.7
-60	13
-80	8.1

Table B6 The impact energy measurements of the H2 steel at various temperatures

Temperature (°C)	**Energy (J)**
-20	278.9
-40	282.2
-60	210.1
-80	173.1
-90	28.2
-90	7.1
-100	10.3
-120	7.1

Table B7 The impact energy measurements of the H3 steel at various temperatures

Temperature (°C)	Energy (J)	% Brittle
40	205.6	20
21	260.2	0
10	187	45
0	89.7	85
-20	77.2	85
-30	27.7	95
-40	24.3	95
-60	13.5	99

Table B8 The impact energy measurements of the H4 steel at various temperatures

Temperature (°C)	Energy (J)
-20	242
-30	241
-40	213
-50	229
-50	204
-50	202
-60	15
-60	9
-70	17
-80	7

Table B9 The impact energy measurements of the H5 steel at various temperatures

Temperature (°C)	Energy (J)
20	224
10	197
0	189
-10	175
-10	40
-10	25
-20	88
-20	45
-30	85
-40	15

Table B10 The impact energy measurements of the C2 steel at various temperatures.

Temperature (°C)	Energy (J)
-20	295.7
-40	282.2
-50	249.8
-60	221
-70	209.7
-70	205.5
-80	16.2
-100	11

Table B11 The impact energy measurements of the C3 steel at various temperatures.

Temperature (°C)	Energy (J)
40	213.2
21	255.8
0	223.9
-10	134.8
-20	92.6
-40	90.3
-60	85.3
-80	10